**UNIVERSITY OF SOUTHERN QUEENSLAND**

# CHARACTERISATION AND STRATEGIC TREATMENT OF DYSTROPHIC MUSCLE

A Dissertation submitted by:

Nicola Laws, BVSc (hons) (UQ),
Cert. Small Animal Medicine (Royal College of Veterinary Surgeons),
MACVSc (Small Animal Medicine)

For the award of

Doctor of Philosophy

2005

# ABSTRACT

The *mdx* mouse is widely used as a model for Duchenne Muscular Dystrophy, a fatal X-linked disease caused by a deficiency of the sub-sarcolemmal protein, dystrophin This dissertation reports characterisation of the features of dystrophy in the *mdx* mouse, including parameters such as electrophysiological and contractile properties of dystrophic cardiac tissue, quantitative evaluation of kyphosis throughout the *mdx* lifespan, and contractile properties of respiratory and paraspinal muscles. Following these characterisation studies, the efficacy of antisense oligonucleotides (AOs) to induce alternative mRNA splicing in *mdx* skeletal muscles (diaphragm and paraspinal muscles) was evaluated.

The left atria of younger (<6 weeks) and older (>15 months) *mdx* mice showed consistently lower basal forces and responsiveness to increased calcium, while action potential duration was significantly shorter in young mice (3 weeks) and older mice (9 and 12 months) ($P<0.05$). Cardiac fibrosis increased with age in *mdx* atria and ventricles and was elevated in young (6-8 weeks) and old (15 months) *mdx* compared to control mice ($P<0.01$). This study provided insights into DMD cardiomyopathy, and suggested that very young or old *mdx* mice provide the most useful models.

*Mdx* mice show thoracolumbar kyphosis like boys with Duchenne Muscular Dystrophy. A novel radiographic index, the Kyphotic Index (KI), was developed and showed that *mdx* mice are significantly more kyphotic from 9 months of age, an effect maintained until 17 months ($P<0.05$). At 17 months, the paraspinal and respiratory muscles (latissimus dorsi, diaphragm and intercostal muscles) are significantly weaker and more fibrotic ($P<0.05$).

Administration of AOs at four sites within the diaphragm at 4 and 5 months of age significantly increased twitch and tetanic forces compared to sham treated *mdx* ($P<0.05$). However, no difference in collagen was evident and dystrophin was not detected, possibly due to the low concentration of AO utilised. This study suggested that AOs can provide functional improvement in treated skeletal muscles.

Monthly injections with AOs into the paraspinal muscles from 2 months to 18 months of age alleviated kyphosis, without significantly altering twitch and tetanic forces of latissimus dorsi, diaphragm and intercostal muscles. There was evidence of less fibrosis in diaphragm and latissimus dorsi muscles ($P<0.05$) and reduced central nucleation of the latissimus dorsi and intercostal muscles ($P<0.05$). Again, dystrophin was not detected by immunoblot.

These studies indicate that very young and old *mdx* mice display previously uncharacterised dystrophic features, and are useful models for testing new therapies such as AOs. Low doses of AOs were shown to be safe and efficacious for long-term use, however there remains a need for testing higher concentrations and improved delivery strategies.

## CERTIFICATION OF DISSERTATION

I certify that the ideas, experimental work, results, analysis and conclusions reported in this dissertation are entirely my own effort, except where otherwise acknowledged. I also certify that the work is original and has not been previously submitted for any other award, except where otherwise acknowledged.

_____ _____

Signature of Candidate Date

ENDORSEMENT

_____ _____

Signature of Supervisor/s Date

_____ _____

# ACKNOWLEDGEMENTS

I wish firstly to acknowledge the help and encouragement of my Principal Supervisor, Dr Andrew Hoey. His dedication and expertise was at all times an inspiration, and his patience and ready availability to answer questions was greatly appreciated.

I am also grateful for the help and friendship of Dr Renee Cornford-Nairn. Renee performed the Western blots included within this dissertation, which was the only experimental work not performed by myself.

Thankyou to Dr Lindsay Brown, Department of Physiology and Pharmacology, University of Queensland for access to his laboratory and his students' helpful assistance in learning several new techniques. In particular, I would like to thank Vincent Chan for his time and patience in showing me aspects of histology and confocal microscopy. Thankyou also to Dr Andrew Fenning for his initial help with microelectrode studies. I am especially grateful to Mr Paul Addison, also of the Department of Physiology and Pharmacology, University of Queensland for his continued advice and encouragement regarding the setting up histology facilities within our own laboratory.

Thankyou to Dr Peter Dunn, who was a willing source of statistical help and advice, in particular for all his help unravelling the vast amount of data generated in the aging mouse heart study. His assistance and explanations enabled me to view the data in a more logical manner.

I received assistance with electronics and constructing MAP and TAP apparatus from Oliver Kinder (Workshop Manager), Graham Holmes and Stewart Cornford (Department of Physics). I am grateful for their expert workmanship, and patience with my many and varied requests for help.

The technical and administrative staff from the Department of Biology, University of Southern Queensland, were a source of constant help and friendship. Thankyou Pat McConnell, Julie Murphy, Adele Jones, Mo Boddington, Vic Schultz, Debbie White, Ros Gill, Kath O'Donnell, Bob Coy and Sandra Sharp. Sandra and Julie's high standards of animal care were always exemplary.

Thankyou to the Oakey Veterinary Hospital for their kind loan of radiographic equipment and facilities for both x-ray studies. Thanks also to Helen Posselt, physiotherapist from Montrose Access, for useful discussions and papers on kypho-scoliosis in boys with Duchenne Muscular Dystrophy.

The staff of the Office of Research and Higher Degrees were always willing to assist in any way they could. Thankyou Ruth Hilton, Christine Bartlett, Trish Lowein and Carla Hamilton for your professionalism and support over the past few years.

Thanks are due also to all the Science IT staff, including Chris de Byl, Sammy Quattromani, Phil Hallas and Steve Payne, for their efforts in keeping the lab computers functioning and sorting out numerous small problems as they arose.

Thankyou to Dr Marie Ward from Auckland University, NZ, who gave advice via e-mail concerning ventricular trabeculae preparations.

Thankyou also to Drs Steve Wilton and Sue Fletcher, and Kaite Honeyman from Neuromuscular Research Institute, University of Western Australia for their generous help and advice with the anti-sense oligonucleotide aspect of this study.

I am grateful for the friendship and help from fellow researchers Christel, Peter, Scott Kershaw, Mike, Dave, Connie, Garth, Scott Fry, Austin, Rebecca, Xiao and Helen

Finally, my love and gratitude to Glen, Michael and Patrick: I cannot thank you enough for the support, tolerance and good humour you showed me at all times.

# TABLE OF CONTENTS

## CHAPTER 1. INTRODUCTION: DUCHENNE MUSCULAR DYSTROPHY, LITERATURE REVIEW AND SCOPE OF STUDY

## CHAPTER 2. THE AGING MDX MOUSE: ATRIAL FUNCTION AND CARDIAC FIBROSIS



## CHAPTER 3. THE AGING *MDX* MOUSE: DIAPHRAGM FUNCTION AND FIBROSIS

## APPENDIX B: RECIPES AND PROTOCOLS

## B1: HYDROXYPROLINE ASSAY



## B2: HISTOLOGY RECIPES AND PROTOCOLS



## B3 : WESTERN BLOT



## B4: SKELETAL MUSCLE ORGAN BATH PROTOCOLS



## B5: MICROELECTRODE STUDIES

# LIST OF FIGURES

# LIST OF TABLES



# LAYOUT OF DISSERTATION

A chapter format has been used for the presentation of data within this thesis as it was felt that individual studies were complete projects in their own right, with differing objectives and sometimes scientific methods. For this reason each chapter included a brief Introduction, Aims, Methods, Statistics, Results and finally Discussion. To prevent excessive repetition of methods these sections were kept brief and explained in greater detail in Appendix B. Likewise, a lengthy review of the published literature for each topic was avoided in Chapter 1, but relevant information was included (where applicable) as individual chapter introductions or within the chapter discussions. Chapter 7 provides an overview of the dissertation, highlighting important conclusions, shortcomings and implications for future study. The objective at all times was to present experimental data in context with the current knowledge base in the subject area, whilst providing new observations and insights.

# PUBLICATIONS

Laws, N., Woolf, P., Lu, S., Conlan, L. & Hoey, A., Research on Skeletal and Cardiac Muscle Dysfunction, *Muscular Dystrophy 2003 Conference,* Perth

Hoey, A., Lu, S., Woolf, P. & Laws, N., 2003, The *Mdx* Mouse as a Model of Heart Dysfunction for DMD, *Cardiomyopathy in Muscular Dystrophy*, Tucson, Session 13:40

Hoey A., van Erp C., Laws N., Lu S. 2004. The aging *mdx* mouse as a model of cardiomyopathy for Duchenne Muscular Dystrophy. *J. Mol. Cell. Cardiol.* 37:174 A36

Laws N., Hoey A. (2004). Progression of kyphosis in *mdx* mice. *J Appl Physiol.* 97:1970-1977

Laws N., Hoey A. (2004). Progression of kyphosis in dystrophin deficient (*mdx)* mice, *Australian Society for Medical Research Postgraduate Conference*, Brisbane

# PRESENTATIONS

Laws N. (2002). The Misunderstood Mouse. *Dept. of Biological and Physical Sciences, University of Southern Queensland Postgraduate conference.*Toowoomba

Laws N. (2003) Cardiac manifestations in the *mdx* mouse model of Duchenne Muscular Dystrophy, *Muscle 2003 Conference*, Canberra

Laws N. (2003). The Misunderstood Mouse II. Is the *mdx* mouse a good model for heart failure in Duchenne Muscular Dystrophy? *Dept. of Biological and Physical Sciences, University of Southern Queensland Postgraduate conference.* Toowoomba

# ABBREVIATIONS

| | |
|---|---|
| AO | antisense oligonucleotide |
| APA | action potential amplitude |
| APD | action potential duration |
| BDM | 2,3-butanedione monoxime |
| BP | base pair |
| BPM | beats per minute |
| DGC | dystrophin-glycoprotein complex |
| $dH_2O$ | distilled water |
| DNA | deoxyribonucleic acid |
| FOC | force of contraction |
| g | gram |
| H&E | haematoxylin and eosin |
| Kb | kilobases |
| K Da | kilodalton |
| LA | left atria |
| LVA | left ventricular apex |
| Lo | optimum length |
| M | molar |
| mM | millimolar |
| MAP | monophasic action potential |
| Mb | megabases |
| mRNA | messenger RNA |
| ms | millisecond |
| N | normolar |
| nNOS | neuronal nitric oxide synthase |
| S.E. | standard error |
| TAP | transmembrane action potential |
| TPF | time to peak force |
| $TR_{50}$ | time for 50% relaxation |
| $TR_{90}$ | time for 90% relaxation |

# CHAPTER 1. INTRODUCTION: DUCHENNE MUSCULAR DYSTROPHY, LITERATURE REVIEW AND SCOPE OF STUDY.

*The disease is one of the most interesting and at the same time most sad…*

*Sir William Gowers, Lancet 1879*

## 1.1 Duchenne Muscular Dystrophy

Muscular dystrophies are a heterogenous group of hereditary diseases characterised by muscle necrosis, progressive muscle wasting and weakness. Phenotypically, they are the result of uncompensated deficiencies in metabolites or proteins, exceeding muscle's demands for differentiation, maturation, growth and repair (Infante and Huszagh, 1999). Abortive cycles of necrosis and repair follow, leading to the eventual loss of satellite cells, endomysial fibrosis and adiposis. The majority of the dystrophies, but not all, are disorders of the dystrophin-glycoprotein complex that spans the sarcolemma, with Duchenne Muscular Dystrophy (DMD) the most prevalent and severe, usually leading to the death of affected males by their third decade.

For the purposes of this review the term dystrophic applies to muscles lacking the protein dystrophin, including the disease in man and several animal models.

### 1.1.1 Brief history of Duchenne Muscular Dystrophy

Clinical descriptions of boys with progressive muscle wasting and weakness, enlarged calves and muscle contractures appeared in the 18$^{th}$ and 19$^{th}$ Centuries, authored by physicians Charles Bell (Edinburgh, 1774), Gaetano Coste (Naples, 1836), Mr Partridge (London, 1847) and W.J. Little (London, 1853). However, the most complete early description of the disease came from Dr Edward Meryon (London, 1851), whose dissertation on 8 affected boys from 3 families suggested a genetic link and gender predilection. He concluded from microscopic analysis that the condition involved muscle tissue, and spared the nervous system. Duchenne de Boulogne reported some 40 cases in the 1850's and 1860's, including more detailed histology obtained from muscle biopsies. (Early history reviewed by (Gowers, 1879) and (Emery and Muntoni, 2003)). Sir William Gowers gave a complete

description of 'Pseudo-hypertrophic Muscular Paralysis' in a series of Lancet papers published in 1879 (Gowers, 1879). He brought attention to the common manifesation of muscular dystrophies now known as 'Gower's manoeuvre', where affected individuals have difficulty rising, using their hands to incrementally walk up their thighs until able to stand (Figure 1.1), and the strong inheritance from the maternal side 'like haemophilia'.

Since these times the classification of different forms of muscular dystrophies, as well as identification of rare forms, has been performed. Becker Muscular Dystrophy (BMD), an allelic form of DMD with a milder phenotype was recognised (Becker and Kiener, 1955). Gene specific probes were developed and the cDNA was cloned and sequenced (Koenig *et al.*, 1987), and the protein dystrophin was identified (Hoffman *et al.*, 1987). Studies on the localisation (Koenig *et al.*, 1988) and function of dystrophin were then undertaken in earnest, most involving the murine model of DMD; the *mdx* mouse, discovered in a colony of C57Bl/10ScSn (Bulfield *et al.*, 1984). The dystrophin-like protein, utrophin, was discovered in 1992 (Tinsley *et al.*, 1992).

Early gene or myoblast transfer studies began in the 1990's and are ongoing. Muscle is a vast organ presenting serious challenges to any somatic gene or cell replacement strategy. Adeno-viral associated mini-dystrophin research holds promise for the future (Xiao *et al.*, 2000; Gregorevic *et al*, 2004). Aminoglycoside antibiotics such as gentamicin can be used to circumvent premature stop codons, and it is hoped new derivative drugs with a wider margin of safety can be used in the 10-15% of boys with this form of genetic defect (Barton-Davis *et al.*, 1999). Anti-sense oligoribonucleotides offer exciting future prospects for safe and effective 'patching' of mis-sense mutations, allowing a read-through of genetic information and production of functional dystrophin-like protein (Wilton *et al.*, 1999; Aartsma-Rus *et al.*, 2002). The anticipation of a number of Stage I clinical trials, provides hope to patients and their families, although researchers agree a genetic 'cure' may realistically be one or two decades away (Scheuerbrandt, 2004). New genotyping techniques will allow tailoring of treatments to specific genetic lesions (Flanigan *et al.*, 2003).

Perhaps the most recent advances in DMD research is into cardiomyopathy in both the *mdx* model and boys with DMD (reviewed by (McNally and Towbin,

2004), (Quinlan *et al.*, 2004),(Yue *et al.*, 2004), and the recognition that best practice treatment guidelines for cardiac monitoring and care (as promoted for respiratory care) can improve longetivity and quality of life (Bushby *et al.*, 2003), (McNally and Towbin, 2004).

### 1.1.2.Clinical features of DMD

Boys with DMD are normal at birth, and clinical signs are not usually detected until after they become ambulatory. There is often delayed motor development (delays in sitting, standing or walking unsupported) or an abnormal gait when walking, running or climbing stairs. Despite an increasing understanding of DMD and better diagnostic testing, the average age at diagnosis in the United Kingdom is 4 years 10 months, almost identical to that of the 1980's (Bushby *et al.*, 1999).

Intellectual milestones can sometimes be delayed, in particular speech development, with 50-70% of DMD children having a delay in speech at presentation. A proportion of boys have behavioural or emotional disturbances, or have intellectual impairment (Emery and Muntoni, 2003).

Enlargement of the calf muscles is a typical early sign, and this hypertrophy can sometimes extend to masseters, deltoids, serrati anterior and quadriceps. Muscle weakness is bilateral and symmetrical, resulting in well-defined physical features including a broad-based waddling gait, pelvic tilting, lumbar lordosis and toe walking. Gower's manoeuvre is often elicited by 4-5 years of age. Shortening of the Achilles tendons and occasionally hip flexors and hamstrings occur (Figure 1.1). Respiratory muscles are never evidently weak in ambulatory children, with forced vital capacity measurements > 70%.

Eventually a child with DMD will become confined permanently to a wheelchair, with the age that this occurs varying from 7-13 years (Emery and Muntoni, 2003). Functional tests, such as the Hammersmith Scale, show a progressive loss in motor function. As the disease progresses and muscle weakness becomes more profound, flexion contractures occur, and a severe kyphoscoliosis develops unless spinal support is provided (Smith *et al.*, 1989).

There is a progressive decline in pulmonary function with age, leading to hypercapnic respiratory failure. The age when vital capacity falls below 1L is a

strong marker of subsequent mortality (5 year survival <8%) (Phillips *et al.*, 2001). Sleep-disordered breathing and nocturnal desaturation are common and severe in DMD patients (Bourke and Gibson, 2002). Cardiac manifestations range from subclinical, progressing to dilated cardiomyopathy and early death from heart failure. Clinically apparent cardiomyopathy is present in all patients over 18 years of age (Nigro *et al.*, 1990), and shortens life expectancy significantly (Eagle *et al.*, 2002).

Sir William Gowers poignant early descriptions of boys with DMD, with its accompanying illustrations (Gowers, 1879) are unfortunately still relevant today. DMD remains a relentlessly progressive disorder causing significant morbidity and early mortality, however the clinical course is altering due to improved physiotherapy, early introduction of antibiotics, influenza vaccination, glucocorticoid regimes, assistive respiratory devices and spinal stabilisation techniques. In particular, nocturnal ventilation has improved survival markedly from 19 years for non-ventilated patients to 25 years for those receiving ventilation (Eagle *et al*., 2002). Improved delivery and organization of care has meant the difference between death in childhood and achieving an independent (although supported) life as adults.

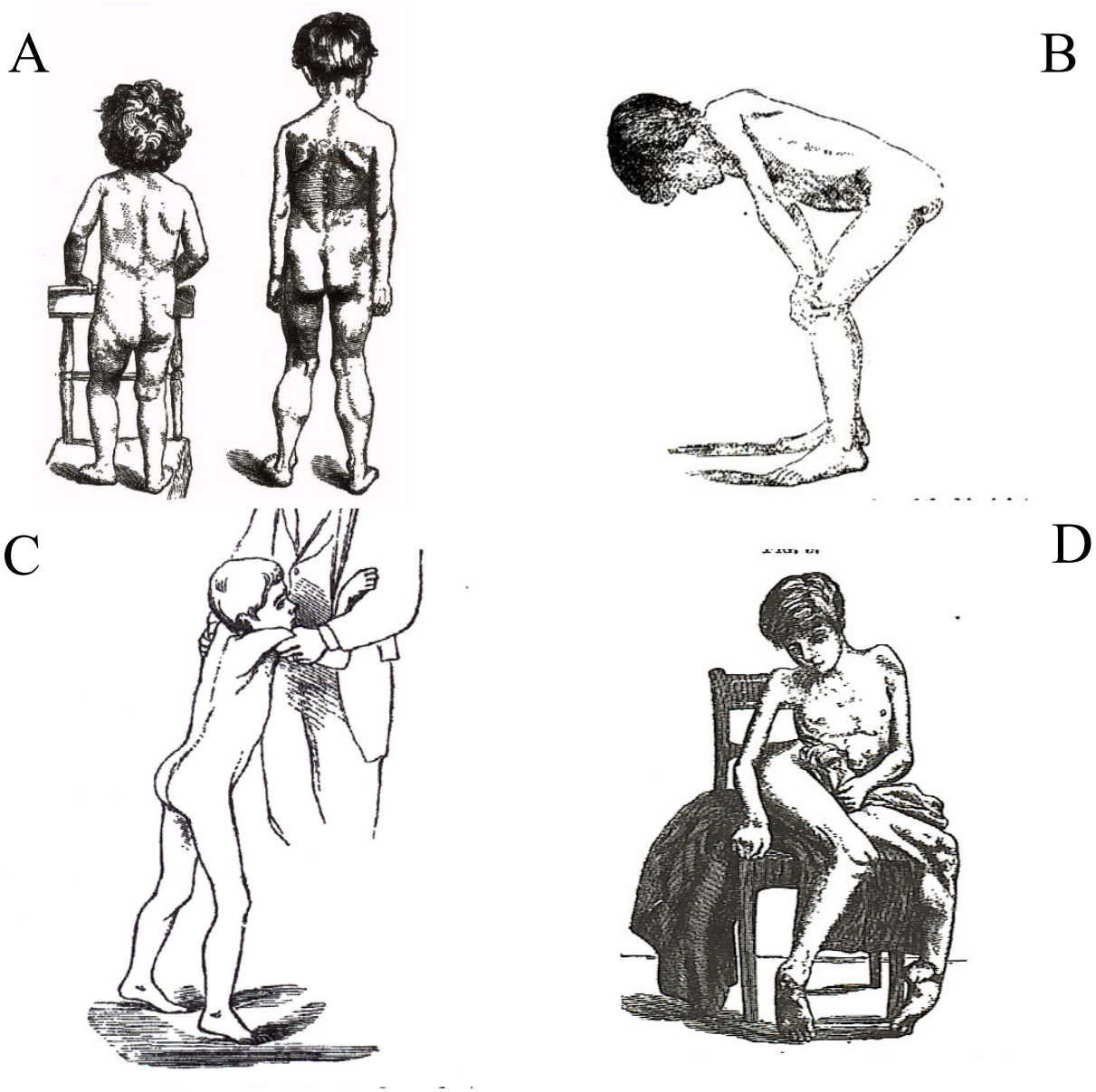


**Fig 1.1** Illustrations from early treatises on Duchenne Muscular Dystrophy.

A. Two young boys showing calf hypertrophy and wide based stance characteristic of DMD.

B. During Gower's manoeuvre, a boy typically uses the strength of his arms and hands pushing against his thighs to help him rise from a sitting position.

C. A patient displaying progressive weakness and lordosis.

D. An advanced case with severe spinal deformity and ligament contractures.

(Figs A, B and D: (Gowers, 1879), C:(Bramwell, 1879))

## 1.2 The dystrophin gene: room for error

### 1.2.1 Incidence of DMD

DMD is the most frequent of the lethal X chromosome-linked recessive disorders, with an occurrence of approximately 1 per 3,500 male births (Emery, 1993). The mutation rate of 1 in 10,000 for the dystrophin gene is one of the highest mutation rates reported, and means 1 in 3 cases of DMD are the result of new, sporadic mutations (Muller *et al.*, 1992).

### 1.2.2 Gene structure and isoforms

The dystrophin gene spans 2.4 megabases at Xp21.1 and comprises at least 85 exons (including at least 7 promoters) that have been well conserved throughout vertebrate evolution (Koenig *et al*., 1987; Koenig *et al*., 1988).

The genomic locus is nearly 200 times greater in size than the 14kb final RNA transcript, with a mean size of exons of 200bp and a mean size of introns of 35kb. The DNA encoding the DMD locus represents 1/1000 of total human DNA, and it has been suggested that the high frequency of DNA mutations is a direct consequence of the sheer size of the gene (Koenig *et al*., 1987).

Dystrophin exists in a number of isoforms, with three full length transcripts referred to as Purkinje (P), Muscle (M) and Brain (B), reflecting those tissues in which they are predominately represented, and at least five other shorter transcripts generated by internal promotors (retina, heart, spinal cord, peripheral nerves and ubiquitous) (Culligan *et al.*, 1998; Pearce *et al.*, 1993; Emery, 2002). Figure 1.2 shows a schematic representation of the human dystrophin gene.

### 1.2.3 Mutation 'hot spots' in DMD

The high mutation rate and large size of the dystrophin gene has led to the characterisation of hundreds of independent mutations, with approximately 65% of patients with DMD having large deletions within the gene, centred around two mutation 'hot spots'(Koenig and Kunkel, 1990). The first is located approximately 1200kb from the 5' end, clustered around Exons 45-55. The second is located 500kb from the 5' end, clustered around Exons 1-20.

The size and position of the deletion does not often correlate with the clinical phenotype observed, an observation largely explained by the reading frame hypothesis (Monaco *et al.*, 1988). The majority of frame-shift deletions in these hot spots result in severe DMD, as no dystrophin is produced. In-frame deletions of the central region of the gene that removes almost 50% of the dystrophin can result in a mild phenotype.

One third of DMD mutations are estimated to arise from point mutations or very small deletions that introduce premature stop codons, and these are not always centred on the mutation hot spots (Lenk *et al.*, 1993).

### 1.2.4 Becker Muscular Dystrophy

DMD is also allelic with a milder condition of similar, but slower clinical course, known as Becker Muscular Dystrophy (BMD) (Becker and Kiener, 1955; Kingston *et al.*, 1983). BMD usually results from mutations that maintain the reading frame, resulting in a partially functional dystrophin transcript (Monaco *et al.*, 1988), however exceptions can occur sometimes with frame shift deletions, truncation mutations or splice site mutations also being described in BMD patients. (See also Sections 1.3.1, 1.3.2)

### 1.2.5 Utrophin

The dystrophin coding region also demonstrates homology with other classes of genes, and the entire dystrophin sequence is similar to that of utrophin (Pearce *et al*., 1993). The autosomal utrophin gene, located on chromosone 6, is another large gene of over 1 Mb in size, encoding the protein utrophin. This protein is present in a wide variety of tissues, with the highest levels in lung and kidney. In developing skeletal muscle it is localised around the entire sarcolemma, however in adults it becomes restricted to the myotendinous junctions and neuromuscular junctions. It has sequence homology to dystrophin of over 80% (Tinsley *et al*., 1992). The utrophin gene is not mutated in DMD, hence the interest in it for gene therapy strategies.

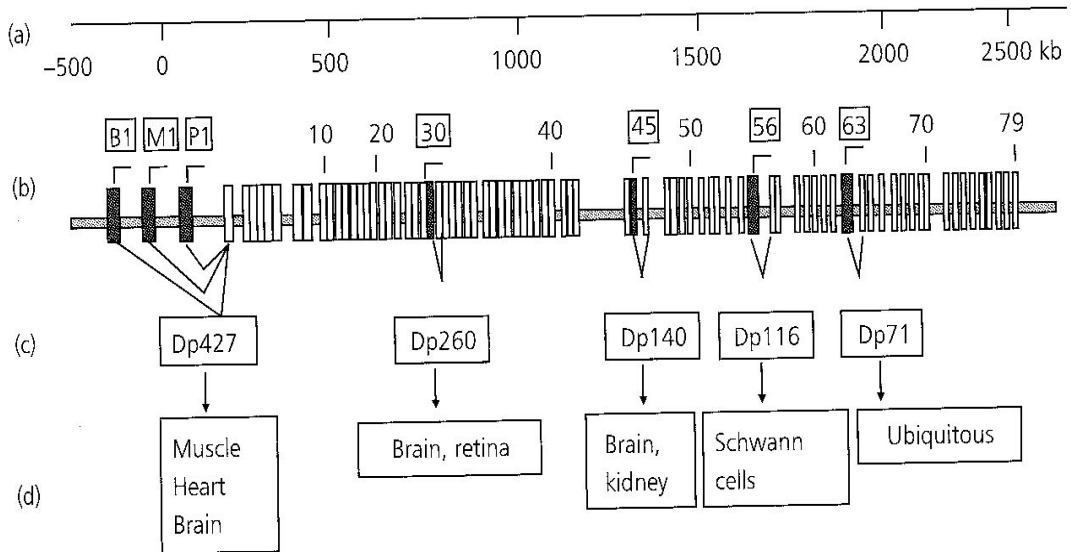


**Fig 1.2** Schematic representation of the dystrophin gene

a) The size occupied by the gene in kilobases (kb)
b) The location of the various first exons and promoters (represented by the boxes above the vertical bars that show the dystrophin exons)
c) Names of the resultant isoforms. B1, M1 and P1 indicate Brain, Muscle and Purkinje cell promoters, encoding for 3 full-length isoforms. They are located before Exon 2
d) Tissues in which the various isoforms are preferentially expressed

(from (Emery and Muntoni, 2003))

## 1.3 Dystrophin : more than a scaffold.

### 1.3.1 Structure of dystrophin

Dystrophin is a minor component (by mass) of skeletal, cardiac and smooth muscle, comprising only 0.002% of its total protein content (Beam, 1988). Despite its low abundance, it is an integral part of the large group of transmembrane and associated proteins known collectively as the dystrophin-glycoprotein complex (DGC). The DGC forms a direct link between the actin cytoskeleton and the extracellular matrix, and breaks in this link at one or more levels give rise to muscular dystrophy phenotypes. Figure 1.3 illustrates the arrangement of dystrophin serving as a bridge between the sarcolemma and sub-sarcolemmal actin filaments.

Full-length dystrophin is a very large molecular weight protein (427 kilodaltons), that is described as having four structural domains (Hoffman *et al*., 1987). The N-terminal domain shows homology to α-actinin and binds F-actin *in vivo* and *in vitro.* One trangenic mouse study indicated that an intact actin-binding domain is not essential (Corrado *et al.*, 1996), however deletions of the amino terminal and rod actin binding domains result in severe pathology (Cox *et al.*, 1994).

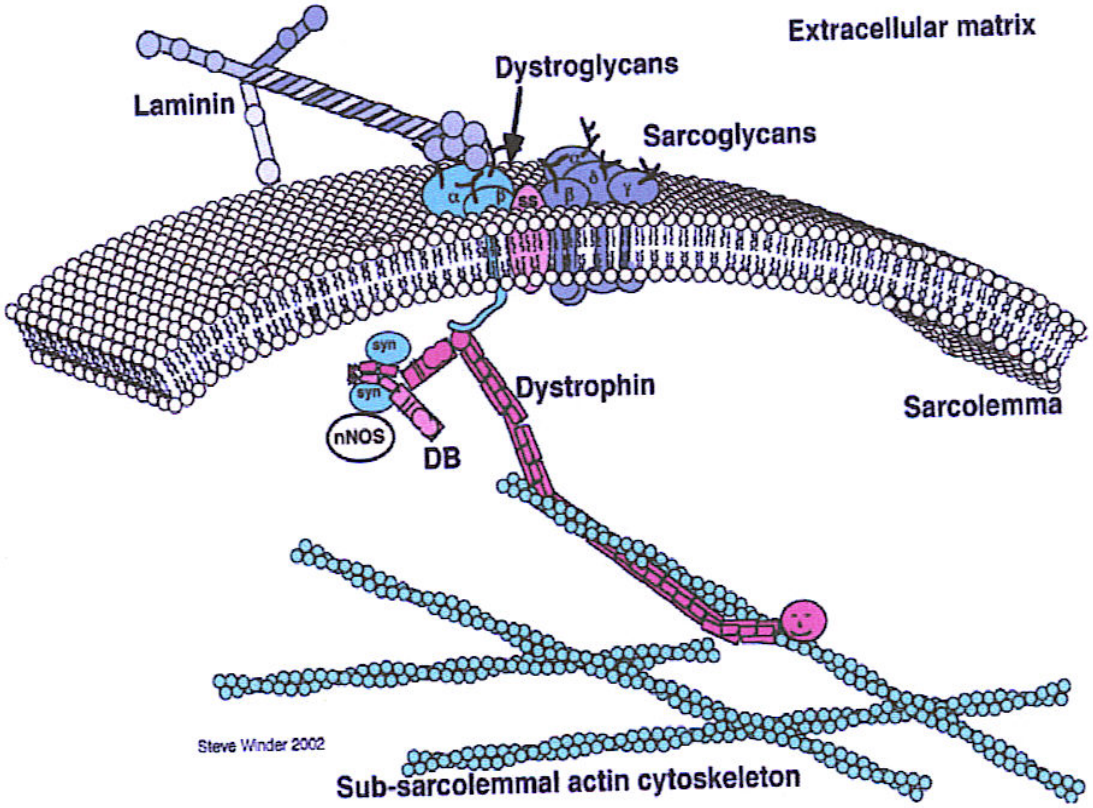


**Fig 1.3** The dystrophin-glycoprotein complex of skeletal muscle. The diagram shows the arrangement of DGC constituents in the sarcolemma and sub-sarcolemmal areas. Abbreviations: ss = sarcospan, DB= dystrobrevin, syn= syntrophin, nNOS= neuronal nitric oxide synthase.
(adapted from (Spence *et al.*, 2002))

A large central rod domain with 24 spectrin-like repeats follows this. The entirety of this domain appears not to be critical, as many mild Becker patients may have large in-frame deletions (for example from exon 17-48) that results in lengthy deletions in the rod domain (England *et al.*, 1990).

The WW region, which separates the rod from the cysteine-rich domain is involved in the interaction of dystrophin with β-dystroglycan, and is a motif found in proteins with signalling and regulatory functions. Next comes the cysteine rich domain containing sequences involved in calcium binding, and calmodulin binding in a calcium dependant manner. Deletions within the cysteine rich regions disrupt the interaction between dystrophin and the glycoprotein complex and leads to severe dystrophic pathology (Rafael *et al.*, 1996).

Coiled-coil regions forming the C-terminus bind dystrobrevin, and the alternatively spliced region binds syntrophin. The exact function of dystrobrevin and syntrophin have not been entirely elucidated, however there is evidence they have roles in cell signalling through their binding with neuronal nitric oxide synthase (nNOS), sodium channels and various kinases. Deletions of the extreme C-terminus and alternatively spliced region have no apparent effect on the function of dystrophin (Rafael *et al*., 1996).

Analysis of dystrophin-deficient *mdx* mice and DMD patients shows that critical mutations causes a loss of the DGC at the myocyte membrane and de-stabilisation of the whole complex, even though the DGC genes are still transcribed and translated (Ervasti *et al.*, 1990).

### 1.3.2 Evidence for a mechanical role for dystrophin

The characterisation of the DGC has provided considerable evidence for dystrophin acting as a link between the glycoprotein complex and the sub-sarcolemmal actin cytoskeleton. The linkage between the cytoskeleton and the extracellular matrix via dystroglycan is a likely mechanism for anchoring muscle cells, stabilising the membrane and protecting the sarcolemma from the stresses involved in muscle contraction (Campbell, 1995).

Dystrophin is localised to the sarcolemma at those areas of muscle under maximum longitudinally and radially transmitted stresses, and at the myotendinous junctions (Bonilla *et al.*, 1988); (Petrof, 1998a).

There is conflicting evidence whether dystrophic muscle is more susceptible to contraction induced injury using *in vivo* and *in vitro* methods. *Mdx* mice subject to markedly increased respiratory muscle workloads by tracheal banding did not show an expected increase in severe diaphragm pathology (Krupnick *et al.*, 2003). Limb muscles subject to eccentric contractions however, did show fibre damage, measured by fluorescent dye leakage (Petrof *et al.*, 1993a; Petrof, 1998a).

Leakage of muscle enzymes (pyruvate kinase and creatine kinase) into the serum occurs in *mdx* mice, DMD patients (and sometimes non-manifesting carriers) and occasionally BMD patients. *Mdx* muscle fibres also show an increased permeability to Evans Blue and Procion Orange, indicative of significant membrane lesions (Matsuda *et al.*, 1995).

### 1.3.3 Cell signalling role for dystrophin

The DGC is a multifunctional protein complex, and there are strong arguments that its primary role is transmembrane signalling (Rando, 2001). The mechanisms of cell death due to mutations of the DGC are related to cell survival pathways and cellular defence mechanisms regulated by those signalling cascades. Components of the DGC are not muscle specific, but are widespread, suggesting universal and vital functions.

There are numerous signalling molecules associated with the DGC, and the list continues to grow. They include calmodulin (which binds dystrophin and syntrophin), calmodulin-regulated kinases, Grb2 and nNOS. nNOS binds to syntrophin, which binds to dystrophin and α-dystrobrevin. The product of nNOS, nitric oxide (NO) has cell protective properties, including actions as a free radical, the induction of cGMP-dependant cell survival pathways and a local vasodilatory effect on vascular smooth muscle, resulting in less ischaemic injury to skeletal muscle cells. nNOS is absent in the sarcolemmal or cytoskeletal fractions of *mdx* mice (Brenman *et al.*, 1995b), however mice deficient in dystrophin and nNOS do not have an exacerbation of muscle pathology (Crosbie *et al.*, 1998);(Chao *et al.*, 1998).

Evidence from transgenic mouse studies expressing the Dp71 isoform further elucidates the role of dystrophin. This isoform restores the DGC at the cell

membrane, however a severe phenotype still results, suggesting that the N and C terminal domains are required for normal dystrophin function, including cell signalling (Cox *et al*., 1994).

### 1.3.4 Calcium homeostasis

Early studies showed increased deposits of calcium (demonstrated by alizarin red stain) in muscle biopsies of DMD patients (Bodensteiner and Engel, 1978). The processes of this calcium entry remain controversial. There is an increased activity of plasma membrane $Ca^{2+}$ channels in myotubes of DMD patients and the *mdx* mouse at a time when dystrophin is first expressed (Fong *et al.*, 1990), although other researchers could not verify these findings in the muscles of young mice (Head, 1993). Patch clamp studies demonstrated calcium entry through novel stretch inactivated ion channels in *mdx* myotubes, which could account for sufficient $Ca^{2+}$ influx to elevate intracellular $Ca^{2+}$ to pathological levels (Franco and Lansman, 1990). Recently new fluorescent techniques showed higher calcium in *mdx* myotubes and adult *mdx* fibres. These effects can be inhibited by the ion channel blockers nifedipine and amiloride(Hopf *et al.*, 1996; Tutdibi *et al.*, 1999).

While some researchers argue that calcium accumulation is secondary to the degenerative processes occurring in dystrophin-deficient muscle, and not an inherent property of it (McArdle *et al.*, 1995; Reeve *et al.*, 1997), there is growing evidence using patch clamp techniques that subsarcolemmal accumulation of calcium in *mdx* muscles is high enough to induce $Ca^{2+}$-induced-$K^+$ release upon depolarisation. In addition there is passive influx of $Ca^{2+}$ and an increased number of entry sites in dystrophic muscle (Mallouk and Allard, 2002; Mallouk *et al.*, 2000)

While it is unlikely that the DgC is an integral component of $Ca^{2+}$ channels itself, it could play a role in the proper organisation of such channels within the membrane, as well as the transmission of mechanical signals to channel gating mechanisms (Rando, 2001).

## 1.4 Pathophysiology of dystrophin deficient muscle

### 1.4.1 Initiation of necrosis

Cell death in dystrophic muscle is not inevitable, but reflects a propensity that varies between muscles, changes with age and differs between species. Many characteristics of dystrophic muscle are stereotypic for necrotic processes, including raised intracellular $Ca^{2+}$, increased volume of the sarcoplasmic reticulum, abnormal morphology of mitochondria and inflammation (Bulfield *et al*., 1984; Anderson *et al.*, 1988); (Cullen M.J. and Jaros, 1988); (Stedman *et al.*, 1991). The initiating event in the dystrophic process remains contentious, with arguments for and against elevated $Ca^{2+}$, membrane damage or apoptosis acting as triggers (Tidball *et al.*, 1995).

There appears to be no close connection between mechanical loading and cell death, with one study showing decreased degeneration in the limb muscles of exercised *mdx* mice (Dupont-Versteegden *et al.*, 1994b), while another contrasting study employing immobilisation of *mdx* hind limbs by splinting also resulted in a significant reduction in degeneration (Mokhtarian *et al.*, 1999). Recent cardiac studies showed that mechanical stress such as exercise or aortic banding was necessary to cause significant heart pathology (Danialou *et al.*, 2001b; Nakamura *et al.*, 2002).

Myonuclear studies demonstrating fragmented double stranded DNA, and abnormal chromatin in *mdx* muscles lends weight to a primary apoptotic process followed by necrosis (Tidball *et al.*, 1995). This scenario does not rule out the role of high intracellular $Ca^{2+}$, as raised calcium is a common occurrence in well-documented models of apoptosis (Cohen and Duke, 1984). High $Ca^{2+}$ can cause necrosis, but may also be an initiator of apoptosis (Tidball *et al*., 1995).

### 1.4.2 Downstream events

The abnormally high $Ca^{2+}$ content of dystrophic muscle activates calcium dependant proteases (especially calpains) that cause widespread proteolysis (Turner *et al.*, 1988; Turner *et al.*, 1993). Proteases can themselves modify calcium leak channels, thus a vicious cycle of disorded calcium homeostasis ensues (Alderton and Steinhardt, 2000). Mitochondrial overload occurs also, with the result being a

reduction in oxidative phosphorylation and eventual cell death. Additional mechanisms play a role in the pathogenesis of DMD, including defective glucose utilisation, a blunted vascular response to exercise, increased susceptibility to cytokines and oxidative stress, and aberrant cell signalling (Rando *et al.*, 1998; Thomas *et al.*, 1998; Heydemann and McNally, 2004). A schematic representation of the patho-physiological sequences in dystrophic muscle is shown in Figure 1.4.

### 1.4.3 Myocyte regeneration and fibrosis

Normal muscle is post-mitotic, but is capable of regenerating due largely to the proliferation of a population of mononuclear muscle precursor cells (satellite cells) within the basement membrane of fibres (Ferrari *et al.*, 1998). In dystrophic muscle, regeneration fails to keep up with necrosis, so that atrophy eventually results. DMD muscle precursor cells in culture show fewer replications than age matched controls, thought to be due to shortened telomere lengths from prior replication cycles *in vivo* (Decary *et al.*, 2000). There may also be a role for insulin-like growth factor 1, as mice over-expressing this cytokine show decreased myonecrosis, improved muscle regeneration and protection against apoptosis (Barton *et al.*, 2002).

Chronic accumulation of fibrous tissue is a hallmark of dystrophy in both boys with DMD and the *mdx* mouse. Studies have demonstrated the role of T lymphocytes in this process, particularly in the diaphragm (Morrison *et al.*, 2000). Transforming growth factor-β1 has also been mooted as a mediator of fibrosis in DMD (Bernasconi *et al.*, 1999) and the canine model of DMD (Passerini *et al.*, 2002).

### 1.4.4 Gene expression

In recent years there has been interest in screening muscle cDNA arrays from DMD patients. Upregulation of 4 mitochondrial mRNA transcripts were found in one study, despite diminished mitochondrial enzyme activity. This upregulation of mRNA in response to low protein levels may be a short-term compensatory response, or due to oxidative damage, which is particularly important in mitochondrial compartments (Tkatchenko *et al.*, 2001). Titin mRNA was markedly downregulated in this study, which, given titin's role in muscle fibre elasticity and

formation of thick filaments, could contribute to sarcomere disorganisation and myofibril fragility during contractions. Another study found 80 downregulated genes, 36% of which were mitochondrial genes, while 12% involved cell signalling or cell growth and differentiation. The largest group of upregulated genes were developmentally regulated genes such as cardiac α-actin, embryonic myosin heavy chain, acetylcholine receptors and others (Chen *et al.*, 2000). Noguchi and coworkers were the first to highlight differences between individual DMD patients at a molecular level, noting differences in gene expression for HLA-related proteins, myosin light chains and troponin T (Noguchi *et al.*, 2003). Temporal gene expression studies from *mdx* diaphragms provided evidence that secondary factors are important in dystrophies, with coordinated increases of many cytokines, chemokines, leucocyte adhesion factors and complement system activators (Porter *et al.*, 2002)

The multitudinous complex pathways involved in the progression of DMD pathology still require extensive unravelling. Debates over initiating events, exacerbating factors, the relative importance of cell signalling pathways, up- or downregulated genes, and oxidative damage are ongoing. Far from being solely academic arguments, the elucidation of these hierarchical or causal relationships will go a long way to influence the development and targeting of future therapies. It is likely that further gene expression profiling will facilitate this process. The lack of inevitability of early and widespread necrosis in all models of dystrophy means novel pharmaco- or genetic therapies could have an eventual role in modifying severe dystrophic phenotypes by controlling downstream events.

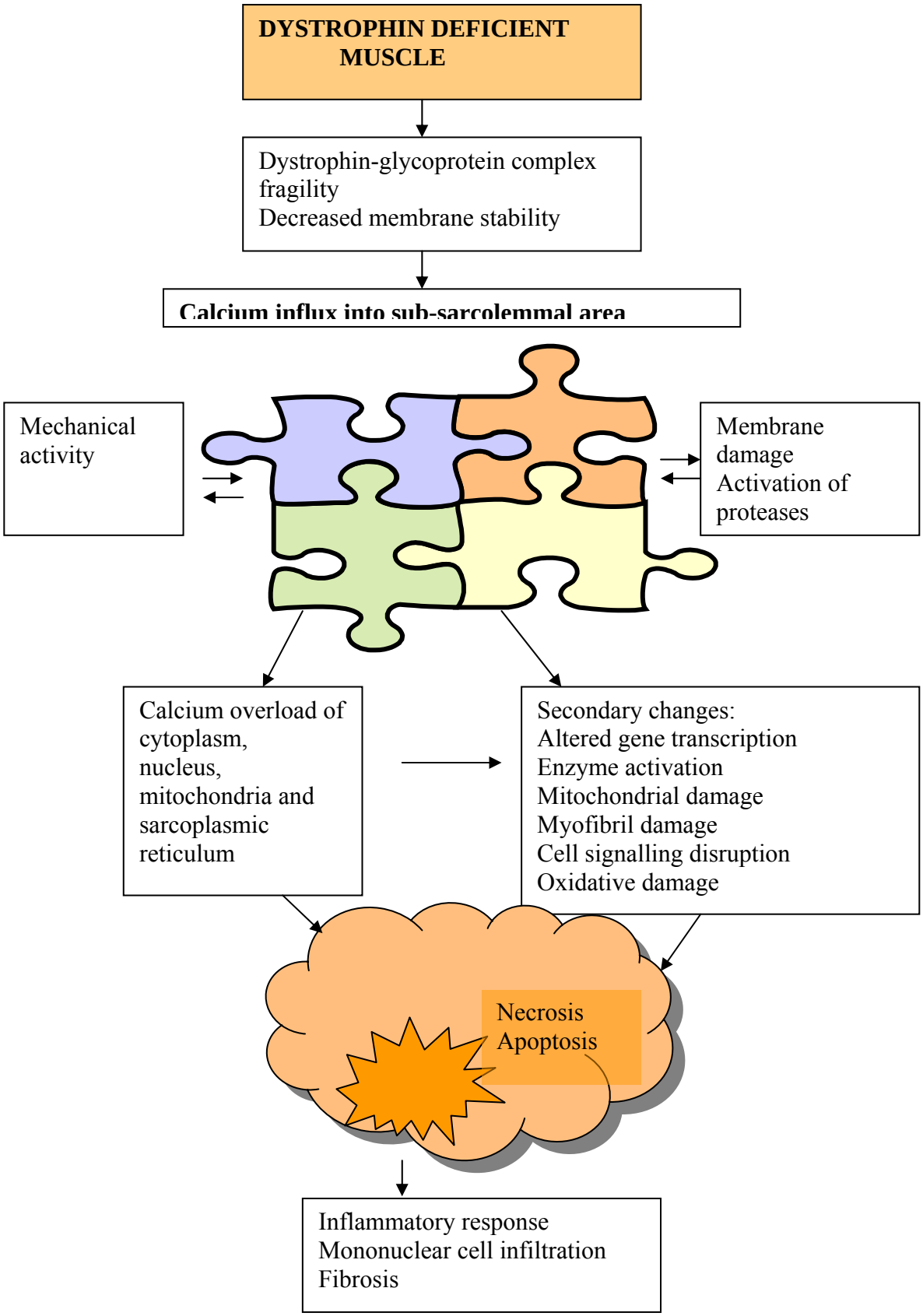


Fig 1.4 Pathophysiological processes occurring in muscle lacking dystrophin

## 1.5 Dystrophin deficiency in species other than man

### 1.5.1 Range of animal models for DMD

There are a number of naturally occurring dystrophin deficient animal species, and many more transgenic models. The most widely used is the muscular dystrophy X-linked mouse (*mdx*), discovered in a colony of C57Bl/10ScSn mice in Scotland when screening the colony for the serum enzymes pyruvate kinase and creatine kinase (Bulfield *et al*., 1984). The canine model for DMD, the Golden Retriever Muscular Dystrophy dog (GRMD) was recorded a few years later (Kornegay *et al.*, 1988). The first dystrophin-deficient cats were shown to have remarkable muscle hypertrophy and histological features of necrosis and regeneration, but not fibrosis (Carpenter *et al.*, 1989). These 3 species will be discussed in greater detail below.

There are a variety of other models including the dystrophic chicken (Dawson, 1966), sheep (Paulson *et al.*, 1966), cow (Poukka, 1966), zebrafish, *Danio reio*, (Chambers *et al.*, 2001; Bolanos-Jimenez *et al.*, 2001; Lu *et al.*, 2003), and nematode, *Caenorrhabditis elegans*, (Mariol and Segalat, 2001). The use of these models is not widespread, due largely to their phenotypic or genetic dissimilarity to DMD.

### 1.5.2 Hypertrophic Feline Muscular Dystrophy cat

The first description of X-linked muscular dystrophy in cats was of two male littermates at 23 months of age (Carpenter *et al*., 1989). Both animals showed pronounced hypertrophy of tongue, neck, trunk, limbs and diaphragm, hypertrophic cardiomyopathy and evidence of muscle fibre necrosis on histological examination. Two domestic shorthair cats with stiff gaits, salivation and lingual hypertrophy were diagnosed with muscular dystrophy based on severe histopathological changes in their skeletal muscles (myocyte hypertrophy, splitting of fibres and calcium deposition) and absence of dystrophin, and were subsequently used to establish a colony of HFMD cats at the University of Berne, Switzerland (Gaschen *et al.*, 1992). Their muscle hypertrophy is a true hypertrophy (rather than pseudohypertrophy as seen in DMD), there is little muscle weakness and, with the exception of diaphragm muscles in older animals (6-9 months of age), they tend not to develop endo- or perimysial fibrosis. The genetic lesion is a deletion of the

muscle and Purkinje promoter (Winand *et al.*, 1994). This tends to be a lethal genetic defect due to secondary complications such as megaoesaphagus (due to constriction by the hypertrophic diaphragm), failure to eat or drink, and renal failure (Gaschen *et al*., 1992). Figure 1.5 shows examples of histopathological and clinical features of FHMD.

### 1.5.3 Golden Retriever Muscular Dystrophy dog

The GRMD dog has been recognised as an excellent model for research into DMD for several decades, and there are now colonies established throughout the world, including the United States, Japan, France and Italy. Like DMD, affected animals show muscle weakness, elevated serum creatine kinase levels, features of multifocal muscle fibre necrosis and regeneration as well as significant fibrosis with contracture (Figure 1.5). Electron microscopy showed disruption of myofibrillar architecture, particularly in the subsarcolemma, and increased numbers and size of mitochondria (Kornegay *et al*., 1988).

The genetic defect is a splice site mutation in Exon 6, leading to deletion of Exon 7 (Fletcher *et al.*, 2001). Interestingly, although no dystrophin is detected by immunohistochemical methods, GRMD dogs may show low level, widespread dystrophin using Western blotting. This suggests that some dogs may use a mechanism of alternative processing of mRNA to overcome their mutation to produce truncated, but functional dystrophin (Schatzberg *et al.*, 1998). This hypothesis could explain the variation in clinical severity noted even within litters (Cooper *et al.*, 1988);(Nguyen *et al.*, 2002), and possibly some boys with DMD where low level dystrophin is also present (Nicholson, 1993).

GRMD dogs develop dilated cardiomyopathy. Echocardiographic studies show reduced fractional shortening and left ejection fractions, and marked left ventricular free wall dysfunction (Chetboul *et al.*, 2004).

There are a number of reported therapy trials using the GRMD dog, including prednisolone studies (Liu *et al.*, 2004), adenoviral vectors expressing utrophin (Cerletti *et al.*, 2003), chimeric oligonucleotide injections (Bartlett *et al.*, 2000); (Fletcher et al., 2001) and haemopoietic stem cell studies (Dell'Agnola *et al.*, 2004). The value of the GRMD model of DMD will become increasingly evident in

future years as research into promising new therapies hurry towards Stage 1 clinical trials.

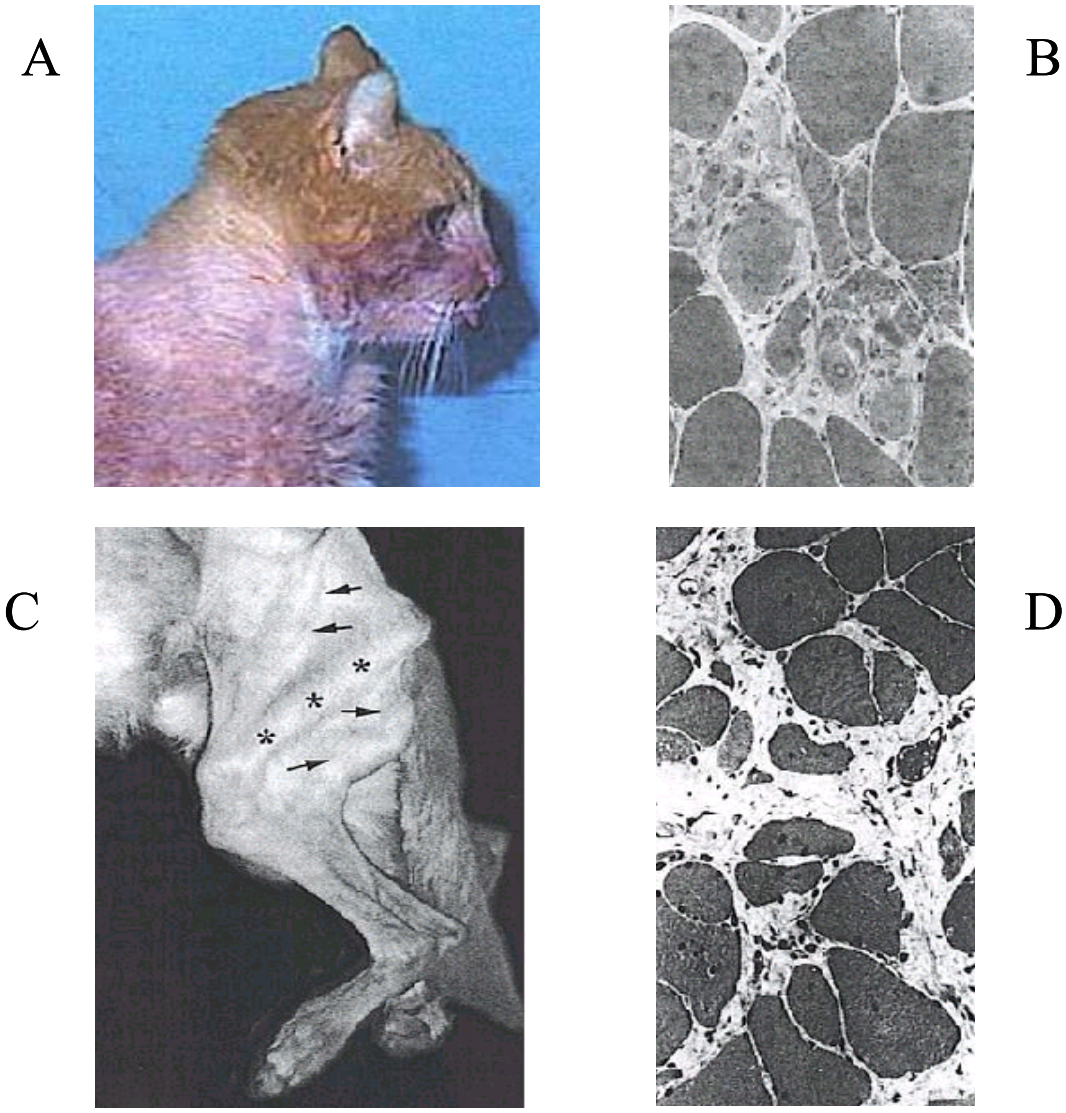


**Fig 1.5** Feline and canine muscular dystrophy

A: Feline hypertrophic muscular dystrophy (FHMD) cat, showing muscle hypertrophy and stiffness of head and neck muscles, failure to groom and tongue protrusion. B: Histology of FHMD animals shows regeneration with central nuclei.

C. Golden Retriever Muscular Dystrophy (GRMD), with pronounced quadriceps and biceps femoris atrophy. In contrast the semimembranosus, semitendinosis and cranial sartorius muscles are spared (arrows).* denotes femur D. The histological features tend to be more severe than FHMD, with endomysial and perimyseal fibrosis prominent. (From A.(Shelton, 1999), B (Carpenter et al., 1989), C:(Kornegay *et al.*, 2003), (Kornegay et al., 1988))

### 1.5.4 The *mdx* mouse

#### 1.5.4 i The natural history of the *mdx*

It is now realised that the *mdx* progresses through distinct stages throughout its lifespan, and demonstrates varying degrees of skeletal muscle pathology and cardiomyopathy depending on age and muscle type (Fig 1.6). These stages impact on research into the pathophysiology of DMD, and the timing of therapies targeting dystrophic muscle.

#### 1.5.4ii Skeletal muscle necrosis

*Mdx* muscles exhibit early necrosis from day 5 after birth, but only in muscles of the head, trunk and girdle. There is an onset of limb muscle degeneration around 2 weeks, with a peak between weeks 5 and 8 weeks (Coulton *et al.*, 1988) or 3 weeks (Grounds and Torrisi, 2004). The number of centrally nucleated fibres increases progressively to reach 50% of all fibres by 2 months and 90% by 3 months as the muscle regenerates. A very high centrally-nucleated fibre count is not general, however, and some muscles such as the diaphragm have a much lower count (Gillis, 1999). Although split fibres are not uncommon in the *mdx*, the presence of connective or adipose tissue is not prominent in mice up to 52 weeks of age (Pastoret and Sebille, 1995b). That study found that histologically degenerating fibres were seen until 104 weeks of age, and in these older mice large areas of muscles were comprised of atrophied fibres surrounded by fibrosis. Evidence of regeneration was rare after 90 weeks.

This evidence of cycles of chronic degeneration of *mdx* muscles is supported by the continual leak of cytosolic enzymes throughout life (Bulfield *et al*., 1984; Coulton *et al*., 1988) and the high protein turnover observed in adult animals (MacLennan and Edwards, 1990).

Some muscles are more selectively affected by dystrophinopathy, especially the diaphragm (Stedman *et al.*, 1991) and postural muscles such as the soleus, intercostals and paraspinals (Lefaucheur *et al.*, 1995). There appears to be a relative sparing of small fast twitch muscles (Lefaucheur *et al*., 1995), and extraocular muscles (Porter *et al.*, 1998).

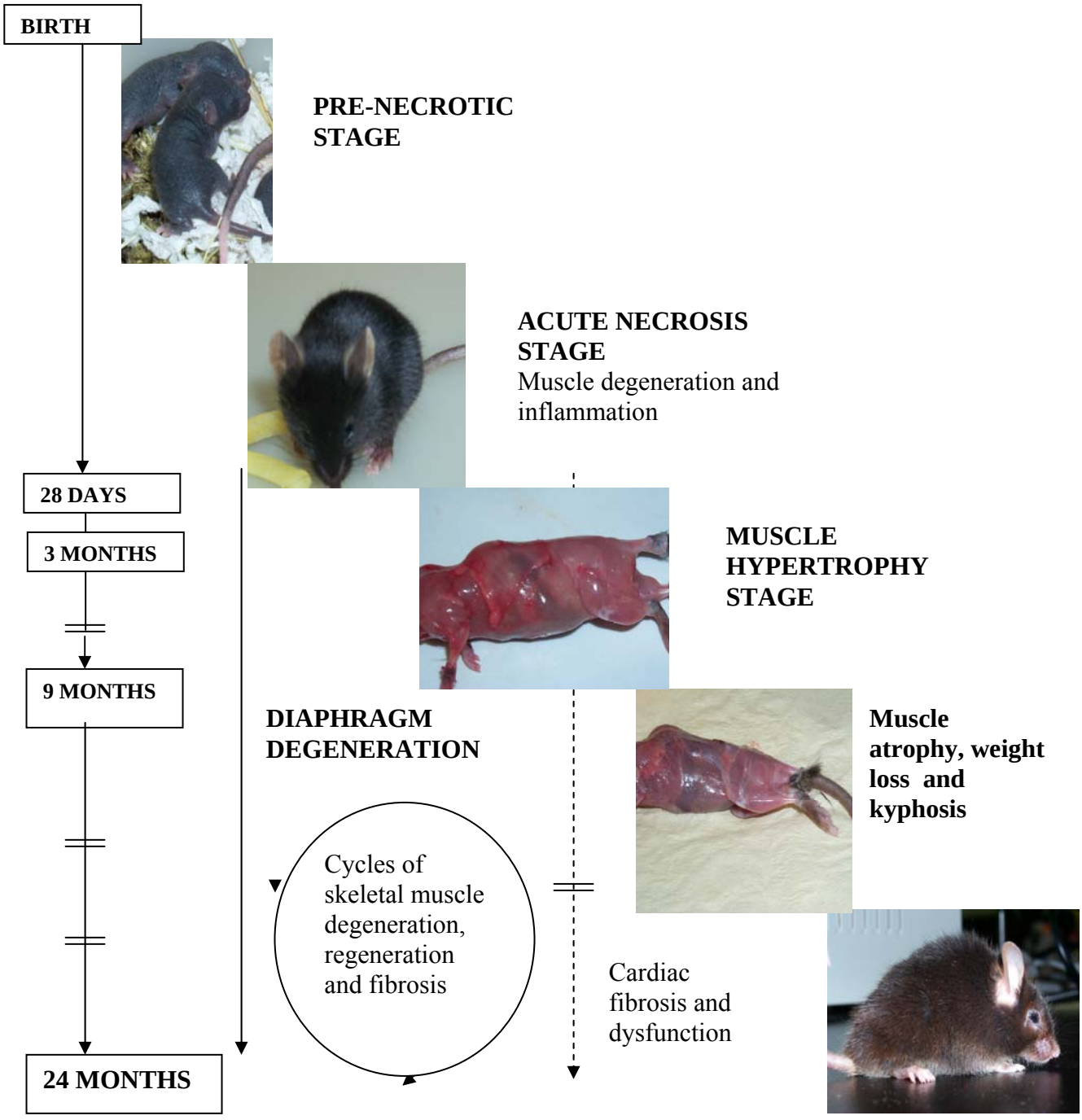


**Fig 1.6** The natural history of the *mdx* mouse.

The dystrophin-deficient mouse model of DMD undergoes various stages throughout its life, including an acute necrotic period at weaning age, muscular hypertrophy between approximately 5-12 months and weight loss and skeletal muscle atrophy between approximately 15-24 months. Diaphragm degeneration is most pronounced, and begins early in life. *Mdx* mice do not display overt heart failure, but cardiac fibrosis increases and heart function declines with age.

1.5.4iii Muscle hypertrophy in the *mdx*

Generalised muscular hypertrophy peaks between 6 and 12 months, then regresses to the point where 18 month old mice show atrophy (Pastoret and Sebille, 1995b). Muscle hypertrophy can be due to fibre hypertrophy, hyperplasia (fibre neosynthesis) or connective tissue proliferation, although none of these theories alone explain the increase in muscle weight or cross-sectional area in the adult *mdx* (De La Porte *et al.*, 1999). Compensatory hypertrophy may occur due to viable fibres contracting synergistically against fibres damaged by the dystrophic process, with observations that the extensor digitorum longus (EDL) and soleus muscles sustain a hypertrophy of 17% and 22% greater respectively than control mice (Lynch *et al.*, 2001). Although various authors state that adult *mdx* muscles are 'bigger and stronger' than age matched C57 muscles (Coulton *et al*., 1988; Partridge, 1997; Pastoret and Sebille, 1995a; Pastoret and Sebille, 1995b; Bobet *et al.*, 1998), when forces are normalised for weight and cross-sectional area, the forces generated are actually less (Lynch *et al*., 2001).

1.5.4 iv The *mdx* diaphragm: the 'gold standard'

Of the skeletal muscles studied in the *mdx* mouse, only the diaphragm exhibits marked and progressive degeneration, fibrosis and functional deficits commensurate with limb muscles of boys with DMD (Stedman *et al*., 1991; Lynch *et al.*, 1997; Lefaucheur *et al*., 1995; Anderson *et al.*, 1998; Coirault *et al.*, 1999). One study found that impaired diaphragm strength was associated with qualitative and quantitative changes in myosin molecular motors that are responsible for generating force, and consequently reduced force per contractile element (cross bridge) contributes to weakness (Coirault *et al.,* 1999). There is also a regional difference in pathology supportive of contraction-induced injury, oxidative damage and muscle use, with those that work harder showing more severe disease, at least in the mouse (Anderson *et al.,* 1998).

1.5.4v Cardiomyopathy in the *mdx*

Data concerning the dystrophic involvement of *mdx* cardiac muscle is both limited and conflicting. There is evidence for substantial cardiac muscle necrosis found in some studies (Lefaucheur *et al*., 1995; Bridges, 1986), but not others

(Torres and Duchen, 1987). Lefaucher *et al* 1995 found foci of inflammation and advanced fibrosis in older (at least 20 months) *mdx* hearts.

Cardiac functional studies lend weight to significant heart pathology, including altered contractility and half relaxation times, and response to exogenous calcium in 12 week old mice (Sapp *et al.*, 1996), and electrocardiographic changes (Chu *et al.*, 2002; Bia *et al.*, 1999). There are also age and sex related differences in cardiac β-adrenoceptors (measured by sensitivity to drugs that either stimulate or block these receptors) between 3 month *mdx* compared to C57 (Lu and Hoey, 2000). Altered action potentials are evidence of changes in membrane ion channels (Pacioretty *et al.*, 1992), and *mdx* animals were found to have a significantly higher intracellular calcium concentration in ventricular cells, suggesting a defective control of calcium may have a role in electrophysiological and contractile properties of cardiomyocytes, as well as a noxious effects on cellular integrity (Alloatti *et al.*, 1995).

Echocardiography of *mdx* hearts demonstrated significant differences in heart rate and left ventricular dimensions from control mice after 40 weeks of age, but not earlier. Fibrosis was seen as a late consequence of dystrophin deficiency (Quinlan *et al*., 2004).

### 1.5.4vi Genetic mutation in the *mdx*

The molecular basis of the disorder in *mdx* mice is a point mutation causing a frameshift and a premature stop codon in exon 23 of the dystrophin gene (3185C>T) (Sicinski *et al.*, 1989). Despite this termination codon, approximately 1% of *mdx* fibres show the presence of dystrophin (so called 'revertant fibres'), possibly as a result of an exon skipping mechanism that restores the in-frame reading of the gene (Wilton *et al.*, 1997a).

More recently mice have been generated with point mutations or deletions in various parts of the dystrophin gene, to aid further understanding of critical functional domains of dystrophin (Im *et al.*, 1996).

### 1.5.4 vii Shortcomings and strengths of the *mdx* model

Researchers have questioned the validity of the *mdx* as a model for human disease, due to the apparent milder phenotype, evidence of skeletal muscle

regeneration, and lack of significant widespread fibrosis and fatty changes following muscle necrosis. It is said to be a better model for regenerative myopathy than degenerative processes. However, it remains the most readily available and economic model for research into DMD.

Dystrophinopathies show a lack of correspondence between phenotype and genotype. As commented by (Partridge, 1991), the ability of dystrophin-deficient animal models, such as the *mdx* mouse, to maintain a considerable muscle mass with a large resistance to pathogenesis offers 'a considerable experimental asset, for it must be accommodated by any coherent theory of pathogenesis of dystrophin deficiency'.

Gene knockouts based on the *mdx* background are useful for loss-of-function or gain-of-function studies. Various transgenic strains, again on the *mdx* background, provide useful insights into the pathogenesis of the disease. The *mdx* mouse is proving to be a useful model for screening compounds for potential treatment of DMD patients. Compounds considered to be showing a positive effect in the *mdx* mouse are being considered for clinical trials.

There is increasing recognition of the importance of cardiomyopathy in DMD, and also recently in *mdx* mice. Like boys with DMD, mice show skeletal muscle degeneration and fibrosis before the onset of significant heart disease, which does not occur until much later in the lifespan. The gradual onset of cardiomyopathy, as well as inherent dysfunction in cardiomyocyte calcium handling, makes it a valid model of DMD cardiomyopathy.

New gene correction therapies will require extensive testing prior to clinical trials, including optimisation of dose, delivery methods and determination of transduction efficiency and safety. The short generation time and lifespan of the *mdx* mouse, as well as its close genetic homology to a large percentage of DMD patients, makes it the ideal model for these studies.

## 1.6 Drug therapy for Duchenne Muscular Dystrophy

There is no cure for DMD, and current palliative therapies are centred on long-term corticosteroid administration (prednisolone or deflazacort), and drugs aimed at treating or alleviating heart failure or respiratory tract complications. The following section reviews current therapy options and research into new treatment modalities.

### 1.6.1 Glucocorticoids

Following almost two decades of use in patients with DMD, it is clear that glucocorticoids can provide short-term functional improvements such as increased muscle strength and prolonged ambulation (Wong and Christopher, 2002).

The precise mechanisms by which glucocorticoids benefit dystrophic muscle are unclear. The possible mechanisms include a benefit to myogenesis (Passaquin *et al.*, 1993); (Anderson *et al.*, 1996), increased muscle mass due to anabolic effects (Rifai *et al.*, 1995), reduction in apoptosis (Lim *et al.*, 2004), stabilisation of the sarcolemma (Jacobs *et al.*, 1996), regulation of intracellular calcium (Metzinger *et al.*, 1995) and possibly immunosuppressive actions due to a reduction of mononuclear cells, although the latter is controversial (Kissel *et al.*, 1993). Gene profiling of *mdx* suggested that genes involved in the immune response are down-regulated, while structural protein genes were up-regulated after treatment with prednisolone (Muntoni *et al.*, 2002).

The systemic effects of steroids are problematic, with a proportion of boys unable to continue treatment due to weight gain, mood swings and cataract development. These changes were found to be significantly less with the oxazolone derivative of prednisolone, deflazacort (Biggar *et al.*, 2001). Boys treated with deflazacort or prednisiolone can walk significantly longer, have improved cardiac and respiratory function and delayed timing for scoliosis surgery (Biggar *et al.*, 2001; Silversides *et al.*, 2003). The mechanisms are again unknown, but *in vit*ro this agent has shown to augment expression of the membrane stabiliser laminin and satellite cell activity and muscle repair (Biggar *et al.*, 2002). Deflazacort is unavailable in some Western countries, such as the United States and Australia, due to legislation restrictions. Moreover, there is no international consensus on the best

dose rates for either glucocorticoid, or optimum age at which treatment should commence.

### 1.6.2 Creatine monohydrate

Phosphocreatine is an important source of quick energy production in muscle, particularly those used for sprinting. Creatine monohydrate is used as a nutritional supplement by athletes, and has shown promise for the treatment of people with neuromuscular disorders. Its beneficial effects are attributed to antioxidant properties, reduction of protein breakdown and enhancement of sarcoplasmic reticulum calcium uptake. In *mdx* mice administered creatinine from a young age, the first wave of acute muscle necrosis was markedly reduced in the extensor digitorum longus (fast twitch muscle), but not the soleus (slow twitch muscle) (Passaquin *et al.*, 2002). Creatine supplementation in DMD patients is more controversial. A four-month trial on boys with DMD showed increased handgrip strength and an increased fat free mass (Tarnopolsky *et al.*, 2004). Another trial provided evidence of increased resistance to fatigue, and improved maximal voluntary contractions of patients (Louis *et al.*, 2003). However a double blind, cross-over trial showed no improvement in quantitative strength tests (Walter *et al*, 2002). Creatine monohydrate is still commonly used as a supplement for boys with DMD.

### 1.6.3 Alternative pharmacological agents

Although gene therapy will likely provide the cure for DMD, success still remains on the distant horizon. In the meantime there is emphasis on developing therapies that alleviate the deleterious consequences of dystrophin deficiency such as muscle necrosis, inflammation and scarring. With a better understanding of the complex pathophysiology of dystrophic muscle and appreciation of downstream events, comes research into new agents such as anti-tumour necrosis factor α, (Remicade®), myostatin blocking agents and others.

Table 1.1 lists current or recently completed clinical trials studying alternative pharmaceutical agents, and Table 1.2 lists some recent drug studies in the *mdx* mouse model of DMD.

**Table 1.1 Clinical trials into alternative drug treatments of DMD**

| Therapeutic agent | Mechanism of action | Benefit or adverse effect | Reference |
|---|---|---|---|
| Albuterol | β-agonist Inhibits proteolysis | Improved muscle strength | (Fowler *et al.*, 2004) |
| Oxandrolone | Anabolic pathways | Increased strength or no benefit | (Fenichel *et al.*, 1997) (Fenichel *et al.*, 2001) |
| Growth Hormone | Anabolic pathways | Improved cardiac function, no effect on muscle strength | (Cittadini *et al.*, 2003) |
| Coenzyme Q | Antioxidant, increased respiratory chain activity | Trials ongoing | http://www.mdausa.org |
| Glutamine and creatine | Modulators of inflammation | No effect on muscle strength | http://www.mdausa.org |

**Table 1.2 Studies into novel therapeutic agents in the *mdx* mouse**

| Therapeutic agent | Mechanism of action | Benefit or adverse effect | Reference |
|---|---|---|---|
| Insulin like Growth Factor (IGF-I) | Anabolic and satellite cell proliferation | Improved contractilty | (Gregorevic *et al.*, 2002) |
| Remicade® | Anti-tumour necrosis factor (TNF α) | Marked protection against acute muscle breakdown | (Grounds and Torrisi, 2004) |
| L-Arginine | Increased NO production by NOS | Upregulation of utrophin at sarcolemma? | (Chaubourt *et al.*, 2002) |
| Anti-myostatin | Antibodies block myostatin action | Hypertrophy and decreased muscle breakdown | (Bogdanovich *et al.*, 2002) |
| Heregulin | Regulates utrophin promoter | Resistance to muscle damage, decreased muscle pathology | (Krag *et al.*, 2004) |
| Leukaemia Inhibitory Factor | Increased myocyte growth and proliferation | Muscle hypertrophy, less degeneration | (White *et al.*, 2001; Austin *et al.*, 2000) |

## 1.7 Gene therapy for Duchenne Muscular Dystrophy

### 1.7.1 Dystrophin expression cassettes

The muscle isoform of dystrophin is encoded on a 14kb mRNA, which is considerably shorter than full-length dystrophin, and effective at preventing dystrophy in *mdx* mice (Cox *et al.*, 1993). It is important that gene regulatory regions are included in dystrophin expression cassettes, including the muscle creatine kinase gene, a polyadenylation signal and an intron.

Despite their reduced size, these cassettes are still too large to fit in most vectors, so much research has focussed on developing mini- or micro dystrophin (*dys*) genes, omitting non essential areas of the gene such as the central rod region and the C-terminal. Micro-*dys* with less than 3 spectrin-like repeats show little function, however clones with 4 or more repeats show normal function (Sakamoto *et al.*, 2002). Successful mini-*dys* transfer encoded by recombinant plasmid DNA has been performed in *mdx* diaphragms and hind limb muscles (Decrouy *et al.*, 1997), showing some protection of injury to muscle fibres.

### 1.7.2 Vectors for gene delivery

The four classes of vectors of most interest in DMD research are adenoviruses (Ad), adeno-associated viruses (AAV), retroviruses and plasmids, although recently equine infectious anaemia lenti-virus has also been utilised for *in-utero* gene delivery (Gregory *et al.*, 2004).

Conventional Ad vectors suffer the limitation of giving rise to transient expression of recombinant genes, with levels declining by 1 week and usually undetectable by 4 weeks. There appears to be recruitment of immune cells (cytotoxic T cells) marking virus-infected cells for destruction (Yang *et al.*, 1995). Improved adenoviruses, the so-called gutted adenoviruses, have emerged and show less immunogenecity, with greater capacity for larger therapeutic genes such as dystrophin (Allamand and Campbell, 2000); (Matecki *et al.*, 2004). Muscle gene therapy utilising Ad vectors will likely require repeat delivery to be effective. Recent reports of intravascular delivery of Ad mediated reporter genes to *mdx* muscles also show promise for the future (Cho *et al.*, 2000).

Retroviral vectors are limited to carrying mini- or micro-*dys*. They are difficult to grow in large quantities, however they are capable of being readily

incorporated into the host genome, potentially allowing persistent gene transfer (VandenDriessche *et al.*, 2002).

Adeno-associated vectors (AAV) are capable of integration into muscle cells and may persist for years (Xiao *et al.*, 2000). It is theoretically possible to administer these agents, then provide booster doses to maintain high levels of expression. They can accommodate only 4.8kb of exogenous sequence (Flotte *et al.*, 1995).

Widespread muscle-specific expression of functional micro-dystrophin in *mdx* was acheieved using vasculature permeabilising agents and delivery via AAV pseudotype 6 vectors, with such methods applicable to a variety of genes in addition to dystrophin (Gregorivic *et al*, 2004).

Naked plasmid DNA shows a remarkable ability to transfer genes to muscle. Plasmids have the advantages of minimal immunogenecity and toxicity, and a large cloning capacity. They should overcome most viral-vector mediated problems, and may be safer. A drawback is their low transfection efficiency when administered by intramuscular injection. Advances in electroporation technology will potentially assist in high level or long lasting gene expression using this method, at least in animal models (Vicat *et al.*, 2000; Murakami *et al.*, 2003). Pre-treatment of muscles with bovine hyaluronidase prior to electroporation greatly enhances transfection (McMahon *et al.*, 2001). Intravascular delivery of these agents also shows potential (Liu *et al.*, 2001a); (Zhang *et al.*, 2004).

Retention of plasmids may be a limitation, and they will either require repeat administration (as for Ad‘s) or modification to enable better integration and persistence.

### 1.7.3 Cardiovascular gene therapy

There have been few studies examining gene transfer into dystrophic cardiac muscle. The challenges for successful gene therapy of cardiac tissue include safe and effective delivery, duration of transgene expression, safety of the vector and the intrinsic properties of cardiac cells. Cardiomyocytes replicate very slowly, and because of their syncytial nature transfection will likely be limited to the immediate vicinity, rather than dispersed via a long length of fibre as occurs in skeletal muscle. Foetal or neonatal administration of genes in mice offers provide evidence of the

potential for treatment of patients at a young age (Gregory *et al*., 2004). AAV mediated micro-*dys* persisted for 10 months post injection. A recent study indicated that dystrophin expression in 50% of heart cells of *mdx* mice would be sufficient to treat cardiomyopathy (Yue *et al*., 2004).

### 1.7.4 Clinical trials into gene therapy for DMD

There are two landmark clinical trials currently underway, or close to commencement.

The first study in France included a completed Stage I trial using intravenous administration of a large number of plasmids containing dystrophin cDNA into the forearms of patients. It has proved to be safe, but dystrophin expression was of the order of 1-10% of myocytes. In the second phase of the trial with Duchenne patients, it is planned to inject large volumes of the naked DNA into the forearm (Thioudellet *et al.*, 2002; Scheuerbrandt, 2004). At present transfection levels are too low to draw conclusions of the validity of these methods.

The second trial, supported by the Muscular Dystrophy Association of America, uses a modified AAV of serotype 2, called AAV 2.5. It contains a mini-*dys* construct, lacking the rod regions R3-R21, and C-terminal end, making it one third as long as normal dystrophin (Wang *et al.*, 2000). A Phase I/II trial will commence in late 2005 after toxicity and biodistribution studies are completed. The trials will involve 6 boys with DMD, older than 10 years. Placebo or vector injections will be administered into biceps muscles, with muscle strength testing and biopsies performed 6 weeks later (Scheuerbrandt, 2004).

## 1.8 *Ex vivo* strategies using myoblasts or stem cells

### 1.8.1 Myoblast transplantation

The basic tenet of myoblast transfer is that its benefit would arise from a generation of significant amounts of donor muscle containing normal dystrophin, and the long-term survival of these donor muscle fibres within the patient's muscles (Partridge *et al.*, 1998). Early trials on myoblast (immature muscle cell) transfer into dystrophic mouse muscles showed some functional benefit in protecting adjacent fibres against necrosis, however effects were limited to a small region surrounding the injection site and there was evidence of immunological rejection of implanted cells (Partridge, 2002). Immunosuppressive drugs can improve therapeutic

outcomes, but may have significant side effects. Autologous myoblast transplantation could overcome rejection problems (Floyd *et al.*, 1998); (Moisset *et al.*, 1998), however myocytes from patients with DMD are not characteristically prolific in cell culture and may not be suitable for this approach.

A family of genes including myoD has been identified that converts non-muscle cells (eg fibroblasts) into muscle cells, and these may provide new sources of cells for gene therapy applications (Weintraub *et al.*, 1989). There are also problems with cell survival that need addressing, however studies examining manipulation of telomerase expression may expand the replicative lifespan of myoblasts from normal and DMD patients (Biggar *et al*., 2002).

### 1.8.2 Stem cell therapy

New approaches involve stem cell recruitment via bone marrow transplantation techniques (Gussoni *et al.*, 1999), or intra-arterial administration into *mdx* limbs (Torrente *et al.*, 2001). Transplantation of myogenic progenitor cells into immunosupressed mice show that they can migrate to necrotic muscle and participate in its regeneration (Ferrari and Mavilio, 2002). Low efficacy of current stem cell approaches will require development of new strategies for expansion and active recruitment to myogenic differentiation.

## 1.9 Strategies to upregulate utrophin

Utrophin is a promising candidate for DMD therapy. Like dystrophin, it is capable of providing cytoskeletal linkage between actin and the extracellular matrix via DGC binding. It shows four structural domains like dystrophin. *Mdx* mice overexpressing a truncated utrophin transgene have reported to show reduced pathology as well as improved muscle function (Deconinck *et al.*, 1997b). Utrophin has the advantage of not being recognised as a neo-antigen in dystrophin-deficient muscle, so cell-mediated immunity problems seen with *dys* transfer should be largely circumvented (Ebihara *et al.*, 2000).

An alternative approach is to increase expression of utrophin to the 2-3 fold increase in protein level required to prevent dystrophic pathology at the translational level via promoter activation, either via the use of small diffusable chemical compounds (such as butyrate derivatives used in β–thalassaemia), or alternative

drugs (Perkins and Davies, 2002). Heregulin, L-arginine, NO or hydroxyurea are thought to act by utrophin promoter activation mechanisms, although there is contention regarding the efficacy of L-arginine in this role (Krag *et al*., 2004; Chaubourt *et al*., 2002).

## 1.10 Gene repair strategies

### 1.10.1 Aminoglycosides

Aminoglycoside antibiotics can suppress nonsense mutations in mammalian cells by the same action as they disrupt translational fidelity in bacteria. They bind a specific site in ribosomal RNA and disturb codon-anticodon recognition (Kaufman, 1999). As *mdx* mice show a nonsense mutation in their dystrophin gene, the aminoglycoside gentamycin can be used to promote translation read-through of the nonsense codon in this species. Initial trials showed a restoration of between 10-20% of normal levels of dystrophin in *mdx* muscles, at a level sufficient to protect against contraction-induced injury (Barton-Davis *et al.*, 1999). This class of antimicrobials cause nephrotoxicity and ototoxicity, especially with long-term use, and more investigation is required regarding optimum dosage and interval between dosages before treatment of the estimated 15% of boys with DMD with premature stop mutations.

Negamycin, a dipeptide antibiotic said to be less toxic than gentamycin, restored dystrophin to skeletal and cardiac muscles of *mdx* mice in one study (Arakawa *et al.*, 2003). Its mechanism of action is binding to a partial sequence of the eukaryotic rRNA decoding A-site.

There have been several clinical trials using these agents. Effect may vary according to position of the stop codon, with some boys demonstrating greater dystrophin expression than others (Politano *et al.*, 2003). Further clinical trails are anticipated, involving the use of gentamycin analogues, PTC124 and geneticin.

### 1.10.2 Antisense oligonucleotides (AOs)

#### 1.10.2i The theoretical basis to AO use:

Genes are organized in genomic DNA with exons (coding sequences) separated by introns (non-coding sequences). Exons contain open reading frames (ORF) of nucleotide triplet codons for amino acids and comprise an initiation codon

and a stop codon. For normal gene function to occur two exons in a series must have triplet codon breakpoints that maintain the correct translational ORF during splicing of intron sequences to form messenger RNA (mRNA). (Fig 1.7)

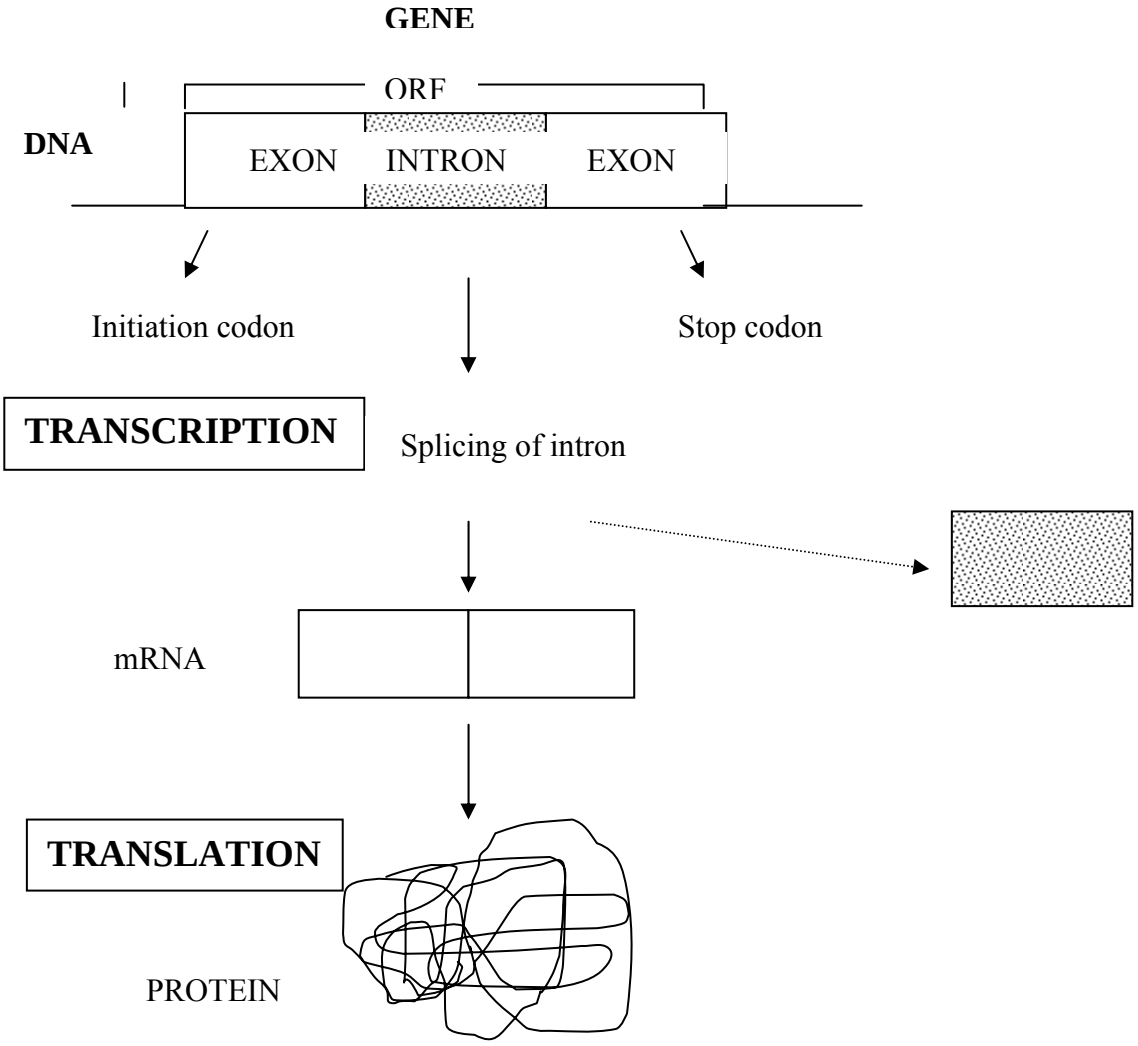


**Fig 1.7** Simplified depiction of events involved in mammalian gene expression.

Analysis of gene sequences of DMD patients revealed that the majority (but not all) showed deletions or point mutations of the gene causing a consequential shifting of the ORF, and the translation to a truncated, abnormal dystrophin (Fig 1.8A). If the deletion were in the area of the gene that maintained the ORF, the resultant protein would be shorter and semi-functional, a so-called Becker Muscular Dystrophy (BMD) protein causing a milder phenotype (Monaco *et al*., 1988) (Fig 1.8B).

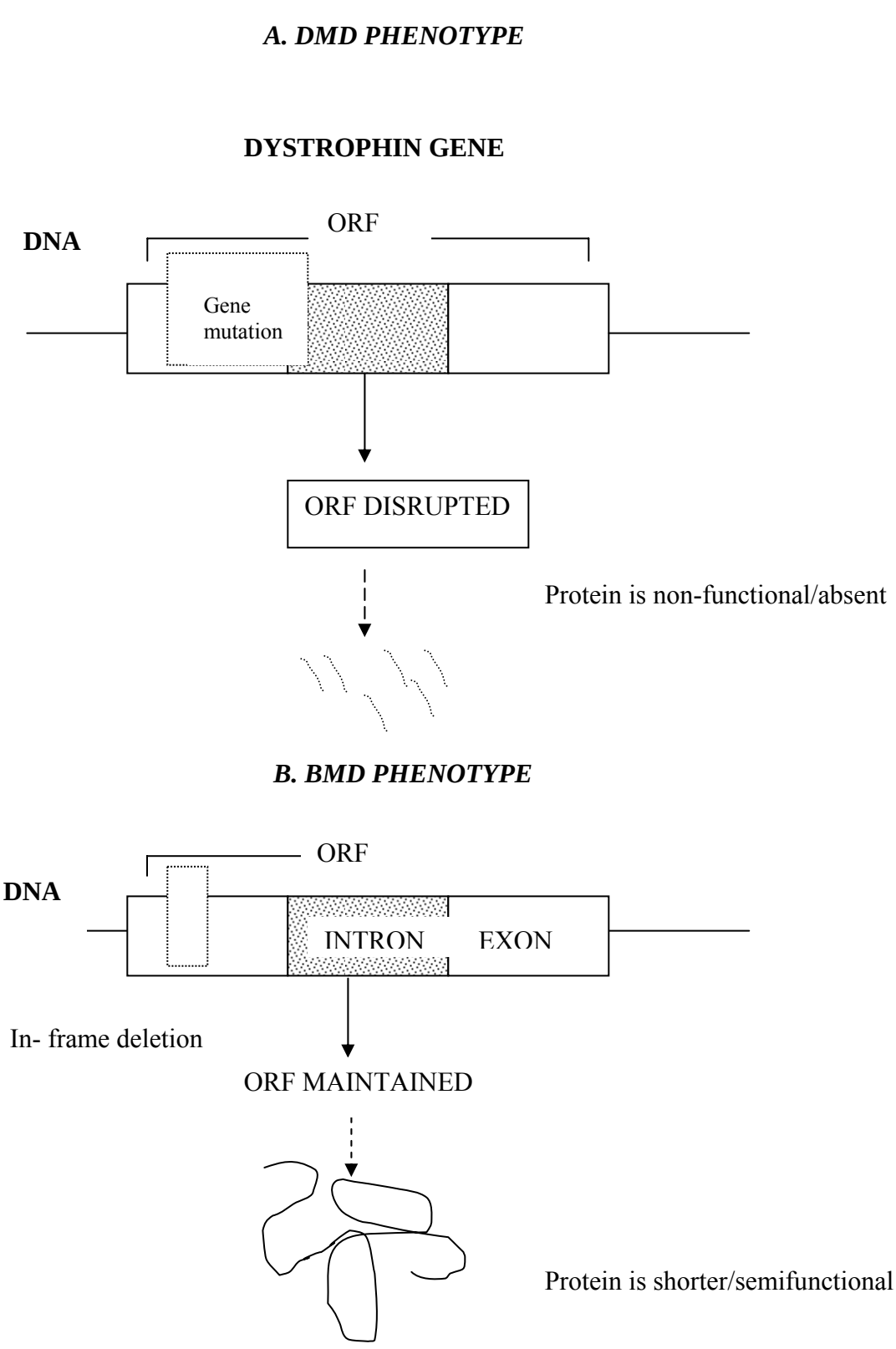


**Fig 1.8** Mutations of the dystrophin gene leading to A. Duchenne Muscular Dystrophy (DMD) or B. Beckers Muscular Dystrophy (BMD), depending upon the site of deletion, and whether the reading frame remains intact or is disrupted. These simplified diagrams apply to point mutations and short deletions and may not apply to large deletions, duplications or mutations at more than one site.

In the *mdx* mouse the nonsense mutation of the dystrophin gene results in termination of translation within Exon 23. Theoretically there should be no functional dystrophin expressed in *mdx* muscles, however occasional (<1%) dystrophin-positive fibres are found. Such fibres are also found in many DMD patients (Fanin *et al.*, 1995). It is proposed that dystrophin arises in these fibres by alternative processing and exon skipping causing in-frame gene transcripts (Wilton *et al.*, 1997a; Wilton *et al.*, 1997b).

Studies have shown that synthesized antisense oligonucleotides (AOs) may operate to induce exon skipping in a similar manner to that occurring in the *mdx* mouse (Wilton *et al.*, 1999; Dunckley *et al.*, 1995). AOs have been utilised to block motifs involved in normal pre-mRNA splicing in *mdx* myoblasts. This causes skipping of exon 23 without disrupting the reading frame, thus potentially allowing synthesis of a shorter, but still functional protein when delivered to *mdx* muscles. (Figure 1.9)

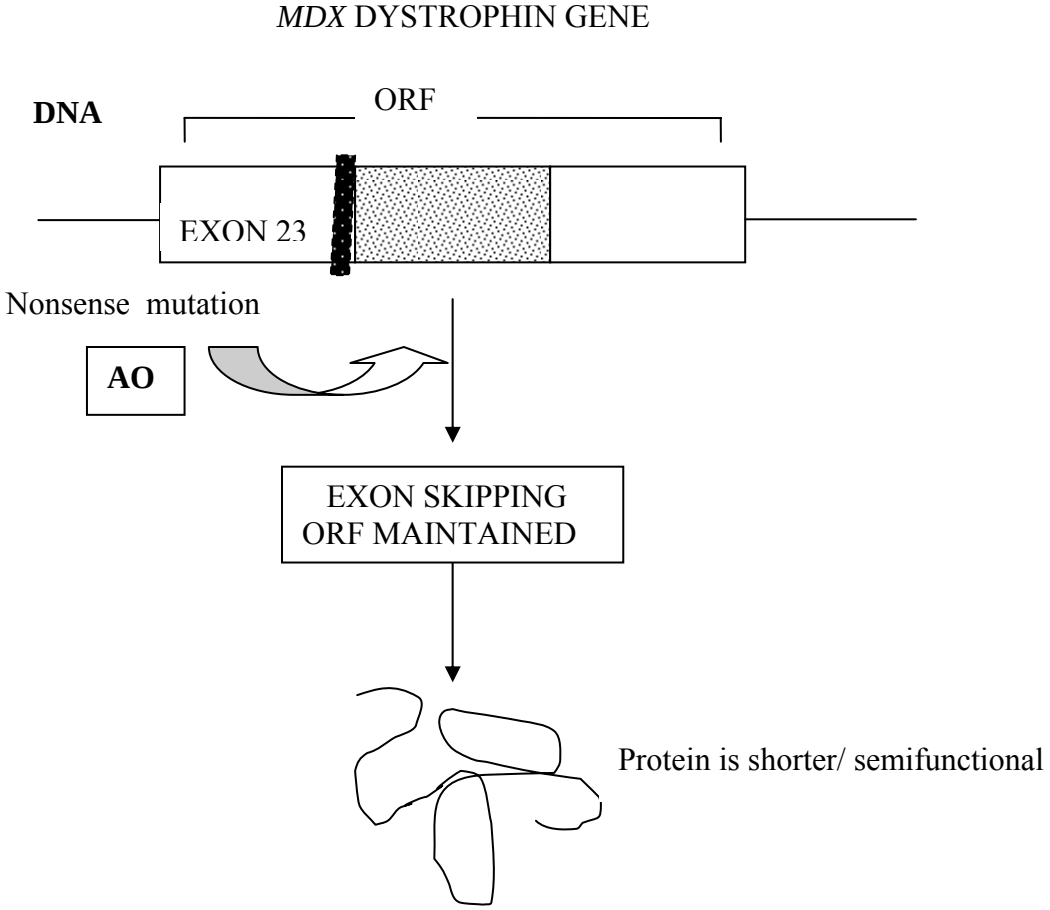


**Fig 1.9** Use of antisense oligonucleotides in *mdx* mice to induce exon-skipping

1.10.2ii The structure and action of AOs

Oligonucleotides have been used for the downregulation of cancer or disease genes, most commonly by base-pairing with a mRNA target and mediating its destruction by RNase H. AOs can also be used to silence mutations that cause aberrant splicing (for example β-Thalaassemia and some cystic fibrosis mutations), thus restoring correct splicing and gene function (Sazani and Kole, 2003). The requirements for the second generation AO's are different - they must not activate RNase H, which would destroy the pre-mRNA target prior to splicing, and they must also be able to compete with splicing factors for access to pre-mRNA located in the nuclei of cells. AO's with modifications to the 2'position, such as 2'-*O*-methyl, or those with backbones based on phosphorothioate or morpholino derivatives are suitable candidates (Sazani and Kole, 2003).

Delivery agents that allow AOs to accumulate in nuclei of cells and bind to the pre-mRNA markedly enhance their efficacy. Cationic liposome formulations or commercial vectors, such as Lipofectin, Eufectin or Lipofectamine are designed to enhance delivery and uptake. These vectors, because of their positive charge, have high affinity for negatively charged cell membranes (Dias and Stein, 2002).

### 1.10.2iii Development of AOs and potential applications

AOs applicable to *mdx* dystrophin were synthesized after sequencing of purified PCR products following long range PCR across introns 22 and 23. Splice sites flanking these introns were identified and 2'O-methyl *dys* 3' and *dys* 5' AOs were designed that would anneal to the 3' and 5' splice sites of the mouse pre-mRNA respectively. These consistently induced skipping of Exon 23 in immortalised mouse myoblast lines (Wilton *et al*., 1999). Since then vast improvements in AO design and efficiency has occurred, including design of AO's directed specifically against the 5' (donor) splice site of intron 23. AOs as small as 17 nucleotides induced strong and consistent exon skipping, with evidence of a Becker-like protein produced in cell lines and *in vivo* (Mann *et al.*, 2002; Mann *et al.*, 2001). Figure 1.10 shows immunohistochemical evidence of successful dystrophin restoration in *mdx* muscle.

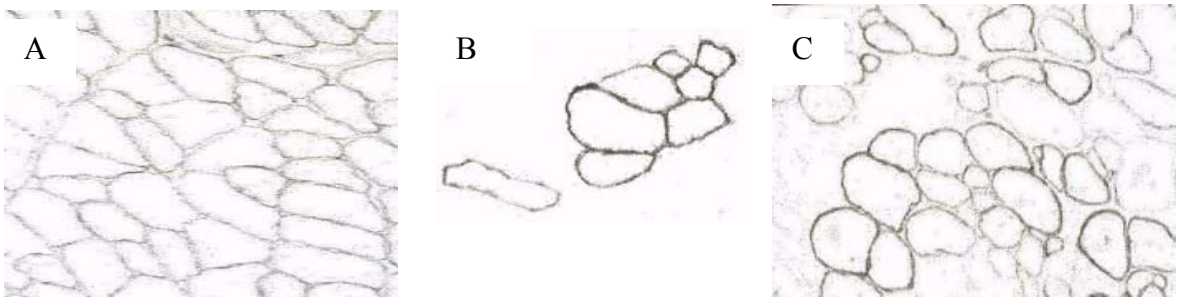


**Fig 1.10** Examples of successful antisense oligonucleotide (AO) treatment, detected by immunostaining. A. Wild-type mice with dystrophin located on the periphery of all fibres. B *Mdx* muscle cells with some revertant fibres showing positive staining. C. *Mdx muscles* following electrotransfer of AO with many fibres staining positive for dystrophin. (Wells *et al.*, 2003)

Optimisation of oligonucleotide composition and delivery methods is vital to the application of this methodology in both the *mdx* mouse model (Wilton *et al*., 1999; Mann *et al.*, 2001) and in DMD cultured muscle cells (Aartsma-Rus *et al*., 2002; van Deutekom *et al.*, 2001). Modification of AO's to a morpholino chemistry is also possible, which creates a neutral molecule with biological stability that can be tethered to a sense 'leash' and delivered as a cationic lipoplex (Gebski *et al.*, 2003). The aim of structural modifications is to create optimal safety, delivery and efficacy of both AO and delivery agent.

Further developments include the application of multiexon skipping strategies using a combination of AOs to skip two or more exons (including an entire stretch from Exon 45-51 in cultured myotubes from one DMD patient) (Aartsma-Rus *et al.*, 2004). Improved delivery using hyaluronidase enhanced electrotransfer was investigated in injected *mdx* limb muscles, with increased dystrophin expression resulting (Wells *et al.*, 2003). Repeated administration and higher dosages of AO's enhanced dystrophin expression (Lu *et al.*, 2004). Linkage of antisense sequences to short nuclear (sn) RNA allows for subcellular localisation and inclusion into spliceosomes, and U7 (a non-spliceosomal snRNA) can be engineered to bind and deliver antisense sequences. AOs linked to U7 sn RNA have been introduced via AAV vectors for high efficiency gene transfer into skeletal

muscle. Administration into *mdx* tibialis anterior muscles showed prolonged expression, reduction of exercised-induced damage, and improved contractility (Goyenvalle *et al*., 2004).

The advantages of an AO approach to therapy are that it is tissue specific and highly sequence specific (Bremmer-Bout *et al.*, 2004). AOs are small compounds, and do not elicit an immune response. The apparent specificity of current AOs suggests that systemic delivery may be possible with targeted exon skipping only occurring in those tissues expressing dystrophin. There is the potential for repeated delivery as there appears to be a natural ability of muscle cells to take up these compounds, as well as a slow turnover of muscle cells *in vivo* (Wilton *et al*., 1999).

The shortcomings of AO therapy at present are the challenges of widespread delivery to many muscle groups, and ensuring persistence in tissues. While some experiments suggest dystrophin persistence following AO treatment is up to 2 months (Lu *et al*., 2003), other studies suggest it may be considerably shorter than this (Wells *et al.*, 2003). The development and refinement of vectors for systemic delivery may overcome these problems.

Unfortunately dystrophinopathies caused by large deletions of the gene will not be amenable to this method of correction, however a hospital database in France indicated that 43% of patients could benefit from skipping a single exon (Goyenvalle *et al*., 2004), and this proportion may be increased if multiple exon skipping can be accomplished (Aartsma-Rus *et al*., 2004).

It must also be recogised that BMD is not a benign disorder, and can result in serious cardiomyopathy and death. However, many BMD patients lead active lives well into middle age (or beyond), and do not suffer the debilitating consequences of respiratory failure or generalised muscle wasting seen in DMD.

Despite these limitations the future for incorporation of AO technology into the treatment of DMD looks promising. The dystrophin gene is uniquely suited to therapeutic exon skipping due the modular and repetitive nature of some of its domains, and the high incidence of point mutations or short deletions. There are now pathways in place for vector mediated delivery and potential rescue of multiple muscle groups, as well as future clinical trials.

## 1.11 Aims and Scope of study

The overall aim of this research project was further characterisation of the *mdx* mouse model of DMD, to enable strategic treatment with antisense oligonucleotides. Particular muscles were targeted in this study, including cardiac muscle, diaphragm, paraspinal and accessory respiratory muscles. Knowledge gained from preliminary characterisation studies were used to optimise methods and choose ages and numbers of mice for subsequent experiments utilising AO's (see Fig 1.11). The exception to this was the cardiac experiments, as it was felt that an in-depth cardiac AO study was beyond the scope of this PhD because of time constraints. The aims and scope of each individual project are listed below.

### 1.11.1 Atrial function and cardiac fibrosis in aging *mdx*

The *mdx* heart has been characterised to an extent previously, and in recent years there have been functional studies using *in vitro* isolated hearts and *in vivo* catheterised hearts. New knowledge has been gained from these studies that confirms the *mdx* mouse as a useful model for DMD cardiomyopathy under certain conditions, notably exercise induced stress, following aortic banding or pharmacologically induced stress (dobutamine or isoprenaline), or perhaps older age. This latter point was published only in late 2004, with reports of echocardiographic data from 40 week old *mdx* suggesting ventricular function was impaired and dilation was present in these older mice, but not before (Quinlan *et al*., 2004). Prior to these studies there was limited functional data available, mostly from young *mdx* atria. The older mouse may be a realistic model for heart disease in DMD, as cardiomyopathy also develops gradually in DMD, often towards the end of the patient's lifespan. Artificially induced heart failure (such as from aortic banding or acute catecholamines challenge) may provide a less realistic model than gradually occurring pathology with compensatory physiological responses and progressive fibrosis.

The aim of this study was to characterise changes in atrial function and cardiac fibrosis throughout the lifespan of the *mdx* mouse. This project used 9 ages of mice (from 3 weeks to 24 months), and measured cardiac morphometry, atrial contractility, responses to exogenous calcium and development of fibrosis as measures of progressive cardiac dysfunction. Cardiac fibrosis has been poorly

documented in the *mdx*, despite it being a significant contributor to DMD cardiomyopathy, and fibrosis in general being a hallmark of dystrophy in any muscle type. This project used two measures of cardiac fibrosis; the first was the colorimetric assay of hydroxyproline, an amino acid constituting some 8% of the total protein content of collagen, the second using collagen specific staining and percentage flourescence of heart sections.

Electrophysiological data was also measured across the age groups of mice, using transmembrane action potentials from isolated left atria. Again, there is little available data from *mdx* mice, and none across the lifespan. There is also conflicting ECG data available in the literature with reports indicating QT intervals as similar, less or greater in *mdx* compared to control mice, and it was hoped action potential data would resolve this. Electrophysiological disturbances may be an inate property of dystrophic muscle, as there is a high incidence of arrythmias and ECG abnormalities in boys with DMD, even at a young age before clinical signs of heart failure.

### 1.11.2 Monophasic action potential measurements and trabeculae contractility

Monophasic action potential measurements using Langendorff preparations and trabeculae contractility was also planned in a separate set of experiments, as it was felt that these parameters would add considerably to our knowledge regarding dystrophic cardiac muscle. There have been no MAP studies reported from *mdx* mice, despite this technique being widely used in transgenic murine models of human cardiomyopathy (especially arrhythmias). There have been few mouse trabeculae or small papillary muscle functional studies, and none in *mdx* mice. Ventricular experiments may provide additional information, especially if there is unequal chamber involvement in the dystrophic process.

Unfortunately there were technical difficulties with these studies, which meant there were too few results to draw conclusions or provide tests of statistical significance. These results are included as Appendix A, including establishment of equipment and setting up of protocols.

### 1.11.3 Diaphragm function and fibrosis in aging *mdx*

The diaphragm is recognised as the muscle that best resembles the severe dystrophic pathology seen in DMD. This study utilised the same age groups of mice as outlined in 1.11.1, and served as a useful preliminary study for a future experiment examining the effects of AOs injected into the diaphragm. Protocols were established, and expertise gained, in skeletal muscle contractility experiments, histology and surgery for diaphragm injections.

### 1.11.4 Progression of kyphosis in aging *mdx* mice

Boys with DMD develop severe kyphoscoliosis unless spinal surgical stabilisation is undertaken. The aim of this study was to characterise the progression of kyphosis in *mdx* mice by monthly radiographs, and development of a novel Kyphotic Index to measure this objectively. Further aims were to assess the contractility of paraspinal and respiratory muscles not previously examined in mice, including latissimus dorsi muscles and an intercostal muscle segments. Fibrosis was also quantitated in these muscles, in addition to the longissimus dorsi muscles and diaphragm. These paraspinal and accessory respiratory muscles were deemed important for both the progression of kyphosis and possibly respiratory dysfunction in *mdx* mice. It was anticipated that knowledge gained from these experiments would further understanding of the dystrophic phenotype, and serve as useful preliminary data for a later experiment administering AOs into paraspinal muscles.

### 1.11.5 AO administration into *mdx* diaphragm muscle

AOs show promise as a gene correction strategy in the treatment of DMD, but for this to be considered successful they must be shown to ameliorate the signs of dystrophin deficiency, including necrosis, fibrosis and muscle weakness. This study examined the effects of two administrations of AOs into *mdx* diaphragms, given one month apart. The aim was to determine if AOs injected into a muscle with known severe dystrophic tendencies is rescued by such therapy, using the endpoints of muscle function *in vitro*, collagen accumulation and dystrophin protein expression by Western blotting.

### 1.11.6 Long term administration of AO's into paraspinal muscles of *mdx*

Any potential therapy for a genetic disorder such as DMD is likely to be given long term, and by repeat administration. Current AO strategies are limited to direct intramuscular injections, and previous studies have looked only at single treatments in young animals. The aim of this study was to examine the efficacy of monthly AO injections into the paraspinal muscles of *mdx* mice for 16 months (following on from 1.11.5). Mice were radiographed once monthly to follow progression of kyphosis in injected, sham-injected and wild-type mice. At the end of the experiment muscles were mounted in organ baths for contractility studies, and fibrosis was measured by hydroxyproline assay and specific collagen stains of histological sections. Western blotting was used to assess efficacy of AO transduction and dystrophin protein expression. This study is unique in applying a dynamic parameter that changes with age (the Kyphotic Index), and measures of contractility and fibrosis at the end of the lengthy experimental period.

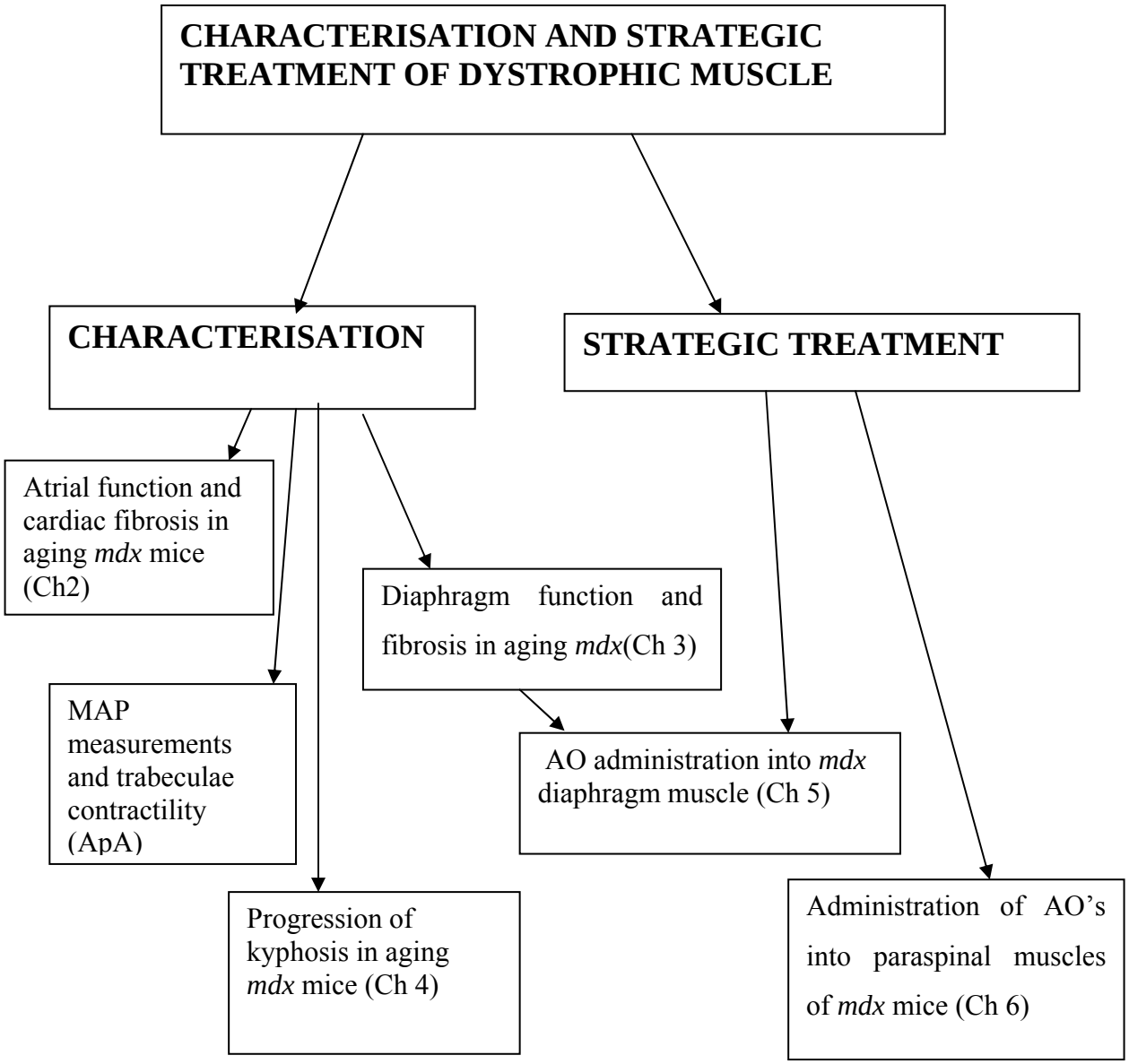


**Fig 1.11** Overall plan of research studies

MAP= monophasic action potential, AO= antisense oligonucleotides, Ch= chapter, Ap= appendix.

# CHAPTER 2. THE AGING *MDX* MOUSE: ATRIAL FUNCTION AND CARDIAC FIBROSIS

## 2.1 Introduction

Boys with DMD often exhibit cardiomyopathy in addition to serious respiratory complications due to diaphragm weakness, thoracic deformity and chronic hypoventilation. A recent survey on survival in DMD patients highlighted that early death from heart failure reduced average life expectancy significantly (Eagle *et al.*, 2002). Symptomatic cardiomyopathy increases with age, with all DMD patients over 18 years having detectable cardiac disease (Nigro *et al.*, 1990). The spectrum of cardiac involvement includes sudden death, isolated conduction defects and dilated or hypertrophic cardiomyopathy. Autonomic imbalance has been demonstrated in DMD patients at an early stage of the disease when cardiopulmonary function is still well preserved (Yotsukura *et al.*, 1995).

Cardiac involvement in *mdx* was noted in early histological studies. Myocardial lesions were observed in 5/10 male *mdx* mice ranging in age from 8-30 weeks (Bridges, 1986). Coulton *et al.*, (1988) found evidence of cardiac myonecrosis and cellular infiltration in 13/65 ventricles examined in mice of 26-303 days old. Foci of inflammation and fibrosis were also found in old *mdx* hearts (greater than 20 months old) (Lefaucheur *et al*., 1995), while another histological study reported the absence of pathological changes in *mdx* hearts examined at different ages (Torres and Duchen, 1987).

Two studies have suggested that *mdx* hearts may be hypertrophic (Danialou et al., 2001b; Megeney *et al.*, 1999), although it has been pointed out that these studies had small sample sizes (5 and 12 mice respectively) that were not large enough to reveal a statistically significant hypertrophy (Yue *et al.*, 2004). Other studies have shown that heart weight normalised to body weight is similar between *mdx* and control mice (Yue *et al*., 2004), and that left ventricle/bodyweight is significantly less in younger and similar in older mice (Lu and Hoey, 2000). There have been no studies to evaluate heart weights in relation to body weight systematically across throughout the *mdx* lifespan, although echocardiographic studies of 8, 29 and 42 week old mice showed the development of dilated cardiomyopathy in 42 week old *mdx*, with increased LV end systolic and diastolic diameters and decreased fractional shortening (Quinlan *et al*., 2004).

Studies of isolated left atria in 12-week-old mice showed *mdx* also have contractile dysfunction compared to wild types (Sapp *et al.*, 1996). These young mice also displayed a reduced responsiveness to calcium and altered atrial twitch characteristics, including delayed relaxation times. *Ex vivo* perfused hearts from young *mdx* provide direct evidence for severe contractile dysfunction and non-ischaemic tissue damage correlated with cardiac workload, indicating dystrophin functions to guard cardiomyocytes from mechanical stress (Danialou et al., 2001b). It has been suggested that 50% dystrophin expression is sufficient to improve heart function in *mdx* mice, as measured by Evans blue dye uptake and left ventricular functional parameters (Yue *et al*., 2004).

Autonomic nervous system dysfunction occurs in *mdx* as well as boys with DMD. There is a marked deterioration in cardiac $\beta_1$-adrenoceptor function in aged (12 month old) male *mdx*, evidenced by a reduced potency and efficacy of (-)-isoprenaline (Lu and Hoey, 2000). Heart rate variability studies on conscious mice suggested an elevated sympathetic tone and blunted parasympathetic activity in *mdx* (Chu *et al.*, 2002).

Quantitative studies of cardiac fibrosis in *mdx* are few. One study revealed a four-fold increased fibrosis in 17-month-old *mdx* hearts compared to controls, with no predilection for the five regions analysed (right ventricle, anterior wall, posterior wall, lateral wall and septum)(Quinlan *et al.*, 2004).

There is a requirement for further cardiac phenotype characterisations of the *mdx* as it increases the knowledge base to help understanding of the pathophysiology of DMD cardiomyopathy. Furthermore, this is important for therapeutic trials involving anti-inflammatory, immune-modulating agents or gene therapy studies that may improve cardiac function.

## 2.2 Aims

The primary aim of the present study was to determine whether cardiac function and electrophysiological properties of *mdx* mice change across their lifespan and vary significantly from wild type mice. In addition, cardiac collagen was measured to assess if *mdx* heart fibrosis increases with age, as occurs in hearts from boys with DMD.

## 2.3 Methods

### 2.3.1 Mouse numbers and groupings

In the initial series of experiments (Study 1), groups of 7-8 male control C57BL/10ScSn (C57) and mutant C57BL/10ScSn *mdx* (*mdx*) mice were utilised for functional studies at 3, 6 and 12 weeks, 6, 9, 12 and 15 months of age. In addition two groups of *mdx* mice only were used at 18 and 24 months of age (because of the unavailability of control mice at these ages). For hydroxyproline assays and morphometry measurements additional age, sex and strain matched tissues were utilised to give an $n$=10-14 per group.

Following examination of the results of these experiments two age groups of C57 and *mdx* mice (6-8 weeks and 15-17 months) were utilised for a more detailed analysis of cardiac fibrosis (Study 2). There were 7-8 mice/age group/ strain for this part of the study. It was anticipated that measuring cardiac fibrosis at 3 different cross-sectional levels of the heart, and an increased $n$ number would improve accuracy, as would performing hydroxyproline assays on ventricular tissue from mid-heart rather than just the tip of the heart apex.

*Mdx* mice were obtained from the USQ Animal House, and C57's from Animal Resource Centre, Nedlands, Western Australia.

The groupings and mouse numbers are shown in Figure 2.1

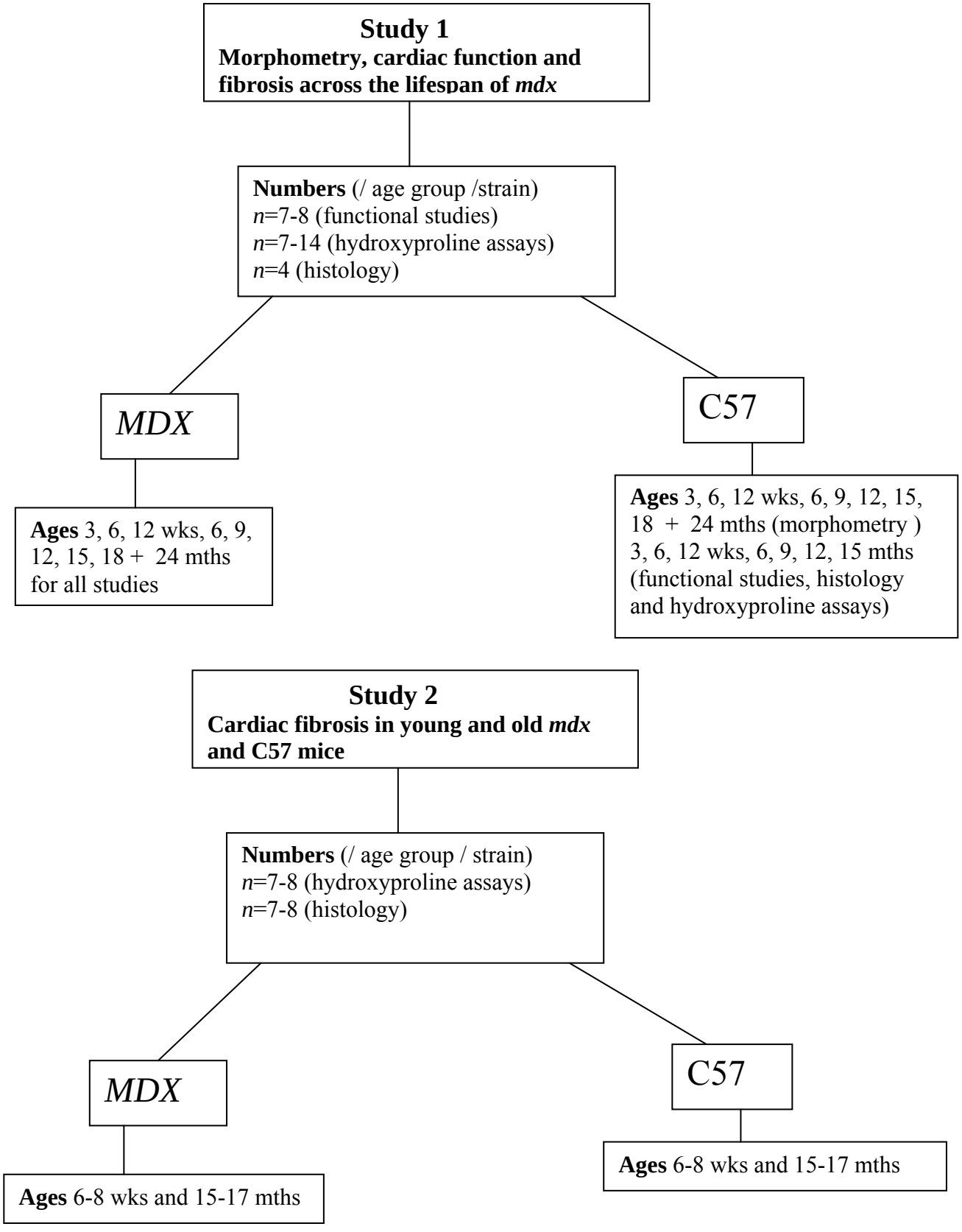


**Fig 2.1** Diagram detailing the mouse numbers and groups for the series of experiments evaluating cardiac function and fibrosis in *mdx* and control (C57) mice.

2.3.2 Transmembrane action potentials and contractility of isolated atria

At the commencement of each experiment mice were weighed, anaesthetised using Tiletamine/Zolazepam at 35 mg/kg subcutaneously (Virbac Laboratories, Australia), then euthanased by exsanguination. Lungs and hearts were removed, and the lungs were rinsed of blood clots, blotted for 3 seconds and weighed.

Each heart was dissected quickly in ice-cold pre-carbogenated (95% $O_2$/5% $CO_2$) Tyrode physiological salt solution (TPSS; mM: NaCl 136.9, KCl 5.4, $MgCl_2H_20$ 1.05, $NaH_2PO_4.2H_2O$ 0.4, $NaHCO_3$ 22.6, $CaCl_22H_2O$ 1.8, glucose 5.5, ascorbic acid 0.3, $Na_2EDTA$ 0.05). The right atria, right ventricular free wall and left ventricle (LV) plus septum were dissected, blotted for 3 seconds and weighed.

The left atria (LA) was removed and a stainless steel hook was positioned into the pulmonary vein opening, before transferring into a 1 ml Perspex organ bath. The LA was pinned onto a small rubber mat, and the hook connected to the force transducer (model AE801, SensoNor, Horten, Norway). The tissue was perfused continuously with carbogenated TPSS at a flow rate of 3mL/min and a temperature of 35±0.5$^oC$. The LA was held at an optimum preload of 3.5±0.5 mN throughout the experiment, and field stimulated via platinum electrodes at 0.5ms pulse width and 1 Hz, 25% above threshold (Grass SD9 stimulator, W. Warwick, RI, USA).

After a 30-minute equilibration period the LA was impaled 4-5 times at different sites with a 3M KCl filled glass microelectrode (World Precision Instruments, New Haven, CT, USA, 150F glass, 10-50MΩ resistance). Data was recorded using a PowerLab and Chart 4.1.1 software (A.D. Instruments, Castle Hill, Australia), at 1000 samples/sec and then an average of the 4-5 recordings was calculated. A concentration response curve (CRC) to $CaCl_2$ was generated following transmembrane action potential (TAP) recordings. Details of the apparatus required for these experiments are provided in Appendix B.

2.3.3 Collagen measurements

At the end of the experiment the LA was blotted briefly and weighed. LA and LV apex were stored at –70$^oC$. For Study 2 the right atria were also stored for hydroxyproline assays. The remainder of left ventricle and septum was fixed sequentially in Telly's fixative (formaldehyde, glacial acetic acid-ethanol fixative, 72 hours), Bouin's solution (formaldehyde, glacial acetic acid-picric acid fixative,

24 hours) and 70% ethanol, prior to paraffin embedding, cutting and staining of 10 micron sections, using 0.1% w/v picrosirius red solution (Sirius Red F3B, Chroma Dyes, Germany in saturated picric acid).

Analysis was performed blinded to the strain or age. Interstitial and perivascular collagen was included, while capsular collagen was excluded from analysis. For Study 1 sections were viewed on a Biorad MRC 1024 confocal scanning microscope with a krypton/argon laser and subjected to a Rhodamine/Texas Red filter of 568nm wavelength. Images were captured using a Biorad Lasersharp 2000 program. Photomicrographs of 4 sections per heart were analysed and averaged for saturated pixel intensity corresponding to collagen fibres, using Scion Image software Beta 4.0.2 (http://www.scioncorp.com). Results are expressed as collagen as a percentage of area of view. An *n* of 4-6 mice per group was compared in this manner.

For Study 2 examining fibrosis in young and old mice, entire hearts were sectioned at 3 levels a) apex, b) mid portion and c) base. Fluorescent microscopy images were acquired from these heart sections using a digital camera (Q imaging Micropublisher 5.0 RTV) coupled to an epifluorescence microscope (Eclipse E600, Nikon, Japan). Four sections per tissue were photographed and analysed using the image analysis program DocuAnalySIS (Soft Imaging System), then averaged. Collagen was expressed as a percentage of the total area of tissue. Good correlation was found between results of slides examined previously using the confocal microscope, and those captured and analysed with this analysis system.

Hydroxyproline (HP) content was also used as a measure of total collagen as described previously (Stegemann and Stalder, 1967), with the following modifications. Tissue was thawed, then hydrolysed in sealed 2 ml cryotubes with 6M HCl overnight at 110$^{o}$C and dried completely using filtered air under pressure and heat (50$^{o}$C). Values are expressed as µg HP/mg tissue wet weight. Appendix B shows details of HP assays, modified for tissue samples less than 20mg, to fit a 2 mL total volume.

### 2.4 Statistics

Results are expressed as means ± S.E. Responses between groups of same aged *mdx* and C57 were compared using Student's unpaired *t*-tests. For Study 2 group mean

differences were determined initially by ANOVA, with *post hoc* application of unpaired Student's t-tests in the event of significant ANOVA. *P* values less than 0.05 were considered statistically significant.

## 2.5 Results

### 2.5.1 Morphometry

Differences in body weight between *mdx* and C57 were evident at various life stages as depicted in Fig 2.2a. At 3 weeks of age, corresponding to the acute muscle necrotic stage, *mdx* mice were significantly lighter ($P<0.001$), and then became heavier than wild type mice with development of muscle hypertrophy (significant at 12 weeks of age ($P<0.05$)). Older *mdx* (at 15 months of age) demonstrated a weight decline relative to C57 mice ($P<0.01$).

Lung weights were less for *mdx* mice at all age groups except 15 months (data not shown), however when adjusted for bodyweight there was no significant difference between *mdx* and wild type mice, except for the 3 week old and 9 month old age groups (Fig 2.2b). Importantly there was no evidence of increased lung/body weight ratios indicative of pulmonary congestion as *mdx* aged.

Total *mdx* heart weights (calculated by addition of individual heart chambers) were less at 3 weeks, and at all ages exceeding 12 months (Fig 2.2c). In contrast heart weight/body weight ratio was higher in *mdx* at 3 weeks (when body weights were less than controls) and lower at 12 weeks when they are undergoing muscle hypertrophy. At all ages exceeing 12 months *mdx* exhibited a lower heart weight/body weight ratio, despite lower body weights (Fig 2.2d). At no time point did *mdx* show increased total heart or individual chamber size, relative to control animals.

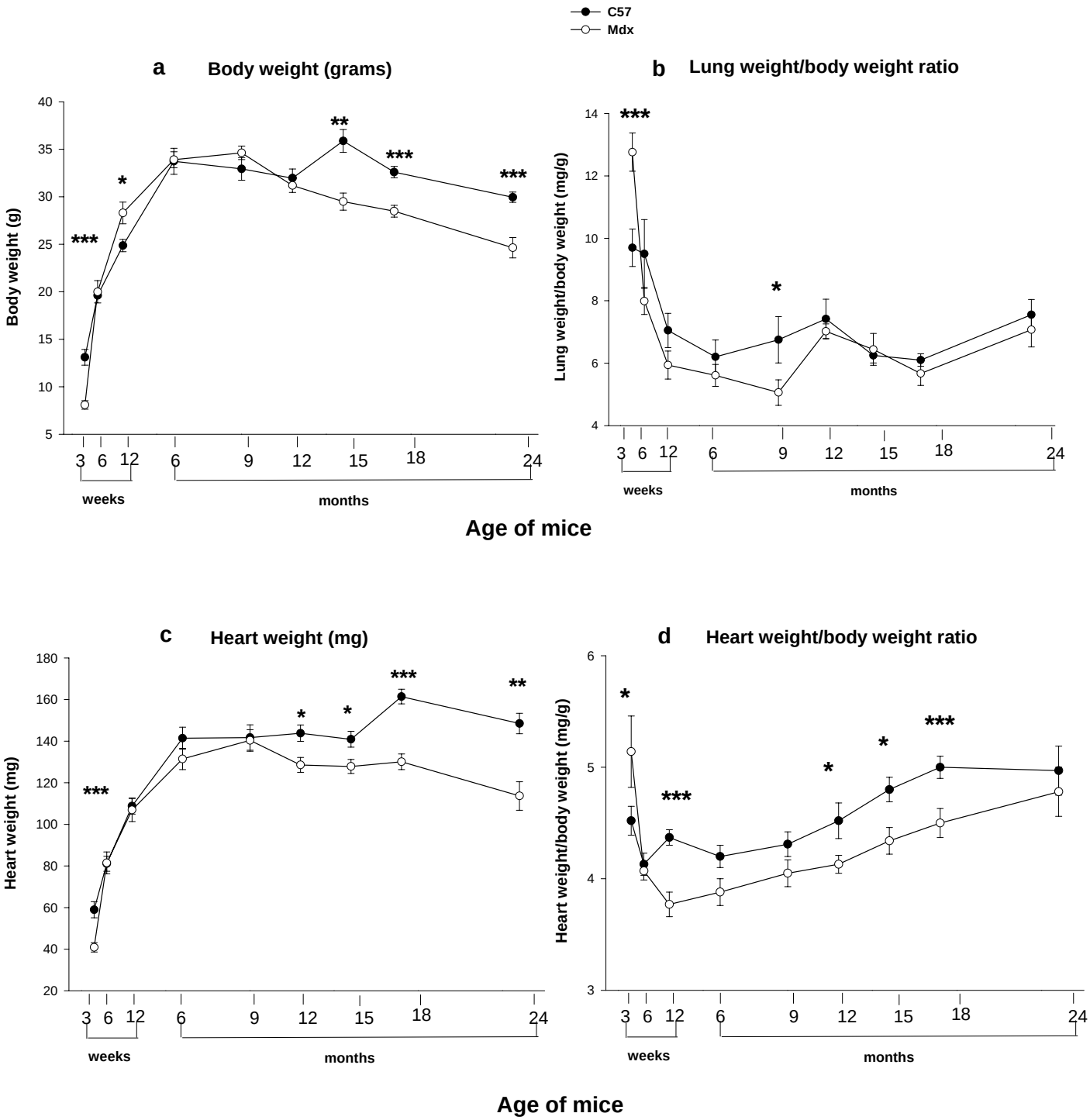


**Fig 2.2** Morphometry data from aging mice. *Mdx* and C57 mice a) Body weights of *mdx* mice are less at 3 weeks of age, and then became significantly less than controls from 15-24 months. b) Lung weight/body weight ratio was greater in *mdx* at 3 weeks when mice were of low body weight, and were then less than control mice (significant at 9 months only). c) Heart weights were greater in control mice, with significance at 3 weeks, then from 12 months to 24 months. d) Heart weight/ body weight ratio was less for *mdx* mice (significant at 3months, then from 12-18 months), however at 3 weeks of age *mdx* showed an increased heart/body weight ratio. $n$=7-8 per strain/age group *** $P$<0.001, ** $P$<0.01, * $P$<0.05.

2.5.2 Transmembrane action potential recordings

The criteria for TAP inclusion were a stable wave-shape with a sequence of more than 10 action potentials, a horizontal diastolic interval, amplitude greater than 70 mV, and an overshoot greater than +10 mV.

APDs were measured at 20, 50 and 90% of repolarisation ($APD_{20}$, $APD_{50}$ and $APD_{90}$ respectively). There was a strong trend of shorter $APD_{90}$ values in all age groups of *mdx*, with significance at 3 weeks, 9 months and 12 months (Fig 2.3). Waveform shape differed between strains as mice aged, with $APD_{50}$ increasing in *mdx* older than 15 months, despite a tendency for a shorter $APD_{90}$ (Fig 2.3 and 2.4) APD increased over the lifespan of both mouse strains

Action potential amplitudes (APA) were not significantly different (C57, 88.5 ± 2.8: *mdx* 87.4 ± 2.1 mV). Rate of upstroke ($dV/dt_{max}$) were not different between strains (C57, 86.3 ± 2.1: *mdx* 91.9±3.7 V/sec). There was no difference in resting membrane potentials at any age groups compared (C57, -76.7 ± 0.73mV: *mdx*, -75.45 ± 0.19mV).

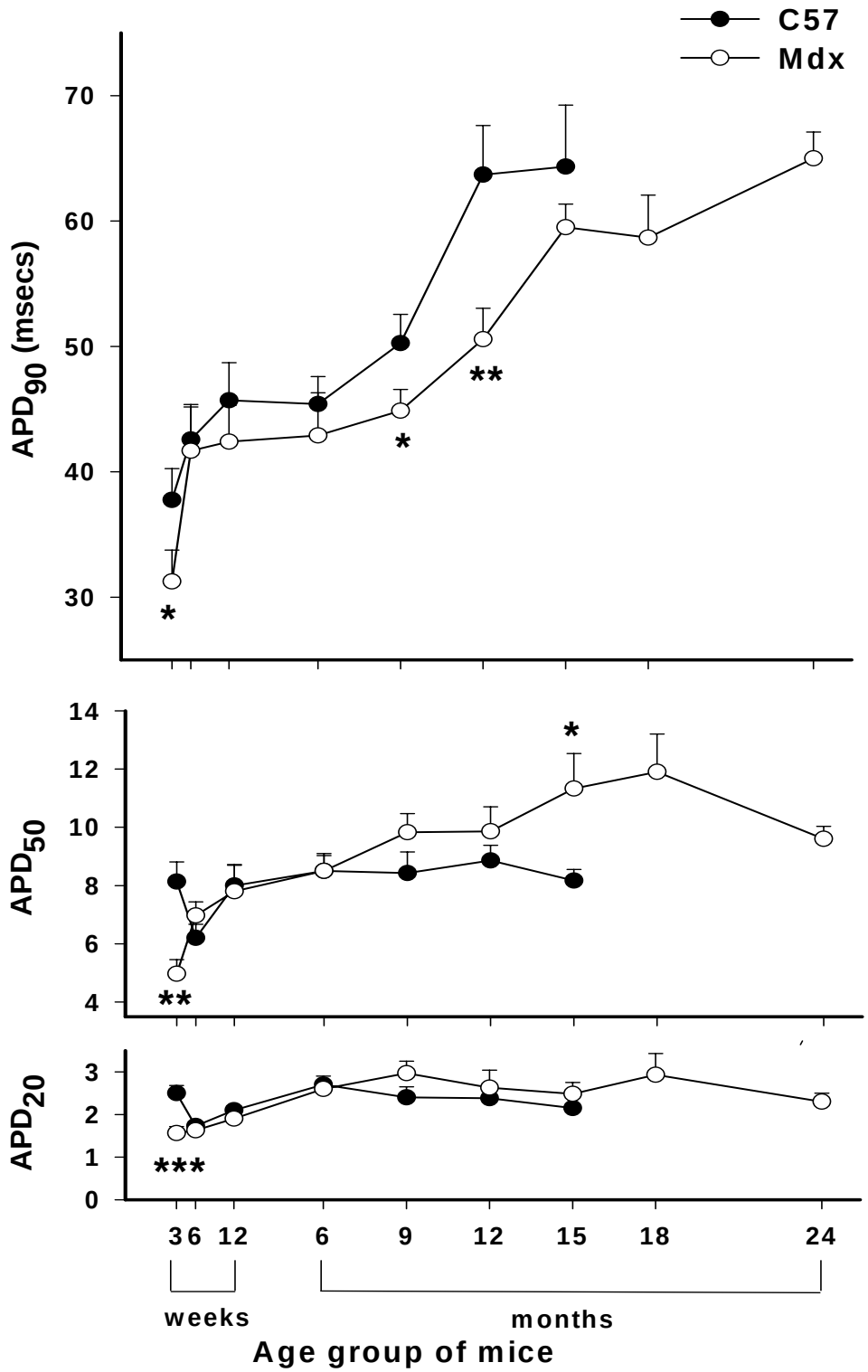


**Fig 2.3** Transmembrane action potential durations (APD) across age ranges of *mdx* (open circles) and control mice (filled circles), measured from left atria. APD $_{20,50,90}$ represents 20%, 50% and 90% repolarisation time. *n*=7-8 per strain/age group. **P<0.01, *P<0.05

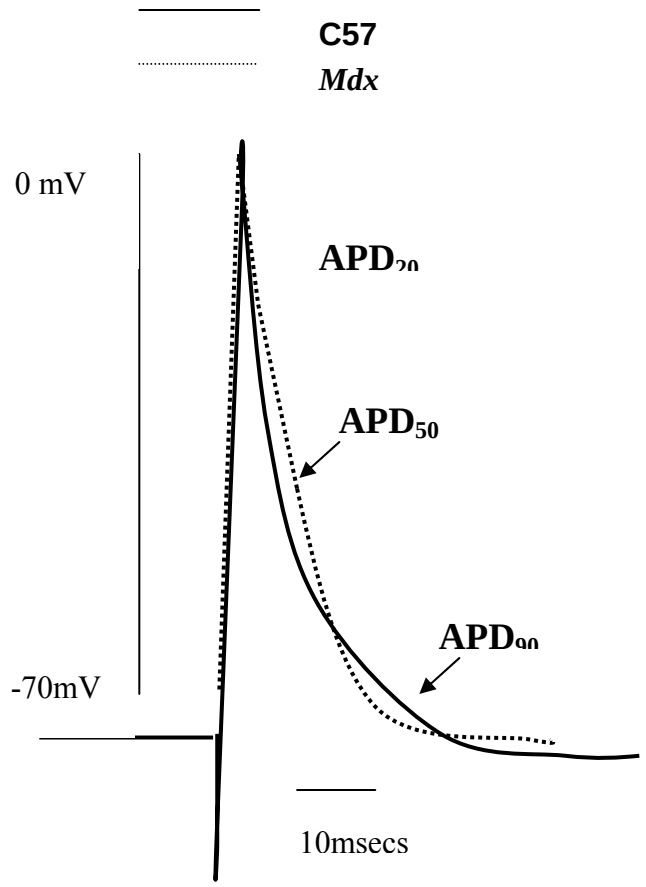


**Fig 2.4** Action Potential waveforms in aged (15 month old) *mdx* (broken line) and C57 (solid line). Action potential amplitudes, and resting membrane potentials were the same for both strains, but $APD_{50}$ was prolonged and $APD_{90}$ shorter in dystrophic atria.

2.5.3 Atrial isometric force and calcium induced inotropy

Basal isometric force production was measured at 1.8 mM $CaCl_2$ (Fig 2.5a). Young *mdx* showed reduced basal force compared to controls, which was significant at 3 and 6 weeks, and redeveloping again at 15 months. In the intervening period force production was not different except for 9 months when *C57* showed smaller forces. A CRC to $CaCl_2$ was also determined for each LA (Fig 2.5b).

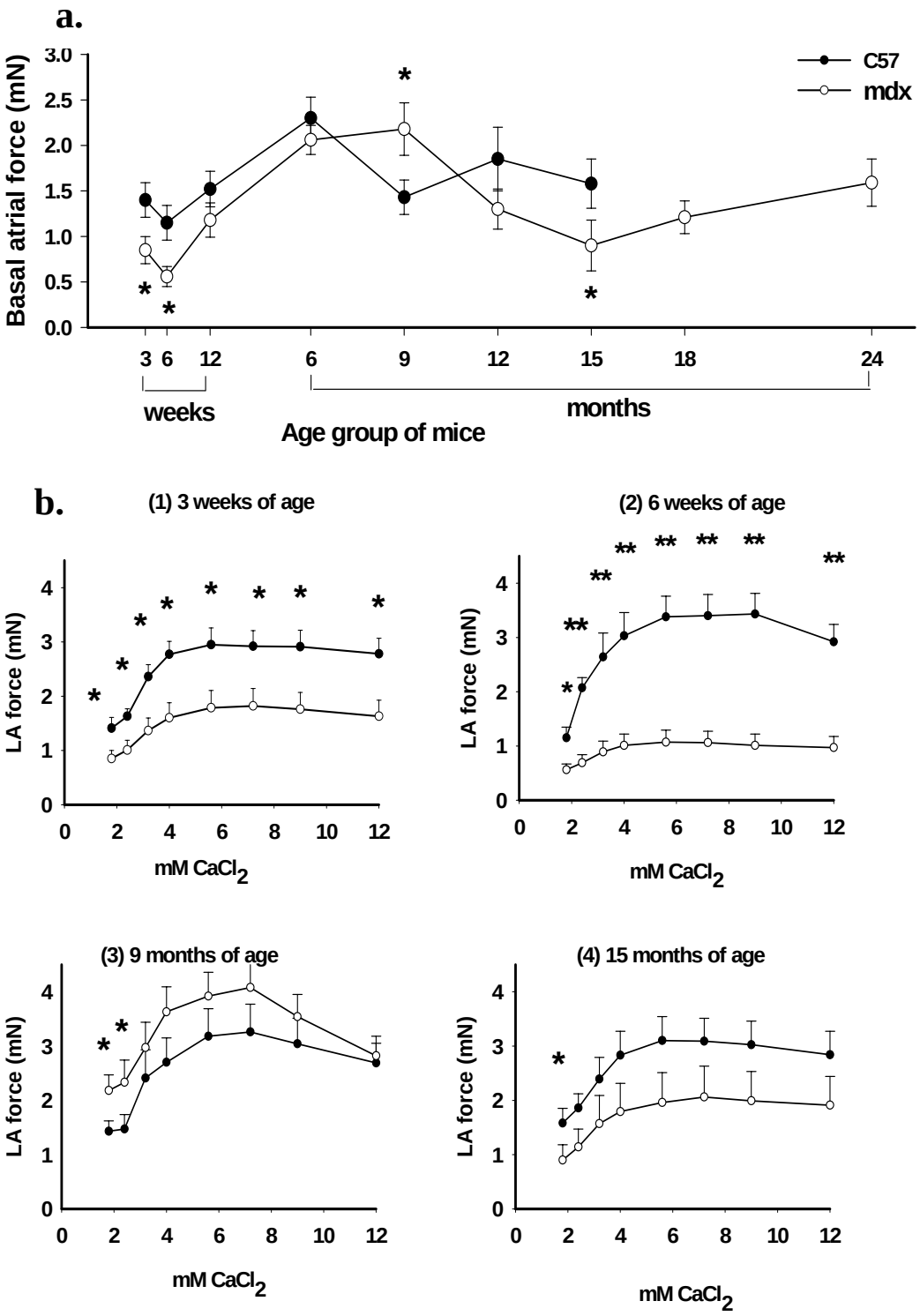


**Fig 2.5** Isometric twitch forces in aging *mdx* (open symbols) and C57 (closed symbols).*n*=7-8 mice per strain/age group.**$P$<0.01,*$P$<0.05 **a.** Basal atrial force of contraction at 1.8mM $CaCl_2$ (mN) **b.** Concentration Response Curves to $CaCl_2$ for 4 ages of mice, from 1.8 mM (basal force) to 12mM $CaCl_2$

There was a significant difference between increases in force of contraction in young *mdx* mice relative to their age-matched controls, with *mdx* showing diminished inotropic responsiveness at 3, 6 and 12 weeks of age, and again at 15 months. As previously noted for basal force generation, 9 month old *mdx* showed increased responsiveness to exogenous calcium. Shapes of CRCs varied, demonstrating a plateau or usually a decline in contractility with maximum calcium loading.

Isometric twitch characteristics varied between mouse strains at ages greater than 12 weeks (Fig 2.6). After this age *mdx* mice showed a prolonged time to 50% relaxation (TR50: $P<0.01$)) and time to 90% relaxation (TR90: $P<0.01$), and mice from 9 months of age showed a delayed time to peak force (TPF: $P<0.05$) also. These parameters increased irrespective of the peak force generated.

**3-12 weeks**

Basal force less

TPF, $TR_{50}$ and $TR_{90}$ similar

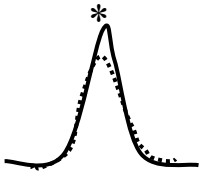


**15 months**

Basal force less

TPF, $TR_{50}$ and $TR_{90}$ prolonged

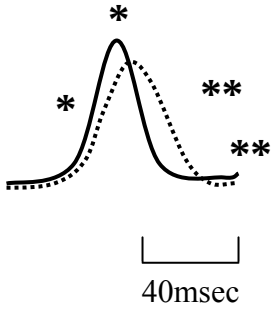


**Fig 2.6** Changes in isometric twitch waveforms with age (C57 solid line, *mdx* dashed line). Young *mdx* mice show similar twitch shape to control mice despite a reduced force, but as *mdx* age time to peak force and time to 50% and 90% relaxation increases. ** $P<0.01$, * $P<0.05$

2.5.4 Collagen measurements

2.5.4a Study 1

LA and LV apex hydroxyproline values across the age ranges are shown in Fig 2.7. There was a 2-4 fold more hydroxyproline (and hence collagen) in atrial compared to ventricular tissue.

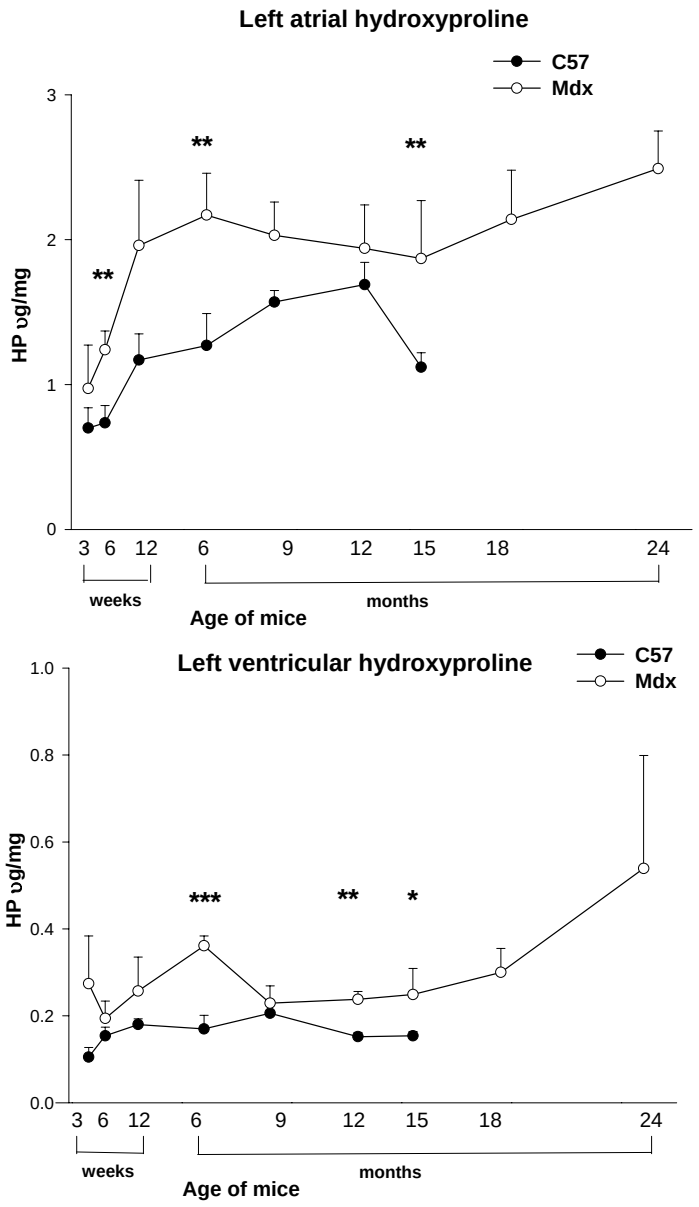


**Fig 2.7** Left atrial and left ventricular hydroxyproline (HP) values for aging mice. There was a tendency for greater fibrosis (measured by HP ) in *mdx* for both tissues, especially after 12 months of age. *n*=7-14 per age per strain. * $P<0.05$, ** $P<0.01$, *** $P<0.001$

The mean ventricular collagen percentage as detected by picrosirius red fluorescence was increased for *mdx* mice, but due to large standard error of means in this strain, this only reached statistical difference at two ages (6 weeks and 15 months) (Fig 2.8a). The box and whiskers plot portrays the trend for increased fibrosis in aging *mdx* hearts, and the spread of data for both strains across their life spans (Fig 2.8b)

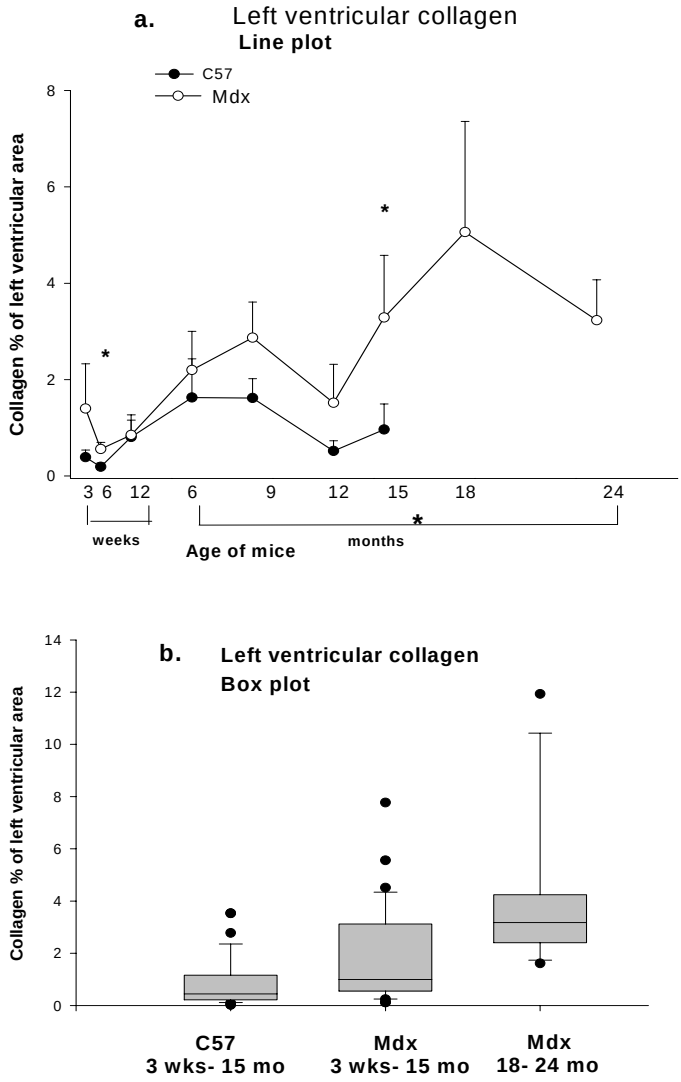


**Fig 2.8a** Left ventricular collagen expressed as percentage of area, as determined by picrosirius red staining and confocal imaging. Results based on 4 sections/heart, *n*= 4 per strain/age. **Fig 2.8b** Box plot using the same data as 3.8a, demonstrating progression of fibrosis in older *mdx* hearts. Median value shown by bar, 1st and 3rd quartiles by box and lowest and highest values for mean LV collagen % of area.
* $P<0.05$

Figure 2.9 shows representative photomicrographs of myocardial sections in young and aged *mdx* and C57 mice. Some *mdx* mice showed marked collagen deposition compared to others of the same strain, or control mice of the same age. This collagen was predominantly localised to interstitial areas in *mdx*, although regions of accumulated perivascular collagen was also noted. An occasional young animal with dramatically increased capsular fibrosis was seen, however this type of collagen was not included in the final analysis due to the sporadic incidence.

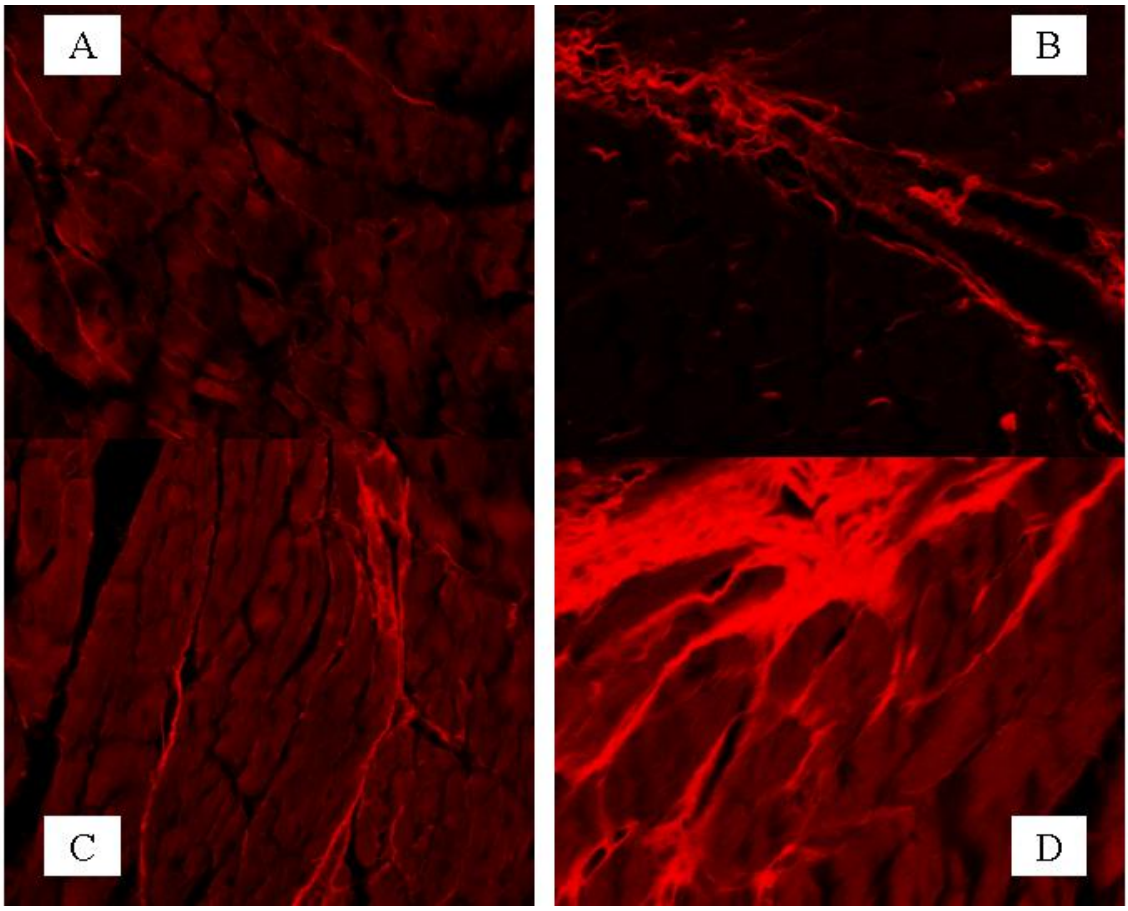


**Fig 2.9** Representative photomicrographs of *mdx* and C57 left ventricular sections cut at 10 microns and stained with picrosirius red. 40X magnification. A.6-week-old C57. Collagen deposition, shown by orange-red staining, is minimal. Collagen averaged over all sections for this animal was 0.13% B. 6-week-old *mdx* (0.69% collagen) C.15-month-old C57 (0.97% collagen). D.15-month-old *mdx*. (7.77% collagen)

2.5.4b Study 2

HP values were greater for *mdx* right atria in young mice (P<0.01), left atria in both young (P<0.05) and old *mdx* (P< 0.001), and left ventricles in young (P<0.05) and old *mdx* (P<0.01). Left ventricular hydroxyproline tended to be 5-10 times less than atrial hydroxyproline. Figure 2.10 shows results of HP assays from atrial and mid ventricular sections.

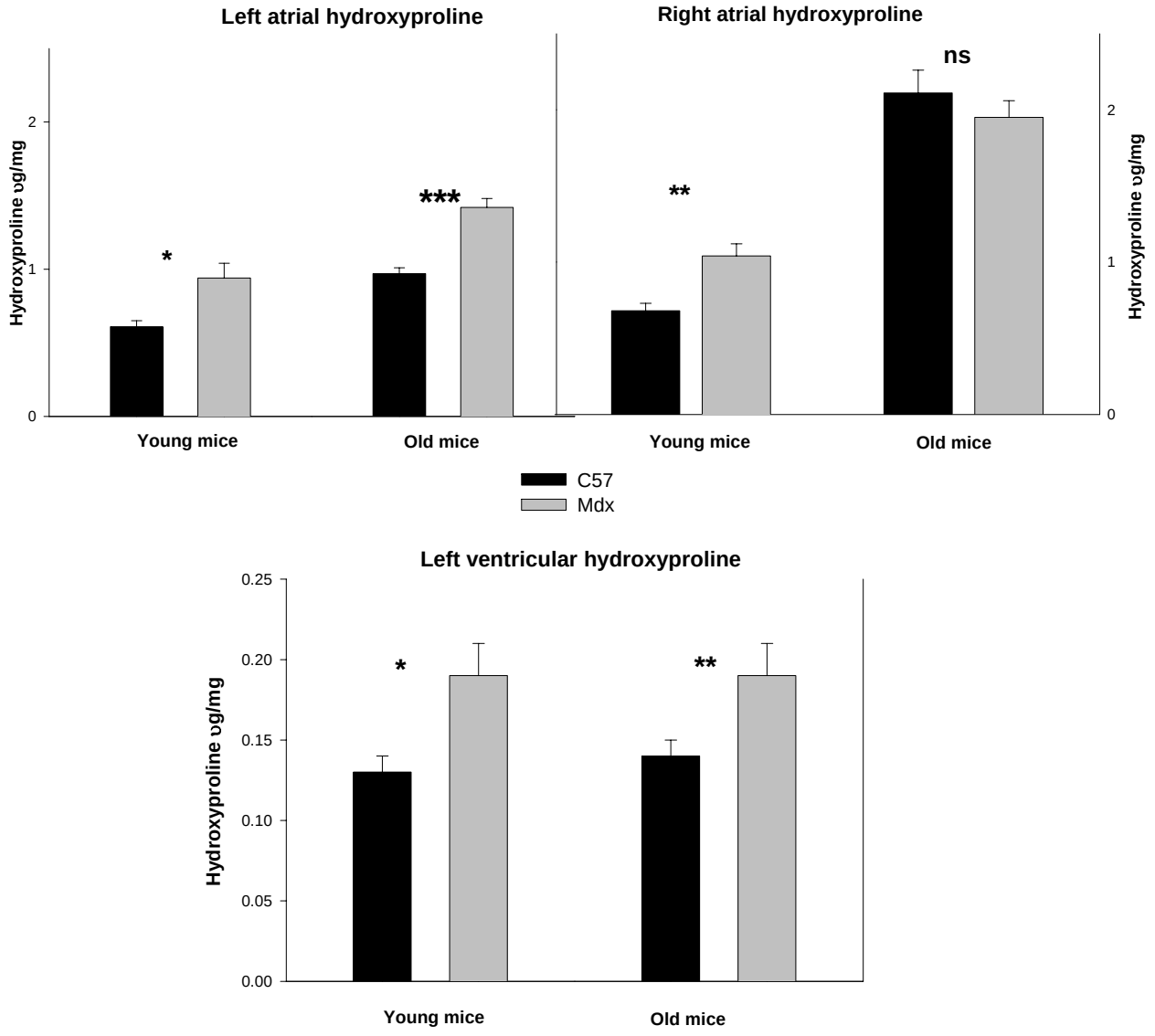


**Fig 2.10** Left atrial, right atrial and left ventricular hydroxyproline (HP) values for young and aged mice. *Mdx* showed greater HP in all tissues except the right atria in old mice. *n*=7-8 per age per strain. * *P*<0.05, ** *P*<0.01, *** *P*<0.001, ns=not significant.

The results of collagen analysis at 3 different levels are shown in Figure 2.11. There was significantly more fibrosis in old compared to young mice of both strains, and *mdx* showed more fibrosis than control mice at both age groups. There was no difference in the extent of fibrosis between levels, with the exception of young *mdx* that had a lower collagen content of the heart apex compared to the mid portion and heart base (P<0.001).

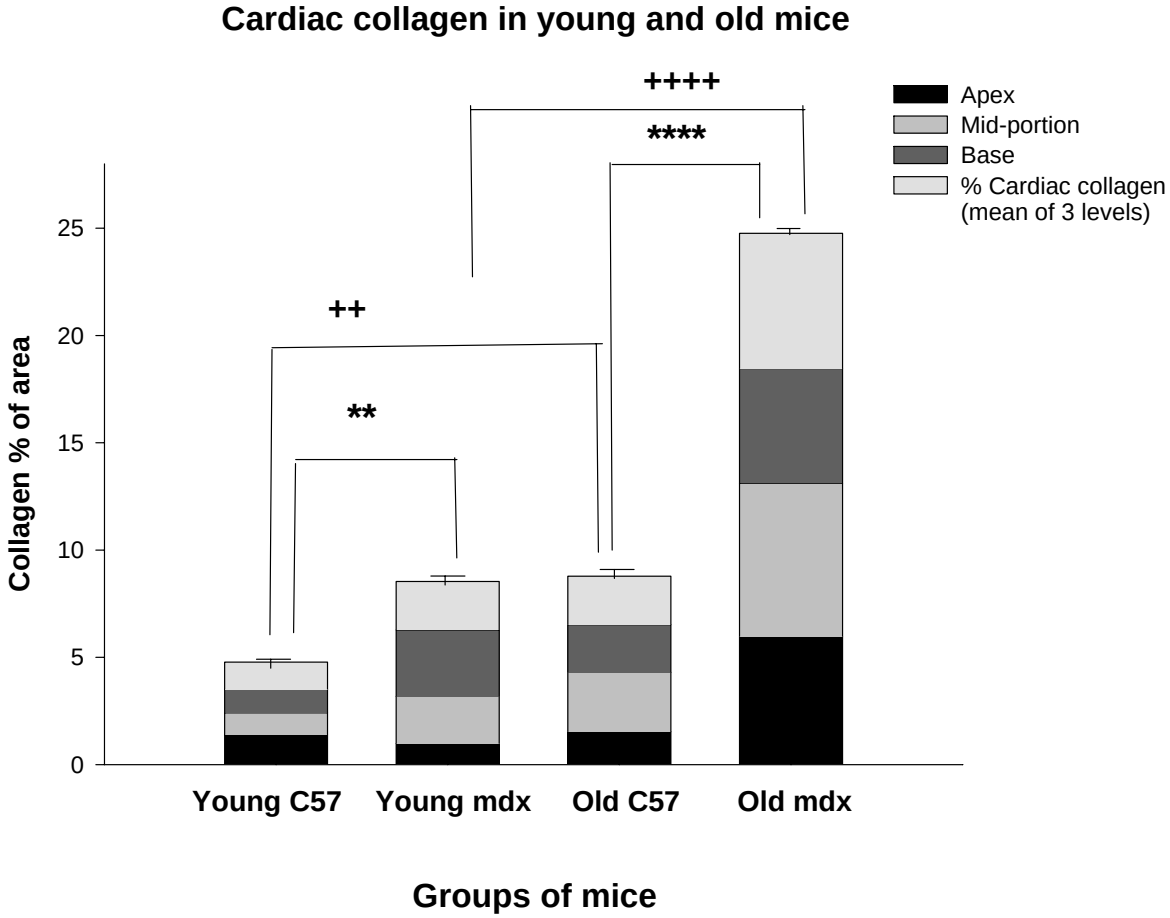


**Fig 2.11** Cardiac collagen in young (6-8 week old) and old 15-17 month old *mdx* and control mice. Interstitial collagen as a percentage of total area was averaged from 4 views at 3 different levels of each heart (apex, mid portion and base). In addition, averages of the 3 levels is shown as the top stack (with error bars corresponding to this mean value only). Collagen increased significantly with age in both strains, but the magnitude of increase was greater for *mdx* mice. *Mdx* had significantly more cardiac collagen compared to age-matched control mice. *n*=7-8 mice/age /strain. *= level of significance between *mdx* and C57 mice, += level of significance between young and old mice of the same strain.

Examples of picrosirius red stained heart samples are shown in Figure 2.12, and Figure 2.13.

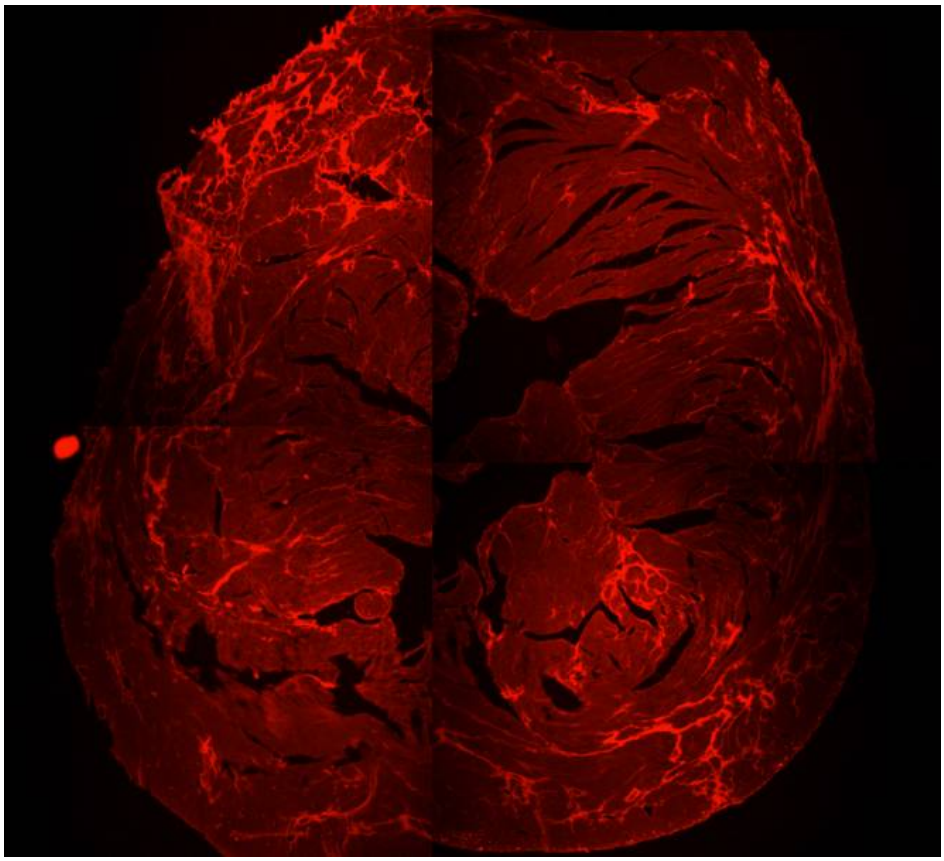

**Fig 2.12** Photomicrograph of a heart apex from a 17-month-old *mdx* mouse (montage of 4x magnification epifluorescent images). Picrosirius staining, representing interstitial collagen, is seen within many regions of this *mdx* heart, however it was also common to find a patchy distribution with dense collagen deposition in only one or two areas. There appeared to be no specific predilection site for fibrosis in *mdx* cardiac muscle, unlike the regional fibrosis seen in hearts from boys with Duchenne Muscular Dystrophy.

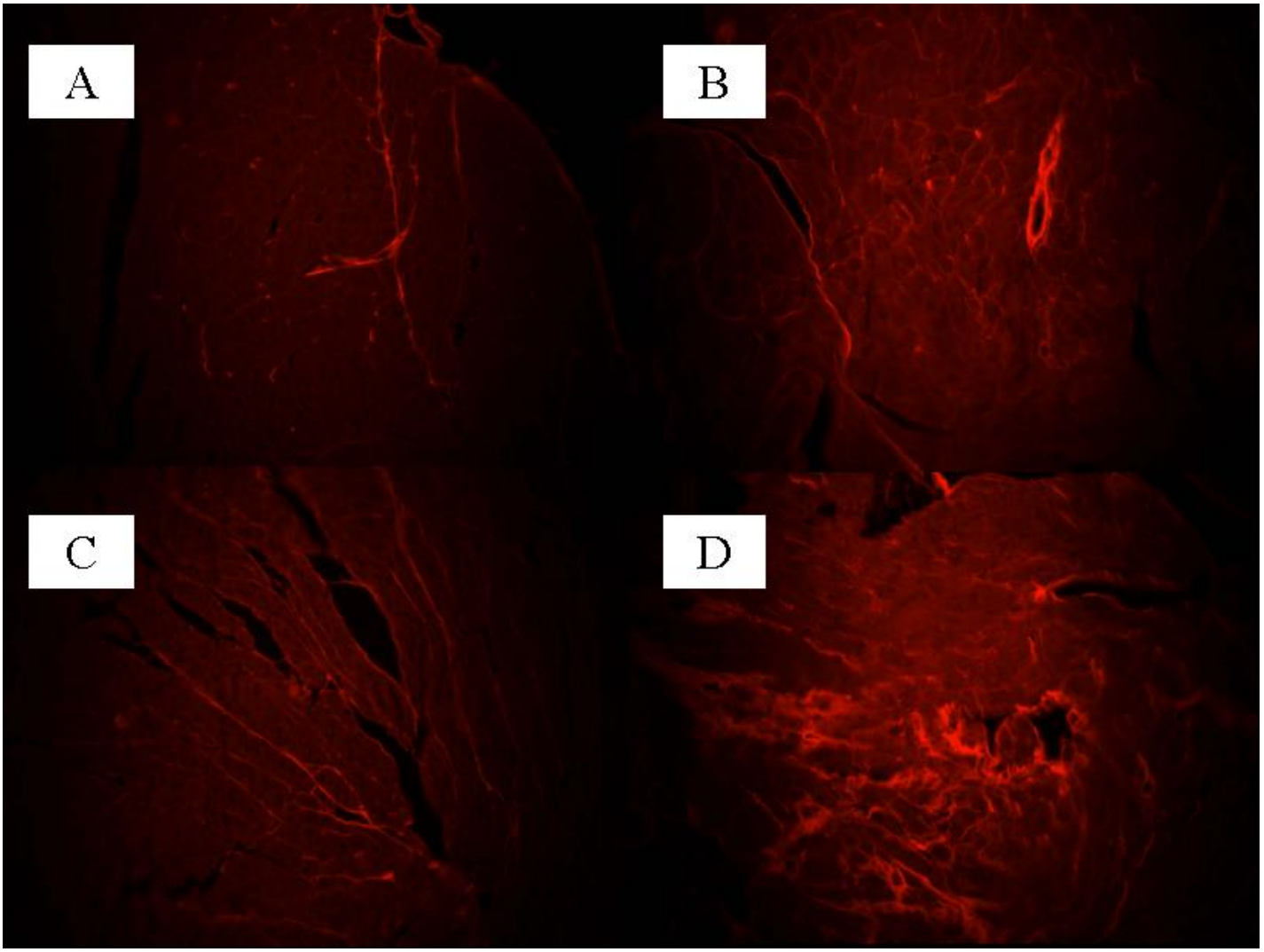


**Fig 2.13** Fibrosis in *mdx* and control mice heart, with images from mid sections of left ventricles. The red staining represents cardiac collagen deposition. A= young (6-8 week old) C57, B= old (17-18 month old ) C57, C= young *mdx*, D= old *mdx*. There was significantly more fibrosis in young and old *mdx* compared to age-matched control hearts. The collagen of older *mdx* was dense and infiltrative, resulting in marked fibre disarray.

## 2.6 Discussion

The comparison of dystrophin-deficient and wild type mice across their lifespan was performed to investigate the progression of cardiac abnormalities with age, hence helping to better define the *mdx* cardiac phenotype, and assess the most appropriate age to use it as a model for DMD. There have been few cardiac studies in this strain providing quantitative data regarding electrophysiology or cardiac fibrosis across the lifespan, despite widespread research into the *mdx* mouse and the high incidence of cardiomyopathy associated with DMD.

In the acute skeletal muscle necrosis phase represented by the 3-week-old mice, *mdx* have greatly reduced body weights compared to controls. There was a lower total heart weight and lung weights at this age ($p<0.05$), although as a proportion of body weight these values were higher, presumably due to the systemic effects of skeletal muscle necrosis causing ill thrift. Body weight curves from older mice agree with other studies, where there is a decline in body weight in older *mdx*, as they again become less active and have more difficulty in obtaining food and water unaided (Pastoret and Sebille, 1995b), although the magnitude of weight loss in the mice in this current study was much less. Differing bodyweights between *mdx* colonies worldwide was highlighted in a recent report, where 3-12 month old *mdx* ranged from 35-50 grams (Murakami *et al.*, 2003). The heaviest *mdx* at this age range bred by the USQ colony was 36.7 grams, with an average of 34.6 ± 0.7g. These differences may be due to husbandry factors, intercurrent disease or perhaps strain variability. As *mdx* mice have been widely used for research since 1984 (Bulfield *et al.*, 1984), and may have been maintained as inbred colonies for long periods, it is plausible that some phenotype diversity between colonies has evolved (with this diversity possibly extending beyond body weight).

Heart weights are reported with organs carefully trimmed of great vessels, pericardium and fat. *Mdx* hearts from 6 weeks of age were smaller than controls with a lowered heart/body weight ratio, in contrast to a former study (Bia *et al.*, 1999). The strain difference in heart weight/body weight ratio at 15 months is a reflection of declining and increasing body weights in *mdx* and C57 respectively, rather than altered cardiac size. Heart weights may be less if there is considerable wall thinning such as dilated cardiomyopathy, however there was no gross evidence

of either hypertrophy or individual chamber dilation. Recent echocardiograph experiments suggest that dilated cardiomyopathy does occur in *mdx* at 42 weeks of age, resulting in increased LV end diastolic and end systolic dimensions and reduced fractional shortening (Quinlan *et al*., 2004).

Lung/body weight ratios are used as a measure of pulmonary congestion, and the lowered ratios in *mdx* indicate that congestive heart failure is not a feature.

There is a shortening of $APD_{90}$ in *mdx* left atria compared to controls. A previous study measured shorter APDs from ventricular cells in *mdx* older than 6 months, and in dystrophic canine (*xmd*) epicardial atrial and ventricular cells (Pacioretty *et al.*, 1992). The genesis of the shorter potential may result from dystrophin's role in receptor/channel localisation. Previous work suggests that the actin-based cytoskeleton is implicated in regulation of both voltage- and ligand–gated ion channels such as L-type $Ca^{2+}$ channels (Sadeghi *et al.*, 2002). In the mouse the transient outward K current ($I_{to}$) has a prominent role in repolarisation, and an enhancement of this current will lead to more rapid repolarisation and shorter duration of electrical potential. The longer $APD_{50}$ at 15 months of age is also noteworthy, with possible mechanisms including increased $I_{Ca}$ or delayed inactivation (as suggested by Sadeghi *et al.*, 2002)

It is difficult to draw conclusions about ventricular repolarisation from *mdx* ECG data reported in the literature. Murine T wave terminations and hence QT intervals are not always readily identifiable (Danik *et al.*, 2002). This is highlighted by 3 studies in *mdx*: in one the QTc was shorter in conscious 10-12 week old mice (C57: 61.6±1.5ms; *mdx*: 55.5±0.5msecs, $P<0.05$) (Chu *et al*., 2002), another found longer durations in similarly aged mice anaesthetised with xylazine-ketamine (C57: 50msecs; *mdx*: 70 msecs, $P<0.003$) (Sadeghi *et al*., 2002), and a third study reported no difference in 2, 6 and 12 month old mice anaesthetised with Hypnorm-Hypnovel (QT stated as 24msecs in both strains) (Bia *et al*., 1999). These discrepancies may be due to drug effects or methodology and could be clarified with telemetry studies, plus isolated and *in vivo* ventricular action potential experiments. In patients with DMD QT dispersion is greater (ie the range between minimum and maximum QT intervals, reflecting regional variations in ventricular recovery), however the minimum QTs were significantly less than normal subjects, indicating shorter electrical repolarisation (Yotsukura *et al.*, 1999).

*Mdx* hearts show reduced contractility compared to control mice at most, but not all, ages studied. This is the first report showing that at specific ages *mdx* isolated atria are capable of generating equivalent forces as C57 under the same conditions and has been previously observed in our laboratory in other groups of 6-12 month old mice (unpublished data). These results are contrary to patients with DMD, who show deteriorating heart function with time, while in *mdx* mice a progression of pathological changes in skeletal muscle occurs also with age, albeit to a milder degree than the acute necrosis period around weaning age (Pastoret and Sebille, 1995b; Lynch *et al*., 2001; Hayes and Williams, 1998).

It is clear that young mice represented in this study by the 3 and 6-week-old groups, have compromised cardiac function. Basal forces are lower, and responsiveness to exogenous $Ca^{2+}$ is blunted and in addition each level of repolarisation ($APD_{20,\ 50\ and\ 90}$) is significantly shortened in the 3-week-old group. Other reports using 12 week old atria show evidence for differing force-frequency relationships, development of diastolic contracture, irregular contractile activity and a lowered efficacy to $CaCl_2$ (Sapp *et al*., 1996; Lu and Hoey, 2000). This weakness might be intrinsic to dystrophic cardiac muscle, due to secondary phenomena, or resulting from a combination of factors. Dystrophic cardiomyocytes have higher intracellular calcium, which initiates proteolysis and consequently tissue necrosis, which could affect contractility (Alloatti *et al.*, 1995). Both *mdx* and DMD myocytes lack neuronal nitric oxide synthase (nNOS), which is thought to contribute to abnormal muscle function and incomplete myofibre regeneration (Brenman *et al.*, 1995a; Chao *et al.*, 1996). Young *mdx* undergoing generalised and severe muscle necrosis may be under considerable stress, and were shown to have a significantly lower metabolic rate and food consumption to controls (Dupont-Versteegden *et al.*, 1994a). It is feasible that a period of relative malnutrition and the existence of widespread inflammatory processes resulting from necrosis may exacerbate cardiac dysfunction, but whether animals then come out of this period with upregulated utrophin or adaptive responses to the calcium overload for a time, or if compensatory myocyte regeneration occurs is only speculative. Absences of dystrophin (and hence effective dystrophin-glycoprotein complexes) render cardiomyocytes more susceptible to mechanical stresses (Danialou *et al.*, 2001a; Kamogawa *et al.*, 2001). There is consensus from recent studies in young mice (8-

12 weeks) that *mdx* have relatively normal cardiac function and mild histopathology under baseline conditions, and mechanical stress induced via aortic banding (Danialou et al., 2001a); (Kamogawa et al., 2001), exercise (Nakamura *et al*., 2002) or pharmacological means such as isoprenaline or dobutamine (Yue et al., 2004);(Quinlan et al., 2004), is necessary to produce significant functional or histological changes. .

Older mice (>15 months in this current study) show deteriorating atrial function, increased fibrosis, and altered twitch morphology, suggesting progressive pathology at the myocyte and organ level as *mdx* age. A recent echocardiographic study did not show differences in chamber dimensions or fractional shortening in *mdx* and control mice until they reached 42 weeks of age (Quinlan *et al*., 2004).

The apparent paradox of shorter $APD_{90}$ and longer contractile rise and relaxation times implies a level of dissociation between the electrical events occurring within the cardiac cell and functioning of the contractile machinery. The alteration in relaxation and contraction times appears to occur in an age-dependant manner, being normal in young mice and greater from 6 months onwards in this study and at 12 weeks in another performed at 25$^{o}$C (which slows contractile kinetics) (Sapp *et al*., 1996). Raised intracellular calcium has been shown to abolish excitation-contraction coupling in isolated skeletal muscles in rat and toad (Lamb *et al.*, 1995). In addition *mdx* extensor digitorum longus muscles, with an inherent intracellular calcium elevation, also displays these properties (De Luca *et al.*, 2001). There is an interplay of events determining lusiotropy, including dissociation of calcium from actin-myosin cross bridges, reuptake of calcium by the sarcoplasmic reticulum and calcium extrusion which may be affected in dystrophic cardiomyocytes.

Hydroxyproline values from left atria and left ventricular apex samples indicate collagen accumulation begins at a young age in *mdx* mice. The LV HP measurements in the first study do not suggest marked fibrosis in dystrophin deficient hearts, but this may be a methodological problem rather than a reflection of true values. A total assay volume of 2 mL precluded use of more than 20 mg of tissue and, because LV was also stored for confocal microscopy, only the tip of the apex was utilised. In the second study samples were taken from mid portions of the heart, and values were perhaps more representative. Right atria were also included

in this study, with HP significantly greater in young, but not old, *mdx* compared to control right atria. The reason for this is unknown, however this structure usually has a dense collagen network, commensurate with its structural and conducting function and fibrosis may progress in aging normal and dystrophic mice.

There was variation in collagen measured by picrosirius red staining and confocal microscopy (Study 1), with large standard error of means for dystrophic, but not for control hearts. This phenomenon also occurred in another study, where 3 times as many dystrophic mice were analysed compared to control mice, yet large standard errors were noted in *mdx* only (Quinlan *et al*., 2004). There was no perceived benefit in using confocal microscopy in this series of experiments, particularly as the number of scans was small (3), and given the added costs of this technique. In Study 2 improvements included the use of more mice, analysing 3 levels of the heart instead of only one and ensuring analysis fairly included non fibrotic as well as fibrotic regions. Fibrosis may not occur equally in all *mdx* hearts, and this is supported by other studies in *mdx* (Lefaucheur *et al*., 1995) and boys with DMD. Although the magnitude of fibrosis (up to 8-10%) is less in *mdx* mice compared to DMD patients, it could still impact on contractile function and electrical impulse propagation in affected animals.

There were several limitations to this study. There were no age matched control mice available to enable valid comparisons of functional and electrophysiology data at 18 and 24 months. Atrial contractile and electrophysiological data may not be commensurate with ventricular function, however isolated left atria were used in order to obtain sufficient statistical results in mice of body weights ranging from 6 to 39 grams. Atrial preparations have been used previously to demonstrate altered contractile function in *mdx* mice (Alloatti *et al*., 1995), and it is known that multifocal dystrophic involvement occurs in all four heart chambers of boys with DMD (Sanyal *et al.*, 1978; Sanyal and Johnson, 1982), and was evident from increased ventricular and atrial collagen in this study. Mouse trabeculae or papillary muscles have a high frequency (~75%) of geometrically unsuitable preparations for working muscle experiments (Gao *et al.*, 1999; Kogler *et al.*, 2001), and it is our laboratory's experience that *mdx* papillary muscle preparations undergo contracture more readily than control mice, presumably as a consequence of their high

intracellular calcium (see Appendix A for details regarding ventricular experiments in *mdx*).

. There have been arguments that the *mdx* is a poor model of cardiomyopathy (Grady *et al.*, 1997) (Megeney *et al*., 1999), however there is evidence from this current investigation, and other previously published work, that significant dystrophic changes do occur in *mdx* hearts which can lead to pathophysiological events not identical with, but similar to, the cardiomyopathy of DMD.

This study concludes that particular ages of *mdx* may be more useful than others for cardiac experiments. The young mouse less than 6 weeks old, undergoing or recovering from widespread muscle necrosis, shows cardiac contractile dysfunction. Mice older than 15 months of age demonstrate altered twitch properties, deterioration in contractile function and fibrosis indicative of ongoing pathology. The inherent dystrophic changes in dystrophin-deficient cardiomyocytes, such as altered calcium metabolism, cellular electrophysiological alterations and nNOS deficiency may be responsible for these changes. A shortened $APD_{90}$ and hence refractory period, in association with other features of dystrophic cardiac cells such as increased intracellular calcium, necrosis and fibrosis can potentially enhance the development of arrhythmias, which are evident in many boys with DMD. Electrophysiological studies such as the transmembrane action potential measurements detailed here, patch clamping or monophasic action potential studies as performed in other murine models of cardiomyopathy are important in understanding electrophysiological disturbances at cell, tissue and organ level.

# CHAPTER 3. THE AGING *MDX* MOUSE: DIAPHRAGM FUNCTION AND FIBROSIS

## 3.1 Introduction

The landmark study by Stedman *et al* was the first to document the severe histological changes in *mdx* diaphragm compared to the control strain, and the concurrent functional deficits of isolated diaphragm strips in organ bath experiments (Stedman *et al.*, 1991). The discovery of a similar pattern of degeneration, fibrosis and severe functional deficits comparable to DMD limb muscles has since extended the application of the *mdx* mouse as an animal model of human disease. These authors compared diaphragm muscle by examining them histologically at two ages (6 and 16 months), by using hydroxyproline analysis as a measure of collagen content (in mice from 12-18 months of age), and by determining functional properties (18-month-old mice). At 6 months of age there was wide variation in myofibre size and architecture, with evidence of continued necrosis and connective tissue proliferation. By 16 months of age they noted extensive myofibre loss and replacement by fibrous tissue in diaphragms from *mdx* compared to C57 mice. Older *mdx* diaphragm strips demonstrated reductions of strength to 13.5% of the levels of control mice, in addition to reduced elasticity, twitch speed and fibre length. Figure 4.1 shows representative H & E stained sections from 18-month-old *mdx* and control mice (sections prepared by author).

A range of further studies examined contractility at 6 weeks, 4 months, 6 months, 8 months, 9 months, 10-13 months, 22-24 months and fibrosis (by hydroxyproline analysis or histological stains) at 3 months, 4 months, 6 months, and 8 months (Petrof *et al.*, 1993b; Dupont-Versteegden et al., 1994b); (Hartel *et al.*, 2001); (Krupnick *et al.*, 2003; Coirault *et al.*, 2003; Coirault *et al.*, 1999; Lynch *et al.*, 1997; Lynch *et al.*, 2001; Gregorevic *et al.*, 2002). However no single study has investigated these parameters across most of the lifespan of *mdx* mice.

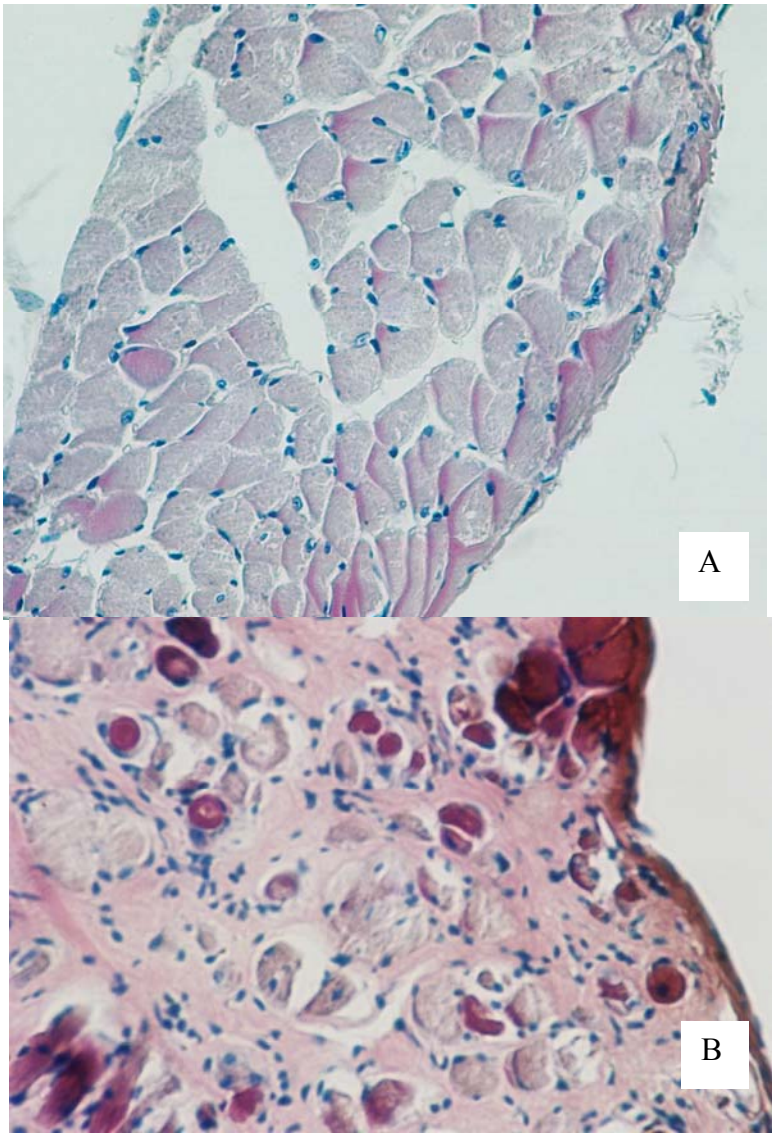


**Fig 3.1** H&E stained diaphragm sections from A) 18-month-old control mouse and B) 18-month old *mdx*. Dystrophic features of collagen accumulation, inflammatory cell infiltration, central nucleation and wide variation in cell size are apparent in the *mdx* diaphragm. (20x magnification)

A lowered threshold of work-induced injury was postulated as a cause of the distinct pattern of dystrophic changes in *mdx* diaphragm muscles (Stedman *et al*., 1991). This was supported by findings of similar but less severe histological changes in the accessory muscles of respiration, which, like the diaphragm, have a constant obligatory workload. Also of interest is the satellite cell reserve within the

diaphragm suggesting that regeneration of myocytes within this organ still occurs, even in old *mdx*. Further studies have shown 70-80% of limb muscles of *mdx* mice have central nuclei, compared to 35% in diaphragm muscle, and that fibre diameter remains smaller in *mdx* diaphragms compared to controls (Louboutin *et al.*, 1993). It has been suggested that the crural diaphragm is subject to more strain, fatigue or contraction induced injury than the costal diaphragm, possibly due to a higher workload and mechanical strain of these fibres in quadrupedal animal (Anderson *et al.*, 1998).

In contrast, evidence is accumulating against the work-overload hypothesis. The decrease in diaphragm strength in *mdx* mice is more pronounced than that predicted by the area of fibrosis alone (Petrof *et al*., 1993b, Lynch *et al.*, 1997), indicative of alternate causes of diaphragm weakness. There is a strong linear relationship between maximum tetanic forces and total number of cross bridges per square millimetre, with *mdx* diaphragm having a 48% reduction in cross bridges (Coirault *et al.*, 1999). There is also evidence that the contractile apparatus of muscle fibres may be intrinsically dysfunctional in *mdx* diaphragms (Coirault *et al*., 1999), even as young as 6 weeks of age when muscle necrosis and fibrosis remain limited (Coirault *et al.*, 2003). These authors found a 37% lower force production in 6-week-old *mdx* mice, despite only 2.8% fibre necrosis and 3.6% collagen surface area occupied. Their conclusions were that *mdx* diaphragm muscle is more prone to degeneration, as a portion of active cross bridges are forced to carry the ventilatory workload. Oxidative damage is a likely contributory factor, with studies showing both a reduction in NO-mediated protection against ischaemia and increased cellular susceptibility to oxidative damage in *mdx* (Disatnik *et al.*, 2000; Rando *et al.*, 1998). Further evidence against the work-overload hypothesis of muscular dystrophy was afforded by tracheal banding experiments, which did not accelerate degeneration in *mdx* diaphragm despite significantly increased inspiratory workloads (Krupnick *et al.*, 2003).

To date, few studies have utilised direct administration of therapeutic agents into *mdx* diaphragm muscle, despite this structure showing the greatest similarity to DMD skeletal muscles, and being a potential treatment paradigm for gene therapies, plasmid or adenovirus delivery, or oligoribonucleotide (AO) administration. Efficient introduction of pure recombinant plasmid DNA into C57BL/6J mice diaphragms was reported (Davis and Jasmin, 1993), and reporter gene delivery has been successful in mouse diaphragms (Liu *et al.*, 2001a; Liu *et al.*, 2001b). It was demonstrated that a controlled release device for Leukaemia Inhibitory Factor (LIF) based on a calcium alginate rod could be sutured to the abdominal surface of the diaphragm to provide LIF for a 3-month period (Austin *et al.*, 2000). These experiments utilised normal mice or young (3 month old) *mdx* mice and it is not clear from these studies whether the significant collagen deposition present in *mdx* diaphragms limits the use of direct injections in this strain. Timing of administration may be critical, with a balance sought between an age of mouse with a large enough body size to make surgery and diaphragm injections practicable, and prior to the period of accelerating degenerative changes and fibrosis, which may limit the spread of injectate within the muscle, and potential success of dystrophin restorative therapies.

## 3.2 Aims

There were 4 aims of the study: a) to gain experience in the dissection and mounting of mouse diaphragm strips in organ bath experiments, b) to establish and optimise hydroxyproline assays for diaphragm tissue within our laboratory, c) to determine the best age range for experiments involving direct administration of AOs into mouse diaphragm muscles, using both functional data and measures of fibrosis and d) to develop expertise in sub-epimyseal diaphragm inoculations in mice.

## 3.3 Methods

### 3.3.1 Mouse numbers and grouping

The same animals used for cardiac studies (Chapter 3) were utilised for diaphragm contractility experiments. There were 7-8 mice per group, with animals aged 3 weeks, 6 weeks, 12 weeks, 6 months, 9 months, 12 months, 15 months, 18 months and 24 months of age (total 105 mice). Age matched male C57 and *mdx*

were utilised, except for 12, 18 and 24 months age groups, where only *mdx* mice were available. A total of 10 C57 and *mdx* mice of mixed ages were used for post-mortem practice diaphragm injections, additional to contractility studies. Hydroxyproline analyses were performed on diaphragm strips from 6 or 7 control and *mdx* mice per age group.

### 3.3.2 Organ bath experiments

The organ bath protocol followed was that used in the laboratory at the time, utilising existing equipment.

Mice were anaesthetised with 50 mg/kg tiletamine/zolazepam (Zoletil, Virbac Australia)) by subcutaneous injection. The diaphragm and surrounding ribs were removed *en bloc* and placed in ice cold Krebs solution, bubbled with 95% $O_2$ and 5% $CO_2$. Strips of diaphragm muscle were prepared for hydroxyproline analysis by snap freezing in liquid nitrogen before storing at –80$^{o}$C. A single diaphragm strip 2-3 mm wide was excised from the right hemidiaphragm for organ bath studies. These were anchored by means of cotton thread to a fixed peg at the rib end, and attached to a force transducer at the tendon end, and placed within a 25ml glass organ bath maintained at 23$^{o}$C. Tissues were stimulated via a Grass S48 stimulator (W. Warwick, RI, USA). Data was collected and analysed using Chart 4.1.1 software on an iMac computer. A square pulse of 0.2 ms duration was dispersed via two platinum plate electrodes positioned at each side of the muscle. Preload was set at 5 mN, frequency of tetanic stimulation at 120 Hz and voltage at 10 volts for all muscle strips.

Reported data was the average of 3 individual single twitch or tetanic stimulations per muscle strip to give an overall mean for that mouse. A fatigue protocol (one tetanic stimulation every 5 secs for 5 minutes) was also performed. Muscles were measured using a digital micrometer, blotted for 3 secs then weighed prior to storage at –80$^{o}$C for subsequent hydroxyproline assays. Cross-sectional area (CSA) and normalisation of forces was calculated as described previously (Lynch *et al*., 2001), where CSA equals weight of tissue divided by length multiplied by 1.06 (the density of mammalian skeletal muscle).

Organ bath protocols were changed subsequently (including more stringent optimisation of preload, voltage and frequency for each muscle preparation), with a

preamplifier to increase stimulation current intensity added to the experimental apparatus. Subsequent diaphragm experiments resulted in greater peak force values for these reasons (see Chapters 5- 7), however these early results are included because they offer useful functional information for aging mice, complimenting hydroxyproline values at the same age groups.

### 3.3.3 Quantitation of collagen

Hydroxyproline content was used as a measure of collagen. Tissues were thawed then hydrolysed in sealed tubes with 6M HCl overnight at 110 $^{o}$C. The samples were dried to entirety using filtered air under pressure and heat (50 $^{o}$C). The rest of the protocol has been described previously (Stegemann and Stalder, 1967), with details of the assay adjusted to a 2 mL total volume provided in Appendix A. Values are expressed as gHP μ/mg tissue wet weight.

### 3.3.4 Diaphragm injection technique

Anaesthesia was induced with 70-mg/kg thiopentone sodium (Nembutal,Boerhinger Ingelheim Australia) given i.p. Hair was clipped from the ventral abdomen of the mouse and a midline laparotomy performed from the xiphisternum caudally. Exposure of the abdominal surface of the diaphragm was achieved by placing a silk suture through the abdominal musculature on each side, then attaching a pair of haemostats to the ends of the threads and holding them away from the body. Magnification was performed initially with 3x magnification glasses, or later, 7x magnification illuminated lenses (Voroscope). 30 gauge 0.3 mL disposable insulin syringes (Omnican 30, Braun, Australia) were used for the injections, which for practice purposes were a total of 34μL of 0.9% saline and 6 μL histological marking dye (Wak-Chemie Medical, Germany). The needle was inserted with the orifice away from the muscle and as much of the length inserted into the muscle as possible. 4 injections of 10 μL were administered at sites around the diaphragm, two in the right and two in the left hemidiaphragms. Success of the procedure was gauged by the spread of staining in the vicinity of the injection site.

### 3.4 Statistics

Results are expressed as mean ± SEM. Variables were compared between experimental groups using Student's t-tests, assuming equal variances. Differences between groups were considered significant when $P<0.05$.

### 3.5 Results

3.5.1 Morphometry

Figure 3.2 shows group mean body weights of mice used for both the aging heart study (Chapter 3) and for this study. Significant differences were observed at 3 weeks of age, when *mdx* were lighter ($P<0.001$), at 12 weeks old when *mdx* were heavier corresponding to their muscle hypertrophy stage ($P<0.05$) and again at 15 months when *mdx* mice were moving less freely around their cages and weight loss was observed ($P<0.01$). This weight loss in *mdx* continued until the end of the study (24 months of age).

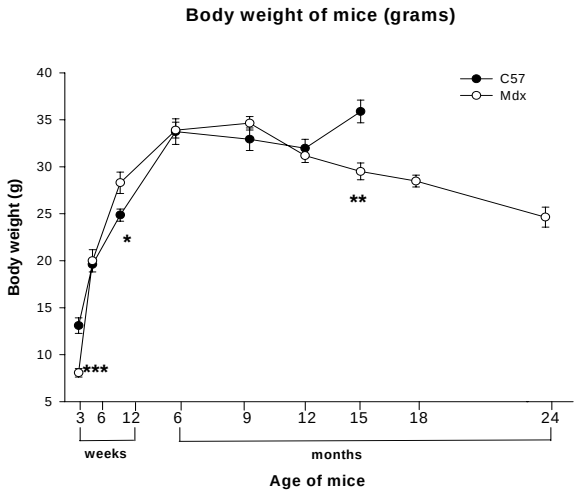


**Fig 3.2** Body weights of aging mice used for diaphragm study and aging heart study. n=7-8 mice per strain per age group, except for 18 months and 24 months when only *mdx* were available. *$P<0.05$, **$P<0.01$, ***$P<0.001$

3.5.2 Diaphragm contractility.

Peak twitch and tetanic forces are shown in Figure 3.3a and b. *Mdx* twitch values were significantly less at 6 weeks and six months *Mdx* tetanus values were similar to control mice at 3, 6 and 12 weeks of age. After this time there was a significant difference between mice strains, with *mdx* having lower values ($P<0.01$). Twitch to tetanus ratios tended to be greater in *mdx* mice compared to controls, showing significance at 6 months of age (C57, 0.18 ± .004; *mdx*, 0.23 ± .02, $P<0.01$) and 15 months of age (C57, 0.19 ± 0.02; *mdx*, 0.29 ± .02, $P<0.01$).
Other twitch characteristics measured including time to peak force (TPF), time for 50% relaxation ($TR_{50}$) and time for 90% relaxation ($TR_{90}$) did not differ significantly between mice strains (data not shown). Percentage fatigue of diaphragm strips was significantly less in *mdx* mice after 9 months of age (C57, 53.49 ± 2.3%; *mdx*, 35.8 ± 5.9%, $P<0.01$), corresponding to the lower tetanic forces achieved in older mice.

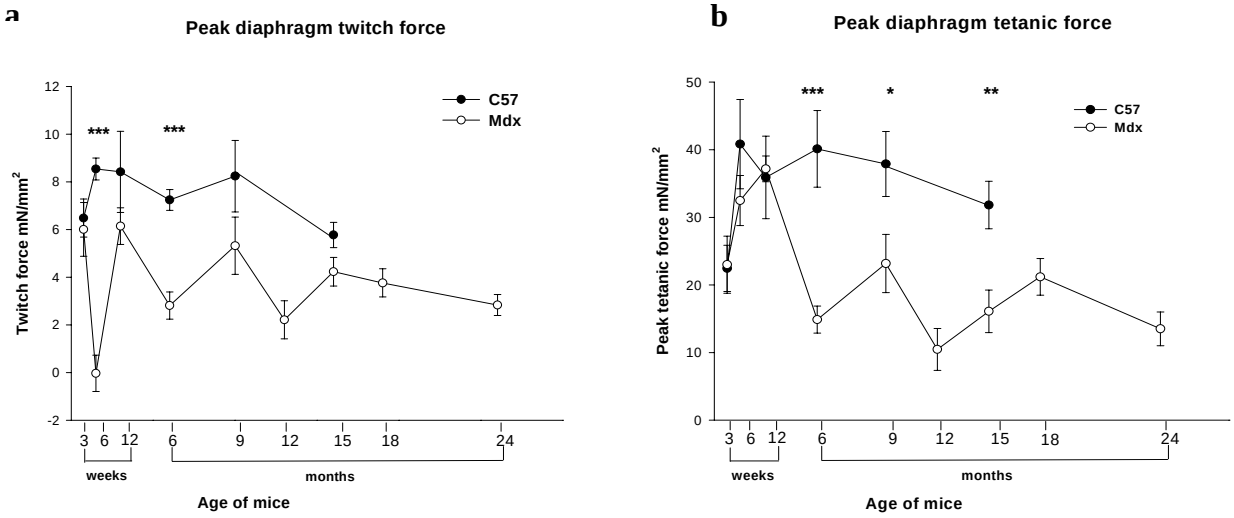


**Fig 3.3a** Peak diaphragm twitch force, normalised to CSA for groups of C57 and *mdx* mice (n= 7-8 mice per strain per age group). There were significant differences between strains at 6 weeks and 6 months of age, with *mdx* showing lower peak twitch forces.

**Fig 3.3b** Peak diaphragm tetanic force normalised to CSA for groups of C57 and *mdx* mice (n= 7-8 mice per strain per age group). Force was similar in young mice (3, 6 and 12 weeks), but became less in *mdx* mice from 6 months of age.

3.5.3 Diaphragm fibrosis

There was a three to four fold increase in HP in old *mdx* mice, compared to young *mdx*. Values tended to remain similar in the age groups of control mice tested. (Figure 3.4)

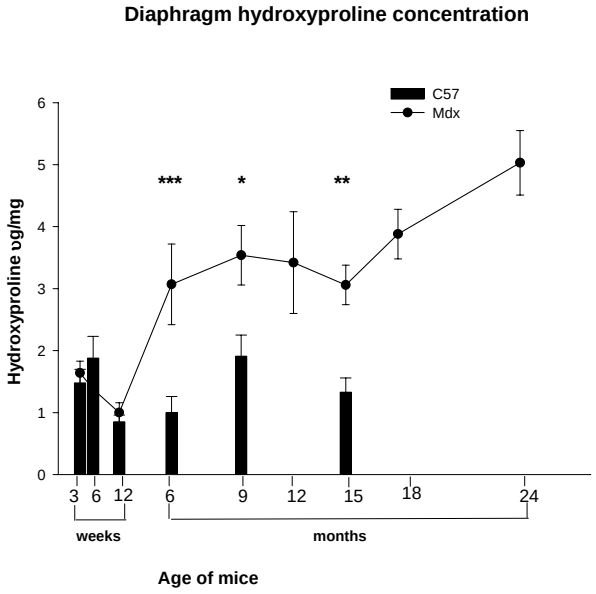


**Fig 3.4** Diaphragm hydroxyproline values, expressed as µg HP/mg tissue wet weight. n=7-8 mice per strain per group. HP values were similar for *mdx* and control mice until 6 months of age, when significant differences were measured. * $P<0.05$, ** $P<0.01$, *** $P<0.001$

### 3.5.4 Diaphragm injections

Young *mdx* mice (< 6 weeks old) and C57 mice of all ages tended to have very thin diaphragm muscles, while older *mdx* had thicker, more opaque muscles that were consequently easier to inject. Success of injections was judged by spread of blue dye in the muscle around the needle tip. This either resulted in a bleb of injectate or sometimes infiltration of dye along the length of muscle fibres, from near the costal margin towards the central tendon. Successful injections were aided by retraction of the costal margin to flatten the diaphragm surface, positioning the mouse on an inclined foam pad to enable the abdominal contents to drop away from the diaphragm, and holding the liver away using gauze swabs and blunt forceps. Occasional injections resulted in blue dye escaping into the thoracic cavity, however with practice correct placement was usually achieved.

## 3.6 Discussion

The *mdx* mouse is a complex model, with differential patterns of dystrophy according to age and the muscles examined. The *mdx* diaphragm is a desirable target for dystrophin restoration strategies because of its severe pathology that begins early and persists throughout the mouse lifespan. There is, however, little available evidence as to the best age to apply such treatments, and only a few references document the use of mouse diaphragm sub-epimysial injections (Davis and Jasmin, 1993; Petrof *et al.*, 1995; Petrof, 1998b)

This present study used the parameters of loss of force production and collagen accumulation as measures of dystrophic pathology. It was hypothesised that success of dystrophin restoring strategies is most likely before significant muscle weakness or fibrosis is present (Chapter 5). Whereas young mice (6 weeks old) have been used for testing of limb injections of AOs (Lu *et al*, 2003), the thinness of diaphragm muscle in control mice and very young *mdx* mice may preclude the efficacy of this procedure until a larger body size is reached.

Organ bath studies of mouse diaphragm muscle are well documented and performed in many laboratories throughout the world, however a review of the literature showed a variation in protocols and peak force values obtained (Stedman

*et al*., 1991; Lynch *et al*., 1997; Coirault *et al*., 1999; Stevens and Faulkner, 2000).

It is essential to optimise procedures within an individual laboratory and for researchers to gain expertise in new experimental techniques. It became apparent that protocols initially in place in our laboratory were resulting in very low force productions (less than 1/3 of those achieved elsewhere), and did not optimise conditions for muscle fibre contractions. Changes for subsequent studies included the careful determination of preload to obtain optimal muscle fibre length ($L_o$) and hence achieve greatest isometric active tension, determination of the frequency resulting in a maximally fused tetanic tension and assessment of optimal stimulus voltage. In addition a preamplifier was added to the experimental apparatus to amplify field stimulation intensity. Unfortunately much of this preliminary experiment was performed before these changes were made, and for comparison sake the rest of the diaphragm preparations were treated similarly. As a consequence maximal force production was considerably underestimated in this series, as tension declines at lengths less than or greater than $L_o$. However, when taken together with hydroxyproline values and information available from published studies, useful conclusions could be still be reached. Figure 3.5 shows the approximate decline in force production with age as well as collagen accumulation.

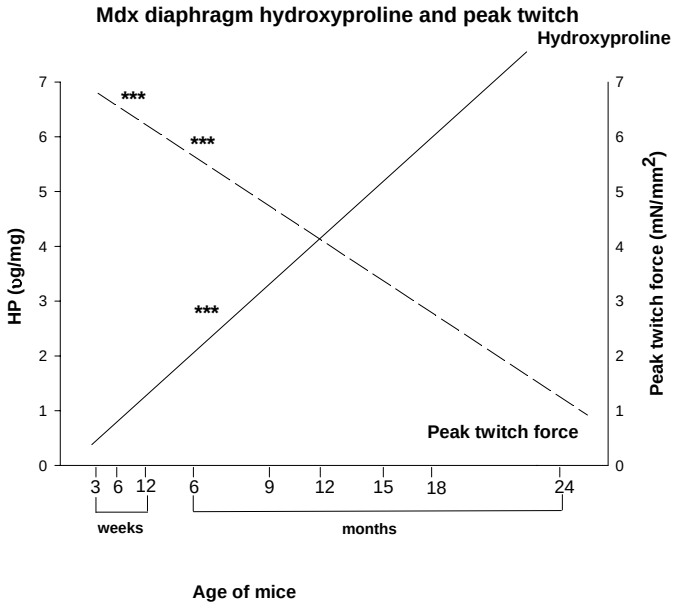


**Fig 3.5** Plot expressing both decline in peak twitch force in aging mdx, compared to increased fibrosis (measured by hydroxyproline analysis). The two lines show averaged values generated by curve fit, and as such represent approximate values only. The asterisks show the age at which significant differences between mdx and control mice for hydroxyproline and twitch force occurred in this study.

It was felt that determination of diaphragm fatigue did not provide useful additional information as muscles showing lower tetanic force production tended to fatigue less (older *mdx* diaphragms). The altered twitch/tetanus ratios could also not be interpreted categorically because of the incorrect optimisation procedures used.

The success of diaphragm injections was cofirmed by visual confirmation. The sites of injections were clearly apparent by the appearance of a raised bleb within the diaphragm musculture. Successful injections occurred infrequently at first, but with repeated practice these injections were possible at four sites in the majority of animals. The dissection of treated diaphragms post mortem also allowed examination and assessment of the spread of dye.

In conclusion this study provided experience in organ bath techniques and highlighted the need for modification and improvements of existing skeletal muscle contractility protocols. Valuable experience in laparotomy and diaphragm injections

in mice was gained. The reliability of hydroxyproline assays as a measure of diaphragm fibrosis was realised. For potential studies employing direct injection of AOs into *mdx* diaphragm muscle it was concluded that such injections should occur well before six months of age, when marked dystrophy is evident. As it was thought that two administrations of AOs four weeks apart were preferential to one injection it was considered that future mice undergo surgery for AO injections at four and five months of age, before sacrifice for organ bath studies, hydroxyproline, histology and Western analysis at six months of age.

# CHAPTER 4. THE AGING *MDX* MOUSE: PROGRESSION OF KYPHOSIS

## 4.1 Introduction

Chest deformity due to scoliosis, kyphosis, lordosis or combined spinal curvatures contribute significantly to the morbidity associated with DMD, and often leads to a restrictive respiratory pattern with diaphragm and inspiratory muscle weakness, ineffective cough mechanisms, mucus plugging of airways and chronic alveolar hypoventilation (Rideau *et al.*, 1981; Seddon and Khan, 2003). Vital capacity (VC) remains normal in patients with neuromuscular disease if respiratory muscle strength is more than 50% of predicted, however when strength is less than this VC becomes diminished to a greater extent than expected (De Troyer *et al.*, 1980; Estenne *et al.*, 1993). This decrease is thought to be associated with a loss of compliance of the chest wall and lungs, with stiffening of ribcage tendons and ligaments and ankylosis of costosternal and thoracovertebral joints (Estenne et al., 1993); (Bach and Kang, 2000). As well as exacerbating respiratory dysfunction in affected boys, kyphoscoliosis negatively impacts on their quality of life in their wheelchair dependant years, with most patients electing surgery for spinal fusion and stabilisation and/or experiencing chronic pain due to poor posture and prolonged sitting (Smith *et al.*, 1989).

The natural course of spinal deformity differs between patients and a classification scheme has been established based on radiographic indices including the Cobb angle, pelvic obliquity, kyphotic index (KI) and sacral angle (Oda *et al.*, 1993). Pulmonary function (as measured by plateau of vital capacity) correlates with the progression of spinal deformity and may be an indicator of the expected progression (Yamashita *et al.*, 2001a; Yamashita *et al.*, 2001b). It has also been suggested that a particular clinical course may correlate with a specific molecular lesion (Hoffman *et al.*, 1989; Hoffman, 1993).

Thoracolumbar kyphosis also occurs in murine models of neuromuscular diseases including the dystrophin deficient (*mdx*) mouse (Lefaucheur *et al.*, 1995), the dystrophin/utrophin deficient (*mdx:utrn*$^{-/-}$) mouse (Grady *et al.*, 1997; Deconinck *et al.*, 1997a) and the kyphoscoliosis (*ky*) mouse (Dickinson and Meikle, 1973; Bridges *et al.*, 1992). Figure 4.1 shows photographs of aged *mdx* and control

mice with skin removed. These images show the muscle atrophy present in old *mdx* mice, and the presence of kyphosis of the thoracolumbar region.

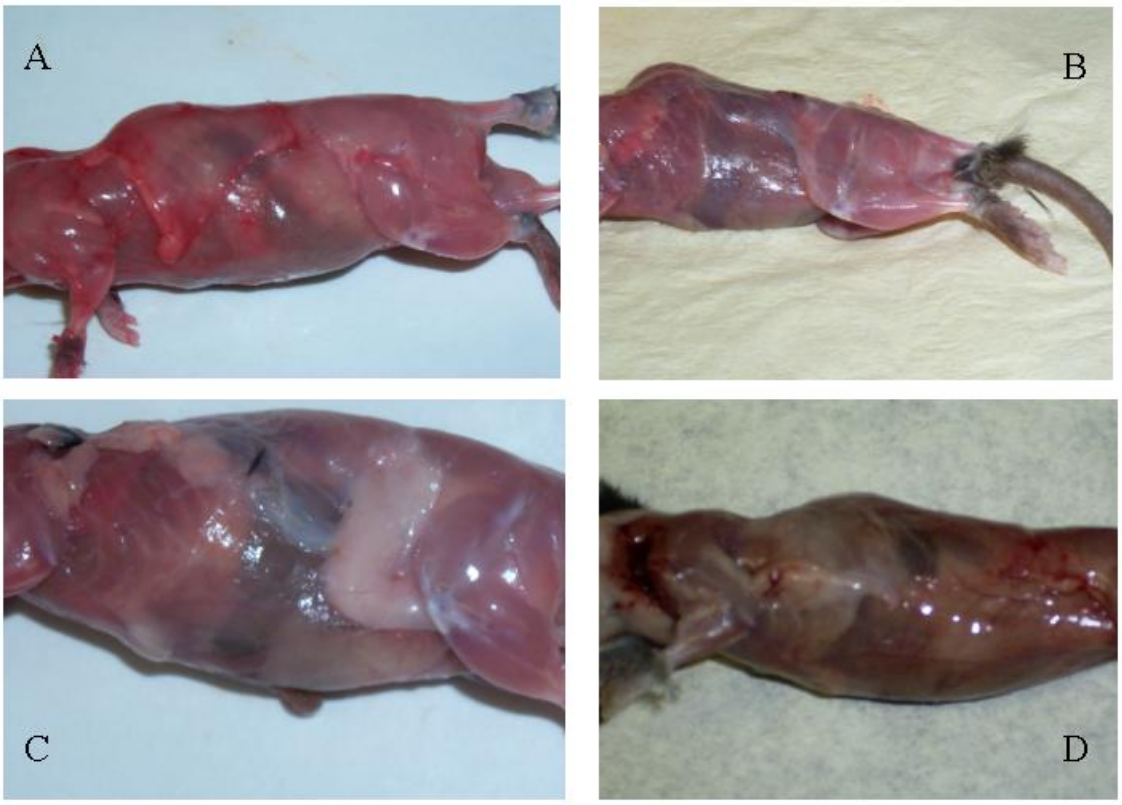


**Fig 4.1** Whole body photographs of A.Young (3mo) *mdx* mouse, B. Aged (22 mo) *mdx*, C. Young C57 mouse and D. Aged C57 mouse. Kyphosis is grossly evident in both strains of mice, but is more pronounced in *mdx.* Also evident is the muscle hypertrophy in young *mdx* mice, and the muscle atrophy and weight loss that occurs with age in this strain.

Although *mdx* diaphragm muscle has been shown to most closely mimic the pathological changes seen in DMD (Stedman *et al*., 1991), there is also histological evidence of necrosis and fibrosis in postural and paraspinal muscles of *mdx* and *mdx:utrn*$^{-/-}$ (Lefaucheur *et al*., 1995; Grady *et al*., 1997; Deconinck *et al*., 1997a). To date limited respiratory studies have been performed in the *mdx* mouse model, however there is recent evidence of significant attenuation of respiratory responses to hypercapnia (a potent ventilatory stimulant) in *mdx* mice compared to control mice, which was thought to be influenced by tumour necrosis factor-α (Gosselin *et al.*, 2003).

## 4.2 Aims

There were three goals in this study: a) Establishment of a novel Kyphotic Index (KI) to quantify the progression of spinal deformity in two groups of aging mice, *mdx* and their aged matched controls. b) Evaluation of contractile function in paraspinal and respiratory muscles (latissimus dorsi muscles and intercostal strips) and comparison to diaphragm muscle as a known standard. The latissimus, a flexor of the brachium, was chosen because of its origin from T8-T12 and the thoracolumbar fascia in the region kyphosis occurs, and due to its well documented contractile properties in other species (James *et al.*, 1997). Functional parameters of intercostal muscles have been reported previously in larger species, but not in mice, therefore intercostal strips comprising four rib sections and adjoining intercostal muscles (external and internal intercostals) were utilised. c) Measurement of fibrosis in the above muscles and longissimus dorsi muscles by means of hydroxyproline measurements and picrosirius red stained sections recording histological changes to evaluate muscle degeneration and regeneration. It was hoped that findings from this study would extend understanding of the *mdx* phenotype and be commensurate with dystrophic changes contributing to thoracolumbar deformity in DMD patients.

## 4.3 Methods

### 4.3.1 Mouse numbers and groupings

Male C57BL/10ScSn mice (control strain) were purchased from Animal Resource Centre, Nedlands, Perth, WA at 7 weeks of age. Male *mdx* mice were bred at the USQ Animal House, Toowoomba, Qld. The mice were housed in groups and given free access to laboratory chow and water, and all experiments were conducted in accordance with guidelines of the USQ Animal Ethics Committee. 4 mice per strain were used for the radiographic study, with one mouse dying during this study. An additional 4 mice per strain were also utilised for contractility experiments, hydroxyproline assays and histology. 17 month old mice were chosen as the aged group because of time restraints of PhD studies, and lack of availability of older mice for the additional functional experiments.

4.3.2 Radiographic studies and establishment of Kyphotic Index

Mice were sedated with Ketamine HCl 50 mg/kg (Ketamil, Troy Laboratories, Australia) in combination with Xylazine HCl 10 mg/kg (Ilium Xylazil-20, Troy Laboratories, Australia) administered by subcutaneous injection. At the end of the procedure atipamezole (Antisedan, Novartis Animal Health, Australia) was given at a dose rate of 0.1 mg/kg to reverse $\alpha$-$_2$ agonist effects of xylazine. Mice were lightly taped to the radiographic cassette using clear adhesive tape. Each animal was individually identified by tail markings, a radiodense (metal) number placed next to them, and a radiographic cassette label indicating date and animal grouping. Konica CM-H medical mammography film was exposed using a portable X-ray unit (either Showa Xray Co Ltd Tokyo, Japan or Porta 1030 model, Job Corporation, Yokohama, Japan). Optimum exposure with this equipment was established at 48KV, 1.8 MAS with a film focal distance of 70 cm. Mice were radiographed once monthly from 4 months until 17 months of age. Figure 4.2 depicts mice undergoing radiography.


**Fig 4.2** Mice undergoing radiography for determination of KI. A. Portable x-ray machine suspended from a timber beam to ensure correct film-focal distance. B. Anaesthetised mice positioned on cassette using clear adhesive tape. A metal number is taped beside each animal for individual identification.

Equipment and procedures conformed to Queensland Department of Health regulations for veterinary radiography, and the correct personal and protective equipment (lead gown and gloves) was worn. Although it was necessary to stay in the room during film exposure the operator was as far from the x-ray beam as allowed by the length of cable. Monitoring of radiation exposure by radiation meters was performed regularly.

Each whole body radiograph was photographed using a tripod mounted Ricoh Caplio RR30 digital camera with images analysed using Scion Image software Beta 4.0.2 (http://www.scioncorp.com). KI was calculated from a line drawn between the caudal margin of the last cervical vertebra, to the caudal margin of the 6$^{th}$ lumbar vertebra (usually corresponding to the cranial border of the wing of the ilium) (Line AB), divided by a line perpendicular to this from the dorsal edge of the vertebra at the point of greatest curvature (Line CD). This correlates as closely as possible to those radiographic parameters used to assess KI in boys with DMD, and is depicted in Figure 4.3a and b

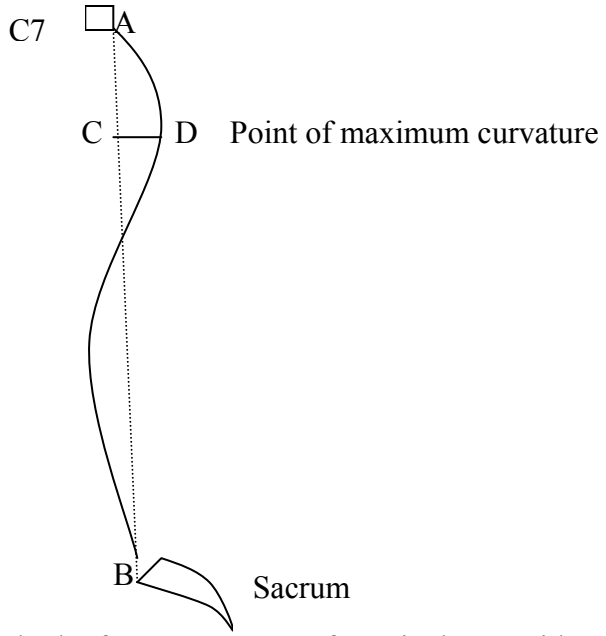


**Fig 4.3a**. Method of measurement of KI in boys with DMD (diagram adapted from(Smith et al., 1989)). With patient in sitting position, measurements are made from a lateral radiograph. AB is length of line drawn from anteroinferior edge of seventh cervical vertebra (C7) to the sacral promontory, and CD is the distance from the line to anterior border of the vertebral body that is furthest from that line. KI= AB/CD

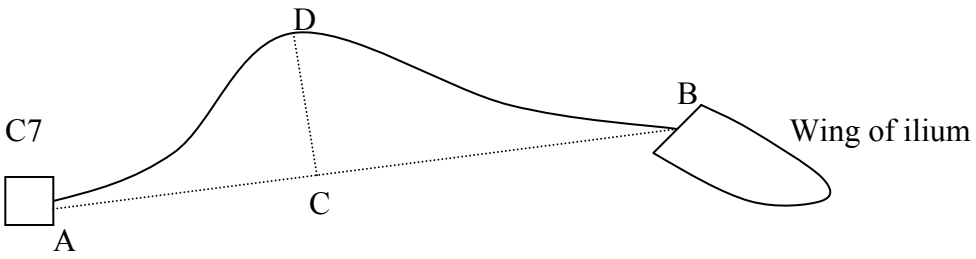


**Fig 4.3b**. KI in mice, calculated from radiographs of anaesthetised mice positioned in right lateral recumbency.
Line AB is the length of a line drawn from posterior edge of C7 to the posterior edge of L6, usually where it contacts the wing of the ilium (which is more consistently identifiable than the sacral border). Line CD is the distance from line AB to the dorsal border of the vertebral body farthest from that line. KI=AB/CD

Trial radiographs of the same animals in 3 positions 1) hind limbs and forelimbs placed in moderate extension, 2) overextension (stretching) of limbs and 3) flexion of forelimbs and hind limbs showed there was some differences in measured KI, considered to be less than 10%. Care was then taken to avoid 2) or 3), and to ensure limbs were only moderately extended. This could be confirmed when radiographs were analysed because the femurs and humeri were close to parallel and perpendicular to the long axis of the spine. Several radiographs that did not meet these criteria or were under or overexposed were excluded from analysis.

4.3.3 Measurement of thoracic area

With radiographs photographed using a fixed film-focal distance and utilising the Scion Image program draw tool, a line was extended around the inside border of the thoracic cavity, from T1 at the thoracic inlet following sternebrae, diaphragm and ventral edge of vertebrae to allow an estimation of thoracic area at age 17 months (Figure 4.4). This measure was repeated three times and results averaged for each animal (n=4 animals per group). Because thoracic area is related to body size the calculated area was normalised for body weight to give a value of thoracic area/body weight ($cm^2$/gram)

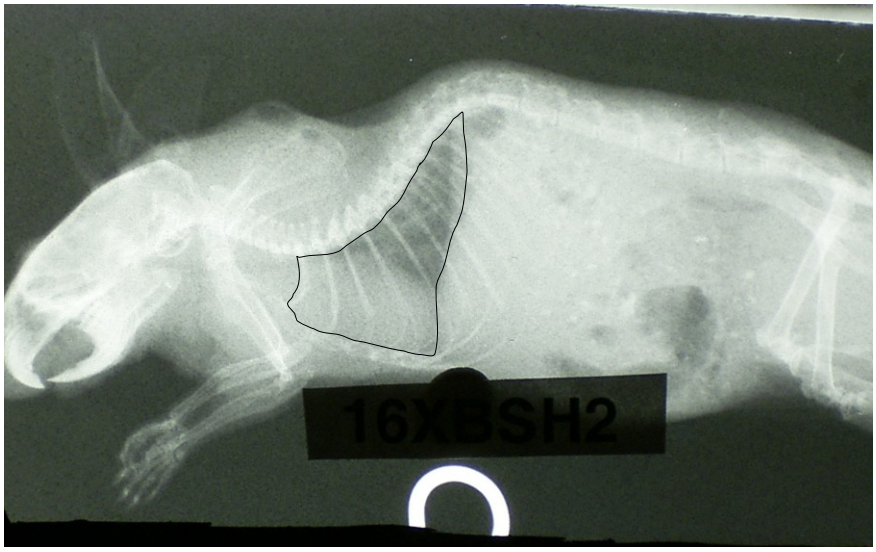

**Fig 4.4** Assessment of thoracic area in mice. A freehand line was drawn digitally following anterior edge of the first rib, sternebrae, diaphragm and ventral vertebral border using Scion Imaging program, and area bound by this line was calculated. This measurement was repeated three times for each mouse and results were averaged. The mouse shown above had a thoracic area of 3.59 $cm^2$.

4.3.4 Contractility studies

17 month old mice were anaesthetised using pentobarbitone sodium (Nembutal, Boehringer Ingelheim, Australia) at 70 mg/kg IP. Cessation of breathing occurred when the thorax was entered. The following muscles were dissected and placed into ice-cold Krebs buffer solution bubbled with carbogen (95% $O_2$/5% $CO_2$), a) diaphragm strip from left midcostal hemi- diaphragm, with placement of silk suture material around the central tendon at one end and a small rib section at the other. b) latissimus dorsi muscle, which is a fan shaped muscle with an aponeurosis originating from the spinal processes of T8-T12 and the thoracolumbar fascia, and a distinct tendon of insertion at the proximal humerus. A needle threaded with 6/0 surgical silk was passed through the aponeurosis and tied with a loop to attach to a force transducer. A short length of silk was also tied at the tendon end to anchor to a fixed peg below the stimulating electrodes and c) intercostal section comprising 4 ribs and their attached intercostal muscles (internal and external), extending from T8-12, adjacent and parallel to the longissimus dorsi muscle. Silk

sutures were passed with a needle around each rib at the top and bottom of the intercostal strip for mounting.

Muscles from the right side were collected and stored for histological analysis and hydroxyproline assays. Contralateral muscles were mounted in water-jacketed glass organ baths, maintained at 23$^{o}$C, using 6/0 silk surgical suture thread attached to a fixed peg at one end and a force transducer at the other. Tissues were stimulated via a Grass S48 stimulator (W. Warwick, RI, USA) and current intensity was amplified using a pre-amplifier (EP500B. Audio Assemblies, Campbellfield, Victoria, Aust). Data was collected and analysed using Chart 4.1.1 software. A square pulse of 0.2ms duration was dispersed via 2 platinum electrodes positioned along the length of the muscle.

Optimum preload ($L_o$) was defined as the length eliciting maximal single twitch force. Optimal voltage was also determined for each preparation, as was the frequency eliciting maximal tetanic force from a range of 50 - 180 Hz. A total of 7-8 mice per group were used for contractility studies. Reported data was the average of 3 individual single twitch or tetanic stimulations per muscle strip after 25 minutes of equilibration and optimisation of conditions. Muscles were measured at $L_o$ using a digital micrometer, blotted for 3 secs then weighed. Cross sectional area (CSA) and normalisation of force was calculated as described previously for diaphragm and latissimus muscles, where CSA equals tissue weight divided by length x 1.06 (density of mammalian muscle) (Lynch *et al*., 2001). Intercostal muscle fibre CSA was shown to vary topographically (Kelsen *et al.*, 1993) and in our preparations a strip comprises both muscle and rib cartilage and internal and external intercostal muscle layers consisting of differing fibre orientations and hence lengths. For these reasons intercostal forces were normalised to weight only. Time to peak force, 50% relaxation time and 90% relaxation time was calculated for each single twitch value.

### 4.3.5 Hydroxyproline analysis

Hydroxyproline content was used as a measure of collagen in diaphragm, intercostal muscles, latissimus dorsi and longissimus dorsi muscles. Muscles were trimmed of fat, ribs and tendons and stored at -80 $^{o}$C. Tissue was thawed then hydrolysed in sealed tubes with 6 M HCl overnight at 110$^{o}$C. The samples were dried to entirety using filtered air under pressure and heat (50$^{o}$C). The rest of the

protocol has been described previously (Stegemann and Stalder, 1967) and Appendix A shows details of the procedure for total assay volumes of 2 mLs. Values are expressed as μg HP/mg tissue wet weight.

4.3.6 Histology

Each tissue (diaphragm, latissimus, longissimus and intercostal muscles) was pinned onto cork at optimal length and then fixed sequentially in Telly's fixative (formaldehyde, glacial acetic acid-ethanol fixative, 72 hours), Bouin's solution (formaldehyde, glacial acetic acid-picric acid fixative, 24 hours) and 70% ethanol, prior to paraffin embedding, cutting and staining of 10 micron sections using 0.1% w/v picrosirius red solution (Sirius Red F3B, Chroma Dyes, Germany in saturated picric acid), a collagen specific stain. Additional 5 micron sections were stained with haematoxylin and eosin for determination of nuclear position. Analysis was performed blinded to the strain of mouse, with sections viewed on a Nikon Eclipse E600 light microscope and captured with a Nikon FDX-35mm camera, then digitised. A visual grading scheme was applied to the picrosirius stained sections, with Grade 1 having minimum interstitial fibrosis (eg <10%), Grade 2 with mild fibrosis (10-25%), Grade 3 with moderate fibrosis (25-50%) and Grade 4 with marked fibrosis (>50%).

**4.4 Statistics**

Pilot experiments on aged mice were performed to estimate standard deviations and suitable sample size. *Post hoc* tests of power confirmed that an $n = 3$ animals for assessment of KI and $n=5$ animals for contractility experiments were adequate (Plummer, 1998). Results are expressed as means ± S.E. Responses between *mdx* and control strain were analysed using Student's unpaired *t*-tests, with the exception of differences in KI, where ANOVA was employed. *P* values less than 0.05 were considered statistically significant.

## 4.5 Results

### 4.5.1 Gross findings

Kyphosis was palpable and clearly evident in all *mdx* mice at 17 months of age. In addition the control strain showed a degree of thoracolumbar kyphosis which was not as pronounced. All animals were ambulatory and in fair-good body condition, however the *mdx* group showed a stiffer gait and moved less freely around their cages.

### 4.5.2 Kyphotic Index

KI as a measure of spinal deformity remained similar for *mdx* and control mice until approximately 9 months of age, after which a significant difference became apparent between *mdx* and normal mice ($P<0.01$ at 9 months). There was a plateau in both mouse strains after this age (Figure 4.5).

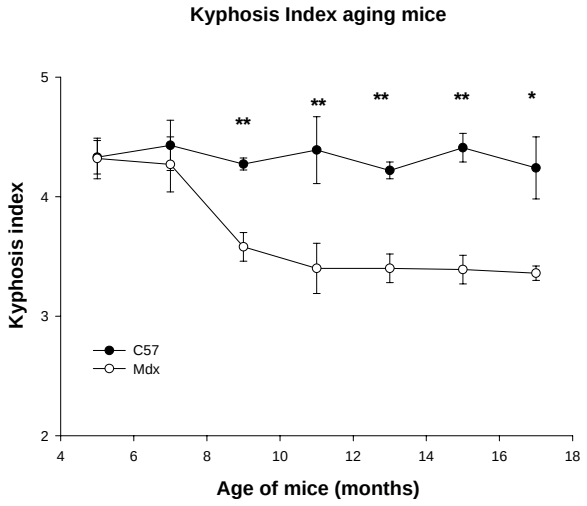


**Fig 4.5** Kyphosis Index of aging *mdx* and control mice. Mice were radiographed monthly from 4 months to 17 months of age and measurements were made every 2 months. $n$=4(*mdx*), $n$=3 (C57) *$P$<0.05, **$P$<0.01.

Figure 4.6 shows examples of radiographs of young (5 months old) and aged (17 month old) *mdx* and control mice, used for determination of KI.

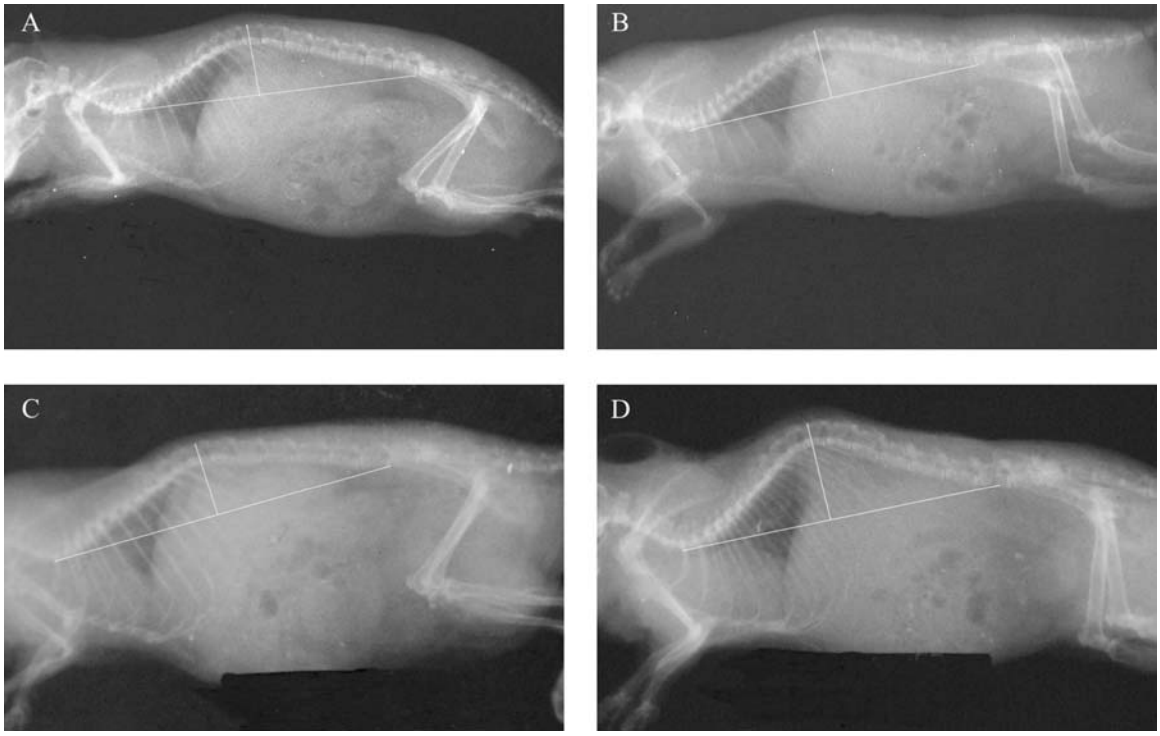


**Fig 4.6** Examples of mouse whole body radiographs used for calculation of kyphotic index. A and C = young and aged (5 month old and 17 month old) control mouse, B and D=young and aged *mdx* mouse. The progression of spinal deformity results in a decrease in KI, and alteration of thoracic shape and size.

4.5.3 Thoracic Area

There was no significant difference in body weights at 17 months of age between *mdx* and C57 mice, however there was a difference ($P<0.05$) between thoracic area and normalised thoracic area in *mdx* and age-matched controls (Table 4.1) with *mdx* mice demonstrating lower values.

**TABLE 4.1** Mean (± SE) of thoracic area, body weight and normalised thoracic area in 17-month-old mice. *n*=3(C57), *n*=4(*mdx*). ***P*<0.05

| | **Thoracic area ($cm^2$)** | **Body weight (g)** | **Thoracic area/bw ($cm^2$/g)** |
|---|---|---|---|
| **Control** | 4.49 ± 0.12 | 32.2 ± 0.86 | 0.14 ± .007 |
| ***Mdx*** | 3.71 ± 0.25 * | 31.65 ± 1.2 | 0.12 ± .004 * |

4.5.4 Muscle contractility

The characteristics (optimal muscle length ($L_o$), average width and weight) of each isolated muscle strip is listed in Table 4.2. The latissimus dorsi muscle showed greatest variation between mouse strains, with *mdx* having considerably heavier (P<0.001) muscles than C57, despite being no significant differences between widths or $L_o$ for these muscle preparations. It is thought that this muscle (in addition to many *mdx* limb muscles) demonstrates considerable hypertrophy during their lifespan with the presence of fibrosis contributing to increased weights. A difference between strains was also apparent during dissection; the diaphragm, intercostals and latissimus muscles of C57 tended to be thin and transparent, while in *mdx* they were thickened and opaque. There was a small difference in average diaphragm width selected for mounting, and, although this is unlikely to affect results, the resultant tissue strip was heavier in the *mdx* group.

**Table 4.2** Mean (± SE) optimum fibre length, weight and width of muscle strips from 17-month-old control and *mdx* mice. *n*=7(C57), *n*=8(*mdx*) ***$P<0.001$ *$P<0.05$

| **Muscle** | **Lo (mm)** | **Weight (mg)** | **Width (mm)** |
|---|---|---|---|
| **Latissimus dorsi** | | | |
| Control | 31.14± 4.2 | 86.56±13.55 | 2.84± 0.4 |
| *mdx* | 31.33± 1.01 | 158.09±10.1*** | 3.68± 0.43 |
| **Intercostal strip** | 8.28± 1.31 | 59.95± 9.04 | 5.53± 1.04 |
| Control | 8.61± 0.39 | 55.65± 3.85 | 4.64± 0.37 |
| *mdx* | | | |
| **Diaphragm strip** | 9.44± 1.34 | 8.15± 0.99 | 1.44± 0.21 |
| Control | 8.56± 0.41 | 12.49± 1.75* | 1.87± 0.18* |
| *mdx* | | | |

*In vitro* isometric contractile properties of these muscles are shown in Table 4.3. All *mdx* muscles examined demonstrated reduced force production (twitch and tetanus) compared to control mice, with *mdx* diaphragm muscle showing the greatest reduction in tension generated (approximately two-thirds that of control mice, $P<0.01$). *Mdx* latissimus dorsi and intercostal strip values were by contrast 50% of control levels for both twitch and tetanus tensions ($P<0.05$ except for latissimus Po ($P<0.01$)). Rise times (TPT) were similar, except for the attenuated diaphragm twitches of the *mdx*, which had significantly shorter TPT ($P<0.001$). Relaxation was prolonged in *mdx* intercostal muscles compared to control levels, reflected by increased $TR_{50}$ and $_{90}$ ($P<0.05$).

| | | TPT (ms) | $TR_{50}$ (ms) | $TR_{90}$ (ms) | $P_t$ ($mN/mm^2$) | $P_o$ ($mN/mm^2$) |
|---|---|---|---|---|---|---|
| **Latissimus dorsi** | Control | 26.5±1.2 | 20.6±0.9 | 43.3±1.5 | 18.76±3.9 | 86.8±13.65 |
| | *Mdx* | 25±1.0 | 20±1.0 | 43.8±3.0 | 10.62±1.19***** | 45.9±5.6****** |
| **Intercostal strip** | Control | 24.2±0.8 | 17.4±0.8 | 36.8±1.7 | 0.23±0.05 | 1.04±0.2 |
| | *Mdx* | 25.8±1.0 | 20.1±1.0***** | 43.0±2.0***** | 0.11±0.02 ***** | 0.58±0.09 ***** |
| **Diaphragm** | Control | 41.5±1.4 | 30.3±0.9 | 62.0±2.3 | 31.93±6.67 | 117.8±23.1 |
| | *Mdx* | 33.1±1.0 ******* | 31.8±1.0 | 62.6±3.0 | 5.83±0.61****** | 31.86±3.2****** |

.

**Table 4.3** Contractile properties of latissimus dorsi muscles, intercostal strips and diaphragm strips from 17-month-old *mdx* and control mice: Time to peak tension (TPT), Time to 50% relaxation ($TR_{50}$), Time to 90% relaxation ($TR_{90}$), peak twitch force ($P_t$) and maximal isometric tetanic force ($P_o$). $n$=7 (C57), $n$=8 (*mdx*) *****$P$<0.05,******$P$<0.01, *******$P$<0.001. $P_t$ and $P_o$ normalised using muscle CSA for diaphragm and latissimus muscles, and wet weight only for intercostal preparations.

4.5.5 Hydroxyproline analysis

Four muscles were used for assays of hydroxyproline content, and results are shown in Figure 4.7. All *mdx* muscles had significantly more HP than control mice, with the diaphragm HP 2.5 times higher than the other muscles examined. Interestingly, control mice also showed a higher level of fibrosis in this organ compared to other respiratory or paraspinal muscles, and when relative values were compared (control HP as a ratio of *mdx* HP) the diaphragm and latissimus displayed an equal tendency for fibrous tissue deposition (0.66), followed by intercostal muscles (0.58) and then longissimus dorsi (0.44). The magnitude of fibrosis may be a reflection of the workload of individual muscles.

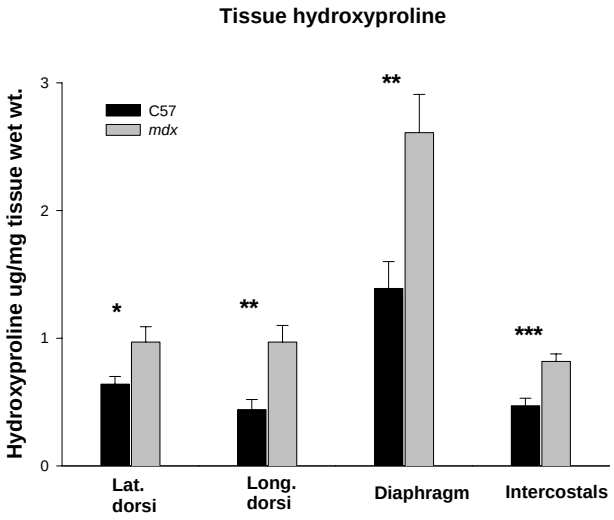


**Figure 4.7** Hydroxyproline content of paraspinal and respiratory muscles in *mdx* and control mice, as a measure of tissue fibrosis. *n*=7(C57), *n*=8 (*mdx*) *****P<0.05, ******P<0.01, *******P<0.001

4.5.6 Histology.

The results of an applied histological grading scheme for muscle sections stained with the collagen specific stain picrosirius red are listed in Figure 4.8. The percentage of centronucleation of muscle fibres as visible on H&E stained sections indicates previous necrosis and degeneration and one or more cycles of regeneration, and is displayed in Figures 4.9 and 4.10. Representative

photomicrographs of all four muscles of *mdx* and control mice stained for collagen are shown in Figure 4.11. It is apparent that *mdx* muscles demonstrate marked heterogeneity in cell size, a high incidence of centrally nucleated fibres, inflammatory cell infiltration and fibrous tissue deposition compared to control muscles.

*Mdx* diaphragm displays the highest scores on histological grading as expected, with marked fibre loss and replacement with interstitial collagen. The intercostals displayed an intensity of picrosirius staining and high score that is not perhaps reflected in measured hydroxyproline content of these tissues. The intercostal muscles are a complex mixed tissue when viewed microscopically, typically comprised of fibres in both cross and oblique section and containing fat and a large blood vessel. The impression in *mdx* sections was for greater disarray in tissue structure, fibre loss, considerable variation in myocyte size, fibrosis and inflammatory cell infiltration.

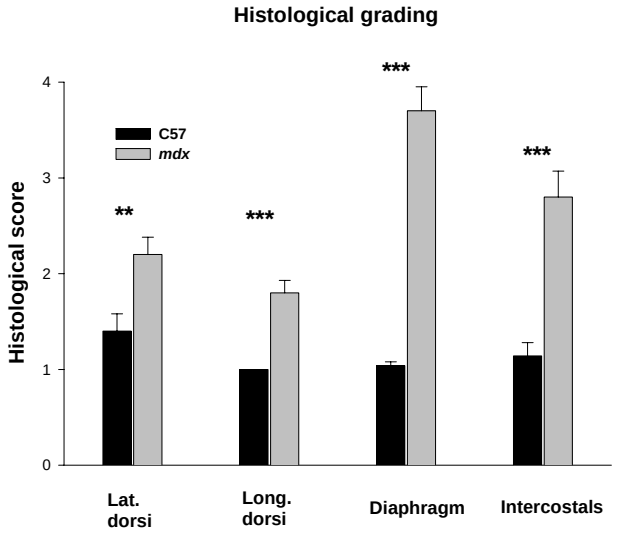


**Fig 4.8** Histological score based on interstitial fibrosis, calculated on picrosirius red stained muscle samples. Scoring scheme was determined on viewing 10 fields per tissue (20X magnification) with a score of 4 indicating greater than 50% fibrosis. $n$=7 (C57), $n$=8 (*mdx*).**$P$<0.01*** $P$<0.001

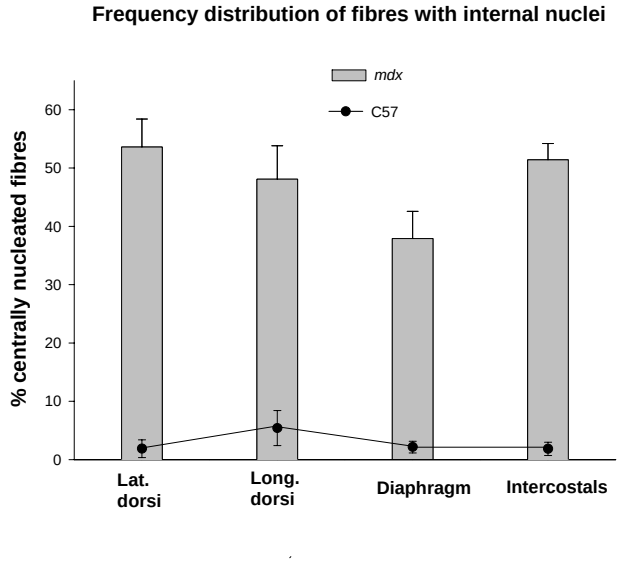


**Fig 4.9** Frequency distribution of internal nuclei in paraspinal and respiratory muscles. Figures are based on counting 100 fibres per muscle on H&E stained sections. *n*=7 (C57), *n*=8 (*mdx*) *P*<0.0001 for all muscles.

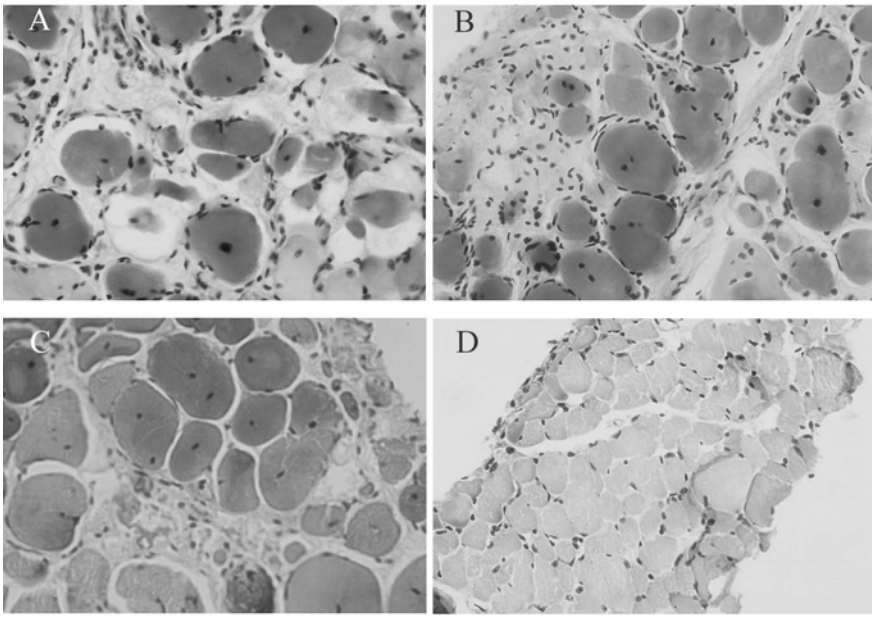


**Fig 4.10** Photomicrographs of haematoxylin and eosin stained sections. A. *Mdx* longissimus, B. *Mdx* intercostals, C. *Mdx* latissimus, D.Control diaphragm. 20X magnification. The *mdx* cells show dystrophic features including centronucleation, variation in fibre size, inflammatory cell infiltration and interstitial fibrosis, indicating cycles of degeneration and regeneration. In contrast the control diaphragm shows greater uniformity of fibre size and little evidence of fibrosis.

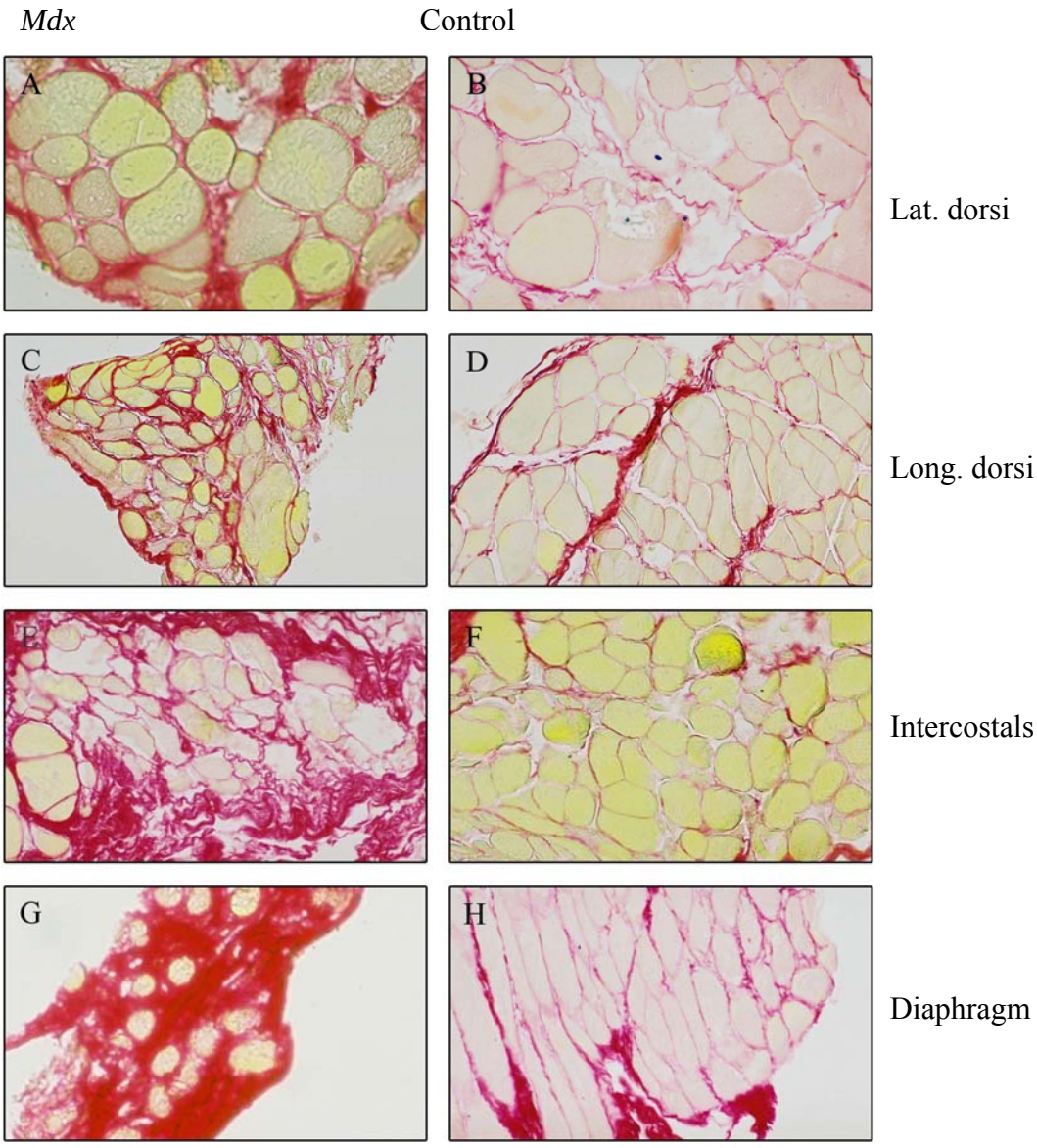


**Fig 4.11.** Picrosirius red stained muscle sections. The dark red stained areas represent collagen. The relative amounts of staining were used to grade samples from 1-4, corresponding with the level of interstitial fibrosis. A,C,E,G:*mdx*. B,C,F,H: C57

A,C =Grade 2, E=Grade 3, G=Grade 4.All control mice were considered Grade 1. Sections C,D and F shown at 10X magnification, other muscles at 20X

## 4.6 Discussion

The *mdx* mouse is the most frequently used animal model for research into DMD, and much of our understanding of the pathophysiology of dystrophic muscle has been gained from studies in this model. They, however, show a milder phenotype than boys with DMD or the Golden Retriever Muscular Dystrophy dog (GRMD).

While a reduction of vertebral support in humans with neuromuscular weakness can show as thoracolumbar deviation in a dorsal or ventral plane (kyphosis or lordosis respectively) or a lateral deviation of the spine due to the effect of gravity (scoliosis), the quadrupedal gait of mice results in the development of kyphosis.

With careful positioning of animals it is possible to accurately measure differences between animals not apparent by observation or palpation. A significant decrease in Kyphotic Index occurred in a group of *mdx* mice at 9 months of age, or at approximately one third of the *mdx* lifespan. This differs from *mdx:utrn*$^{-/-}$ which shows an earlier onset of spinal deformity (Deconinck *et al*., 1997a; Grady *et al*., 1997) This difference is probably attributable to the muscle hypertrophy demonstrable in most skeletal muscle of *mdx*, which for a time maintains whole muscle strength, although *in vitro* organ bath studies of the paraspinal muscles indicates that normalised forces (maximum isometric tension per unit cross-sectional area) are weaker. This is in agreement with experiments conducted on limb muscles (Lynch *et al*., 2001).

It is likely that the level of anaesthesia of mice will affect KI, and early trials utilizing only light sedation resulted in animals struggling against the tape restraint causing movement blur. Ketamine/xylazine combination provided muscle relaxation as well as immobilisation, and offered the benefit of allowing xylazine reversal by atipamezole, which may enhance recovery in aged *mdx* with cardiac impairment. Right lateral recumbent views were chosen for ease and consistency, allowing up to 6 mice per cassette to be radiographed. It is also possible to choose prone positioning with cross table lateral views, however this would allow only two mice to be radiographed at one time. There was also concern that the heavy shoulder and hind limb musculature of young *mdx* (3-12 months old, corresponding to muscle hypertrophy stage) would hinder correct positioning when prone.

Thoracic area measurements of *mdx* was less than those of control mice, and it is likely that such thoracic deformity in aged *mdx* will affect pulmonary function (or contribute to the reduced lifespan of more severely kyphotic *mdx:utrn*$^{-/-}$ (Deconinck *et al*., 1997a)). Certainly in DMD patients diaphragmatic and respiratory muscle weakness coupled with severe thoracic deformity leads to hypoventilation and hypoxaemia, sleep abnormalities and susceptibility to respiratory tract infections (Sivak *et al.*, 1999; Seddon and Khan, 2003).

Certain *mdx* skeletal muscles show profound dystrophic changes, particularly the diaphragm, slow twitch limb muscles and postural muscles (Stedman *et al*., 1991; Lefaucheur *et al*., 1995; Pastoret and Sebille, 1995b). These are muscles with either an obligatory constant workload or a role in resisting gravitational forces compared to fast twitch, intermittently active muscles such as the extensor digitorum longus. The diaphragm was utilised in these experiments because its contractile, morphometric and histopathologic properties are well documented (Stedman *et al*., 1991; Coirault *et al*., 1999; Anderson *et al*., 1998) and it serves as a useful benchmark for the severity of dystrophic changes in other less well-characterised muscles. *Mdx* diaphragm strips generate significantly lower maximum tensions compared to age-matched control mice as reported previously (Lynch *et al*., 1997; Stedman *et al*., 1991) and there was an inverse relationship between twitch force and hydroxyproline content. Histological changes showed severe interstitial fibrosis and myocyte disarray typical of this organ in *mdx* mice.

It is apparent that differential levels of dystrophic pathology exist between the four *mdx* muscles examined. The diaphragm has been shown previously to be an atypical tissue by virtue of its low percentage centronucleation, despite extensive fibrotic infiltration (Boland et al, 1995). These reasons for this are not clear (Anderson *et al*, 1998; Krupnick *et al*, 2003). There is no published data available regarding paraspinal and intercostal muscle pathology in *mdx*, or the usefulness of counts of incidence of central nuclei in these muscles as a quantitative measure of dystrophy.

It is perhaps not surprising that intercostal muscles are also subject to a high degree of dystrophic changes as they have an augmentative, though lesser, role than the diaphragm in respiration. During inspiration contraction of the parasternal intercostals causes elevation of the ribs and flaring of the sternum synergistic to

diaphragmatic contractions (Farkas *et al.*, 1985). Several of the *mdx* intercostal sections examined scored equally to diaphragm strips (Grade 4, equivalent to >50% fibrosis). The discordance between histological scores of fibrosis and hydroxyproline levels in intercostal muscles may be a factor of both the extent of infiltration and the density of the collagen in this tissue; i.e fibrosis is more extensive, but less dense.

The intercostal muscles showed prolonged relaxation properties, with significant increases in $TR_{50}$ and $TR_{90}$ compared to control mice. Separation of internal and external intercostal muscle layers was not performed due to the risk of damage to individual fibres. The direction of dissection was parallel to external intercostal fibres, as external intercostal muscle fibres contribute most to force generation during normal respiratory movements. Previous intercostal studies on larger species including rabbits (Citterio *et al.*, 1982), dogs (Decramer *et al.*, 1985; Farkas *et al*., 1985) and hamsters (Kelsen *et al*., 1993 ; Kelsen *et al.*, 1994) utilised separated muscles. The preparations spanning 4 ribs were very similar in dimensions to these hamster preparations, and were also extrapolated from studies in guinea pigs where tracheal segments comprising a series of tracheal rings are mounted via silk suture around cartilages in organ bath experiments (Mardini *et al.*, 1986) (Chitano *et al.*, 2002).

The latissimus dorsi is a fan shaped muscle, which because of its superficial position on the trunk is easily dissected. This muscle also showed centronucleation and fibrosis, with reduced $P_t$ and $P_o$ seen in other skeletal muscles of older *mdx*. Previous contractility studies using rabbit latissimus dorsi confirm its fast twitch properties (James *et al*., 1997). Twitch kinetics from these experiments suggest the latissimus dorsi is also a fast twitch muscle in older mice, although this needs to be verified by fibre typing.

The longissimus dorsi is an important member of the erector spinae group, involved in spinal rotation and extension. It is not amenable to organ bath studies because of multiple branching and insertions on many vertebral processes, however there was histological and biochemical evidence of dystrophy similar to the other *mdx* muscles examined.

In humans, comparisons have been made between limb muscle and joint contracture seen in neuromuscular diseases, and the fibrosis and contracture of respiratory muscles, stiffening of tendons and ligaments of the rib cage and ankylosis of costovertebral and costosternal articulations (Bach and Kang, 2000). Failure to fully expand the lungs causes increases in lung tissue and chest wall elastance and decreases in compliance (Misuri *et al.*, 2000), alterations that contribute markedly to the total mechanical work of breathing.

Although the spinal deformity of dystrophin deficient mice is not as extreme as that seen in patients with DMD, the hallmarks of dystrophy, muscle weakness and fibrosis, and not just aging *per se*, appear to be implicated in the progression of kyphosis and thoracic deformity in this model. It is likely also that the relative inactivity of aged *mdx* mice compared to their control strain, noted by ourselves and others (Pastoret and Sebille, 1995b), is due in large part to the presence of these skeletal malformations and associated muscle contracture and increase in stiffness. It is only conjecture at this stage that significant respiratory insufficiency may also occur in *mdx* mice and could be implicated in this failure to move freely.

In conclusion, this study demonstrated the application of a radiographic index for the measurement of kyphosis in mice, and showed how this index changed in *mdx* mice compared to control mice. The measurement of kyphosis by radiographic indices presented here is a method of quantitative comparison between mouse strains and may also have application for long-term therapeutic studies or gene therapy trials in the *mdx* or other kyphotic mouse strains.

# CHAPTER 5: ANTISENSE OLIGONUCLEOTIDE ADMINISTRATION INTO *MDX* DIAPHRAGM MUSCLE.

## 5.1 Introduction

DMD is the most common human X-linked genetic disorder. The disease remains a prime target for gene therapy because of its monogenic nature, prevalence and the distressing and relentless clinical course of those affected, however the obstacles in the path of a cure are many. Muscle is a vast organ, representing greater than 30% of total body protein, host immune defences are effective against transplanted myoblasts, stem cells or vectors, the gene in entirety is too large for administration via viral vectors, and finally the complexity of the gene and the variety of sites and categories of mutations within the locus itself all hinder progress towards an effective, safe and lifelong therapy.

Antisense oligoribonucleotides (AOs) have been explored as a gene correction therapy, aimed at restoring frame-disrupting mutations. They are composed of 2'-O-methyl ribonucleotide analogues, which bind to a homologous sequence and cause a manipulation ('exon-skipping') of primary transcript processing. They have the advantage of not undergoing extensive degradation by endogenous ribonucleases.

In *mdx* cell culture AOs have been shown to induce exon-skipping resulting in the production of a truncated, yet still functional protein, coined a 'Becker-like' protein, due to the similarity between the patchy sarcolemmal distribution and shortened dystrophin of patients with Becker Muscular Dystrophy (BMD), a milder allelic form of DMD (Mann *et al.*, 2001; Mann *et al.*, 2002). AO mediated skipping of multiple dystrophin exons has also been achieved in cultured human muscle cells (Aartsma-Rus *et al.*, 2002).

AO mediated exon-skipping resulted in dystrophin production in *mdx* limb muscles (Mann et al., 2001); (Lu et al., 2003), shown by immunohistochemistry and Western blotting. There has been one published study looking at function of AO treated *mdx* muscle which showed partial restoration of function in injected tibialis anterior muscles, with significant improvement in force production evident when comparing treated and untreated *mdx* muscles (Lu *et al*., 2003).

Due to the severity of dystrophy in *mdx* diaphragm muscle and its similarities to the pathology of DMD, it is an attractive target for AO administration as a 'proof of principle' treatment modality.

## 5.2 Aims

The aim of these experiments was to determine the effect of AOs injected into *mdx* mice diaphragms (as a continuation of work outlined in Chapter 4). Contractility studies were undertaken as a measure of efficacy of the AOs in restoring (or partially restoring) function. In addition, histological measures of degeneration and regeneration (centronucleation and fibre diameter analysis) and tissue fibrosis were also used. Hydroxyproline was utilised as a biochemical marker of fibrosis in treated diaphragm segments. Finally Western blotting was used to measure the level of dystrophin protein production in treated muscles.

## 5.3 Methods

### 5.3.1 Mouse numbers and grouping

Male mice were 16 weeks of age at the time of the first surgical procedure, 20 weeks of age for the second administration, and 25-27 weeks old when euthanased. There were six groups of mice: a. *mdx* AO (*n*=10), b. *mdx* sham (saline) (*n*=4), c. *mdx* sham (lipofectin) (*n*=4), d.C57 sham (saline) (*n*=4) and e.C57 sham (lipofectin) (*n*=5). For the purposes of Western blotting an extra group of mice was used (n=6), where histology dyes were combined with AOs for more accurate localisation of the sites of injections. The groupings of animals are shown in Figure 5.1.

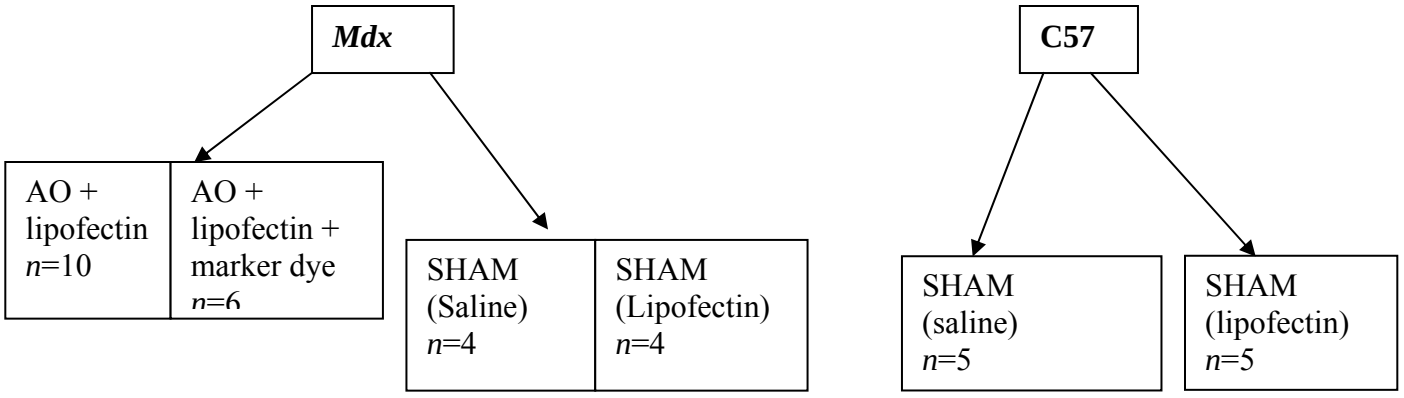


**Fig 5.1** Grouping and numbers of mice for diaphragm AO study.

5.3.2 Anaesthesia and surgery

Anaesthesia was induced with ketamine HCl 50 mg/kg (Ketamil, Troy Laboratories, Australia) and xylazine HCl 10 mg/kg (Ilium Xylazil-20, Troy Laboratories, Australia). A midline laparotomy was performed under sterile surgical conditions to expose the diaphragm. Injections were constituted as described below and injected in two sites on both hemi-diaphragms, using 29 gauge needles and 0.3ml paediatric insulin syringes (Braun Omnican 30). Sites of AO injections are shown in Figure 5.2.

Muscle and skin incisions were closed with 4/0 Maxon and 5/0 Novafil synthetic suture material. After surgery buprenorphine 1 mg/kg (Temgesic, Reckitt Benckiser, Australia) and atipamezole 1mg/kg (Antisedan, Novartis Animal Health, Australia) were administered for analgesia and reversal of xylazine, respectively. Sterile saline (0.5mL) was also injected subcutaneously for maintenance of hydration. Mice were monitored post-operatively until ambulatory and were examined daily, with the appearance of the surgical wound, appetite, activity and weight recorded for 7 days post operatively. All experiments were carried out under USQ Animal Ethics Committee guidelines.

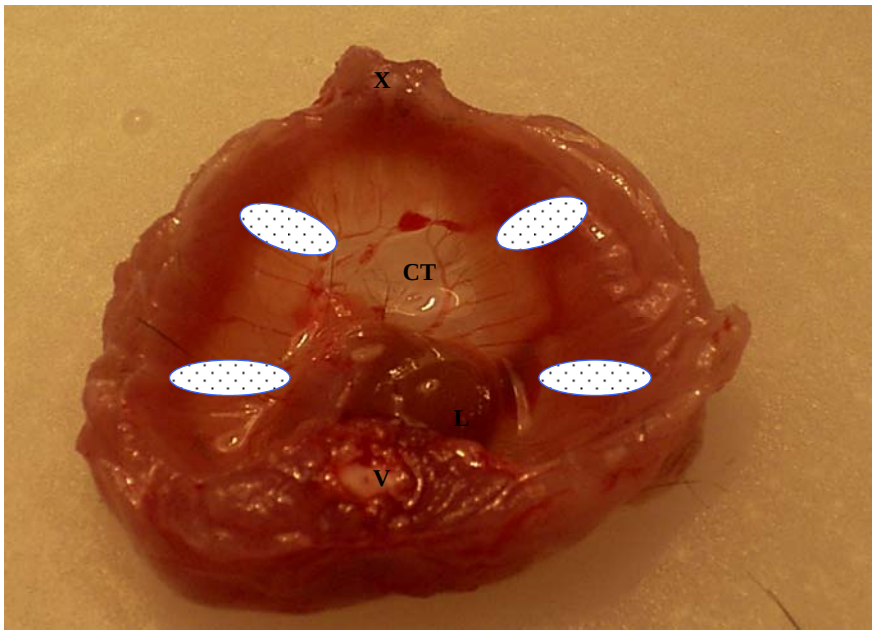


**Fig 5.2** Approximate sites of AO injections. The green ovals represent regions of spread of injectate within the diaphragm muscle. X=xiphisternum, V=lumbar vertebra, CT=central tendon, L=liver, a remnant of which was visible in this cadaver specimen.

5.3.3 Oligonucleotides

The AO used was M23D (+02-18), as defined previously (Mann *et al*., 2002) and shown in Figure 5.3. AOs were synthesised on an Expedite 8909 Nucleic Acid Synthesiser at the Australian Neuromuscular Research Institute, University of Western Australia. The conditions for transfection had been optimised previously (Mann *et al*., 2002). Briefly, complexes of Lipofectin (Life Technologies, Melbourne, Australia) were prepared in a 2:1 Lipofectin/AO ratio (w/w) in sterile 0.9% saline. Lipofectin and AO were incubated separately with saline for 30 minutes prior to mixing; the AO/Lipofectin complex was then used within 30-45 minutes. Approximately 1 µg of AO was administered per injection site. Sham injections comprised the same volume of Lipofectin or saline. 6 mice were treated with AO/Lipofectin as above, with 2 µL histology marker dye added to the 40 µL volume (Wak-Chemie Medical, Germany). The dye was autoclaved in cryotubes prior to use, with the resultant paste reconstituted in sterile saline.

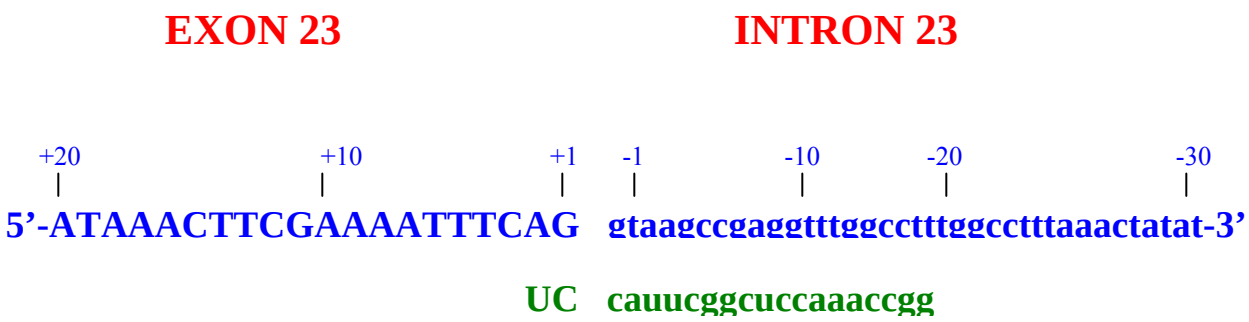


**Fig 5.3** Representation of the genomic sequence of the boundary between Exon 23 (upper case letters) and Intron 23 (lower case letters) of the mouse dystrophin gene. The numbers above the sequence are used to designate the target homology of the AO M23D(+2-18), where M=murine, 23= exon number, D=Donor splice site, (+-)=annealing coordinates. +2 is the last two exonic bases and –18 represents the first bases of intron 23 (Mann *et al*., 2002; Wells *et al*., 2003)

5.3.4 Contractility studies

Mice were anaesthetised with 70 mg/kg thiopentone sodium (Nembutal, Boeringer Ingelheim, Australia) by intraperitoneal injection. The diaphragm and surrounding ribs were removed *en bloc* and placed in ice cold Krebs solution, bubbled with 95% $O_2$ and 5% $CO_2$. Strips of diaphragm muscle were prepared for hydroxyproline analysis and Western blotting by snap freezing in liquid nitrogen before storing at –80$^{o}$C. Another muscle strip was pinned to cork and placed in Telly's solution prior to Bouin's fixation and eventual storage in 70% ethanol. Three diaphragm strips, each 2-3 mm wide were excised for *in vitro* studies (two strips from the right hemidiaphragm and one from the left). These were anchored by means of surgical silk to a fixed peg at the rib end, and attached to a force transducer at the tendon end, and placed within a 25 mL glass organ bath maintained at 23$^{o}$C. Tissues were stimulated via a Grass S48 stimulator (W. Warwick, RI, USA) and signal current intensity were amplified using a pre-amplifier (EP500B. Audio Assemblies, Campbellfield, Victoria, Aust). Data was collected and analysed using Chart 4.1.1 software on an iMac computer. A square pulse of 0.2 ms duration was dispersed via two platinum plate electrodes positioned at each side of the muscle.

Optimum preload ($L_o$) was defined as the length eliciting maximal single isometric twitch force. Optimal voltage was also determined for each preparation, as was the frequency eliciting maximal tetanic force. Reported data was the average of 3 individual single twitch or tetanic stimulations per muscle strip, with those three diaphragm strip values then averaged to give an overall mean for that muscle (=Averaged Values) or the maximum force achieved for that diaphragm (=Maximum Values). A fatigue protocol (one tetanic stimulation every 5 secs for 5 minutes) and recovery from fatigue (a single tetanic stimulation 5 minutes later) was also performed. Muscles were measured at $L_o$ using a digital micrometer, blotted for 3 secs then weighed prior to storage at –80$^{o}$C, and subsequent Western blotting. CSA and normalisation of force was calculated as described previously (Lynch *et al*., 2001).

5.3.5 Hydroxyproline analysis

Hydroxyproline content was used as one measure of collagen content of diaphragm tissue. Tissues were thawed and weighed, then hydrolysed in sealed tubes with 6 M

HCl overnight at 110°C. The samples were dried to entirety using air under pressure and heat (50°C). The rest of the protocol is described in detail in Appendix B. Values are expressed as μg HP /mg tissue wet weight.

### 5.3.6 Western blotting

Muscle samples were homogenised in 19 vol. of extraction buffer, and total protein was quantified with a Bio-Rad DC Protein Assay Kit. 100 μg of total protein from each sample was loaded onto a 4-12% polyacrylamide gel containing 0.2% SDS in tris-glycine buffer. Samples were electrophoresed for 5-6 hours at 20-25mA (temperature limited to approximately 16°C), before blotting onto a nitrocellulose membrane. The membrane was probed with NCL-DYS2 primary antibody (1:100, NovoCastra, Newcastle, UK) for 120 minutes followed by 3 washes in TBST buffer. The bound primary antibody was detected by horseradish-peroxidase conjugated rabbit anti-mouse secondary antibody (1:1000; DakoCytomation, Denmark) and Lumi-Light Western Blotting Substrate (Roche Diagnostics, Mannheim, Germany). The intensity of the bands obtained from the AO treated mice were compared with sham injected *mdx* and C57 mice. Details of the Western protocol used are listed in Appendix B.

### 5.3.7 Histology of diaphragm samples

Tissues for histological analysis were paraffin embedded. Blocks were cut at 10 μm prior to staining with picrosirius red (F3B, Chroma Dyes, Germany). Analysis was performed blinded to the treatment group. Fluorescent microscopy images were acquired using a digital camera (Q imaging Micropublisher 5.0 RTV) coupled to an epifluorescence microscope (Eclipse E600, Nikon, Japan). Four sections per diaphragm were photographed and analysed using the image analysis program DocuAnalySIS (Soft Imaging System), then averaged. Results are expressed as collagen as a percentage of area. H&E stained sections of 5 μm thickness were viewed using bright field, with images acquired and analysed using the same equipment. Percentages of muscle fibres with centralised nuclei were determined in 100 fibres per diaphragm.

## 5. 4 Statistics

The level of significance of treatment with AOs was determined using t-tests. Data was pooled from the sham groups because of a lack of difference between sham treatments- ie *mdx* AO were compared with *mdx* sham (saline and lipofectin), and C57 sham (saline and lipofectin) treated mice. Data is expressed as means ± SE, with significance defined as a $P<0.001$, 0.01 or 0.05 as appropriate.

## 5.5 Results

### 5.5.1 Mouse survival and evaluation of surgery

2 mice died within 7 days of the surgical procedure. These were both *mdx* treated with AO/lipofectin complex plus histology marker dye. Affected mice were hunched and inappetant, and on post-mortem examination both showed a thoracic effusion, with small amounts of blue stain present within the fluid. Wak-Chemie product data sheet does not recommend use of the histological marker in living subjects, although it has been used successfully in AO treated mice previously (Mann *et al*., 2001). It is also likely that autoclaving of the product causes denaturation, manifest as a granular appearance despite retaining its staining properties. It is probable that escape of dye into the thorax occurred inadvertently during diaphragm injections.

The success of the injection procedure was subjective, and gauged by the formation of a distinct bleb of injectate at each site, or spread of blue stain along diaphragm muscle fibres in mice where marker dye was used. The site of previous injections could often be detected as a small area of blood vessel infiltration or grey scar tissue.

### 5.5.2 Body weight

*Mdx* mice were heavier at all time points compared to C57 mice. At the end of the experimental period *mdx* were 35.2 ± 0.63g compared to 30.9 ± 1.32g for wild type mice ($p<0.01$). Weight gain for the 9-11 weeks of the project was 4.1 ± 0.24g (*mdx*) and 2.54 ± 0.65 g (C57). There were no significant differences in body weights between AO and sham treated *mdx* mice.

5.5.3 Contractility studies

The sham treated *mdx* group showed force deficits of 52% (twitch force) and 44% (tetanic force), compared to wild-type mice, whereas the *mdx* AO treated mice showed a deficit or 35% and 25.2% for twitch and tetanic forces respectively (Figures 5.4 and 5.5). Twitch and tetanus forces of the AO treated *mdx* compared to sham-treated *mdx* were increased by 33.8% and 33.9% respectively.

.

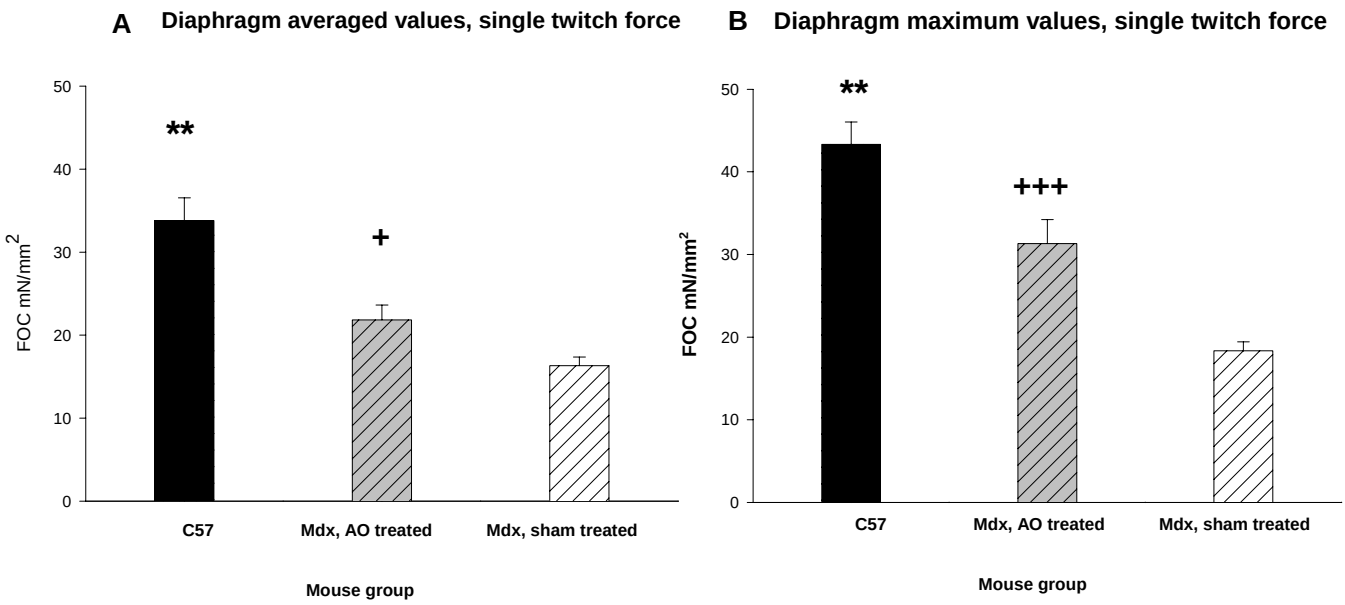


**Fig 5.4** Twitch force results displayed as : A. The average of 3 diaphragm strips, or B. Single maximum value from mice treated with injections of antisense oligoribonucleotides (AO) or saline or Lipofectin (sham treated). FOC= Force of contraction ***$P$<0.001, ** $P$<0.01, * $P$<0.05. n= 10 (C57), 9 (*Mdx* AO) and 8 (*Mdx* sham) ****** =difference between C57 and *Mdx*, AO treated. + = difference between *Mdx*, AO treated and *Mdx*, sham treated.

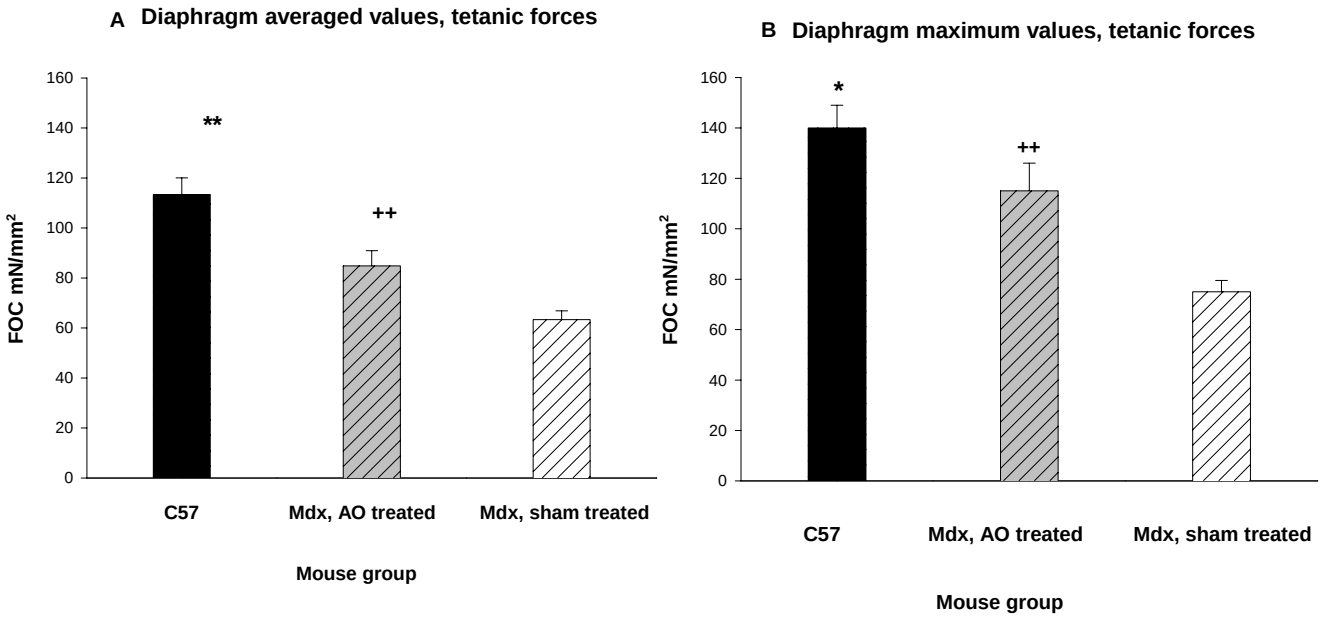


**Fig 5.5** Tetanic force results displayed as : A The average of 3 diaphragm strips, or B Single maximum value from mice treated with injections of antisense oligoribonucleotides (AO) or saline or Lipofectin (sham treated).

Maximum tetanic contractions for AO treated *mdx* were closer to wild type mice values when analysed by this method. FOC= Force of contraction ** $P<0.01$, * $P<0.05$. n= 10 (C57), 9 (*Mdx* AO) and 8 (*Mdx* sham). ****** =difference between C57 and *Mdx*, AO treated. ++ = difference between *Mdx*, AO treated and *Mdx*, sham treated.

Twitch:tetanus ratios were identical for *mdx* AO and sham treated *mdx* when considering averaged values, and these were significantly less than the C57 group (Figure 5.6). For maximum forces the twitch/tetanus ratio was significantly higher in *mdx*, AO treated compared sham treated mdx mice ( $P<0.05$) (Figure 6.5).

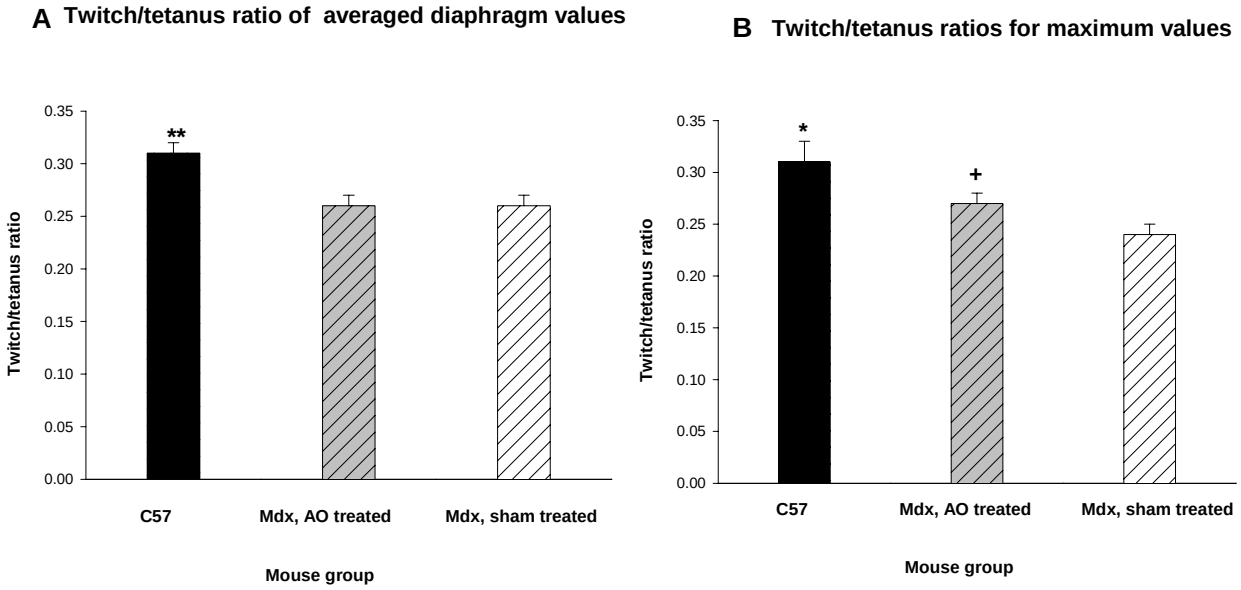


**Fig 5.6** Twitch /tetanus ratio of isolated diaphragm strips from mice treated with injections of antisense oligoribonucleotides (AO) or saline or Lipofectin (sham treated). A) There was no difference between treated and untreated *mdx*, however there were significant differences between both *mdx* groups and wild type mice for averaged values. B) For maximum force values of *mdx*, AO treated were closer to wild type values, although there was still a significant difference between these groups (P<0.05). ** P<0.01, n= 10 (C57), 9 (*Mdx* AO) and 8 (*Mdx* sham) ***** =difference between C57 and *Mdx*, AO treated. **+** = difference between *Mdx*, AO treated and *Mdx*, sham treated.

Fatigue percentage and percentage loss of force (determined by the loss of force of single tetanic stimulus after the 5 min fatigue protocol) were similar between groups of mice, and these values are shown in Table 5.1.

**Table 5.1** Percentage fatigue of diaphragm strips, using a 5-minute protocol with one tetanic stimulation every 5 secs. Loss of force involved measuring one tetanic contraction 5 minutes after the fatigue protocol, expressed as a % reduction in force compared to the initial contraction. n= 10 (C57), 9 (*Mdx* AO) and 8 (*Mdx* sham)

| | **Averaged values** | | | **Maximum values** | | |
|---|---|---|---|---|---|---|
| | **C57** | ***Mdx*, AO** | ***Mdx*,sham** | **C57** | ***Mdx*, AO** | ***Mdx*,sham** |
| **% fatigue** | 42 ± 7 | 49 ± 4 | 45 ± 5 | 49 ± 8 | 50 ± 4 | 60 ± 6 |
| **Loss of force (%)** | 20 ± 6 | 20 ± 4 | 24 ± 5 | 25 ± 7 | 19 ± 3 | 31 ± 8 |

5.5.4 Hydroxyproline analysis

HP values were significantly greater in both sham injected and AO injected mice, compared to C57 mice. Mean HP values were greater in AO treated *mdx* compared to sham treated *mdx*, however these differences were not statistically significant as shown in Figure 5.7

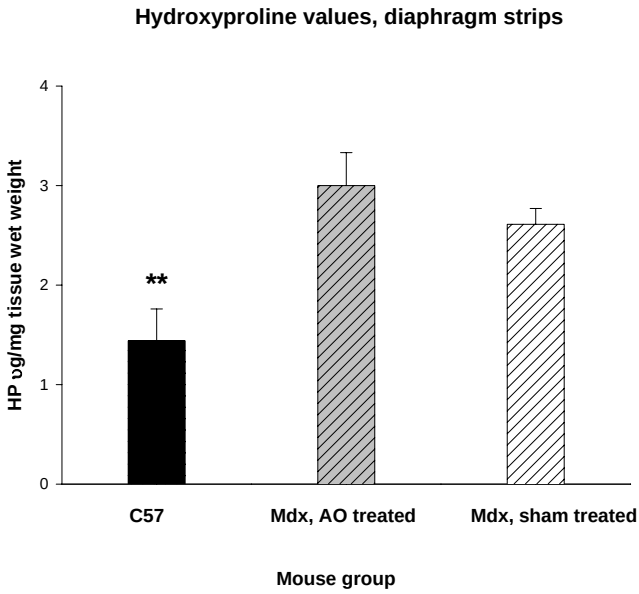


**Fig 5.7** Hydroxyproline values of diaphragm strips. There was no significant difference between *Mdx*, AO treated and *Mdx*, sham treated mice. ** $P<0.01$, n= 10 (C57), 9 (*Mdx* AO) and 8 (*Mdx* sham).

5.5.5 Western Analysis

Western blot analysis of dystrophin expression of diaphragms from wild type mice showed a strong expression of full length dystrophin (Figure 5.8). No dystrophin was detected in homogenates of AO treated or sham treated *mdx* diaphragm samples. This procedure was repeated multiple times using different muscle samples with similar results.

**Fig 5.8** Western blot of individual diaphragm strips from C57 and 3 different AO injected *mdx* mice. Only the band of full length dystrophin in the C57 diaphragm is evident (arrowhead).

5.5.6 Histology

Histological determination of fibrosis showed that *mdx* diaphragms had approximately twice the percentage of fibrosis of wild type diaphragms at this age (C57; 6.1 ± .6%, *mdx*; 13.9 ± .6%, $P< 0.01$). There was no difference in percentage fibrosis between AO treated and sham treated *mdx* (Figure 5.9A). Wild type mice showed a low incidence of centrally nucleated muscle fibres compared to both AO treated and sham treated *mdx*. These differences are displayed in Figure 5.9B. Photomicrographs of representative sections are shown in Figure 5.10 and 5.11.

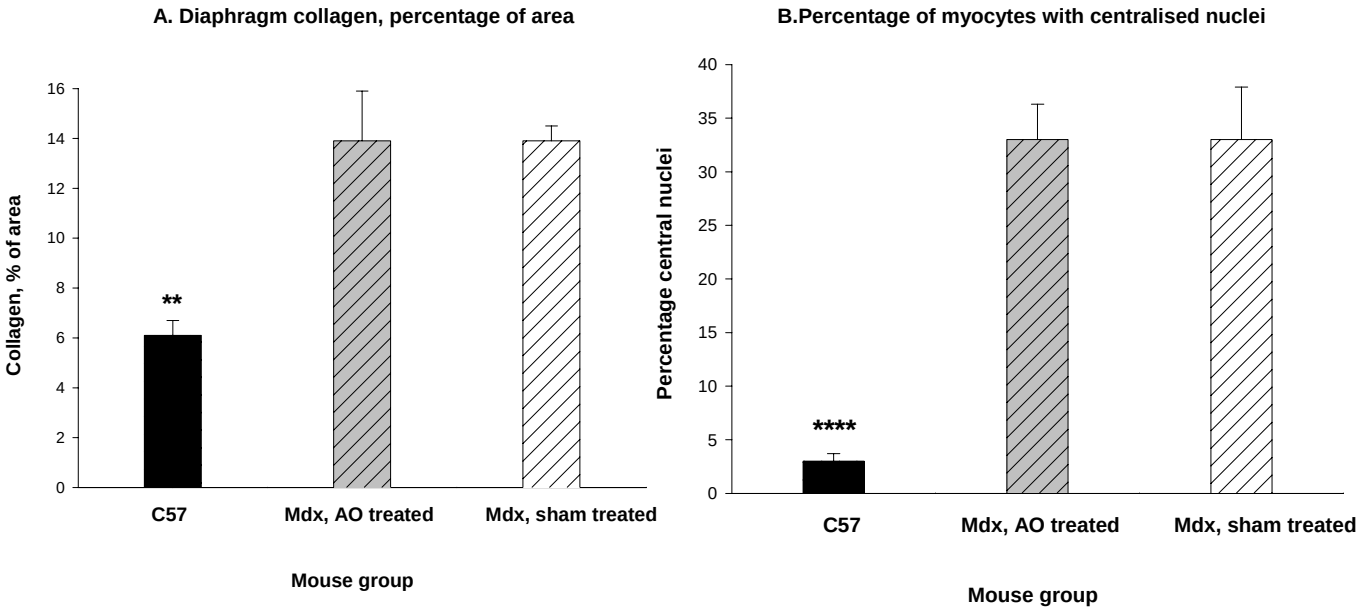


**Fig 5.9** Histological analysis of diaphragm muscle from antisense oligonucleotide (AO) treated and sham treated mice. A. Collagen (as a percentage of area) determined from picrosirius stained sections. B. Percentage of diaphragm fibres with centralised nuclei determined from H & E stained sections. Note the similarity between *mdx* AO and sham treated mice in both diaphragm collagen and centralised nuclei, and the significant differences between *mdx* and wild type mice for both parameters. ** $P<0.01$, **** $P<0.0001$, n= 8 (C57), 6 (*Mdx* AO) and 6 (*Mdx* sham).

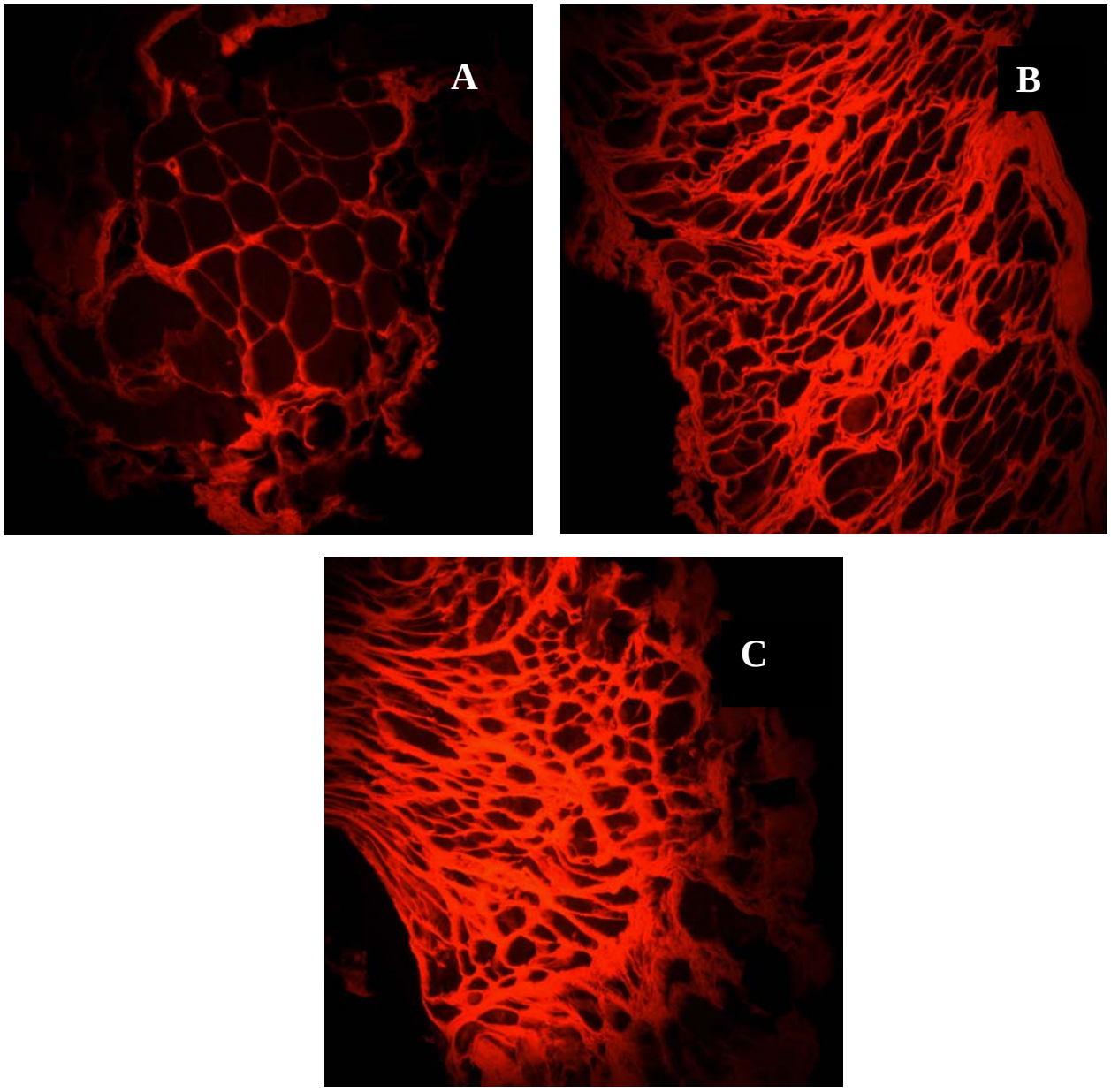


**Fig 5.10** Representative photomicrographs of picrosirius red stained diaphragm muscle sections (20x magnification). A. C57, B *Mdx* AO treated and C *Mdx* sham treated diaphragms. Interstitial collagen was significantly less in wild type mice compared to either AO treated or sham treated *Mdx* groups. The dense interstitial collagen network of *mdx* diaphragm muscle is apparent.

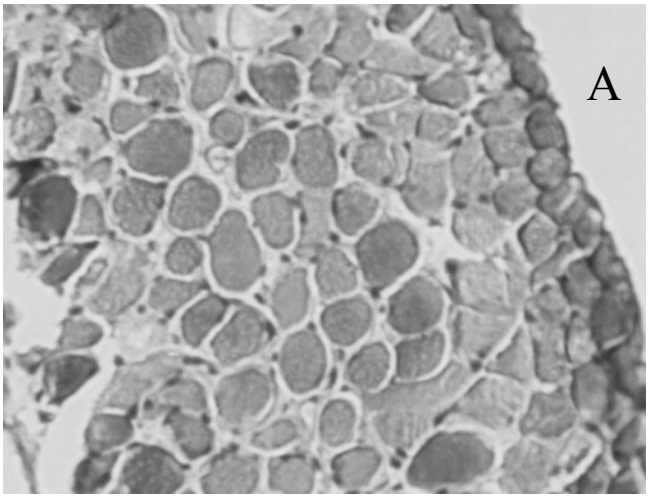


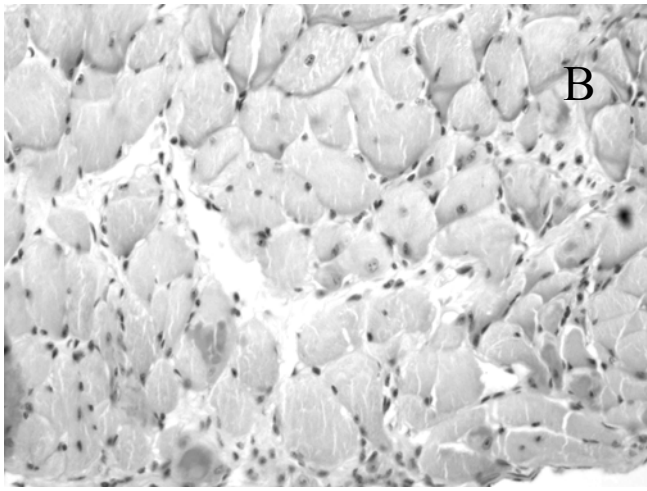


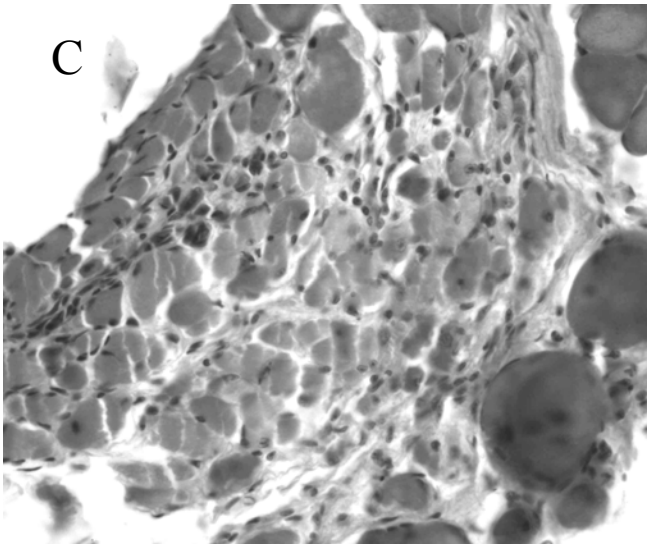


**Fig 5.11** H & E stained diaphragm muscle sections (20x magnification). A. C57, B *Mdx* AO treated and C *Mdx* sham treated. The percentage of centrally nucleated fibres was significantly greater in *Mdx* AO and sham treated muscles compared to wild type mice. Other dystrophic features such as marked variation in cell size, inflammatory cell infiltration and interstitial fibrosis was also evident in *mdx* diaphragms.

## 5.6 Discussion

Recent studies have shown the potential of AO therapy, both in *mdx* cell culture and limb muscles (Mann *et al*., 2001; Mann *et al*., 2002; Lu *et al*., 2003). This current work is novel in applying AOs to *mdx* diaphragm muscle, an organ at greater risk of dystrophic changes, even in young mice. It tests the ability of injected AOs to restore function in diaphragm muscle and investigates whether tissue fibrosis is alleviated.

The diaphragm is less accessible than limb muscles, and there have been few studies determining route, frequency and methods of drug delivery. Controlled release devices for Leukaemia Inhibitory Factor based on calcium alginate rods were sutured to *mdx* diaphragms for a three-month period, and this treatment was shown to ameliorate dystrophic abnormalities (Austin *et al*., 2000). Pure recombinant plasmid DNA and a *lacZ* reporter gene was introduced into mouse diaphragms without causing significant damage, while proving that 41 ± 3 muscle fibres had the potential to be stained from an individual injection site, with fibres frequently showing staining along their entire length. These results were superior to results obtained with similar injections into hind limb muscles (Davis and Jasmin, 1993). Adeno-virus mediated gene transfer into *mdx* diaphragms was successful, however contractile function was impaired, thought to be due to direct cytotoxic effects of viral proteins (Petrof *et al.*, 1995). Intravenous (tail vein injections) and occlusion of the vena cava below the diaphragm allowed reporter gene delivery to mice diaphragms, with expression peaking at 6 days and declining slowly (Liu *et al*., 2001a).

In the current study injections of AO/Lipofectin complex at 4 distinct sites improved twitch and tetanic force production in *mdx* mice diaphragm strips. Contractility data was viewed in 2 ways; firstly by evaluation of normalised forces averaged for 3 diaphragm strips, and secondly by consideration of the maximal twitch and tetanic forces achieved for each diaphragm (Figures 5.4 and 5.5). The two methods were utilised because it is likely that some fibres were more successfully transfected than others, with subsequent force production better reflected by maximal twitch and tetanus forces as compared to averaged values. All 3 groups of mice showed increased force production when maximal values were evaluated, however these increases were greater for *mdx* AO treated mice. Twitch

force and tetanic forces improved 33.9% and 25.3% respectively; when comparing AO with sham treated *mdx* using averaged values. For maximal twitch and tetanus values these gains in function were 70.9% and 53%. Regional variations in diaphragm dystrophy have been noted previously (Anderson *et al*., 1998), or alternatively the variation in force production may better reflect regions of optimal AO delivery and transfection. The benefits were greater for twitch compared to tetanic contractions, as it is probable that patchy sarcolemmal distribution of dystrophin occurs (similar to BMD), resulting in lesser values for fused tetanic contractions where there is recruitment of both dystrophin-positive and negative fibres. The twitch/tetanus ratio was also increased and closer to wild-type mice when maximal values were analysed, due to the higher twitch forces achieved (Figure 5.6). A published observation that dystrophin expression in 17% of mouse diaphragm fibres protected all fibres present within the muscle bundle from the damaging effects of repetitive lengthening contractions suggests that efficiency of transduction need not be close to 100% to obtain significant functional benefits (Decrouy *et al.*, 1997)

There were still significant shortfalls in force values between C57 and AO treated mice. The method of delivery and dosage is one possible explanation. Small volumes of injectate were administered at only four sites around the diaphragm, and although previous work suggests that there is spread along the length of muscle fibres and through the 8-10 cell depth of the diaphragm (Davis and Jasmin, 1993), there was no way of assessing whether tissue strips taken for contractility studies corresponded exactly with injection sites in this current study. There is recent evidence that higher dosages of AOs are required, and persistence of AOs in tissues using direct injection techniques is short (Wells *et al*., 2003). An additional reason why force values did not reach those generated by control mice is the degree of fibrosis of this organ, with even young mice showing extensive collagen deposition.

There was no reduction in tissue collagen in AO treated mice compared to *mdx* mice, as determined by hydroxyproline analysis. In the two histological parameters examined (percentage centralised nuclei and percentage fibrosis), there was no difference detected between AO and sham treated *mdx* mice. At the age of euthanasia (6 months) there is already established dystrophy in *mdx* diaphragms, including variable fibre sizes and fibrosis, as evident on H&E and picrosirius

stained sections. In the future it may be preferable to use younger mice for such studies, before diaphragm fibrosis is as pronounced.

There are several possible reasons for the failure to detect protein expression by Western blot. The dosage of AO used (1 μg per injection site, total of 4 μg per diaphragm) may have been insufficient and dystrophin expression was short-lived or there was interference with the Western procedure due to the presence of the marker dye. The first explanation is the most likely, as more recent work using 3-9 μg per injection (Lu *et al*., 2003) or 8 μg per injection of AO (Wells *et al*., 2003) has shown enhanced transfer and expression The latter authors also suggest that AO-induced dystrophin expression is transient, possibly due to both the loss of the AO and to protein turnover. A recent publication showed that single intravenous administration of the same AO bound to the coblock polymer F127, was sufficient to induce dystrophin, which was demonstrated by immunohistochemical methods but not by Western blots. Three weekly intravenous treatments, however, resulted in increased efficiency of dystrophin induction, successfully demonstrated by Western blotting in many muscles (Lu et al., 2004).

The concentration of AO used was based on prior published studies (Mann et al., 2001); (Gebski et al., 2003), and advice that higher concentrations of AOs may cause tissue necrosis (S. Fletcher, *pers comm*.). Previous studies have utilised the same histology marker dyes in cell culture and *in vivo*, without hindrance to protein detection (Mann *et al*., 2001). Much effort was spent optimising the Western procedure used, including different membranes, buffers and antibody concentrations, which was successful at detecting very low levels of dystrophin in diluted homogenates from C57 muscle with as little as 5 μg of loaded protein (Appendix B).

In conclusion, this study showed that AO injections have the potential to improve contractility of *mdx* diaphragm muscle, even at presumably very low levels of protein expression (ie below that detectable using Western blotting). Diaphragm function, however, is not restored to that displayed by wild-type mice, and in addition tissue fibrosis in 6 month old mice is not reduced. Further refinements of this study would include the use of younger animals, administration of increased AO concentrations, or investigating methods of whole diaphragm delivery, such as intravascular administration with temporary caval occlusion. Immunohistochemical

techniques may be beneficial in showing low levels of AO expression.

# CHAPTER 6. LONG TERM ADMINISTRATION OF ANTISENSE OLIGONUCLEOTIDES INTO THE PARASPINAL MUSCLES OF *MDX* MICE

## 6.1 Introduction

Antisense oligoribonucleotides have become an attractive tool for the study and potential treatment of DMD that results from mutations in the dystrophin gene, which interrupt the reading frame and cause a complete loss of dystrophin.

AOs alter splicing so that the open reading frame is restored and the severe DMD phenotype is converted to a milder BMD phenotype. BMD patients have mutations that are not frame-shifting and result in an internally deleted, but partially functional dystrophin that retains it's N- and C- terminal ends (Koenig *et al*., 1989).Exon skipping has been successful in cells derived from the *mdx* mouse (Wilton *et al*., 1999; Mann *et al*., 2002; Mann *et al*., 2001; Lu *et al*., 2003) and various DMD patients (van Deutekom *et al*., 2001; Aartsma-Rus *et al*., 2002).

Functional properties of AO treated muscle were examined 3-4 weeks after a single administration into *mdx* tibialis anterior muscle (Lu *et al*., 2003). This muscle typically undergoes early necrosis but exhibits milder pathology to that seen in the diaphragm (Boland *et al*., 1995; Boland B. *et al*., 1995), the intercostal muscles, or those skeletal muscles involved with postural activity (Lefaucheur *et al*., 1995). Because age-related diminution of efficiency is a common feature of viral and non-viral gene delivery into skeletal muscle (particularly in dystrophic conditions with increased extra-cellular matrix), protein expression was examined in mice of 6 months of age and was shown to be similar to 2 and 4 week old animals (Lu *et al*., 2003). In that study dystrophin persisted for up to 2 months, however another group found that AO-induced dystrophin expression is much more transient, possibly due to both a loss of AO and protein turnover (Wells *et al*., 2003).

There have been no studies documenting AO use in very old *mdx* mice despite their skeletal muscles undergoing cycles of degeneration and regeneration, and showing pathology late in life closer to DMD dystrophinopathy (Lefaucheur *et al*., 1995; Pastoret and Sebille, 1995b). There is a need to apply AOs to a range of muscles over an extended period of time in order to assess the functional changes in those muscles and extend the therapeutic applicability of these techniques. This

current study utilises mice up to 18 months of age, and is also novel for administering AOs as deep lumbar injections and assessing respiratory and paraspinal muscle function.

## 6.2 Aims

The aims of this study were to determine changes in function of intercostal muscles and latissimus dorsi muscles following 15 monthly deep intramuscular injections of AOs into paraspinal muscles. Diaphragm muscle strips were also examined to compare the severity of dystrophy with the paraspinal and accessory respiratory muscles. This study follows on from previous work (Chapter 4) determining the usefulness of the Kyphotic Index (KI) in measuring kyphosis in older *mdx*. Monthly radiographs were taken for the calculation of KI, which was compared in AO and sham treated mice. In addition, hydroxyproline assays and histological measures of fibrosis and muscle degeneration and regeneration were utilised to evaluate the effects of therapy. Finally Western blotting was used to determine expression of dystrophin protein.

## 6.3 Methods

### 6.3.1 Mouse numbers and grouping

Three groups of mice were utilised; a) C57 mice, sham injected, b) *Mdx* mice, sham injected and c) *Mdx* mice, AO injected. Mice were males at 8 weeks old at the beginning of the experiment and 18 months at the time of euthanasia. 6 mice were assigned to each group, however 2 died (one C57 and one sham injected *mdx*). One of these mice failed to recover from anaesthesia and the other died in its cage of unknown causes. These groupings are shown in Figure 6.1

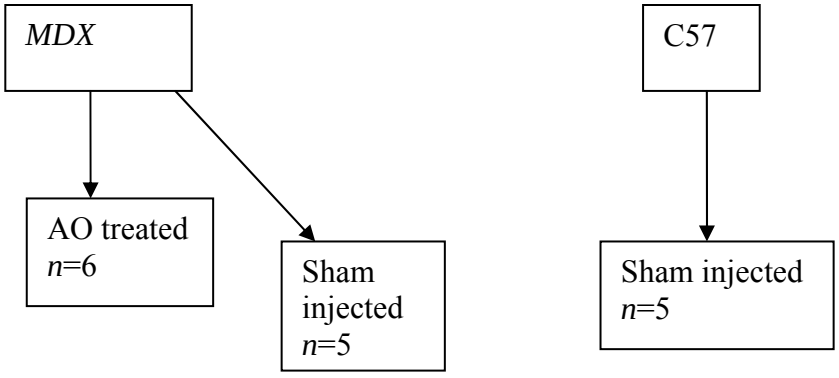


**Fig 6.1** Mouse numbers and groups for long-term administration of Antisense oligonucleotides (AOs) into the paraspinal muscles.

### 6.3.2 Anaesthesia for radiography and administration of AOs

Anaesthesia was induced with ketamine HCl 50 mg/kg (Ketamil, Troy Laboratories, Australia) and xylazine HCl 10 mg/kg (Ilium Xylazil-20, Troy Laboratories, Australia) subcutaneously prior to administration of AOs and radiography.

The hair over the dorsum was clipped, and the skin cleaned with ethanol prior to AO injections. The mice were positioned in ventral recumbency, and firm index finger and thumb pressure was applied to elevate and clearly visualise the lumbar musculature.

At the end of the procedure atipamezole 1mg/kg (Antisedan, Novartis Animal Health, Australia) was administered subcutaneously for the reversal of xylazine. Mice were kept warm and monitored until ambulatory.

### 6.3.3 Antisense oligoribonucleotides

The AO used was M23D (+02-18), as defined previously (Mann *et al*., 2002) and represented in Figure 6.2. AOs were synthesised on an Expedite 8909 Nucleic Acid Synthesiser at Australian Neuromuscular Research Institute, University of Western Australia. The conditions for transfection had been optimised previously (Mann *et al*., 2002). Complexes of Lipofectin (Life Technologies, Melbourne, Australia) were prepared in a 2:1 Lipofectin/AO ratio (w/w) in sterile 0.9% saline. Lipofectin and AO were incubated separately with saline for 30 minutes prior to mixing; the AO/Lipofectin complex was then used within 30-45 minutes.

The injection sites were into the paraspinal muscles adjacent and parallel to the thoracolumbar vertebrae. The needles were placed deep into the longissimus dorsi muscles, orientated in a cranial direction and kept as flat as possible. Evidence from preliminary experiments using several cadaver specimens injected with dye showed that the majority of the injectate remained within the longissimus dorsi muscles, but a small amount spread within the dorsal portion of the latissimus dorsi muscle, or sometimes into adjacent intercostal muscles (Figure 6.3). These variations may be due to the needle depth, or occasionally a small volume of

injectate could travel via fascial planes to other muscle regions. This variation in distribution was not a concern, as it was likely that each muscle had a contributory role in the progression of kyphosis, and the latissimus and intercostals were also used in contractility studies. Three evenly spaced injections were administered on each side of the spine, to give a total of 6 µg of AO per mouse in a total volume of 40 µL. Sham injections comprised the same volume of saline. Saline was utilised instead of Lipofectin, based on advice from previous studies where there was no difference found between saline or Lipofectin sham groups (S Fletcher, *pers comm*.) At the time of the final procedure (18 months of age) the AO treated *mdx* had 2 µL histology marker dye added to the 40 µL volume (Wak-Chemie Medical, Germany). The dye was autoclaved in cryotubes prior to use, with the resultant granular paste reconstituted in sterile saline.

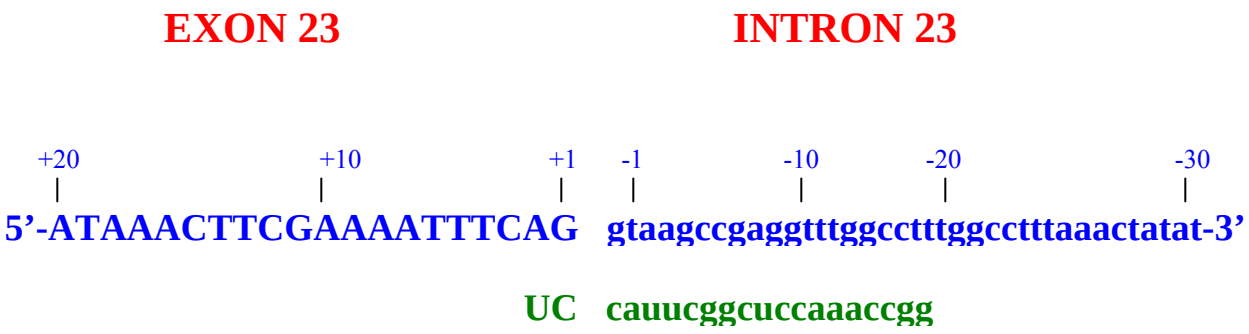


2'-O-methyl modified antisense oligonucleotide M23D(+2-18)

**Fig. 6.2** Representation of the genomic sequence of the boundary between Exon 23 (upper case letters) and Intron 23 (lower case letters) of the mouse dystrophin gene. The numbers above the sequence are used to designate the target homology of the AO M23D(+2-18), where M=murine, 23= exon number, D=Donor splice site, (+-)=annealing coordinates. +2 is the last 2 exonic bases and –18 represents the first bases of intron 23 (Mann *et al*., 2002; Wells *et al*., 2003)

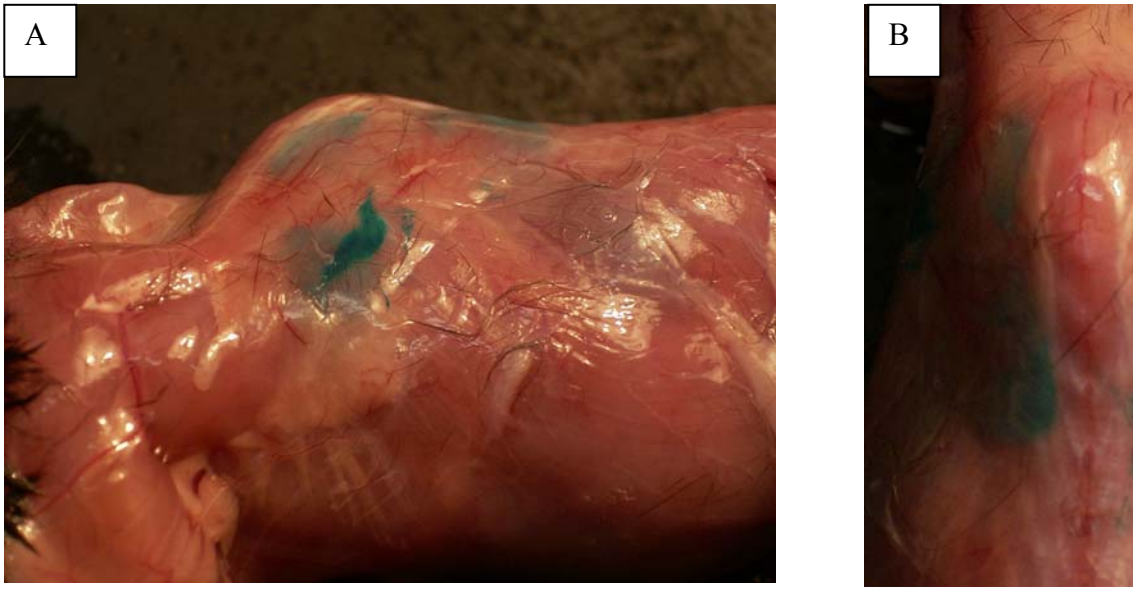


**Fig 6.3** Photographs showing the spread of antisense oligonucleotide/ histology dye injections in the paralumbar muscles of *mdx* mice. A. Lateral view of skinned mouse, with spread of injectate in longissimus muscle (top) and latissimus muscle (below). B. Dorsoventral view showing spread within longissimus muscles. In some mice there was clear staining of intercostal segments also.

6.3.4 Radiography and determination of Kyphosis Index

After induction of anaesthesia and administration of AOs, mice were lightly taped to the radiographic cassette using clear adhesive tape. Each animal was individually identified by tail markings, a radiodense (metal) number placed next to them, and a radiographic cassette label indicating date and animal grouping. Konica CM-H medical mammography film was exposed using a portable X-ray unit (either Showa Xray Co Ltd Tokyo, Japan or Porta 1030 model, Job Corporation, Yokohama, Japan).

Each whole body radiograph was photographed using a tripod mounted Ricoh Caplio RR30 digital camera with images analysed using Scion Image software Beta 4.0.2 (http://www.scioncorp.com). KI was calculated from a line drawn between the caudal margin of the last cervical vertebra, to the caudal margin of the 6$^{th}$ lumbar vertebra (usually corresponding to the cranial border of the wing of the ilium) (Line AB), divided by a line perpendicular to this from the dorsal edge of the vertebra at

the point of greatest curvature (Line CD), as described in Chapter 4. Measurements for each mouse were repeated 3 times and the results were averaged.

6.3.5 Contractility studies

18-month-old mice were anaesthetised using pentobarbitone sodium (Nembutal, Boehringer Ingelheim, Australia) at 70 mg/kg IP. Cessation of breathing occurred when the thorax was entered. The following muscles were dissected and placed into ice-cold Krebs buffer solution bubbled with carbogen (95% $O_2$/5% $CO_2$); a) diaphragm strip from left midcostal hemi-diaphragm b) latissimus dorsi muscle and c) intercostal section comprising 4 ribs and their attached intercostal muscles (internal and external), extending from T8-12, adjacent and parallel to the longissimus dorsi muscle. Muscle dissections are described in greater detail in Chapter 4.

Muscles from the left side were collected and stored for Western analysis, histology and hydroxyproline assays. Contralateral muscles were mounted in water-jacketed glass organ baths, maintained at 23$^{o}$C, using 6/0 silk surgical thread to attach to a fixed peg at one end and a force transducer at the other. Tissues were stimulated via a Grass S48 stimulator (W. Warwick, RI, USA) and current intensity was amplified using a pre-amplifier (EP500B. Audio Assemblies, Campbellfield, Victoria, Aust). Data was collected and analysed using Chart 4.1.1 software. A square pulse of 0.2ms duration was dispersed via 2 platinum electrodes positioned along the length of the muscle.

Optimum preload ($L_o$) was defined as the length eliciting maximal single twitch force. Optimal voltage was also determined for each preparation, as was the frequency eliciting maximal tetanic force from a range of 50 - 180 Hz. Reported data was the average of 3 individual single twitch or tetanic stimulations per muscle strip after 25 minutes of equilibration and optimisation of conditions. Muscles were measured at $L_o$ using a digital micrometer, blotted for 3 secs then weighed. Cross sectional area (CSA) and normalisation of force was calculated as described previously for diaphragm and latissimus muscles, where CSA equals tissue weight divided by length x 1.06 (density of mammalian muscle) (Lynch *et al*., 2001). Intercostal muscle fibre CSA was shown to vary topographically (Kelsen *et al*., 1993) and in our preparations a strip comprises both muscle and rib cartilage and

internal and external intercostal muscle layers consisting of differing fibre orientations and hence lengths. For these reasons intercostal forces were normalised to weight only. Time to peak force, 50% relaxation time and 90% relaxation time was calculated for each single twitch value.

### 6.3.6 Hydroxyproline analysis

Hydroxyproline content was used as a measure of collagen in diaphragm, intercostal muscles, latissimus dorsi and longissimus dorsi muscles. Muscles were trimmed of fat, ribs and tendons and stored at -80 $^{o}$C. Tissue was thawed then hydrolysed in sealed tubes with 6 M HCl overnight at 110 $^{o}$C. The samples were dried to entirety using filtered air under pressure and heat (50$^{o}$C). The rest of the protocol has been described previously (Stegemann and Stalder, 1967) and Appendix B gives details of the procedure for total assay volumes of 2 mLs. Values are expressed as μg HP/mg tissue wet weight.

### 6.3.7 Histology

Each tissue (diaphragm, latissimus dorsi, longissimus dorsi and intercostal muscles) was pinned onto cork at optimal length and then fixed sequentially in Telly's fixative (formaldehyde, glacial acetic acid-ethanol fixative, 72 hours), Bouin's solution (formaldehyde, glacial acetic acid-picric acid fixative, 24 hours) and 70% ethanol, prior to paraffin embedding, cutting and staining of 10μm sections using 0.1% w/v picrosirius red solution (Sirius Red F3B, Chroma Dyes, Germany in saturated picric acid), a collagen specific stain. Instead of applying the histological grading scheme used in Chapter 4, an image analysis program was utilised to grade collagen as a percentage of tissue area. Fluorescent microscopy images were acquired using a digital camera (Q imaging Micropublisher 5.0 RTV) coupled to an epifluorescence microscope (Eclipse E600, Nikon, Japan). Four sections per tissue were photographed and analysed using the image analysis program DocuAnalySIS (Soft Imaging System), then averaged. Additional 5 μm sections were stained with haematoxylin and eosin and viewed using bright field, with images acquired and analysed using the same equipment. Percentages of muscle fibres with centralised

nuclei were determined in 200 fibres per muscle. Analysis was performed blinded to the strain of mouse.

## 6.4 Statistics

Pilot experiments on aged mice were performed for a previous experiment to estimate standard deviations and suitable sample size (Chapter 5). *Post hoc* tests of power (Plummer, 1998) confirmed that an $n = 3$ animals for assessment of KI and $n=5$ animals for contractility experiments of the latissimus, longissimus and diaphragm muscles were adequate. Results are expressed as means±S.E. Responses between *mdx* and control strain were analysed using Student's unpaired *t*-tests, with the exception of differences in KI, where ANOVA was employed. $P < 0.05$ were considered statistically significant.

## 6.5 Results

### 6.5.1 Evaluation of long term AO administration

All mice tolerated the injection procedure well, with no adverse effects noted in surviving animals. At the conclusion of the experiment all mice showed a degree of palpable thoracolumbar kyphosis, which was less pronounced in the control strain. There were no significant differences in body weights between the three groups (C57 30.4 ± 1.03g; *mdx* sham treated 31.4 ± 0.88g; *mdx* AO treated 31 ± 0.98g)

### 6.5.2 Kyphotic Index

KI as measure of spinal deformity was initially less for both sham and AO treated *mdx* mice compared to control mice ($P<0.01$ at 6 months of age). The AO treated *mdx* showed a tendency to a greater KI (and hence less thoracic deformity) than sham treated *mdx* after that age, although this only reached statistical significance at 10 months and again by the end of the experiment (18 months of age). AO treated *mdx* mice also had a lower KI compared to control mice from 8 to 18 months of age, however at 16 and 18 months there was no statistical significance between the two groups. The data was also analysed with the inclusion of aging C57 and *mdx* from a previous study (Chapter 4). This ensured a greater *n* number (n= 8 (C57), 6 (*Mdx* AO) and 9 (*Mdx*)), which reduced some of the intergroup variability.

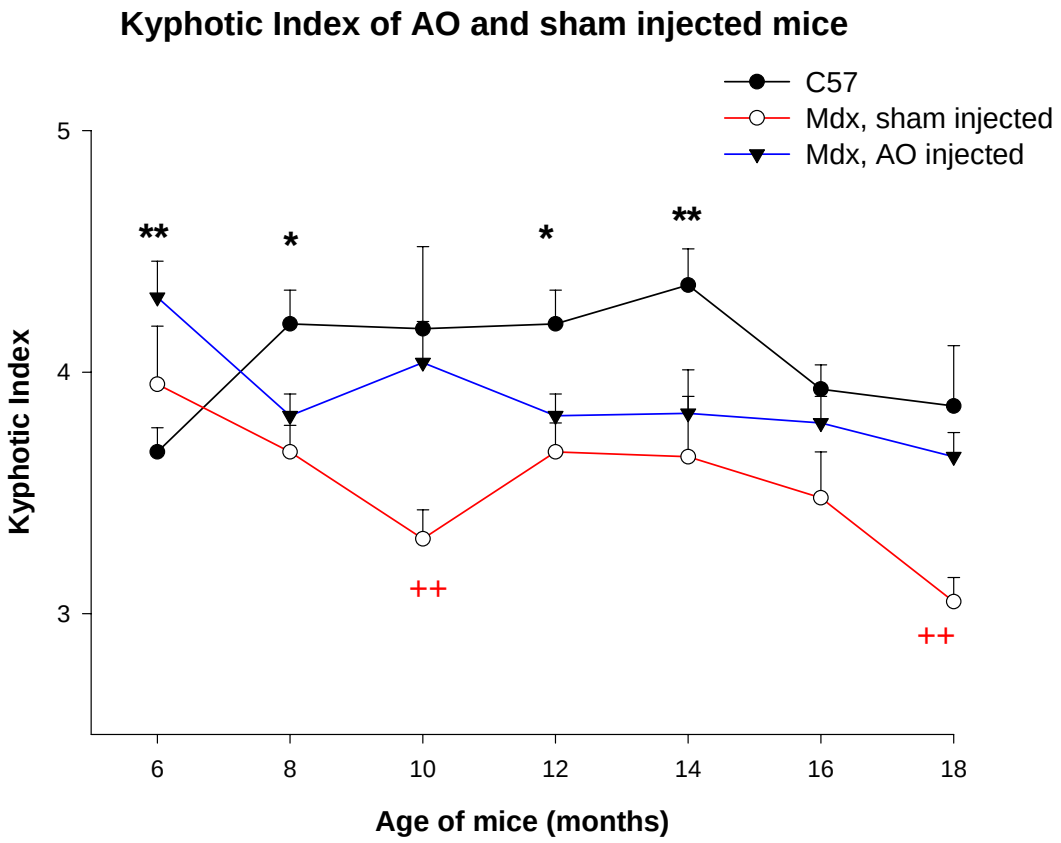


This was believed to be acceptable as all mice were x-rayed on the same day each month and were of a similar age and weight. There was again evidence of reduced kyphosis in AO treated *mdx* mice, with statistical significance between treated and untreated *mdx* at 10, 12, 16 and 18 months of age. The AO treated mice however still demonstrated a reduced KI at most time points. Measured KI of the 3 mouse groups is shown in Figure 6.4.A and B.

Examples of radiographs from aged (18 month old mice) are shown in Figure 6.5.

**Fig 6.4A** Kyphotic Index as a measure of thoracolumbar deformity in antisense oligonucleotide (AO) treated *Mdx*, sham (saline) treated *Mdx* and C57 mice. AO/Lipofectin complex or saline were injected intramuscularly into the paraspinal muscles once monthly from 2-18 months of age. KI was calculated from lateral radiographs. n= 5 (C57), 6 (*Mdx* AO) and 5 (*Mdx* sham). * $P<0.05$, ** $P<0.01$ (comparing AO treated *Mdx* and C57 mice), and ++ $P<0.01$ (comparing AO treated *Mdx* and sham injected *Mdx*).

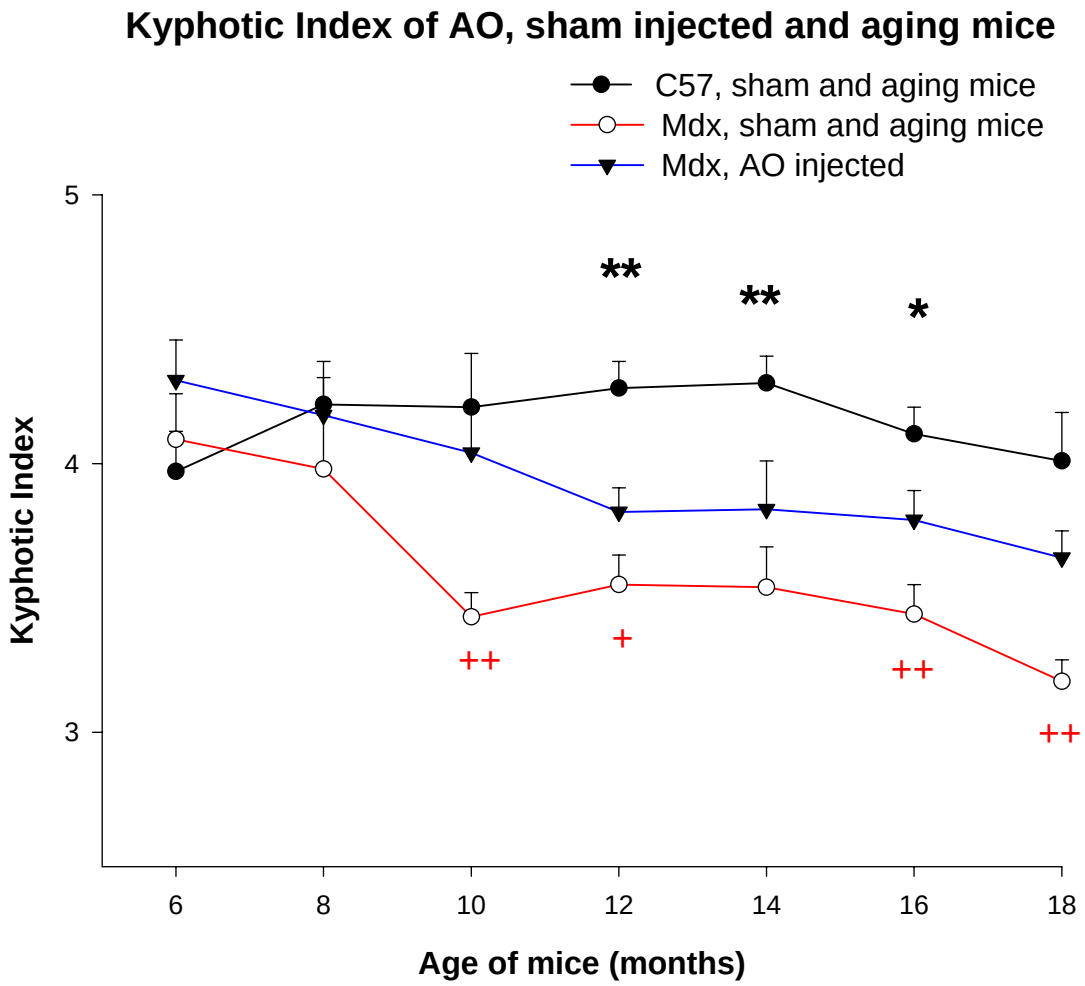


**Fig 6.4B** Kyphotic Index as a measure of thoracolumbar deformity in antisense oligonucleotide (AO) treated *Mdx*, sham (saline) treated *Mdx* and C57 mice and additional untreated *Mdx* and C57 mice. AO/Lipofectin complex or saline were injected intramuscularly into the paraspinal muscles once monthly from 2-18 months of age. KI was calculated from lateral radiographs. n= 8 (C57), 6 (*Mdx* AO) and 9 (*Mdx*). * $P<0.05$, ** $P<0.01$ (comparing AO treated *Mdx* and C57 mice), and ++ $P<0.01$ (comparing AO treated *Mdx* and sham injected *Mdx*). There was evidence of reduced kyphosis in AO treated *Mdx* compared to sham injected and untreated *Mdx*, which reached statistical significance at 10, 12, 16 and 18 months of age.

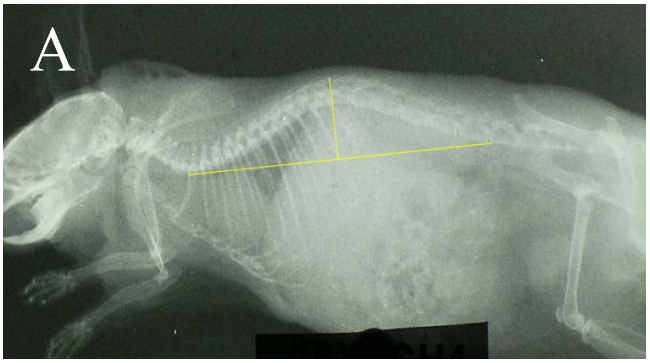


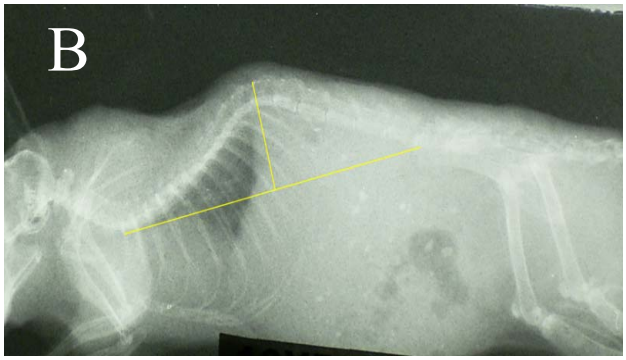


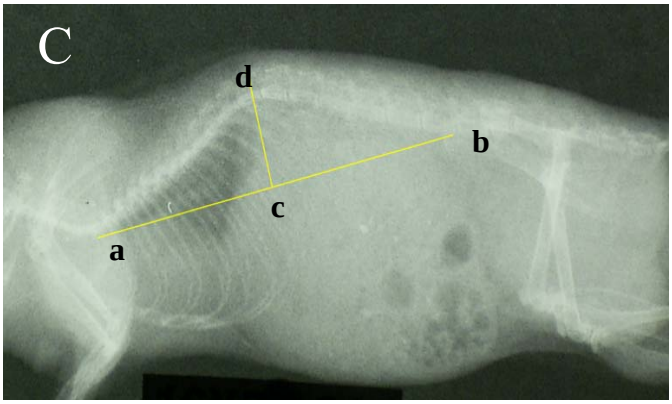


**Fig 6.5** Representative radiographs from 18 month old mice treated with either antisense oligonucleotide (AO) injections or sham (saline) injections into the paraspinal muscles. The yellow lines represent those constructed for the measurement of the Kyphotic Index (KI) = length of line ab/cd. A) C57 sham injected mouse. KI= 3.86 B) *Mdx* sham injected. KI=3.05 C) *Mdx* AO treated. KI=3.65. In the above examples kyphosis is more pronounced in the *Mdx* sham injected mouse, resulting in a lower KI.

6.5.3 Muscle contractility

The characteristics of each isolated muscle (optimal length (Lo), weight and width) are shown in Table 6.1. There was a significant increase in weights of all *mdx* muscle preparations (sham and AO treated) compared to wild type mice. This weight increase of the latissimus dorsi and diaphragm muscles was attributable in part to their greater widths ($P<0.05$). Diaphragm strips are cut from the entire organ, and therefore width could vary from section to section, however the latissimus is an entire muscle that has a distinctive fan shape. It is possible that a measurement of a long muscle of varying widths was not entirely accurate. It is also likely that dystrophic changes, including collagen and fat deposition and muscle hypertrophy, also play a role in the increased weight of most *mdx* muscles. There were no significant differences in muscle morphometry between AO and sham treated *mdx*.

**Table 6.1** Mean (± SE) optimum fibre length (Lo), weight and width of paraspinal and respiratory muscle strips from 18-month-old sham treated control mice, sham treated *mdx* mice and antisense oligonucleotide treated *mdx* mice. n= 5 (C57), 6 (*Mdx* AO) and 5 (*Mdx* sham). * $P<0.05$, ** $P<0.01$ (comparing AO treated *Mdx* and C57 mice). ++ $P<0.01$ (comparing C57 and sham injected *Mdx*).

| Muscle | Lo (mm) | Weight (mg) | Width (mg) |
|---|---|---|---|
| **Latissimus dorsi** | | | |
| Control | 33.04 ± 2.2 | 77 ± 8.2 | 2.34 ± 0.2 |
| Sham *mdx* | 32.7 ± 2.14 | 121.6 ± 14.2 + | 3.02 ± 0.3 |
| AO *mdx* | 34.4 ±0.69 | 140.6 ± 8.8 * | 3.27 ±0.29 * |
| **Diaphragm strip** | | | |
| Control | 8.1 ± 0.78 | 6.08 ± 1.2 | 1.26 ± 0.12 |
| Sham *mdx* | 7.94 ± 0.74 | 10.92 ± 1.85 + | 1.92±0.31 + |
| AO *mdx* | 7.63 ± 0.28 | 9.36 ± 0.82 * | 2.1 ± 0.13 * |
| **Intercostal strip** | | | |
| Control | 7.61 ± 0.99 | 48.2 ± 6.4 | 5.37 ± 0.55 |
| Sham *mdx* | 8.05 ± 0.89 | 79.82 ± 5.5 ++ | 6.88 ± 0.89 |
| AO *mdx* | 8.53 ± 0.21 | 82.96 ± 2.8 ** | 5.86 ± 0.17 |

*In vitro* normalised twitch and tetanic forces of the three skeletal muscles examined are shown in Figure 6.6 (A, B and C).

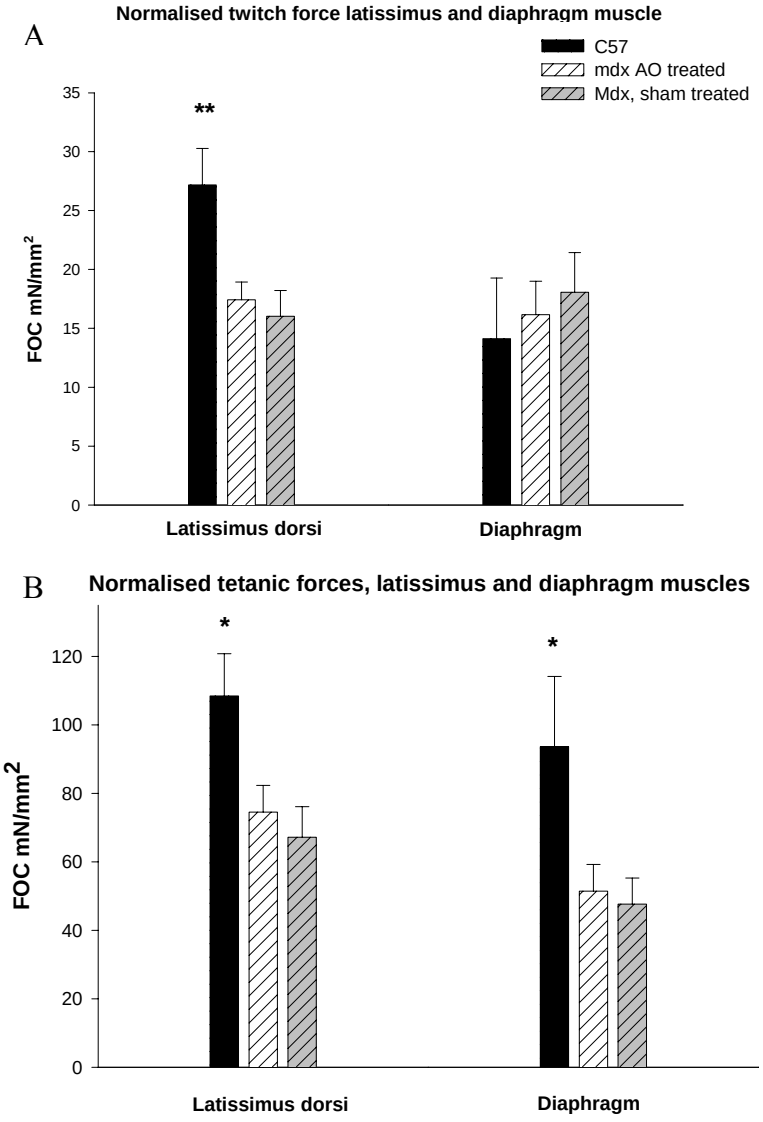

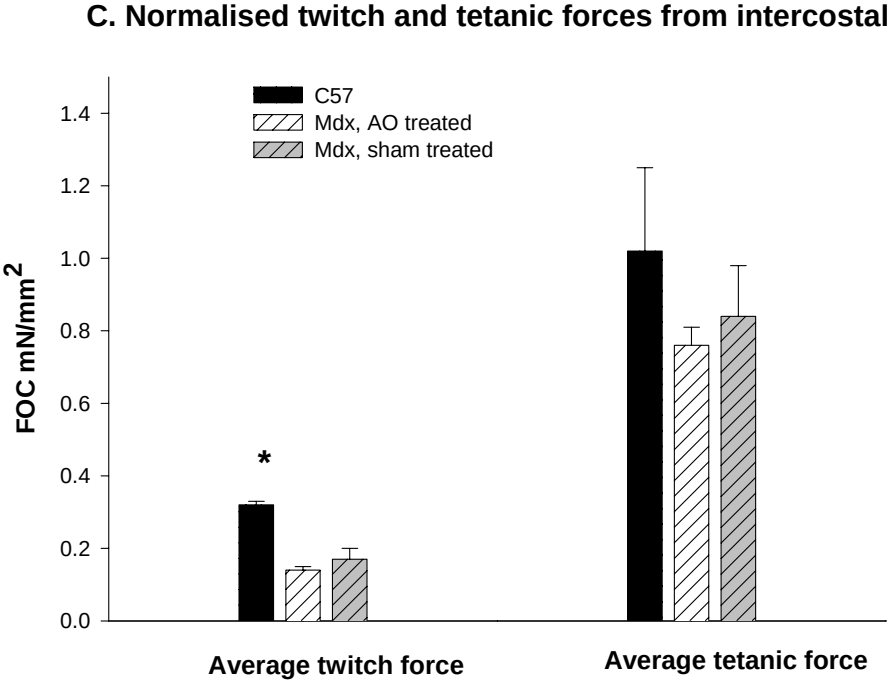


**Fig 6.6** Isometric twitch and tetanic forces from latissimus dorsi, diaphragm and intercostal strips from 18-month-old sham injected control mice, antisense oligonucleotide (AO) injected and sham injected *mdx*. A) Peak twitch forces of latissimus and diaphragm muscles in the three groups of mice. B) Peak tetanic forces of latissimus and diaphragm muscles. C) Twitch and tetanic forces of intercostal muscle strips. There were significantly greater twitch and tetanus forces in control mice compared to mdx for all muscles, however there was no difference in force between AO treated and sham injected mice.

FOC= Force of contraction ** $P<0.01$, * $P<0.05$. n= 5 (C57), 6 (*Mdx* AO) and 5 (*Mdx* sham) ** =difference between C57 and *Mdx*, AO treated.

6.5.4 Quantitation of collagen

The hydroxyproline content of four paraspinal and respiratory muscles (latissimus dorsi, longissimus dorsi, diaphragm and intercostal muscles) is shown in Figure 6.7. All *mdx* muscles demonstrated approximately twice the hydroxyproline levels compared to control mice ($P<0.05$), with the diaphragm showing the greatest evidence of fibrosis of the four tissue types. There was a trend for lower hydroxyproline levels of diaphragm and intercostal muscles in *mdx* AO treated mice, however this did not reach statistical significance. The greater fibrosis of *mdx* diaphragms was also apparent on picrosirius stained sections of these muscles. *Mdx* AO treated latissimus and diaphragm muscles showed significantly less fibrosis than sham treated *mdx* when analysed by this method (Figure 6.8). Examples of histological sections are shown in Figure 6.9.

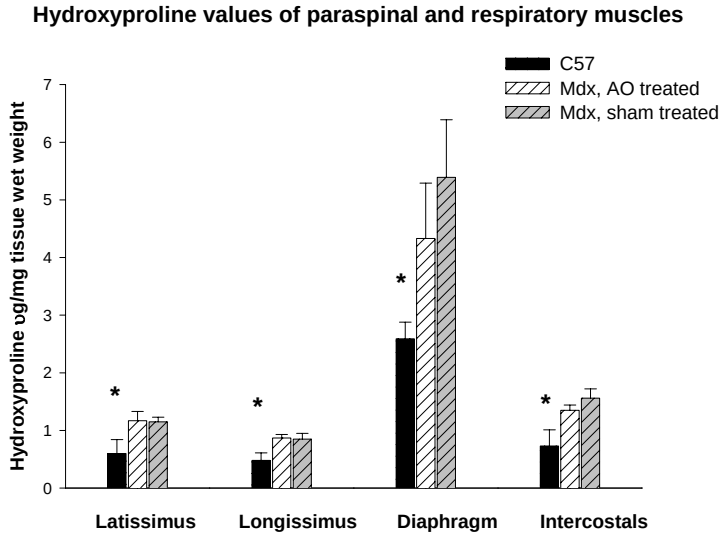


**Fig 6.7** Hydroxyproline (HP) content of latissimus dorsi, longissimus dorsi, diaphragm and intercostal muscles in control mice, sham treated *mdx* and antisense oligonucleotide (AO) treated *mdx* mice. Tissue fibrosis, as measured by HP content, was significantly greater in all *mdx* muscles compared to controls. * $P<0.05$. n= 5 (C57), 6 (*Mdx* AO) and 5 (*Mdx* sham).

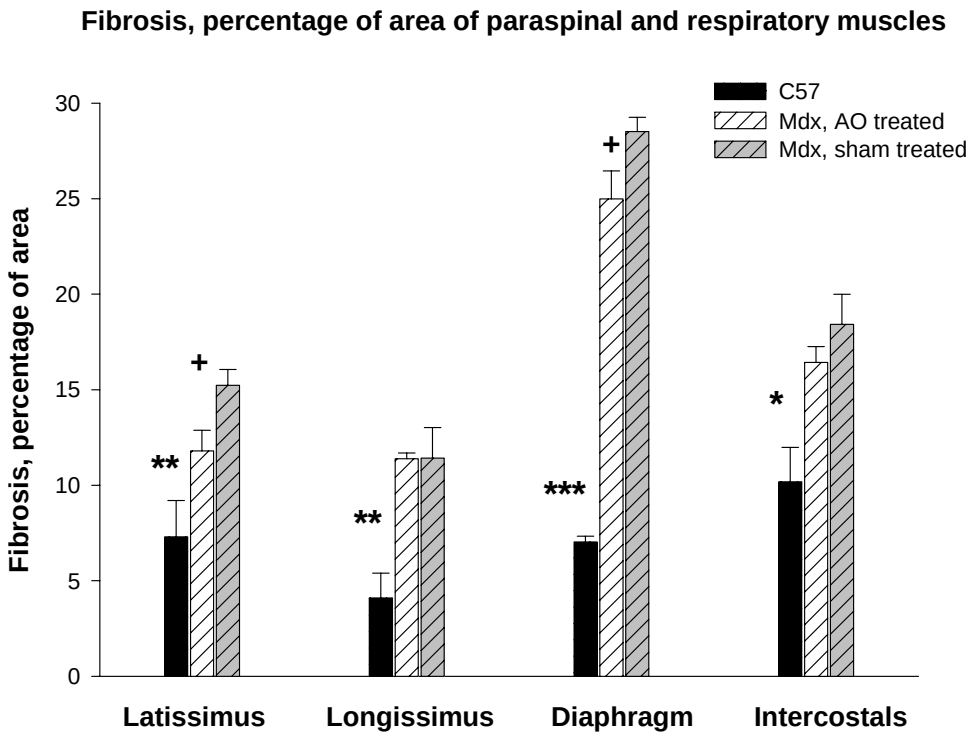


**Fig 6.8** Fibrosis of latissimus dorsi, longissimus dorsi, diaphragm and intercostal muscles in control mice, sham treated *mdx* and antisense oligonucleotide (AO) treated *mdx* mice. Tissue fibrosis, as measured by analysis of picrosirius stained tissues was significantly greater in all *mdx* muscles compared to controls. For diaphragm and latissimus dorsi muscles there was significantly less fibrosis in AO treated *mdx* compared to sham treated *mdx*. n= 5 (C57), 6 (*Mdx* AO) and 5 (*Mdx* sham). * $P<0.05$, ** $P<0.01$, $P<0.001$ (comparing AO treated *Mdx* and C57 mice). + $P<0.05$ (comparing C57 and sham injected *Mdx*).

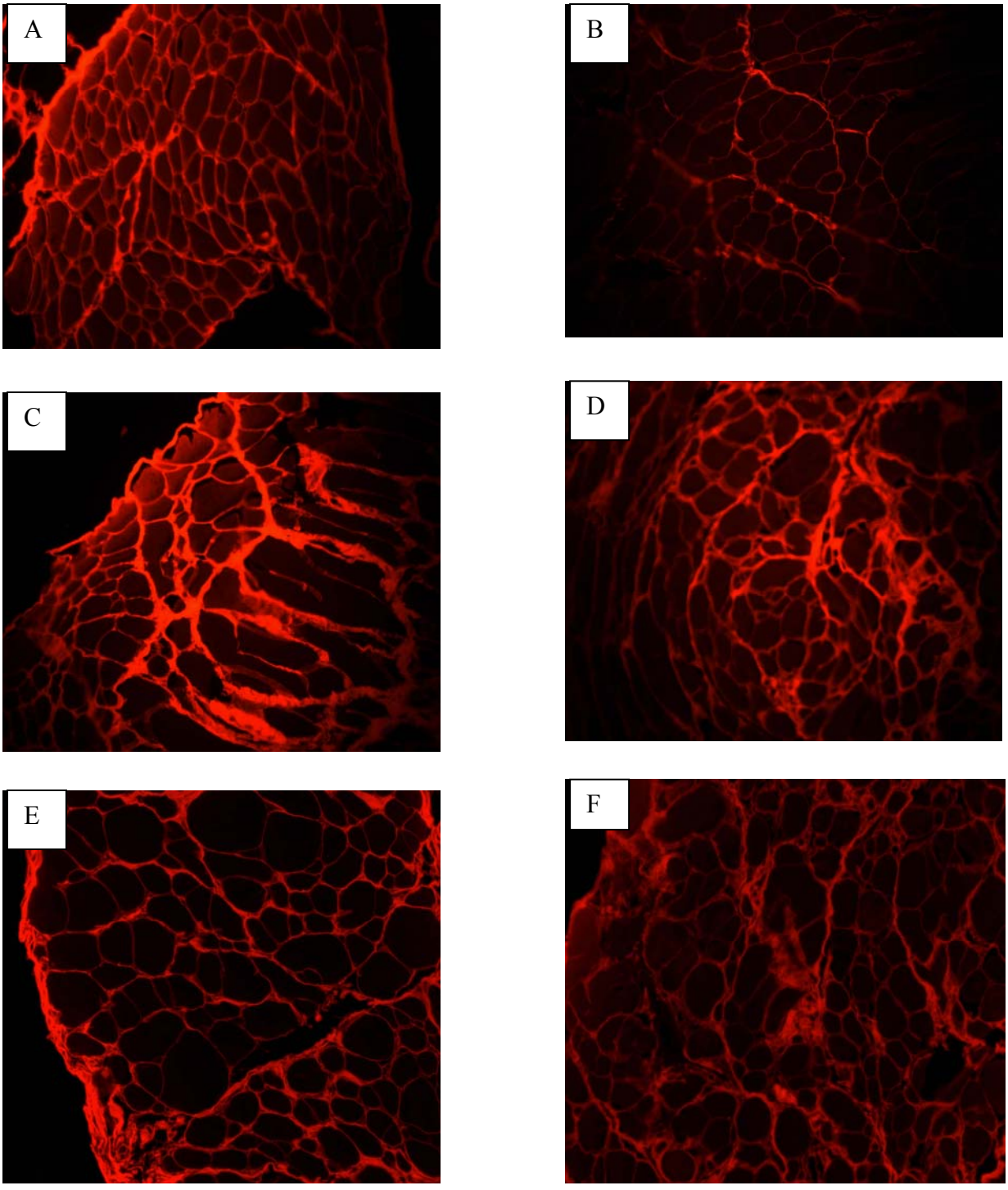


**Fig 6.9i)** Latissimus dorsi (A,C,E) and longissimus dorsi muscle sections (B,D.F) stained with picrosirius red. *Mdx* mice (C,D) showed significantly greater fibrosis than control mice (A,B). In addition to the dense interstitial collagen network of dystrophin deficient muscle, there was also irregular myocyte size and fibre disarray. In antisense oligonucleotide (AO) treated mice there was a small, but statistically significant decrease in percentage fibrosis of the latissimus dorsi muscles (E), but not the longissimus dorsi muscles (F), compared to sham treated *mdx*.

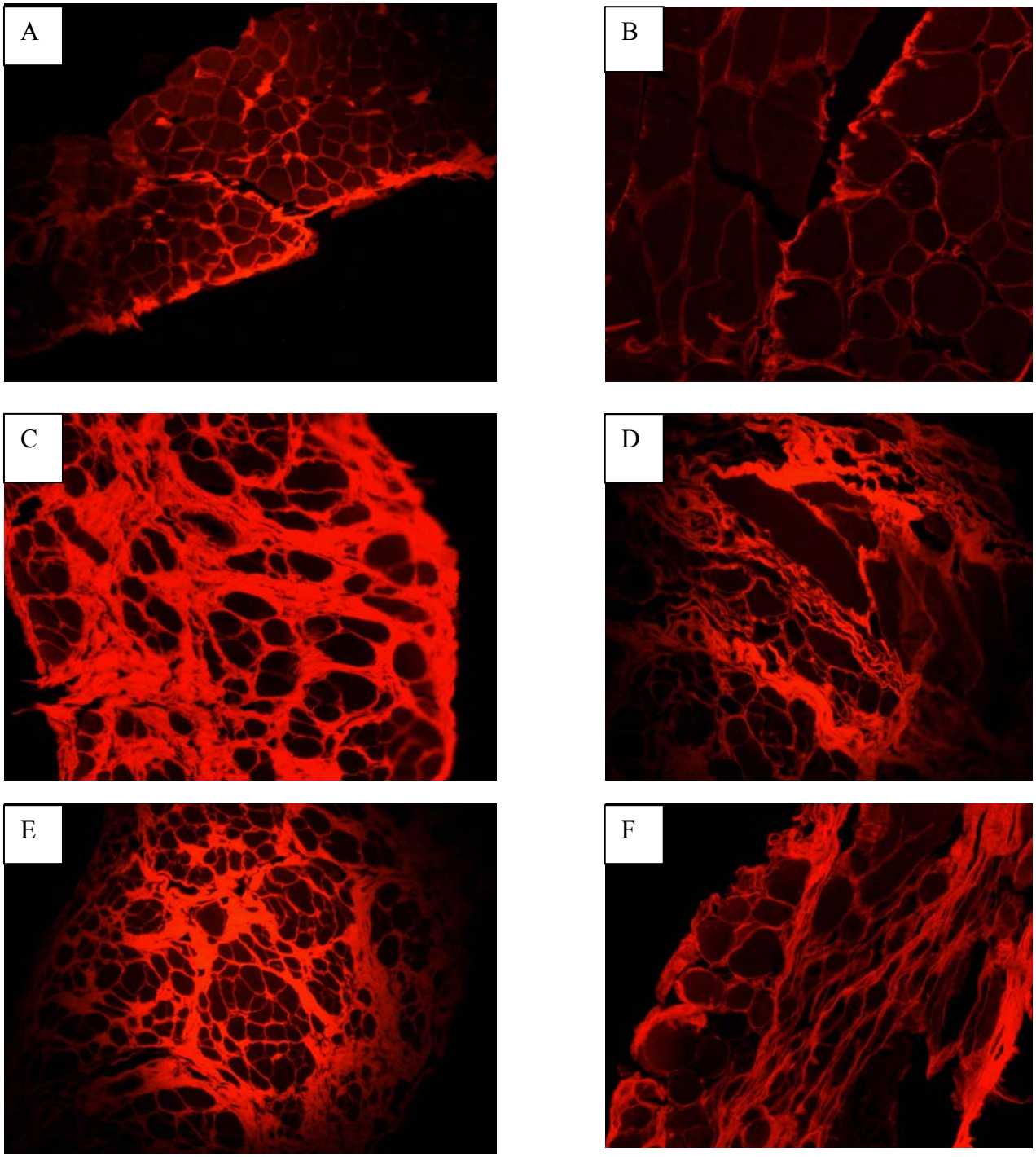


**Fig 6.9ii)** Diaphragm muscle sections (A,C,E) and intercostal sections (B,D,F) stained with picrosirius red. Sham treated *mdx* mice (C,D) showed significantly greater fibrosis than control mice (A,B), demonstrated in these photomicrographs as bright red bands of dense interstitial collagen. Antisense oligonucleotide treated mice showed a small but significant, decrease in diaphragm collagen (E), but not the intercostal muscles (F) when compared to sham treated *mdx*.

6.5.5 Histology

The characteristics of dystrophy, including variability in fibre size; centrally located nuclei, split and fused fibres, inflammatory cell infiltration and myocyte disarray, were apparent in all H&E stained *mdx* muscles. These changes were more pronounced in the diaphragm and intercostal muscles than the latissimus and longissimus dorsi muscles. There was a lower incidence of centrally nucleated fibres in AO treated *mdx* latissimus muscles ($P<0.05$) and intercostal muscles ($P<0.01$), although there was still considerable discrepancy between these treated muscles and control mice ($P<0.001$). The frequency of centrally nucleated myocytes is shown in Figure 6.10, and representative photomicrographs in Figure 6.11.

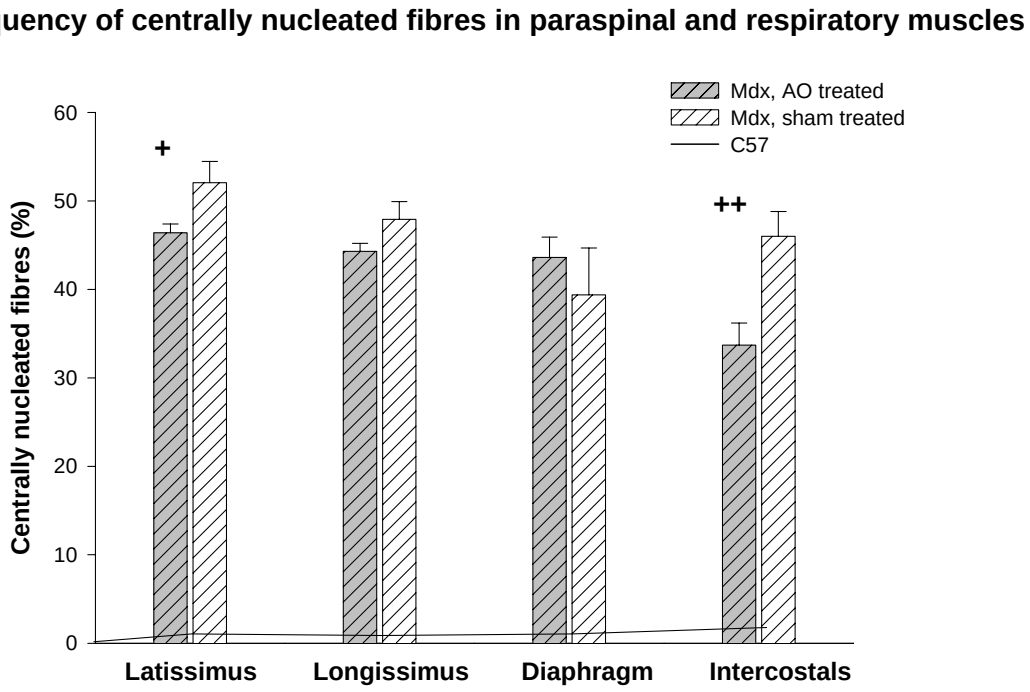


**Fig 6.10** Incidence of muscle fibres with centrally located nuclei from control mice, antisense oligonucleotide (AO) treated *mdx* and sham treated *mdx* mice. The control mice characteristically showed peripheral nuclei (with their frequency here represented by the solid line adjacent to x-axis). There was a reduction in the percentage of central nucleation in AO treated latissimus and intercostal muscles. n= 5 (C57), 6 (*Mdx* AO) and 5 (*Mdx* sham). P<0.001 when comparing *mdx* and C57 mice). + $P<0.05$, ++ $P<0.01$ (comparing AO and sham injected *mdx*).

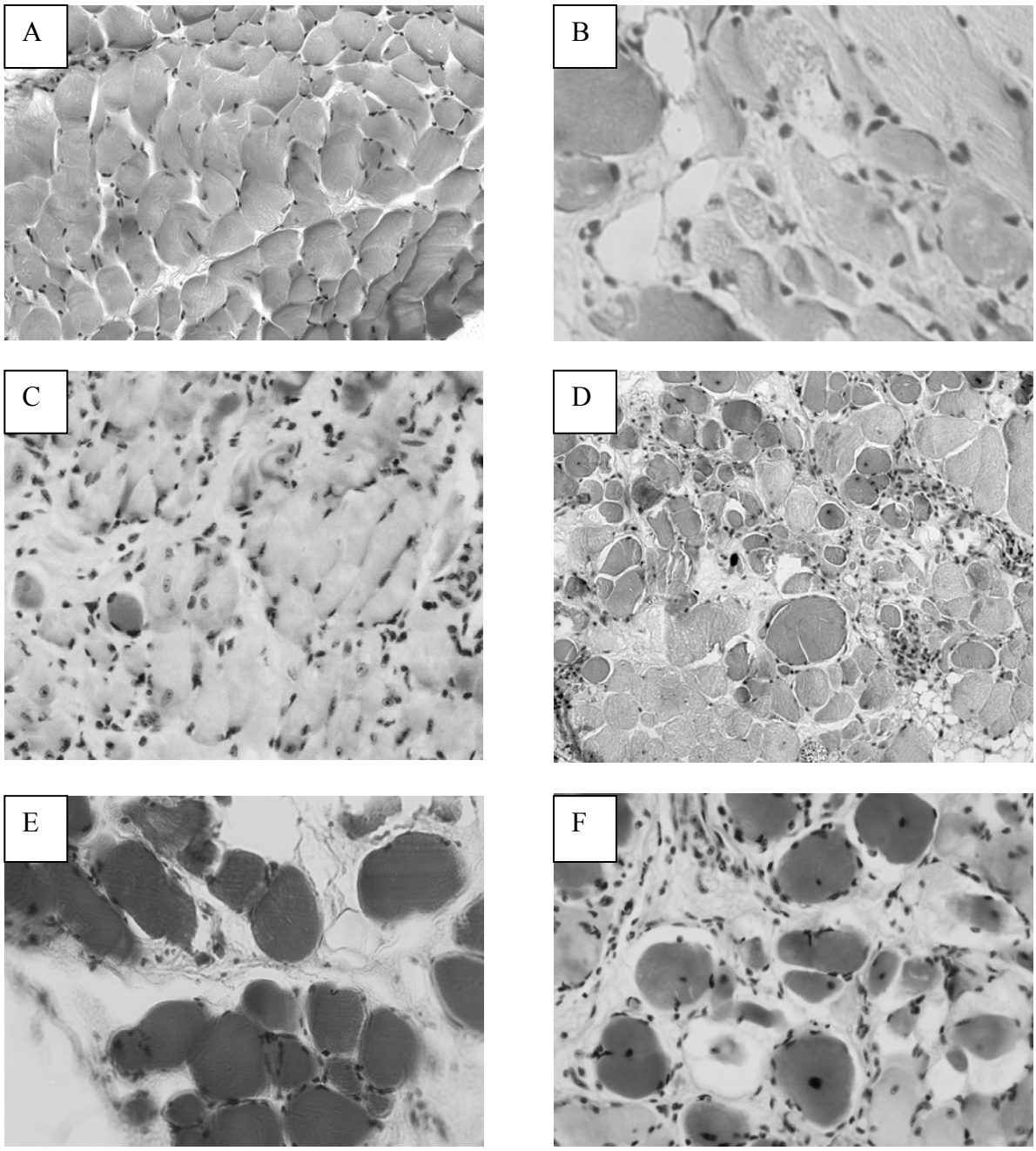


**Fig 6.11(i)** Representative H&E photomicrographs of latissimus dorsi (A,C,E) and longissimus dorsi muscles (B,D,F). Control mice muscle (A,B) had peripheral nuclei and little interstitial inflammation. Sham injected *mdx* mice (C,D) in contrast showed central nucleation and inflammatory cell infiltration typical of dystrophin deficient muscle. Antisense oligonucleotide (AO) injected *mdx* latissimus dorsi myocytes (E) had significantly fewer central nuclei than sham treated *mdx*. In this cluster of cells collagen is still evident but cells show peripheral nuclei, suggestive of less degeneration. AO treated *mdx* longissimus dorsi muscle (F), in contrast shows many centrally nucleated fibres.

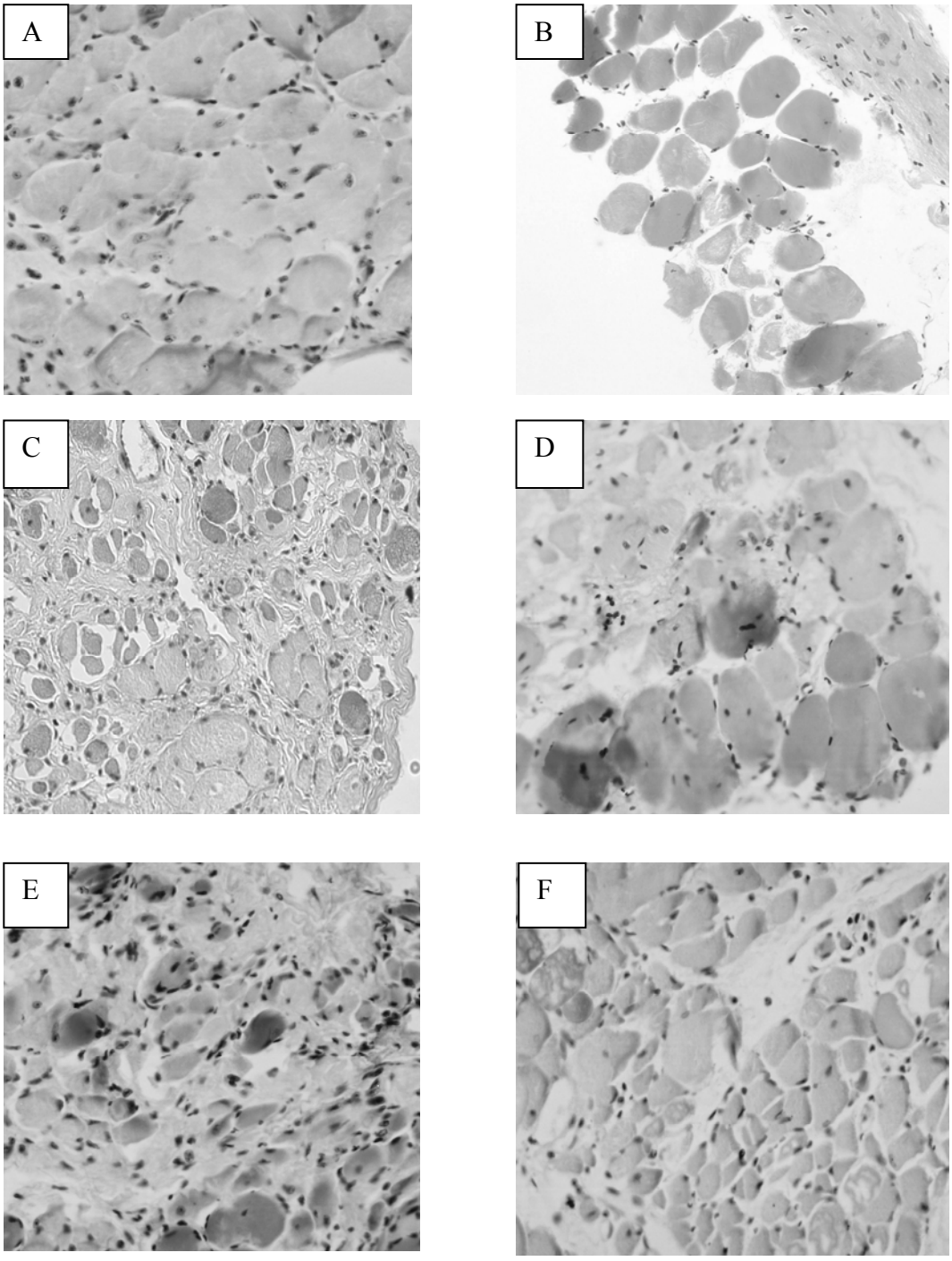


**Fig 6.11(ii)** Representative H&E photomicrographs of diaphragm sections (A,C,E) and intercostal muscles (B,D,F). Control diaphragm (A) and intercostal muscles (B) show homogeneity in size and shape compared to sham treated *mdx* diaphragm sections (C) and intercostal muscles (D). Diaphragm section from AO injected *mdx* (E) showed no significant difference in central nucleation compared to sham injected *mdx*, however the AO treated *mdx* intercostals displayed milder pathology. This group of mice showed significantly less central nucleation than sham treated *mdx* ($P<0.05$).

6.5.6 Western blots

Western blot analysis of C57 lumbar muscles showed full-length dystrophin at the predicted site (427 kDa), however it was not possible to detect dystrophin in AO treated *mdx* muscles. The Western blots were repeated several times with similar results (see Appendix B for details). Results from Western blots are shown in Figure 6.12.

**Fig 6.12** Western blot of paraspinal muscles of control mice, sham injected *mdx* mice and antisense oligonucleotide (AO) injected *mdx*. Only the C57 dystrophin band is evident. Muscles blotted in order were C57 longissimus, sham injected *mdx* longissimus, AO treated *mdx* longissimus (2 different mice) and AO treated *mdx* latissimus (2 different mice).

## 6.6 Discussion

Antisense oligonucleotide therapy of DMD is a promising approach to the disease in those boys whose genetic defect is amenable to forced alternative splicing. There are, however, a number of questions raised by this mode of therapy - including the safest and most efficacious route of administration, timing, long-term efficacy, and level of dystrophin expression required to ameliorate symptoms. There is much work still needed using animal models such as the *mdx* mouse and GRMD dog before clinical trials can progress.

This project examined the outcomes of once monthly AO injections administered into the paraspinal muscles of *mdx* mice aged from 2-18 months of age. These ages were chosen as, although *mdx* show the most severe necrosis at weaning age, they continue to experience cycles of degeneration and regeneration throughout life, with gradual development of severe or moderate dystrophy in muscles such as the diaphragm, postural muscles and accessory respiratory muscles.

(Stedman *et al*., 1991; Pastoret and Sebille, 1995b; Lefaucheur, 1995). In addition, other important clinical features of DMD such as thoracolumbar deformity was documented previously (Laws and Hoey, 2004).

AO injections were well tolerated by the mice, and there was no apparent local swelling, loss of appetite or stiffness of gait following monthly treatments.

The KI of the AO treated mice tended to be greater than sham injected mice (indicating less kyphosis) at all time points from 8-18 months of age, however there was only statistical difference between groups at 10 and 18 months of age. There was incongruity between KI in this series of radiographs (involving a larger *n*) than a previous study (Chapter 4), as the control mice in this study showed a decline in KI at 16 and 18 months of age, bringing them closer in value to *mdx* mice. The KI of AO treated *mdx* mice tended to plateau from 8-18 months of age, compared to fluctuating values in the other two groups of mice, making it more difficult to draw conclusions on the validity of statistical tests of significance (Fig 6.4A). When additional mice were included in the analysis there was less intergroup variabilty (and consequently smaller error bars). It was felt that inclusion of the additional untreated *mdx* and C57 mice was statistically valid as there were no significant difference in KI between them and sham injected mice. This also indicated that using more animals may improve a) the assessment of KI in *mdx* and control mice across their lifespan (despite tests of power suggesting fewer mice were adequate) and b) the evaluation of therapeutic interventions measuring this parameter.

The contractility data presented in Figure 6.6 shows the specific twitch and tetanic forces of control mice was greater than *mdx* mice, with the exception of diaphragm single twitch data (Fig 6.6i). This was an unexpected result and was also contradictory to the specific tetanic forces obtained from the same muscle preparations, however other authors have noted the discrepancies between forces normalised for mass or cross-sectional area in old mice skeletal muscle (Hayes and Williams, 1998). When diaphragm twitch forces were normalised for muscle weight only they were significantly greater for control mice (C57; 3.15 ± 0.42 mN/mg, *mdx* sham treated; 1.39 ± 0.25 mN/mg, *mdx* AO treated : 1.48 ± 0.19. $P<0.01$). Absolute twitch forces for diaphragm strips were also greater for control mice, although this did not reach statistical significance (C57; 18.9 ± 6.5 mN, *mdx* sham treated; 14 ± 2 mN, *mdx* AO treated : 13.6 ± 1.6mN).

There was no significant difference in force production of any examined muscle type for AO treated *mdx* compared to sham treated *mdx*. An inadequate dosage or distribution of AO to the muscles in question is likely to be the primary explanation for this result. AO transfection is a local phenomenon, limited by concentration, the spread of injectate within tissues and degree of internalisation of AO by myocytes. Although evidence of dye was observed within other tissues such as latissimus dorsi or occasionally intercostal muscle regions, a dilution of effects could also result from this spread, i.e. there was less AO available to transfect fewer cells. Tissues with the most staining were reserved for Western blotting to maximise detection of dystrophin, but this could mean that the muscles strips used for contractility studies were less likely to have successfully incorporated AOs. In addition this project examined function at one time point only (18 months old), and there may be a diminution of efficacy of AO therapy in dystrophic muscle with age, as satellite cell reserves and regenerative ability of muscle wanes and fibrosis advances. This latter point may explain the discrepancy between improvement in KI and lack of improvement in contractility.

The two methods of measuring collagen are complimentary with results generally in agreement, however certain results obtained in this study were equivocal. There was no significance difference between AO and sham treated muscles using HP assays, but significantly less interstitial collagen in diaphragm and latissimus muscles when collagen specific stains were analysed. The advantage of histological staining methods is the ability to visualise and record the extent of fibrosis, however the number of fields of view examined (or the number of levels of sectioning) limits the accuracy of analysis. AO therapy is unlikely to influence fibrosis in diaphragm muscle because direct injections were not employed, however it may have provided benefit in areas of latissimus muscles.

Evaluation of central nucleation in *mdx* myocytes demonstrated the attenuation of dystrophic pathology in other studies, including adeno-associated virus vector-mediated gene therapy (Wang *et al*., 2000; Yoshimura *et al.*, 2004; Fabb *et al.*, 2002) and stimulation of calcineurin signalling (Chakkalakal *et al.*, 2004). The percentage decrease in centrally nucleated fibres in this current study, although significant from untreated muscles, is only small. This contrasts to successful gene therapy studies where 75-98% of fibres showed peripheral nuclei

and consistent fibre sizes and shapes (Wang *et al*., 2000; Yoshimura *et al*., 2004). In these studies they injected vectors and min-*dys* into single muscles rather than over a wider area, and accurate localisation of transduced fibres was possible by histology and immunohistochemical methods.

It was not possible to demonstrate dystrophin expression in longissimus dorsi and latissimus dorsi muscle samples by Western blotting, despite the presence of strong dye staining to enable localisation of the sites of AO injection. This is most likely a result of low dosage of AO administered, as detailed in the diaphragm study (Chapter 5). In the time since both these studies were undertaken other researchers have shown that up to 8 fold increased amounts of AO are required for *in vivo* studies in *mdx* muscles (Lu *et al*., 2003; Wells *et al*., 2003). Immunohistochemical methods have recently been proved to be more sensitive than Western blotting for demonstraing low level dystrophin induction follwing AO administration (Lu et al., 2004).

In conclusion, this study did provide some evidence that long term AO administration reduced muscle pathology in *mdx* mice, and at many time points significantly altered the dystrophic phenotype of kyphosis present in this strain, (comparing AO treated with sham injected *mdx*). There was still evidence of greater kyphosis in treated mice compared to control This study also showed that significantly higher levels of AO are needed for *in vivo* experiments than that which achieved transfection of myocytes in cell culture in previous studies. The confounding problems of all gene modulating therapies currently considered for DMD clinical trails are exemplified here; the need for high efficiency widespread transfer, high biological activity, persistent expression and efficient target delivery throughout the lifespan.

# CHAPTER 7: CONCLUSIONS AND IMPLICATIONS FOR FURTHER STUDY

*Regarding every disease now incurable we may entertain the hope that our powerlessness may not be permanent, and that we, or those that come after us, may speak of it in very different terms…*

*Sir William Gowers, Lancet 1879*

Duchenne Muscular Dystrophy can be regarded as a prototype disease. It is common, knows no geographical or socio-economic boundaries and is always fatal. The dystrophin gene, the largest in the human body, has been studied for decades and its structure and mutations can now be considered well characterised. There are several naturally occurring laboratory animals, and many more man-made ones, that are excellent models for different aspects of study. There are research centres throughout the world dedicated solely to research into muscular dystrophies. It is likely the discovery of a genetic cure for DMD will release the floodgates for treatment of many other genetic diseases of lesser prevalence in society.

Dystrophin's countless roles are being revealed gradually; it is a strut that maintains structural stability and helps to resist the forces of muscular contractions, it is integrally involved in those contractions via connections to actin, it binds important molecules such as nNOS, calmodulin, dystrobrevin and ion channels, either directly or indirectly. These various and vital roles suggest that successful treatment can only come about through dystrophin replacement strategies, rather than anti-inflammatory drugs, hormone intervention, immune modulators or channel blockers, which influence only part of the complex.

Whilst there is hope for successful treatment in the future for boys affected with DMD, the pathways to it are far from clear. Parents are confused: will a 'cure' involve stem cell therapy, gene transfer via plasmids or viruses, a series of injections such as geneticin, or a system of applying molecular 'patches' using antisense oligonucleotides? The complexity of the gene and variety of mutations arising within it also suggest than a standard form of treatment is unlikely, but rather that therapy will be customised for every patient, based on individual genotyping and accurate determination of each mutation.

Exon skipping strategies utilising AOs hold great promise for those patients with point mutations and short deletions, as demonstrated by *mdx* muscles *in vivo* and cultured human muscle cells. The challenges include devising methods for widespread delivery, refinement of AO chemistry and ensuring persistence of dystrophin expression in all muscle types, including the heart and the diaphragm.

This dissertation sought to examine several muscles uniquely involved in the dystrophic phenotype and previously either less well characterised, or uncharacterised, in the *mdx* mouse model. These included cardiac muscle, accessory respiratory muscles and paraspinal muscles. In addition *mdx* diaphragm muscle was utilised as an example of skeletal muscle severely affected by the dystrophic process, and most representative of the profound dystrophy seen in DMD. Following these characterisation studies strategic administration of AOs was performed in diaphragm and paraspinal muscles, and the effects evaluated.

*Mdx* cardiomyopathy varies with the life stage. Young mice (3 weeks of age, or corresponding to the acute muscle necrosis stage) showed significantly lower heart weights and atrial contractility compared to control mice. 3 and 6 week old *mdx* showed blunted atrial responsiveness to increasing concentrations of calcium. 15-month-old *mdx* also displayed lower atrial forces compared to C57 mice. Isometric twitch characteristics altered with age, with 15-month-old mice showing lower basal forces and prolonged rise and relaxation times. Electrophysiological differences were evident in dystrophic hearts when action potential durations were measured by transmembrane glass microelectrodes. There was a strong trend for shorter $APD_{90}$ in *mdx* mice (significant at 3 weeks, 9 months and 12 months), while $APD_{50}$ increased in mice over 15 months of age. The apparent paradox of slowed twitch properties, shortened $APD_{90}$ and prolonged $APD_{50}$ provide evidence for dissociation between cell contractile machinery and electrical events, in addition to dysregulation of ion channels in *mdx* cardiomyocytes. These properties, and the development of increasing interstitial fibrosis with age in *mdx* hearts, provide insights into DMD cardiomyopathy including ECG disturbances and the tendency for arrhythmias. Differences between human and murine disease were noted: *mdx* hearts can show equivalent function to control hearts at many ages, and fibrosis is patchy and diffuse, rather than localised and severe, as occurs in boys with DMD. There was no evidence of dilated cardiomyopathy in *mdx*, although this occurs

commonly in DMD. In conclusion this study showed that young (<6 weeks) and old (>15 months) *mdx* mice were most useful for cardiac studies, when contractile dysfunction and electrophysiological disturbances were significant.

Spinal deformity is common in DMD, and also occurs in the *mdx* mouse, in the form of thoracolumbar kyphosis. A novel radiographic index extrapolated from the Kyphotic Index used in children, was developed and applied to aging C57 and *mdx* mice. KI remained the same until approximately 9 months of age, after which it became significantly less in *mdx* mice (indicating more severe kyphosis). Muscles associated with spinal and thoracic deformity were isolated and used for contractility studies, measurements of interstitial collagen, and histological measures of muscle degeneration and regeneration. The latissimus dorsi, intercostal muscles and diaphragm muscles of the *mdx* mouse showed reduced twitch and tetanic force production, increased central nucleation (indicating myocyte regeneration) and increased fibrosis. This study was the first to apply such a radiographic index to an animal model, and evaluate the effects of dystrophy of the paraspinal and respiratory muscles in the progression of kyphosis.

AOs were administered once monthly by intramuscular injection into the paraspinal muscles of mice from 2-18 months of age. KI was measured from monthly radiographs and found to be greater in AO compared to sham treated *mdx* at 10-18 months of age (significant at 10, 12, 16 and 18 months). There was still significant discrepancy in KI however, between AO treated *mdx* and C57 mice. There was no improvement in force production of latissimus dorsi, intercostal muscles or diaphragm in AO treated mice, but there was some reduction in fibrosis measured by histological stains specific for collagen in AO treated latissimus dorsi muscles and diaphragm. The frequency of centrally nucleated fibres was significantly less for AO treated latissimus dorsi and intercostal muscles. Dystrophin expression could not be demonstrated by Western blot. The conclusion from this study was that some benefit to the dystrophic phenotype in the form of reduced kyphosis was observed after long-term administration of AOs. The concentration of AOs was thought to be too low to result in persistent expression of dystrophin, and higher concentrations were indicated. More sensitive dystrophin detection methods, such as immunostaining or RT-PCR should also be evaluated.

The *mdx* diaphragm shows necrosis and fibrosis from an early age, with the histological changes closely mimicing that seen in skeletal muscles of boys with DMD. Organ bath studies measuring contractility of diaphragm strips, hydroxyproline analysis and histological measures of fibrosis and degeneration and regeneration were shown to be reliable indicators of the extent of dystrophy in this organ. From preliminary studies using mice from 3 weeks to 15 months of age, it was decided to use 4-month-old mice for the administration of AOs directly into diaphragm muscle. Two procedures one month apart were performed, involving sub-epimyseal injections of AO/lipofectin complex at four sites around the diaphragm. Mice were sacrificed one month after the second procedure and diaphragm strips were dissected for contractility studies. Twitch and tetanic forces were significantly greater in AO treated diaphragms compared to sham injected, but fibrosis was not alleviated. The frequency of centrally nucleated fibres was also similar between AO and sham treated *mdx*. Western blotting again failed to demonstrate dystrophin production, thought to be due to a low concentration of AO. This study was the first to show evidence of functional benefits after AO treatment in muscle with a tendency for severe dystrophy, and provides additional evidence that this mode of treatment may be a safe and efficacious form of therapy if vectors for systemic delivery are developed.

From the studies outlined above and consideration of published work, it is clear that AO strategies are ready for human trials. The proof of principle that AOs successfully induce exon skipping in both *mdx* and DMD cells was followed by studies showing improved function in *mdx* limb muscles, with a lack of inflammatory response and toxicity. Long term AO use was safe and well tolerated in *mdx* mice, and alleviated kyphosis compared to sham injected mice. Diaphragm function was improved after two injections of AO, albeit of a lower concentration than would be considered for future trials. Recent advances including systemic delivery via intravenous injections, the feasibility of double or multi-exon skipping and the development of viral vectors expressing antisense sequences offer hope. Considerable challenges remain, including the effective delivery of AOs that induce persistent expression of dystrophin, which is able to provide functional benefits across a wide range of muscle types and alleviate the serious pathology associated with DMD.

# BIBLIOGRAPHY

Aartsma-Rus, A., Bremmer-Bout, M., Janson, A., den Dunnen, J., van Ommen, G. and van Deutekom, J. (2002) Targeted exon skipping as a potential gene correction therapy for Duchenne Muscular Dystrophy, *Neuromuscul Disord,* **12 Suppl,** 71-74.

Aartsma-Rus, A., Janson, A., Kaman, W., Bremmer-Bout, M., van Ommen, G., den Dunnen, J. and van Deutekom, J. (2004) Antisense-induced multiexon skipping for Duchenne muscular dystrophy makes more sense, *Am J Hum Genet,* **74,** 83-92.

Alderton, J. M. and Steinhardt, R. A. (2000) Calcium Influx through Calcium Leak Channels Is Responsible for the Elevated Levels of Calcium-dependent Proteolysis in Dystrophic Myotubes, *J. Biol. Chem.,* **275,** 9452-9460.

Allamand, V. and Campbell, K. P. (2000) Animal models for muscular dystrophy: valuable tools for the development of therapies,*Hum. Mol. Genet.,* **9,** 2459-2467.

Alloatti, G., Gallo, M. P., Penna, C. and Levi, R. C. (1995) Properties of Cardiac Cells from Dystrophic Mouse, *Journal of Molecularand Cell Cardiology,* **27,** 1775-1779.

Anderson, J., Bressler, B. and Ovalle, W. (1988) Functional regeneration in the hindlimb skeletal muscle of the mdx mouse, *J Muscle Res Cell Motil,* **9,** 499-515.

Anderson, J., Garrett, K., Moor, A., McIntosh, L. and Penner, K. (1998) Dystrophy and myogenesis in mdx diaphragm muscle, *Muscle Nerve,* **21,** 1153-65.

Anderson, J., McIntosh, L. and Poettcker, R. (1996) Deflazacort but not prednisone improves both muscle repair and fiber growth in diaphragm and limb muscle in vivo in the mdx dystrophic mouse, *Muscle Nerve,* **19,** 1576-85.

Arakawa, M., Shiozuka, M., Nakayama, Y., Hara, T., Hamada, M., Kondo, S. i., Ikeda, D., Takahashi, Y., Sawa, R., Nonomura, Y., Sheykholeslami, K., Kondo, K., Kaga, K., Kitamura, T., Suzuki-Miyagoe, Y., Takeda, S. i. and Matsuda, R. (2003) Negamycin Restores Dystrophin Expression in Skeletal and Cardiac Muscles of mdx Mice, *J Biochem (Tokyo),* **134,** 751-758.

Austin, L., Bower, J., Bennett, T., Lynch, G., Kapsa, R., White, J., Barnard, W., Gregorevic, P. and Byrne, E. (2000) Leukemia inhibitory factor ameliorates muscle fiber degeneration in the mdx mouse, *Muscle Nerve,* **23,** 1700-5.

Bach, J. R. and Kang, S.-W. (2000) Disorders of Ventilation : Weakness, Stiffness, and Mobilization,*Chest,* **117,** 301-303.

Bartlett, R., Stockinger, S., Denis, M., Bartlett, W., Inverardi, L., Le, T., thi Man, N., Morris, G., Bogan, D., Metcalf-Bogan, J. and Kornegay, J. (2000) In vivo targeted repair of a point mutation in the canine dystrophin gene by a chimeric RNA/DNA oligonucleotide, *Nat Biotechnol,* **18,** 615-22.

Barton, E. R., Morris, L., Musaro, A., Rosenthal, N. and Sweeney, H. L. (2002) Muscle-specific expression of insulin-like growth factor I counters muscle decline in mdx mice, *J. Cell Biol.,* **157,** 137-148.

Barton-Davis, E. R., Cordier, L., Shoturma, D. I., Leland, S. E. and Sweeney, H. L. (1999) Aminoglycoside antibiotics restore dystrophin function to skeletal muscles of mdx mice, *J. Clin. Invest.,* **104,** 375-381.

Beam, K. G. (1988) Localizing the gene product, *Nature,* **333,** 798-799.

Becker, P. and Kiener, F. (1955) [A new x-chromosomal muscular dystrophy], *Arch Psychiatr Nervenkr Z Gesamte Neurol Psychiatr,* **193,** 427-48.

Bernasconi, P., Di Blasi, C., Mora, M., Morandi, L., Galbiati, S., Confalonieri, P., Cornelio, F. and Mantegazza, R. (1999) Transforming growth factor-beta1 and fibrosis in congenital muscular dystrophies, *Neuromuscul Disord,* **9,** 28-33.

Bia, B., Cassidy, P., Young, M., Rafael, J., Leighton, B., Davies, K., Radda, G. and Clarke, K. (1999) Decreased myocardial nNOS, increased iNOS and abnormal ECGs in mouse models of Duchenne Muscular Dystrophy, *J Mol Cell Cardiol,* **31,** 1857-62.

Biggar, W., Gingras, M., Fehlings, D., Harris, V. and Steele, C. (2001) Deflazacort treatment of Duchenne Muscular Dystrophy, *J Pediatr,* **138,** 45-50.

Biggar, W., Klamut, H., Demacio, P., Stevens, D. and Ray, P. (2002) Duchenne muscular dystrophy: current knowledge, treatment, and future prospects, *Clin Orthop***, 401,** 88-106.

Bobet, J., Mooney, R. F. and Gordon, T. (1998) Force and stiffness of old dystrophic (mdx) mouse skeletal muscles, *Muscle & Nerve,* **21,** 536-539.

Bodensteiner, J. and Engel, A. (1978) Intracellular calcium accumulation in Duchenne dystrophy and other myopathies: a study of 567,000 muscle fibers in 114 biopsies, *Neurology,* **28,** 439-446.

Bogdanovich, S., Krag, T., Barton, E., Morris, L., Whittemore, L., Ahima, R. and Khurana, T. (2002) Functional improvement of dystrophic muscle by myostatin blockade, *Nature,* **420,** 418-21.

Boland, B., Himpens B., Denef J.F. and Gillis J.M. (1995) Site-dependent pathological differences in smooth muscles and skeletal muscles of the adult mdx mouse, *Muscle & Nerve,* **18,** 649-657.

Boland B., Himpens B., Denef J.F. and Gillis J.M. (1995) Site-dependent pathological differences in smooth muscles and skeletal muscles of the adult mdx mouse, *Muscle & Nerve,* **18,** 649-657.

Bolanos-Jimenez, F., Bordais, A., Behra, M., Strahle, U., Sahel, J. and Rendon, A. (2001) Dystrophin and Dp71, two products of the DMD gene, show a different pattern of expression during embryonic development in zebrafish, *Mech Dev,* **102,** 239-41.

Bonilla, E., Samitt, C., Miranda, A., Hays, A. P., Salviati, G., DiMauro, S., Kunkel, L. M., Hoffman, E. P. and Rowland, L. P. (1988) Duchenne Muscular Dystrophy: Deficiency of Dystrophin at the Muscle Cell Surface, *Cell,* **54,** 447-452.

Bourke, S. and Gibson, G. (2002) Sleep and breathing in neuromuscular disease, *Eur Respir J,* **19,** 1194-201.

Bramwell, B. (1879) Case of pseudo-hypertrophic paralysis, *Lancet,* **114,** 194-5.

Bremmer-Bout, M., Aartsma-Rus, A., de Meijer, E., Kaman, W., Janson, A., Vossen, R., van Ommen, G., den Dunnen, J. and van Deutekom, J. (2004) Targeted exon skipping in transgenic hDMD mice: A model for direct preclinical screening of human-specific antisense oligonucleotides, *Mol Ther,* **10,** 232-40.

Brenman, J., Chao, D., Xia, H., Aldape, K. and Bredt, D. (1995a) Nitric oxide synthase complexed with dystrophin and absent from skeletal muscle sarcolemma in Duchenne Muscular Dystrophy, *Cell,* **82,** 743-52.

Brenman, J. E., Chao, D., S.,, Xia, H., Aldape, K. and Bredt, D. S. (1995b) Nitric Oxide Synthase Complexed with Dystrophin and Absent from Skeletal Muscle Sarcolemma in Duchenne Muscular Dystrophy,*Cell,* **82**.

Bridges, L. (1986) The association of cardiac muscle necrosis and inflammation with the degenerative and persistent myopathy of MDX mice, *J Neurol Sci,* **72,** 147-57.

Bridges, L., Coulton, G., Howard, G., Moss, J. and Mason, R. (1992) The neuromuscular basis of hereditary kyphoscoliosis in the mouse.,*Muscle Nerve,* **15,** 172-9.

Bulfield, G., Siller, W., Wight, P. and Moore, K. (1984) X chromosome-linked muscular dystrophy (mdx) in the mouse, **81,** 1189-1192.

Bushby, K., Hill, A. and Steele, J. (1999) Failure of early diagnosis in symptomatic Duchenne muscular dystrophy. *Lancet,* **353,** 557-8.

Bushby, K., Muntoni, F. and Bourke, J. (2003) 107th ENMC international workshop: the management of cardiac involvement in muscular dystrophy and myotonic dystrophy. 7th-9th June 2002, Naarden, the Netherlands, *Neuromuscul Disord,* **13,** 166-72.

Campbell, K. (1995) Three muscular dystrophies: loss of cytoskeleton-extracellular matrix linkage. *Cell,* **80,** 675-9.

Carpenter, J., Hoffman, E., Romanul, F., Kunkel, L., Rosales, R., Ma, N., Dasbach, J., Rae, J., Moore, F. and McAfee, M. (1989) Feline muscular dystrophy with dystrophin deficiency. *Am J Pathol,* **135,** 909-919.

Cerletti, M., Negri, T., Cozzi, F., Colpo, R., Andreetta, F., Croci, D., Davies, K., Cornelio, F., Pozza, O., Karpati, G., Gilbert, R. and Mora, M. (2003)

Dystrophic phenotype of canine X-linked muscular dystrophy is mitigated by adenovirus-mediated utrophin gene transfer, *Gene Ther,* **10,** 750-7.

Chakkalakal, J. V., Harrison, M.-A., Carbonetto, S., Chin, E., Michel, R. N. and Jasmin, B. J. (2004) Stimulation of calcineurin signaling attenuates the dystrophic pathology in mdx mice,*Hum. Mol. Genet.,* **13,** 379-388.

Chambers, S., Dodd, A., Overall, R., Sirey, T., Lam, L., Morris, G. and Love, D. (2001) Dystrophin in adult zebrafish muscle.,*Biochem Biophys Res Commun,* **286,** 478-83.

Chao, D., Gorospe, J., Brenman, J., Rafael, J., Peters, M., Froehner, S., Hoffman, E., Chamberlain, J. and Bredt, D. (1996) Selective loss of sarcolemmal nitric oxide synthase in Becker muscular dystrophy, *J. Exp. Med.,* **184,** 609-618.

Chao, D., Silvagno, F. and Bredt, D. (1998) Muscular dystrophy in mdx mice despite lack of neuronal nitric oxide synthase, *J Neurochem,* **71,** 784-9.

Chaubourt, E., Voisin, V., Fossier, P., Baux, G., Israel, M. and De La Porte, S. (2002) Muscular nitric oxide synthase (muNOS) and utrophin, *J Physiol Paris,* **96,** 43-52.

Chen, Y.-W., Zhao, P., Borup, R. and Hoffman, E. (2000) Expression profiling in the muscular dystrophies: identification of anovel aspects of molecular pathophysiology,*The Journal of Cell Biology,* **151,** 1321-13336.

Chetboul, V., Carlos, C., Blot, S., Thibaud, J., Escriou, C., Tissier, R., Retortillo, J. and Pouchelon, J. (2004) Tissue Doppler assessment of diastolic and systolic alterations of radial and longitudinal left ventricular motions in Golden Retrievers during the preclinical phase of cardiomyopathy associated with muscular dystrophy, *Am J Vet Res,* **65,** 1335-41.

Chitano, P., Cox, C. M. and Murphy, T. M. (2002) Relaxation of guinea pig trachealis during electrical field stimulation increases with age, *J Appl Physiol,* **92,** 1835-1842.

Cho, W., Ebihara, S., Nalbantoglu, J., Gilbert, R., Massie, B., Holland, P., Karpati, G. and Petrof, B. (2000) Modulation of Starling forces and muscle fiber maturity permits adenovirus-mediated gene transfer to adult dystrophic (mdx) mice by the intravascular route, *Hum Gene Ther,* **11,** 701-14.

Chu, V., Otero, J., Lopez, O., Sullivan, M., Morgan, J., Amende, I. and Hampton, T. (2002) Electrocardiographic findings in mdx mice: a cardiac phenotype of Duchenne Muscular Dystrophy, *Muscle Nerve,* **26,** 513-9.

Cittadini, A., Ines Comi, L., Longobardi, S., Rocco Petretta, V., Casaburi, C., Passamano, L., Merola, B., Durante-Mangoni, E., Sacca, L. and Politano, L. (2003) A preliminary randomized study of growth hormone administration in Becker and Duchenne muscular dystrophies., *Eur Heart J* **24,** 664-672.

Citterio, G., Agostoni, E., Piccoli, S. and Sironi, S. (1982) Selective activation of parasternal muscle fibers according to breathing rate, *Respir Physiol,* **48,** 281-95.

Cohen, J. and Duke, R. (1984) Glucocorticoid activation of a calcium-dependent endonuclease in thymocyte nuclei leads to cell death, *J. Immunol.,* **132,** 38-42.

Coirault, C., Lambert, F., Marchand-Adam, S., Attal, P., Chemla, D. and Lecarpentier, Y. (1999) Myosin molecular motor dysfunction in dystrophic mouse diaphragm, *Am J Physiol Cell Physiol,* **277,** C1170-1176.

Coirault, C., Pignol, B., Cooper, R. N., Butler-Browne, G., Chabrier, P.-E. and Lecarpentier, Y. (2003) Severe muscle dysfunction precedes collagen tissue proliferation in mdx mouse diaphragm,*J Appl Physiol,* **94,** 1744-1750.

Cooper, B., Winand, N., Stedman, H., Valentine, B., Hoffman, E., Kunkel, L., Scott, M., Fischbeck, K., Kornegay, J. and Avery, R. (1988) The homologue of the Duchenne locus is defective in X-linked muscular dystrophy of dogs, *Nature,* **334,** 154-6.

Corrado, K., Rafael, J., Mills, P., Cole, N., Faulkner, J., Wang, K. and Chamberlain, J. (1996) Transgenic mdx mice expressing dystrophin with a deletion in the actin- binding domain display a "mild Becker" phenotype, *J. Cell Biol.,* **134,** 873-884.

Coulton, G., Morgan, J., Partridge, T. and Sloper, J. (1988) The mdx mouse skeletal muscle myopathy: 1.A histological, morphometric and biochemical investigation, *Neuropath. Appl. Neurobiol. Berl,* **77,** 69-81.

Cox, G., Cole, N., Matsumura, K., Phelps, S., Hauschka, S., Campbell, K., Faulkner, J. and Chamberlain, J. (1993) Overexpression of dystrophin in transgenic mdx mice eliminates dystrophic symptoms without toxicity, *Nature,* **364,** 725-9.

Cox, G., Sunada, Y., Campbell, K. and Chamberlain, J. (1994) Dp71 can restore the dystrophin-associated glycoprotein complex in muscle but fails to prevent dystrophy, *Nat Genet,* **8,** 333-9.

Crosbie, R., Straub, V., Yun, H., Lee, J., Rafael, J., Chamberlain, J., Dawson, V., Dawson, T. and Campbell, K. (1998) mdx muscle pathology is independent of nNOS perturbation, *Hum. Mol. Genet.,* **7,** 823-829.

Cullen M.J. and Jaros, E. (1988) Ultrastructure of the skeletal muscle in the X chromosome-linked dystrophic (mdx) mouse, *Acta Neuropathologica,* **77,** 69-81.

Culligan, K., Mackey, A., Finn, D., Maguire, P. and Ohlendieck, K. (1998) Role of dystrophin isoforms and associated proteins in muscular dystrophy (review). *Int J Mol Med,* **2,** 639-48.

Danialou, G., Comtois, A. S., Dudley, R., Karpati, G., Vincent, G., Des Rosiers, C. and Petrof, B. J. (2001) Dystrophin-deficient cardiomyocytes are abnormally vulnerable to mechanical stress-induced contractile failure and injury, *FASEB J,* **10,** 01-0030fje

Danik, S., Cabo, C., Chiello, C., Kang, S., Wit, A. L. and Coromilas, J. (2002) Correlation of repolarization of ventricular monophasic action potential with ECG in the murine heart, *Am J Physiol Heart Circ Physiol,* **283,** H372-381.

Davis, H. and Jasmin, B. (1993) Direct gene transfer into mouse diaphragm, *FEBS Lett,* **333,** 146-50.

Dawson, D. M. (1966) Leakage of enzymes from denervated and dystrophic chicken muscle, *Arch Neurol,* **14,** 321-325.

De La Porte, S., Morin, S. and Koenig, J. (1999) Characteristics of skeletal muscle in mdx mutant mice, *International Review of Cytology,* **191,** 99-148.

De Luca, A., Pierno, S., Liantonio, A., Cetrone, M., Camerino, C., Simonetti, S., Papadia, F. and Camerino, D. C. (2001) Alteration of excitation-contraction coupling mechanism in extensor digitorum longus muscle fibres of dystrophic mdx mouse and potential efficacy of taurine, *Br. J. Pharmacol.,* **132,** 1047-1054.

De Troyer, A., Borenstein, S. and Cordier, R. (1980) Analysis of lung volume restriction in patients with respiratory muscle weakness, *Thorax,* **35,** 603-610.

Decary, S., Hamida, C., Mouly, V., Barbet, J., Hentati, F. and Butler-Browne, G. (2000) Shorter telomeres in dystrophic muscle consistent with extensive regeneration in young children, *Neuromuscul Disord,* **10,** 113-20.

Deconinck, A., Rafael, J., Skinner, J., Brown, S., Potter, A., Metzinger, L., Watt, D., Dickson, J., Tinsley, J. and Davies, K. (1997a) Utrophin-dystrophin-deficient mice as a model for Duchenne Muscular Dystrophy, *Cell,* **90,** 717-27.

Deconinck, N., Tinsley, J., De Backer, F., Fisher, R., Kahn, D., Phelps, S., Davies, K. and Gillis, J. (1997b) Expression of truncated utrophin leads to major functional improvements in dystrophin-deficient muscles of mice, *Nat Med,* **3,** 1216-21.

Decramer, M., Reid, M. and De Troyer, A. (1985) Relationship between parasternal intercostal length and rib cage displacement in dogs, *J Appl Physiol,* **58,** 1517-20.

Decrouy, A., Renaud, J., Davis, H., Lunde, J., Dickson, G. and Jasmin, B. (1997) Mini-dystrophin gene transfer in mdx4cv diaphragm muscle fibers increases sarcolemmal stability, *Gene Ther,* **4,** 401-8.

Dell'Agnola, C., Wang, Z., Storb, R., Tapscott, S. J., Kuhr, C. S., Hauschka, S. D., Lee, R. S., Sale, G. E., Zellmer, E., Gisburne, S., Bogan, J., Kornegay, J. N., Cooper, B. J., Gooley, T. A. and Little, M.-T. (2004) Hematopoietic stem cell transplantation does not restore dystrophin expression in Duchenne muscular dystrophy dogs,*Blood,* **104,** 4311-4318.

Dias, N. and Stein, C. A. (2002) Antisense Oligonucleotides: Basic Concepts and Mechanisms, *Mol Cancer Ther,* **1,** 347-355.

Dickinson, A. and Meikle, V. (1973) Genetic kyphoscoliosis in mice, *Lancet,* **1,** 1186.

Disatnik, M., Chamberlain, J. and Rando, T. (2000) Dystrophin mutations predict cellular susceptibility to oxidative stress, *Muscle Nerve,* **23,** 784-92.

Dunckley, M., Manoharan, M., Villiet, P., Eperon, I. and Dickson, G. (1995) Modification of splicing in the dystrophin gene in cultured Mdx muscle cells by antisense oligoribonucleotides, *Hum. Mol. Genet.,* **7,** 1083-1090.

Dupont-Versteegden, E., Baldwin, R., McCarter, R. and Vonlanthen, M. (1994a) Does muscular dystrophy affect metabolic rate? A study in mdx mice, *J Neurol Sci,* **121,** 203-7.

Dupont-Versteegden, E. E., McCarter, R. J. and Katz, M. S. (1994b) Voluntary exercise decreases progression of muscular dystrophy in diaphragm of mdx mice, *Journal of Applied Physiology,* **77,** 1736-1741.

Eagle, M., Baudouin, S., Chandler, C., Giddings, D., Bullock, R. and Bushby, K. (2002) Survival in Duchenne Muscular Dystrophy: improvements in life expectancy since 1967 and the impact of home nocturnal ventilation, *Neuromuscul Disord,* **12,** 926-9.

Ebihara, S., Guibinga, G.-h., Gilbert, R., Nalbabtoglu, J., Massie, B., Karpati, G. and Petrof, B. (2000) Differential effects of dystrophin and utrophin gene transfer in immunocompetent muscular dystrophy (mdx) mice, *Physiol Genomics,* **3,** 133-144.

Emery, A. (2002) Muscular dystrophy into the new millennium, *Neuromuscul Disord,* **12,** 343-9.

Emery, A. and Muntoni, F. (2003) *Duchenne Muscular Dystrophy,* Oxford University Press, Oxford.

England, S., Nicholson, L., Johnson, M., Forrest, S., Love, D., Zubrzycka-Gaarn, E., Bulman, D., Harris, J. and Davies, K. (1990) Very mild muscular dystrophy associated with the deletion of 46% of dystrophin, *Nature,* **343,** 180-2.

Ervasti, J., Ohlendieck, K., Kahl, S., Gaver, M. and Campbell, K. (1990) Deficiency of a glycoprotein component of the dystrophin complex in dystrophic muscle, *Nature,* **345,** 315-9.

Estenne, M., Gevenois, P., Kinnear, W., Soudon, P., Heilporn, A. and De Troyer, A. (1993) Lung volume restriction in patients with chronic respiratory muscle weakness: the role of microatelectasis,*Thorax,* **48,** 698-701.

Fabb, S. A., Wells, D. J., Serpente, P. and Dickson, G. (2002) Adeno-associated virus vector gene transfer and sarcolemmal expression of a 144 kDa micro-dystrophin effectively restores the dystrophin-associated protein complex and inhibits myofibre degeneration in nude/mdx mice, *Hum. Mol. Genet.,* **11,** 733-741.

Fanin, M., Danieli, G., Cadaldini, M., Miorin, M., Vitiello, L. and Angelini, C. (1995) Dystrophin-positive fibers in Duchenne dystrophy: origin and correlation to clinical course, *Muscle Nerve,* **18,** 1115-20.

Farkas, G. A., Decramer, M., Rochester, D. F. and De Troyer, A. (1985) Contractile properties of intercostal muscles and their functional significance, *J Appl Physiol,* **59,** 528-535.

Fenichel, G., Pestronk, A., Florence, J., Robison, V. and Hemelt, V. (1997) A beneficial effect of oxandrolone in the treatment of Duchenne muscular dystrophy: a pilot study, *Neurology,* **48,** 1225-1226.

Fenichel, G. M., Griggs, R. C., Kissel, J., Kramer, T. I., Mendell, J. R., Moxley, R. T., Pestronk, A., Sheng, K., Florence, J., King, W. M., Pandya, S., Robison, V. D. and Wang, H. (2001) A randomized efficacy and safety trial of oxandrolone in the treatment of Duchenne dystrophy, *Neurology,* **56,** 1075-1079.

Ferrari, G., Cusella-, G., Angelis, D., Coletta, M., Paolucci, E., Stornaiuolo, A., Cossu, G. and Mavilio, F. (1998) Muscle Regeneration by Bone Marrow-Derived Myogenic Progenitors, *Science,* **279,** 1528-1530.

Ferrari, G. and Mavilio, F. (2002) Myogenic stem cells from the bone marrow: a therapeutic alternative for muscular dystrophy? *Neuromuscul Disord,* **12 Suppl 1,** S7-10.

Flanigan, K., von Niederhausern, A., Dunn, D., Alder, J., Mendell, J. and Weiss, R. (2003) Rapid direct sequence analysis of the dystrophin gene, *Am J Hum Genet,* **72,** 931-9.

Fletcher, S., Ly, T., Duff, R., McC Howell, J. and Wilton, S. (2001) Cryptic splicing involving the splice site mutation in the canine model of Duchenne muscular dystrophy, *Neuromuscul Disord,* **11,** 239-43.

Flotte, T., Barraza-Ortiz, X., Solow, R., Afione, S., Carter, B. and Guggino, W. (1995) An improved system for packaging recombinant adeno-associated virus vectors capable of in vivo transduction, *Gene Ther,* **2,** 29-37.

Floyd, S., Clemens, P., Ontell, M., Kochanek, S., Day, C., Yang, J., Hauschka, S., Balkir, L., Morgan, J., Moreland, M., Feero, G., Epperly, M. and Huard, J. (1998) Ex vivo gene transfer using adenovirus-mediated full-length dystrophin delivery to dystrophic muscles, *Gene Ther,* **5,** 19-30.

Fong, P., Turner, P., Denetclaw, W. and Steinhardt, R. (1990) Increased activity of calcium leak channels in myotubes of Duchenne human and mdx mouse origin, *Science,* **250,** 673-675.

Fowler, E. G., Graves, M. C., Wetzel, G. T. and Spencer, M. J. (2004) Pilot trial of albuterol in Duchenne and Becker muscular dystrophy, *Neurology,* **62,** 1006-1008.

Franco, A. and Lansman, J. (1990) Calcium entry through stretch-inactivated ion channels in mdx myotubes, *Nature,* **344,** 670-3.

Gao, W. D., Perez, N. G., Seidman, C. E., Seidman, J. G. and Marban, E. (1999) Altered cardiac excitation–contraction coupling in mutant mice with familial hypertrophic cardiomyopathy, *J. Clin. Invest.,* **103,** 661-666.

Gaschen, F., Hoffman, E., Gorospe, J., Uhl, E., Senior, D., Cardinet, G. and Pearce, L. (1992) Dystrophin deficiency causes lethal muscle hypertrophy in cats, *J Neurol Sci,* **110,** 149-59.

Gebski, B. L., Mann, C. J., Fletcher, S. and Wilton, S. D. (2003) Morpholino antisense oligonucleotide induced dystrophin exon 23 skipping in mdx mouse muscle, *Hum. Mol. Genet.,* **12,** 1801-1811.

Gillis, J. (1999) Understanding dystrophinopathies: an inventory of the structural and functional consequences of the absence of dystrophin in muscles of the mdx mouse, *J Muscle Res Cell Motil,* **20,** 605-25.

Gosselin, L., Barkley, J., Spencer, M., McCormick, K. and Farkas, J. (2003) Ventilatory dysfunction in mdx mice: impact of tumour necrosis factor–α deletion, *Muscle & Nerve,* **28,** 336-343.

Gowers, W. (1879) Clinical Lecture on Pseudo-hypertrophic Muscular Paralysis, *Lancet,* **114,** 1-2, 37-39, 73-75, 113-116.

Goyenvalle, A., Vulin, A., Fougerousse, F., Leturcq, F., Kaplan, J.-C., Garcia, L. and Danos, O. (2004) Rescue of Dystrophic Muscle Through U7 snRNA-Mediated Exon Skipping, *Science*, **306,** 1796-1799.

Grady, R., Teng, H., Nichol, M., Cunningham, J., Wilkinson, R. and Sanes, J. (1997) Skeletal and cardiac myopathies in mice lacking utrophin and dystrophin: a model for Duchenne Muscular Dystrophy, *Cell,* **90,** 729-38.

Gregorevic, P., Plant, D. R., Leeding, K. S., Bach, L. A. and Lynch, G. S. (2002) Improved Contractile Function of the mdx Dystrophic Mouse Diaphragm Muscle after Insulin-Like Growth Factor-I Administration, *Am. J. Pathol.,* **161,** 2263-2272.

Gregorevic, P., Blankinship, MJ, Allen, JM, Crawford, RW, Meuse, L, Miller DG, Russell, DW, Chamberlain, JS. (2004), Systemic delivery of genes to striated muscle using adeno-associated viral vectors, *Nat Med,* **8,** 782-3

Gregory, L., Waddington, S., Holder, M., Mitrophanous, K., Buckley, S., Mosley, K., Bigger, B., Ellard, F., Walmsley, L., Lawrence, L., Al-Allaf, F., Kingsman, S., Coutelle, C. and Themis, M. (2004) Highly efficient EIAV-mediated in utero gene transfer and expression in the major muscle groups affected by Duchenne muscular dystrophy, *Gene Ther,* **11,** 1117-25.

Grounds , M. and Torrisi, J. (2004) Anti-TNF{alpha} (Remicade(R)) therapy protects dystrophic skeletal muscle from necrosis, *FASEB J.,* **18,** 676-682.

Gussoni, E., Soneoka, Y., Strickland, C., Buzney, E., Khan, M., Flint, A., Kunkel, L. and Mulligan, R. (1999) Dystrophin expression in the mdx mouse restored by stem cell transplantation, *Nature,* **401,** 390-4.

Hainsey, T., Senapati, S., Kuhn, D. and Rafael, J. (2003) Cardiomyopathic features associated with muscular dystrophy are independent of dystrophin absence in cardiovasculature, *Neuromuscul Disord,* **13,** 294-302.

Hartel, J., Granchelli, J., Hudecki, M., Pollina, C. and Gosselin, L. (2001) Impact of prednisone on TGF-beta1 and collagen in diaphragm muscle from mdx mice, *Muscle Nerve,* **24,** 428-32.

Hayes, A. and Williams, D. A. (1998) Contractile function and low-intensity exercise effects of old dystrophic (mdx) mice, *Am J Physiol Cell Physiol,* **274,** C1138-1144.

Head, S. (1993) Membrane potential, resting calcium and calcium transients in isolated muscle fibres from normal and dystrophic mice, *J. Physiol.,* **469,** 11-19.

Heydemann, A. and McNally, E. M. (2004) Regenerating More Than Muscle in Muscular Dystrophy, *Circulation,* **110,** 3290-3292.

Hoffman, E. (1993) Genotype/phenotype correlations in Duchenne/Becker dystrophy, *Mol Cell Biol Hum Dis Ser,* **3,** 12-36.

Hoffman, E., Brown, R. and Kunkel, L. (1987) Dystrophin: the protein product of the Duchenne Muscular Dystrophy locus,*Cell,* **51,** 919-28.

Hoffman, E., Kunkel, L., Angelini, C., Clarke, A., Johnson, M. and Harris, J. (1989) Improved diagnosis of Becker muscular dystrophy by dystrophin testing, *Neurology,* **39,** 1011-1017.

Hopf, F. W., Turner, P. R., Denetclaw, W. F., Jr, Reddy, P. and Steinhardt, R. A. (1996) A critical evaluation of resting intracellular free calcium regulation in dystrophic mdx muscle, *Am J Physiol Cell Physiol,* **271,** C1325-1339.

Im, W, Phelps, S, Copen, E, Adams, E, Slighton, J. and Chamberlain, J (1996) Differential expression of dystrophin isoforms in strains of mdx mice with different mutations, *Hum Mol Genetics,* **5,** 1149-1153

Infante, J. and Huszagh, V. (1999) Mechanisms of resistance to pathogenesis in muscular dystrophies, *Mol Cell Biochem,* **195,** 155-67.

Jacobs, S., Bootsma, A., Willems, P., Bar, P. and Wokke, J. (1996) Prednisone can protect against exercise-induced muscle damage, *J Neurol,* **243,** 410-6.

James, R. S., Cox, V. M., Young, I. S., Altringham, J. D. and Goldspink, D. F. (1997) Mechanical properties of rabbit latissimus dorsi muscle after stretch and/or electrical stimulation, *J Appl Physiol,* **83,** 398-406.

Kamogawa, Y., Biro, S., Maeda, M., Setoguchi, M., Hirakawa, T., Yoshida, H. and Tei, C. (2001) Dystrophin-deficient myocardium is vulnerable to pressure overload in vivo, *Cardiovasc Res,* **50,** 509-15.

Kaufman, R. J. (1999) Correction of genetic disease by making sense from nonsense, *J. Clin. Invest.,* **104,** 367-368.

Kelsen, S., Sexauer, W., Mardini, I. and Criner, G. (1994) The comparative effects of elastase-induced emphysema on costal and crural diaphragm and parasternal intecostal muscle contractility, *Am J Respir Crit Care Med,* **149,** 168-173.

Kelsen, S. G., Bao, S., Thomas, A. J., Mardini, I. A. and Criner, G. J. (1993) Structure of parasternal intercostal muscles in the adult hamster: topographic effects, *J Appl Physiol,* **75,** 1150-1154.

Kingston, H., Harper, P., Pearson, P., Davies, K., Williamson, R. and Page, D. (1983) Localisation of gene for Becker muscular dystrophy, *Lancet,* **2,** 1200.

Kissel, J., Lynn, D., Rammohan, K., Klein, J., Griggs, R., Moxley, R., 3d, Cwik, V., Brooke, M. and Mendell, J. (1993) Mononuclear cell analysis of muscle biopsies in prednisone- and azathioprine-treated Duchenne muscular dystrophy, *Neurology,* **43,** 532-536.

Koenig, M., Beggs, A., Moyer, M., Scherpf, S., Heindrich, K., Bettecken, T., Meng, G., Muller, C., Lindlof, M. and Kaariainen, H. (1989) The molecular basis for Duchenne versus Becker muscular dystrophy: correlation of severity with type of deletion, *Am J Hum Genet,* **45,** 498-506.

Koenig, M., Hoffman, E., Bertelson, C., Monaco, A., Feener, C. and Kunkel, L. (1987) Complete cloning of the Duchenne Muscular Dystrophy (DMD) cDNA and preliminary genomic organization of the DMD gene in normal and affected individuals, *Cell,* **50,** 509-17.

Koenig, M. and Kunkel, L. (1990) Detailed analysis of the repeat domain of dystrophin reveals four potential hinge segments that may confer flexibility, *J. Biol. Chem.,* **265,** 4560-4566.

Koenig, M., Monaco, A. and Kunkel, L. (1988) The complete sequence of dystrophin predicts a rod-shaped cytoskeletal protein, *Cell,* **53,** 219-26.

Kogler, H., Soergel, D. G., Murphy, A. M. and Marban, E. (2001) Maintained contractile reserve in a transgenic mouse model of myocardial stunning, *Am J Physiol Heart Circ Physiol,* **280,** H2623-2630.

Kornegay, J., Cundiff, D., Bogan, D., Bogan, J. and Okamura, C. (2003) The cranial sartorius muscle undergoes true hypertrophy in dogs with golden retriever muscular dystrophy, *Neuromusc. Disord.,* **13,** 493-500.

Kornegay, J., Tuler, S., Miller, D. and Levesque, D. (1988) Muscular dystrophy in a litter of golden retriever dogs, *Muscle Nerve,* **11,** 1056-64.

Krag, T. O. B., Bogdanovich, S., Jensen, C. J., Fischer, M. D., Hansen-Schwartz, J., Javazon, E. H., Flake, A. W., Edvinsson, L. and Khurana, T. S. (2004) Heregulin ameliorates the dystrophic phenotype in mdx mice, *PNAS,* **101,** 13856-13860.

Krupnick, A. S., Zhu, J., Nguyen, T., Kreisel, D., Balsara, K. R., Lankford, E. B., Clark, C. C., Levine, S., Stedman, H. H. and Shrager, J. B. (2003) Inspiratory loading does not accelerate dystrophy in mdx mouse diaphragm: implications for regenerative therapy, *J Appl Physiol,* **94,** 411-419.

Lamb, G., Junankar, P. and Stephenson, D. (1995) Raised intracellular [Ca2+] abolishes excitation-contraction coupling in skeletal muscle fibres of rat and toad, *J Physiol (Lond),* **489,** 349-362.

Laws, N. and Hoey, A. J. (2004) Progression of kyphosis in mdx mice, *J Appl Physiol***, 97,** 1970-1977

Lefaucheur, J. P., Pastoret, C. and Sebille, A. (1995) Phenotype of Dystrophinopathy in old *mdx* mice, *The Anatomical Record,* **242,** 70-76.

Lenk, U., Hanke, R., Thiele, H. and Speer, A. (1993) Point mutations at the carboxy terminus of the human dystrophin gene: implications for an association with mental retardation in DMD patients, *Hum. Mol. Genet.,* **2,** 1877-1881.

Lim, J., Kim, D. and Bang, M. (2004) Effects of exercise and steroid on skeletal muscle apoptosis in the mdx mouse.,*Muscle Nerve,* **30,** 456-62.

Liu, F., Liang, K. W. and Huang, L. (2001a) Systemic Administration of Naked DNA: Gene Transfer to Skeletal Muscle,*Mol. Interv.,* **1,** 168-172.

Liu, F., Nishikawa, M., Clemens, P. and Huang, L. (2001b) Transfer of full-length dystrophin gene transfer to the diaphragm muscle of DMD (mdx/mdx) mice through systemic administration of plasmid DNA.,*Mol Ther,* **4,** 45-51.

Liu, J., Okamura, C., Bogan, D., Bogan, J., Childers, M. and Kornegay, J. (2004) Effects of prednisone in canine muscular dystrophy, *Muscle Nerve,* **30,** 767-73.

Louboutin, J., Fichter-Gagnepain, V., Thaon, E. and Fardeau, M. (1993) Morphometric analysis of mdx diaphragm muscle fibres. Comparison with hindlimb muscles, *Neuromuscul Disord,* **3,** 463-9.

Louis, M., Lebacq, J., Poortmans, J., Belpaire-Dethiou, M., Devogelaer, J., Van Hecke, P., Goubel, F. and Francaux, M. (2003) Beneficial effects of creatine supplementation in dystrophic patients, *Muscle Nerve,* **27,** 604-10.

Lu, Q., Mann, C., Lou, F., Bou-Gharios, G., Morris, G., Xue, S., Fletcher, S., Partridge, T. and Wilton, S. (2003) Functional amounts of dystrophin produced by skipping the mutated exon in the mdx dystrophic mouse, *Nat Med,* **9,** 1009-14.

Lu, Q. L., Rabinowitz, A., Chen, Y. C., Yokota, T., Yin, H., Alter, J., Jadoon, A., Bou-Gharios, G. and Partridge, T. (2004) Systemic delivery of antisense oligoribonucleotide restores dystrophin expression in body-wide skeletal muscles, *PNAS,* 0406700102.

Lu, S. and Hoey, A. (2000) Age- and sex-associated Changes in Cardiac B1-adrenoceptors from The Muscular Dystrophy (mdx) Mouse, *Journal of Molecular and Cell Cardiology,* **32,** 1661-1668.

Lynch, G. S., Hinkle, R. T., Chamberlain, J. S., Brooks, S. V. and Faulkner, J. A. (2001) Force and power output of fast and slow skeletal muscles from mdx mice 6-28 months old, *J. Physiol.,* **535,** 591-600.

Lynch, G. S., Rafael, J. A., Hinkle, R. T., Cole, N. M., Chamberlain, J. S. and Faulkner, J. A. (1997) Contractile properties of diaphragm muscle segments

from old mdx and old transgenic mdx mice, *Am J Physiol Cell Physiol,* **272,** C2063-2068.

MacLennan, P. and Edwards, R. H. T. (1990) Protein turnover is elevated in muscle of *mdx* mice in vivo, *Biochem J,* **268,** 795-797.

Mallouk, N. and Allard, B. (2002) Ca2+ Influx and Opening of Ca2+-Activated K+ Channels in Muscle Fibers from Control and mdx Mice, *Biophys. J.,* **82,** 3012-4955.

Mallouk, N., Jacquemond, V. and Allard, B. (2000) Elevated subsarcolemmal Ca2+ in mdx mouse skeletal muscle fibers detected with Ca2+-activated K+ channels, *PNAS,* **97,** 4950-4955.

Mann, C., Honeyman, K., McClorey, G., Fletcher, S. and Wilton, S. (2002) Improved antisense oligonucleotide induced exon skipping in the mdx mouse model of muscular dystrophy, *J Gene Med,* **4,** 644-54.

Mann, C. J., Honeyman, K., Cheng, A. J., Ly, T., Lloyd, F., Fletcher, S., Morgan, J., Partridge, T. A. and Wilton, S. D. (2001) Antisense-induced exon skipping and synthesis of dystrophin in the mdx mouse, *Proceedings of the National Academy of Sciences of the United States of America,* **98,** 42-47.

Mardini, I., Schlenker, E. and Burbach, J. (1986) Effects of dystrophy and age on hamster tracheal smooth muscle function, *Respir Physiol,* **66,** 157-70.

Mariol, M. and Segalat, L. (2001) Muscular degeneration in the absence of dystrophin is a calcium-dependent process, *Curr Biol,* **11,** 1691-4.

Matecki, S., Dudley, R. W. R., Divangahi, M., Gilbert, R., Nalbantoglu, J., Karpati, G. and Petrof, B. J. (2004) Therapeutic gene transfer to dystrophic diaphragm by an adenoviral vector deleted of all viral genes, *Am J Physiol Lung Cell Mol Physiol,* **287,** L569-576.

Matsuda, R., Nishikawa, A. and Tanaka, H. (1995) Visualization of dystrophic muscle fibers in mdx mouse by vital staining with Evans blue: evidence of apoptosis in dystrophin-deficient muscle, *J Biochem (Tokyo),* **118,** 959-64.

McArdle, A., Edwards, R. and Jackson, M. (1995) How does dystrophin deficiency lead to muscle degeneration?--evidence from the mdx mouse., *Neuromuscul Disord,* **5,** 445-56.

McMahon, J., Signori, E., Wells, K., Fazio, V. and Wells, D. (2001) Optimisation of electrotransfer of plasmid into skeletal muscle by pretreatment with hyaluronidase - increased expression with reduced muscle damage,*Gene Ther,* **8,** 1264-70.

McNally, E. and Towbin, J. (2004) Cardiomyopathy in muscular dystrophy workshop. 28-30 September 2003, Tucson, Arizona, *Neuromuscul Disord,* **14,** 442-8.

Megeney, L. A., Kablar, B., Perry, R. L. S., Ying, C., May, L. and Rudnicki, M. A. (1999) Severe cardiomyopathy in mice lacking dystrophin and MyoD, *PNAS,* **96,** 220-225.

Metzinger, L., Passaquin, A., Leijendekker, W., Poindron, P. and Ruegg, U. (1995) Modulation by prednisolone of calcium handling in skeletal muscle cells, *Br J Pharmacol,* **116,** 2811-2816.

Misuri, G., Lanini, B., Gigliotti, F., Iandelli, I., Pizzi, A., Bertolini, M. G. and Scano, G. (2000) Mechanism of CO2 Retention in Patients With Neuromuscular Disease, *Chest,* **117,** 447-453.

Moisset, P., Gagnon, Y., Karpati, G. and Tremblay, J. (1998) Expression of human dystrophin following the transplantation of genetically modified mdx myoblasts, *Gene Ther,* **5,** 1340-6.

Mokhtarian, A., Lefaucheur, J. P., Even, P. C. and Sebille, A. (1999) Hindlimb immobilization applied to 21-day-old mdx mice prevents the occurrence of muscle degeneration, *J Appl Physiol,* **86,** 924-931.

Monaco, A., Bertelson, C., Liechti-Gallati, S., Moser, H. and Kunkel, L. (1988) An explanation for the phenotypic differences between patients bearing partial deletions of the DMD locus, *Genomics,* **2,** 90-5.

Morrison, J., Lu, Q. L., Pastoret, C., Partridge, T. and Bou-Gharios, G. (2000) T-Cell-Dependent Fibrosis in the mdx Dystrophic Mouse, *Lab. Invest.,* **80,** 881- 91

Muller, B., Dechant, C., Meng, G., Liechti-Gallati, S., Doherty, R., Hejtmancik, J., Bakker, E., Read, A., Jeanpierre, M. and Fischbeck, K. (1992) Estimation of the male and female mutation rates in Duchenne Muscular Dystrophy (DMD). *Hum Genet,* **89,** 204-6.

Muntoni, F., Fisher, I., Morgan, J. and Abraham, D. (2002) Steroids in Duchenne muscular dystrophy: from clinical trials to genomic research, *Neuromuscul Disord,* **12 Suppl 1,** S162-5.

Murakami, T., Nishi, T., Kimura, E., Goto, T., Maeda, Y., Ushio, Y., Uchino, M. and Sunada, Y. (2003) Full-length dystrophin cDNA transfer into skeletal muscle of adult mdx mice by electroporation, *Muscle Nerve,* **27,** 237-41.

Nakamura, A., Yoshida, K., Takeda, S., Dohi, N. and Ikeda, S. (2002) Progression of dystrophic features and activation of mitogen-activated protein kinases and calcineurin by physical exercise, in hearts of mdx mice, *FEBS Lett,* **520,** 18-24.

Nguyen, F., Cherel, Y., Guigand, L., Goubault-Leroux, I. and Wyers, M. (2002) Muscle lesions associated with dystrophin deficiency in neonatal golden retriever puppies, *J Comp Pathol,* **126,** 100-8.

Nicholson, L. (1993) The "rescue" of dystrophin synthesis in boys with Duchenne muscular dystrophy.,*Neuromuscul Disord,* **3,** 525-31.

Nigro, G., Comi, L., Politano, L. and Bain, R. (1990) The incidence and evolution of cardiomyopathy in Duchenne Muscular Dystrophy, *Int J Cardiol,* **26,** 271-7.

Noguchi, S., Tsukahara, T., Fujita, M., Kurokawa, R., Tachikawa, M., Toda, T., Tsujimoto, A., Arahata, K. and Nishino, I. (2003) cDNA microarray analysis of individual Duchenne muscular dystrophy patients, *Hum. Mol. Genet.,* **12,** 595-600.

Oda, T., Shimizu, N., Yonenobu, K., Ono, K., Nabeshima, T. and Kyoh, S. (1993) Longitudinal study of spinal deformity in Duchenne muscular dystrophy, *J Pediatr Orthop,* **13,** 478-88.

Pacioretty, L., Cooper, B. and Gilmour, R. (1992) Cellular Electrophysiology of Murine and Canine Cardiac Muscle in Duchenne Muscular Dystrophy, *Biophys. J.,* **61,** A306.

Partridge, T. (1991) Animal models of muscular dystrophy--what can they teach us? *Neuropathol Appl Neurobiol,* **17,** 353-63.

Partridge, T. (1997) In *Dystrophin-Gene, Protein and Cell Biology*. Ed Brown, S and Lucy, A, Cambridge University Press, Cambridge

Partridge, T. (2002) Myoblast transplantation, *Neuromuscul Disord,* **12 Suppl,** 3-5.

Partridge, T., Lu, Q., Morris, G. and Hoffman, E. (1998) Is myoblast transplantation effective? *Nat Med,* **4,** 1208-9.

Passaquin, A., Metzinger, L., Leger, J., Warter, J. and Poindron, P. (1993) Prednisolone enhances myogenesis and dystrophin-related protein in skeletal muscle cell cultures from mdx mouse, *J Neurosci Res,* **35,** 363-72.

Passaquin, A., Renard, M., Kay, L., Challet, C., Mokhtarian, A., Wallimann, T. and Ruegg, U. (2002) Creatine supplementation reduces skeletal muscle degeneration and enhances mitochondrial function in mdx mice, *Neuromuscul Disord,* **12,** 174-82.

Passerini, L., Bernasconi, P., Baggi, F., Confalonieri, P., Cozzi, F., Cornelio, F. and Mantegazza, R. (2002) Fibrogenic cytokines and extent of fibrosis in muscle of dogs with X-linked golden retriever muscular dystrophy, *Neuromuscul Disord,* **12,** 828-35.

Pastoret, C. and Sebille, A. (1995a) Age-related differences in regeneration of dystrophic (mdx) and normal muscle in the mouse, *Muscle & Nerve,* **18,** 1147-1154.

Pastoret, C. and Sebille, A. (1995b) mdx mice show progressive weakness and muscle deterioration with age, *Journal of Neurological Sciences,* **129,** 97-105.

Paulson, G., Pope, A. and Baumann, C. (1966) Lactate dehydrogenase levels in tissue and serum of normal and dystrophic lambs, *Experimental biology and medicine,* **122,** 321-4.

Pearce, M., Blake, D., Tinsley, J., Byth, B., Campbell, L., Monaco, A. and Davies, K. (1993) The utrophin and dystrophin genes share similarities in genomic structure, *Hum. Mol. Genet.,* **2,** 1765-1772.

Perkins, K. and Davies, K. (2002) The role of utrophin in the potential therapy of Duchenne muscular dystrophy, *Neuromuscul Disord,* **12 Suppl 1,** S78-89.

Petrof, B. (1998a) The molecular basis of activity-induced muscle injury in Duchenne muscular dystrophy, *Mol Cell Biochem,* **179,** 111-23.

Petrof, B. (1998b) Respiratory muscles as a target for adenovirus-mediated gene therapy, *Eur Respir J,* **11,** 492-497.

Petrof, B., Acsadi, G., Jani, A., Massie, B., Bourdon, J., Matusiewicz, N., Yang, L., Lochmuller, H. and Karpati, G. (1995) Efficiency and functional consequences of adenovirus-mediated in vivo gene transfer to normal and dystrophic (mdx) mouse diaphragm, *Am. J. Respir. Cell Mol. Biol.,* **13,** 508-517.

Petrof, B., Shrager, J., Stedman, H., Kelly, A. and Sweeney, H. (1993a) Dystrophin Protects the Sarcolemma from Stresses Developed During Muscle Contraction, *PNAS,* **90,** 3710-3714.

Petrof, B. J., Stedman, H. H., Shrager, J. B., Eby, J., Sweeney, H. L. and Kelly, A. M. (1993b) Adaptations in myosin heavy chain expression and contractile function in dystrophic mouse diaphragm, *Am J Physiol Cell Physiol,* **265,** C834-841.

Phillips, M. F., Quinlivan, C. M., Edwards, R. H. T. and Calverly, P. M. A. (2001) Changes in Spirometry Over Time as a Prognostic Marker in Patients with Duchenne Muscular Dystrophy, *Am. J. Respir. Crit. Care Med.,* **164,** 2191-2194.

Plummer, J. (1998) How many animals? *ANZCCART News,* **Vol 11,** 1-3.

Politano, L., Nigro, G., Nigro, V., Piluso, G., Papparella, S., Paciello, O. and Comi, L. (2003) Gentamicin administration in Duchenne patients with premature stop codon. Preliminary results, *Acta Myol,* **22,** 15-21.

Porter, J., Rafael, J., Ragusa, R., Brueckner, J., Trickett, J. and Davies, K. (1998) The sparing of extraocular muscle in dystrophinopathy is lost in mice lacking utrophin and dystrophin, *J. Cell Sci.,* **111,** 1801-1811.

Porter, J. D., Khanna, S., Kaminski, H. J., Rao, J. S., Merriam, A. P., Richmonds, C. R., Leahy, P., Li, J., Guo, W. and Andrade, F. H. (2002) A chronic inflammatory response dominates the skeletal muscle molecular signature in dystrophin-deficient mdx mice, *Hum. Mol. Genet.,* **11,** 263-272.

Poukka, R. (1966) Tissue lipids in calves suffering from muscular dystrophy.,*Br J Nutr,* **20,** 245-56.

Quinlan, J., Hahn, H., Wong, B., Lorenz, J., Wenisch, A. and Levin, L. (2004) Evolution of the mdx mouse cardiomyopathy: physiological and morphological findings.,*Neuromuscul Disord,* **14,** 491-6.

Rafael, J., Cox, G., Corrado, K., Jung, D., Campbell, K. and Chamberlain, J. (1996) Forced expression of dystrophin deletion constructs reveals structure-function correlations, *J. Cell Biol.,* **134,** 93-102.

Rando, T. (2001) The dystrophin-glycoprotein complex, cellular signalling, and the regulation of cell survival in the muscular dystrophies, *Muscle & Nerve,* **24,** 1575-1594.

Rando, T., Disatnik, M., Yu, Y. and Franco, A. (1998) Muscle cells from mdx mice have an increased susceptibility to oxidative stress, *Neuromuscul Disord,* **8,** 14-21.

Reeve, J., McArdle, A. and Jackson, M. (1997) Age-related changes in muscle calcium content in dystrophin-deficient mdx mice, *Muscle Nerve,* **20,** 357-60.

Rideau, Y., Jankowski, L. and Grellet, J. (1981) Respiratory function in the muscular dystrophies.,*Muscle Nerve,* **4,** 155-64.

Rifai, Z., Welle, S., Moxley, R. T., 3rd, Lorenson, M. and Griggs, R. C. (1995) Effect of prednisone on protein metabolism in Duchenne dystrophy, *Am J Physiol Endocrinol Metab,* **268,** E67-74.

Sadeghi, A., Doyle, A. D. and Johnson, B. D. (2002) Regulation of the cardiac L-type Ca2+ channel by the actin-binding proteins alpha -actinin and dystrophin, *Am J Physiol Cell Physiol,* **282,** C1502-1511.

Sakamoto, M., Yuasa, K., Yoshimura, M., Yokota, T., Ikemoto, T., Suzuki, M., Dickson, G., Miyagoe-Suzuki, Y. and Takeda, S. (2002) Micro-dystrophin cDNA ameliorates dystrophic phenotypes when introduced into mdx mice as a transgene, *Biochem Biophys Res Commun,* **293,** 1265-72.

Sanyal, S. and Johnson, W. (1982) Cardiac conduction abnormalities in children with Duchenne's progressive muscular dystrophy: electrocardiographic features and morphologic correlates, *Circulation,* **66,** 853-863.

Sanyal, S., Johnson, W., Thapar, M. and Pitner, S. (1978) An ultrastructural basis for electrocardiographic alterations associated with Duchenne's progressive muscular dystrophy, *Circulation,* **57,** 1122-1129.

Sapp, J. L., Bobet, J. and Howlett, S. E. (1996) Contractile properties of myocardium are altered in dystrophin-deficient mdx mice, *Journal of Neurological Science,* **142,** 17-24.

Sazani, P. and Kole, R. (2003) Therapeutic potential of antisense oligonucleotides as modulators of alternative splicing, *J. Clin. Invest.,* **112,** 481-486.

Schatzberg, S., Anderson, L., Wilton, S., Kornegay, J., Mann, C., Solomon, G. and Sharp, N. (1998) Alternative dystrophin gene transcripts in golden retriever muscular dystrophy, *Muscle Nerve,* **21,** 991-8.

Scheuerbrandt, G. (2004) Assoc Monegasque Contre les Myopathies and Duchenne Parent project France, Monaco.

Seddon, P. C. and Khan, Y. (2003) Respiratory problems in children with neurological impairment, *Arch. Dis. Child.,* **88,** 75-78.

Shelton, G. (1999), Vol. 2004 Veterinary Neurology and Neurosurgery.

Sicinski, P., Geng, Y., Ryder-Cook, A., Barnard, E., Darlison, M. and Barnard, P. (1989) The molecular basis of muscular dystrophy in the mdx mouse: a point mutation, **244,** 1578-80.

Silversides, C. K., Webb, G. D., Harris, V. A. and Biggar, D. W. (2003) Effects of deflazacort on left ventricular function in patients with Duchenne Muscular Dystrophy, *The American Journal of Cardiology,* **91,** 769-772.

Sivak, E., Shefner, J. and Sexton, J. (1999) Neuromuscular disease and hypoventilation, *Curr Opin Pulm Med,* **5,** 355-62.

Smith, A., Koreska, J. and Moseley, C. (1989) Progression of scoliosis in Duchenne muscular dystrophy, *J Bone Joint Surg Am,* **71,** 1066-1074.

Spence, H., Chen, Y. and Winder, S. (2002) Muscular dystrophies, the cytoskeleton and cell adhesion, *Bioessays,* **24,** 542-52.

Stedman, H. H., Sweeney, H. L., Shrager, J. B., Maguire, H. C., Panettieri, R. A., Petrof, B., Narusawa, M., Leferovich, J. M., Sladky, J. T. and Kelly, A. M. (1991) The mdx mouse diaphragm reproduces the degenerative changes of Duchenne Muscular Dystrophy, *Nature,* **352,** 536-539.

Stegemann, H. and Stalder, K. (1967) Determination of Hydroxyproline, *Clin. Chim. Acta,* **18,** 267-273.

Stevens, E. D. and Faulkner, J. A. (2000) The capacity of mdx mouse diaphragm muscle to do oscillatory work, *J Physiol (Lond),* **522,** 457-466.

Tarnopolsky, M. A., Mahoney, D. J., Vajsar, J., Rodriguez, C., Doherty, T. J., Roy, B. D. and Biggar, D. (2004) Creatine monohydrate enhances strength and body composition in Duchenne muscular dystrophy, *Neurology,* **62,** 1771-1777.

Thioudellet, C., Blot, S., Squiban, P., Fardeau, M. and Braun, S. (2002) Current protocol of a research phase I clinical trial of full-length dystrophin plasmid DNA in Duchenne/Becker muscular dystrophies. Part I: rationale, *Neuromuscul Disord,* **12 Suppl 1,** S49-51.

Thomas, G. D., Sander, M., Lau, K. S., Huang, P. L., Stull, J. T. and Victor, R. G. (1998) Impaired metabolic modulation of alpha -adrenergic vasoconstriction in dystrophin-deficient skeletal muscle, *PNAS,* **95,** 15090-15095.

Tidball, J., Albrecht, D., Lokensgard, B. and Spencer, M. (1995) Apoptosis precedes necrosis of dystrophin-deficient muscle, *J Cell Sci,* **108,** 2197-2204.

Tinsley, J., Blake, D., Roche, A., Fairbrother, U., Riss, J., Byth, B., Knight, A., Kendrick-Jones, J., Suthers, G. and Love, D. (1992) Primary structure of dystrophin-related protein, *Nature,* **360,** 591-3.

Tkatchenko, A., Pietu, G., Cros, N., Gannoun-Zaki, L., Auffray, C., Leger, J. and Dechesne, C. (2001) Identification of altered gene expression in skeletal muscles from Duchenne muscular dystrophy patients, *Neuromuscul Disord,* **11,** 269-77.

Torrente, Y., Tremblay, J.-P., Pisati, F., Belicchi, M., Rossi, B., Sironi, M., Fortunato, F., El Fahime, M., D'Angelo, M. G., Caron, N. J., Constantin, G., Paulin, D., Scarlato, G. and Bresolin, N. (2001) Intraarterial Injection of Muscle-derived CD34+Sca-1+ Stem Cells Restores Dystrophin in mdx Mice, *J. Cell Biol.,* **152,** 335-348.

Torres, L. and Duchen, L. (1987) The mutant mdx: inherited myopathy in the mouse. Morphological studies of nerves, muscles and end-plates, *Brain,* **110,** 269-299.

Turner, P., Schultz, R., Ganguly, B. and Steinhardt, R. (1993) Proteolysis results in altered leak channel kinetics and elevated free calcium in mdx muscle, *J Membr Biol,* **133,** 243-51.

Turner, P., Westwood, T., Regen, C. and Steinhardt, R. (1988) Increased protein degradation results from elevated free calcium levels found in muscle from mdx mice, *Nature,* **335,** 735-8.

Tutdibi, O., Brinkmeier, H., Rudel, R. and Fohr, K. J. (1999) Increased calcium entry into dystrophin-deficient muscle fibres of MDX and ADR-MDX mice is reduced by ion channel blockers, *J Physiol (Lond),* **515,** 859-868.

van Deutekom, J. C. T., Bremmer-Bout, M., Janson, A. A. M., Ginjaar, I. B., Baas, F., den Dunnen, J. T. and van Ommen, G.-J. B. (2001) Antisense-induced exon skipping restores dystrophin expression in DMD patient derived muscle cells, *Hum. Mol. Genet.,* **10,** 1547-1554.

VandenDriessche, T., Naldini, L., Collen, D. and Chuah, M. (2002) Oncoretroviral and lentiviral vector-mediated gene therapy, *Methods Enzymol,* **346,** 573-89.

Vicat, J., Boisseau, S., Jourdes, P., Laine, M., Wion, D., Bouali-Benazzouz, R., Benabid, A. and Berger, F. (2000) Muscle transfection by electroporation

with high-voltage and short-pulse currents provides high-level and long-lasting gene expression, *Hum Gene Ther,* **11,** 909-16.

Walter, M, Reilich, P, Lochmuller, H, Kohnen, R, Schlotter, B, Hautmann, H, Dunkl, E, Pongratz, D And Muller-Felber, W (2002) Creatine monohydrate in myotonic dystrophy: a double blind, placebo-controlled clinical study, *J Neurology* **249 (12),** 1717-22

Wang, B., Li, J. and Xiao, X. (2000) From the Cover: Adeno-associated virus vector carrying human minidystrophin genes effectively ameliorates muscular dystrophy in mdx mouse model, *PNAS,* **97,** 13714-13719.

Weintraub, H., Tapscott, S., Davis, R., Thayer, M., Adam, M., Lassar, A. and Miller, A. (1989) Activation of muscle-specific genes in pigment, nerve, fat, liver, and fibroblast cell lines by forced expression of MyoD, PNAS **86,** 5434 -5438.

Wells, K., Fletcher, S., Mann, C., Wilton, S. and Wells, D. (2003) Enhanced in vivo delivery of antisense oligonucleotides to restore dystrophin expression in adult mdx mouse muscle, *FEBS Lett,* **552,** 145-9.

White, J., Bower, J., Kurek, J. and Austin, L. (2001) Leukemia inhibitory factor enhances regeneration in skeletal muscles after myoblast transplantation, *Muscle Nerve,* **24,** 695-7.

Wilton, S., Dye, D., Blechynden, L. and Laing, N. (1997a) Revertant fibres: a possible genetic therapy for Duchenne muscular dystrophy? *Neuromuscul Disord,* **7,** 329-35.

Wilton, S., Dye, D. and Laing, N. (1997b) Dystrophin gene transcripts skipping the mdx mutation, *Muscle Nerve,* **20,** 728-34.

Wilton, S., Lloyd, F., Carville, K., Fletcher, S., Honeyman, K., Agrawal, S. and Kole, R. (1999) Specific removal of the nonsense mutation from the mdx dystrophin mRNA using antisense oligonucleotides, *Neuromuscul Disord,* **9,** 330-8.

Winand, N., Edwards, M., Pradhan, D., Berian, C. and Cooper, B. (1994) Deletion of the dystrophin muscle promoter in feline muscular dystrophy, *Neuromuscul Disord,* **4,** 433-45.

Wong, B. and Christopher, C. (2002) Corticosteroids in Duchenne muscular dystrophy: a reappraisal, *J Child Neurol,* **17,** 183-90.

Xiao, X., Li, J., Tsao, Y.-P., Dressman, D., Hoffman, E. P. and Watchko, J. F. (2000) Full Functional Rescue of a Complete Muscle (TA) in Dystrophic Hamsters by Adeno-Associated Virus Vector-Directed Gene Therapy,*J. Virol.,* **74,** 1436-1442.

Yamashita, T., Kanaya, K., Kawaguchi, S., Murakami, T. and Yokogushi, K. (2001a) Prediction of progression of spinal deformity in Duchenne muscular dystrophy: a preliminary report, *Spine,* **26,** E223-6.

Yamashita, T., Kanaya, K., Yokogushi, K., Ishikawa, Y. and Minami, R. (2001b) Correlation between progression of spinal deformity and pulmonary function in Duchenne muscular dystrophy, *J Pediatr Orthop,* **21,** 113-6.

Yang, Y., Li, Q., Ertl, H. and Wilson, J. (1995) Cellular and humoral immune responses to viral antigens create barriers to lung-directed gene therapy with recombinant adenoviruses,*J. Virol.,* **69,** 2004-2015.

Yoshimura, M., Sakamoto, M., Ikemoto, M., Mochizuki, Y., Yuasa, K., Miyagoe-Suzuki, Y. and Takeda, S. (2004) AAV vector-mediated microdystrophin

expression in a relatively small percentage of mdx myofibers improved the mdx phenotype, *Mol Ther,* **10,** 821-8.

Yotsukura, M., Sasaki, K., Kachi, E., Sasaki, A., Ishihara, T. and Ishikawa, K. (1995) Circadian rhythm and variability of heart rate in Duchenne-type progressive muscular dystrophy, *Am J Cardiol,* **76,** 947-51.

Yotsukura, M., Yamamoto, A., Kajiwara, T., Nishimura, T., Sakata, K., Ishihara, T. and Ishikawa, K. (1999) QT dispersion in patients with Duchenne-type progressive muscular dystrophy, *Am Heart J,* **137,** 672-7.

Yue, Y., Skimming, J. W., Liu, M., Strawn, T. and Duan, D. (2004) Full-length dystrophin expression in half of the heart cells ameliorates {beta}-isoproterenol-induced cardiomyopathy in mdx mice, *Hum. Mol. Genet.,* **13,** 1669-1675.

Zhang, G., Ludtke, J., Thioudellet, C., Kleinpeter, P., Antoniou, M., Herweijer, H., Braun, S. and Wolff, J. (2004) Intraarterial delivery of naked plasmid DNA expressing full-length mouse dystrophin in the mdx mouse model of Duchenne Muscular Dystrophy, *Hum Gene Ther,* **15,** 770-82.

# APPENDIX A: DEVELOPMENT OF NEW TECHNIQUES

## A1: CARDIAC MONOPHASIC ACTION POTENTIALS

### A1.1 Introduction

Boys with DMD show a high prevalence of atrial and ventricular arrhythmias, however the mechanisms of disturbed rhythm and conduction are not well understood (Sanyal and Johnson, 1982; Perloff, 1984). QT dispersion, a measure of QT interval variability, is seen in congenital arrhythmias such as congenital long-QT syndrome, torsades de pointes and various cardiomyopathies. A high degree of QT dispersion (>60ms) was found in a study of 67 DMD patients (Yotsukura *et al.*, 1999), and these authors demonstrated the association between QT dispersion and severity of ventricular arrhythmias with a probable relationship to regional myocardial derangement.

Abnormal ECGs have been observed in *mdx* mice, attributed in one study to the deficiency in nNOS activity seen in this strain (Bia *et al.*, 1999). There is controversy regarding QT intervals in *mdx*, due possibly to difficulties in determining the termination of the murine T wave (Bia *et al*., 1999; Chu *et al.*, 2002; Danik *et al.*, 2002)).

Monophasic action potentials (MAPs) are extracellular recordings that can replicate the repolarisation time course of transmembrane action potentials (TAPs) with high fidelity. MAPs can be recorded from the endocardium and epicardium of *in vivo* or *in vitro* beating hearts in human and animal subjects. The MAP accurately reflects the duration as well as configuration of the repolarisation phase of the TAP, although action potential amplitude and upstroke velocity is much less (Franz, 1999). They are hence useful as a link between basic and clinical electrophysiology in arrhythmia research, including studies of various transgenic mice models of human cardiomyopathy (Casimiro *et al.*, 2001; Franz, 1999; Knollmann *et al*., 2001a ; Knollmann *et al.*, 2001b).

MAP measurements would be a useful tool to further investigate the electrophysiological properties of *mdx* hearts, thus enhancing both the understanding of repolarisation and genesis of arrhythmias in dystrophic cardiac tissue, and helping to resolve controversies regarding the *mdx* cardiac phenotype.

## A1.2 Methods

A1.2.1 Langendorff perfused murine heart model

Hearts were isolated from 6-8 week old and 15 month old *mdx* and C57 mice.n=14-15/group

Mice were anaesthetised with 60 mg/kg sodium pentobarbital administered intra-peritoneally. A thoracotomy was performed and hearts were excised into room temperature perfusion fluid. The aorta was cannulated under magnification using a blunt ended 21 gauge needle, and the coronary circulation perfused at 80 mmHg with modified Krebs-Henseleit buffer containing (mM) NaCl 119, $NaHCO_3$ 2, KCl 4.7, MgCl 1.2, $KH_2PO4$ 1.2, EDTA 0.5, glucose 11 and pyruvate 2. The concentration of $CaCl_2$ was 1.25mM. Buffer was equilibrated with 95% $O_2$ and 5% $CO_2$ at 37$^oC$ for 1 hour, giving a pH of 7.4, and was filtered inline using 0.45 μm filter to remove microparticles. The left ventricle was vented with a polyethylene apical drain, and the heart was then immersed in warmed perfusate in a jacketed glass bath maintained at 37$^oC$, where it rested horizontally. The temperature of the perfusion fluid was monitored continuously by a needle thermistor at the entry of the aortic cannula. The heart was paced by attaching electrodes to either the right atrium or ventricle and stimulating via a Grass SD9 stimulator. Settings= voltage threshold + 20%, (usually 2-3 volts but sometimes requiring a higher voltage to capture initially (up to 60 V)), 2 ms duration, frequency 6.9 Hz. This frequency achieved a heart rate of 420 bpm.

Perfusion pressure was also measured and maintained at 80mm Hg. Data was recorded at 2 kHz on a PowerLab data acquisition system (AD Instruments, Castle Hill, Australia) and 4 kHz for ECG channels. The experimental apparatus for MAP is shown in Figure A1.1.

The organ bath used was a Radnoti water-jacketed glass dish, modified with a Perspex insert to support and prevent free swinging of the heart for the purposes of recording MAPs. A simultaneous volume conducted ECG was also recorded with the recording electrodes and earth electrodes positioned in the perfusion fluid in close proximity to the heart.

**Fig A1.1** Langendorff experimental setup for ECG and MAP recordings

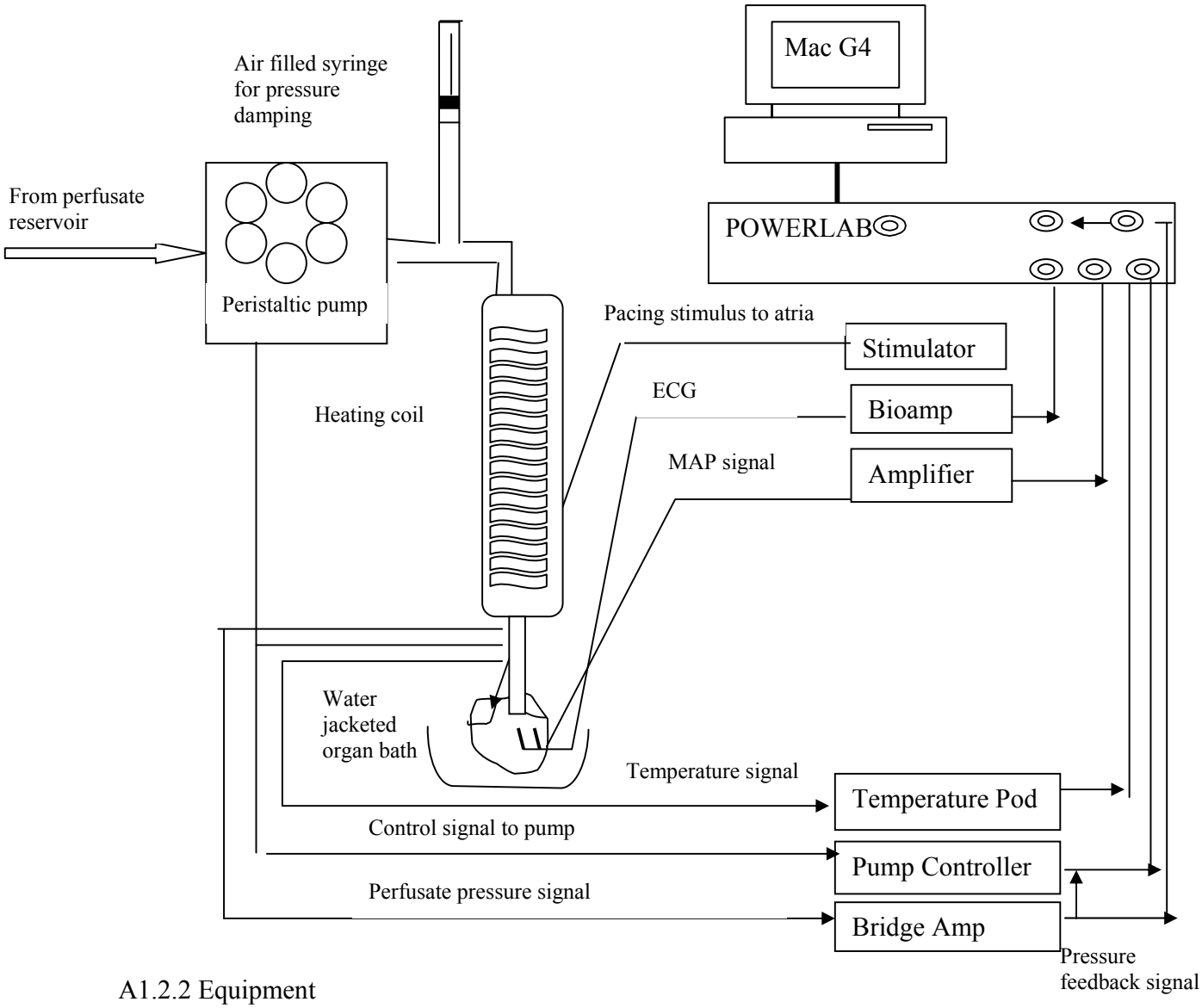


A1.2.2 Equipment

Shallow water-jacketed organ bath (Radnoti)

Glass heating coil (Radnoti)

Tubing and connectors (Radnoti)

Sterivex-HV 0.45µm filter unit (Millipore Corporation, US)

Animal Bioamp (ADI, Castle Hill, Australia)

Gilson pump

MLT844 Physiological Pressure Transducer (ADI)

Clip-on Domes for MLT844 (ADI)

Grass SD9 stimulator

Temperature pod for thermistor

Thermistor (ADI)

Custom made MAP electrodes

Custom made ECG electrodes

Suction

Heated water bath

Arterial clips and clip applicator, fine forceps and scissors

.

A1.2.3 Monophasic Action Potential Recordings

A 0.25mm MAP recording probe was constructed according to published protocols (Knollmann *et al*., 2001a) and consisted of an elastic strand of twisted double silver wires (95% purity), insulated with Teflon sleeves except for the very tips. The ends were deflected by 90$^{o}$ for the distal 3mm. Both tips were galvanically chlorinated to eliminate DC current offset. The MAP exploring electrode was smoothed to a rounded surface. The reference electrode was placed 1 mm proximal from the tip electrode to avoid simultaneous contact with the myocardium (Figure A1.2). The method used for chloriding silver wires is shown in Figure A1.3.

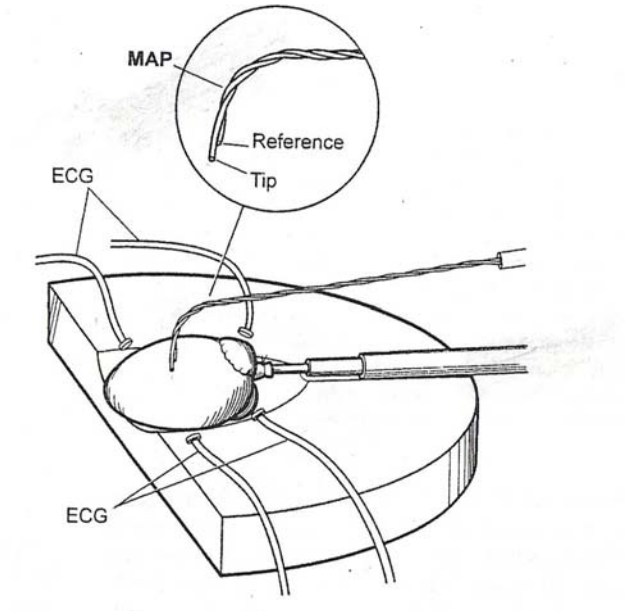


**Fig A1.2** Experimental setup and detail of monophasic action potential electrode used in a Langendorff-perfused mouse heart. The MAP electrodes and four silver/ silver chloride electrodes recording the surface ECG are shown. (Knollmann *et al.*, 2001a)

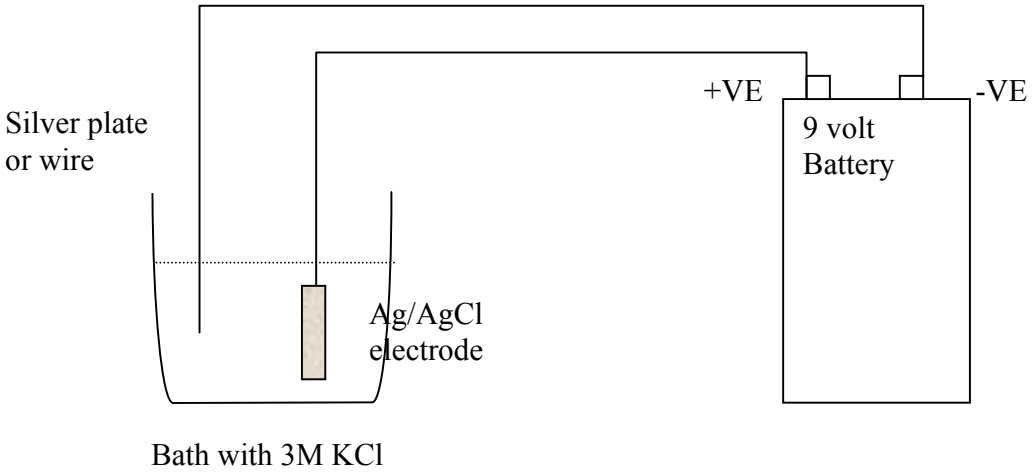


**Fig A1.3** Method of galvanically chloriding silver wire to create MAP or ECG electrodes. The wire is attached to a 9-volt battery and submerged in a saturated KCl solution for 5-10 minutes. Successful chloriding is seen by the formation of a dull grey discolouration to the wire. The silver chloride coating is fragile and impermanent, requiring the process to be repeated every few days.

The MAP probe was lowered by hand perpendicularly onto the epicardial surface of the heart until gentle but stable contact pressure was achieved, resulting in the development of MAP signals.

MAP recordings were made from different aspects of the heart by rotating the heart horizontally to expose the right or left ventricle to the MAP electrode. To obtain endocardial recordings the electrode was placed on right or left ventricle via a small hole in either atrium and made to contact the endocardium by directing the tip against the ventricular wall.

MAP recordings were preamplified with a DC coupled differential preamplifier, digitised at 2 kHz sampling rate and stored and analysed using a PowerLab data acquisition system.

**A1.3 Quality criteria for MAP recordings from murine hearts**.

Table A1 details those criteria that ensure murine MAP recordings are faithful in accurately reproducing the wave shape of TAP recordings from mouse hearts. Representative murine MAPs are shown in Figure A1.4

**Table A1** MAP quality criteria (adapted from Knollmann *et al*., 2001a and Franz, 1999)

1. Fast, clean upstroke (phase 0)
2. No major contamination by intrinsic deflection or QRS
3. Stable MAP wave shape with horizontal diastolic baseline
4. Rapid early repolarisation ($APD_{50}$ 3-11 ms depending on recording site)
5. No 'spike and dome' morphology
6. An inflection point (plateau) below the 50% repolarisation level

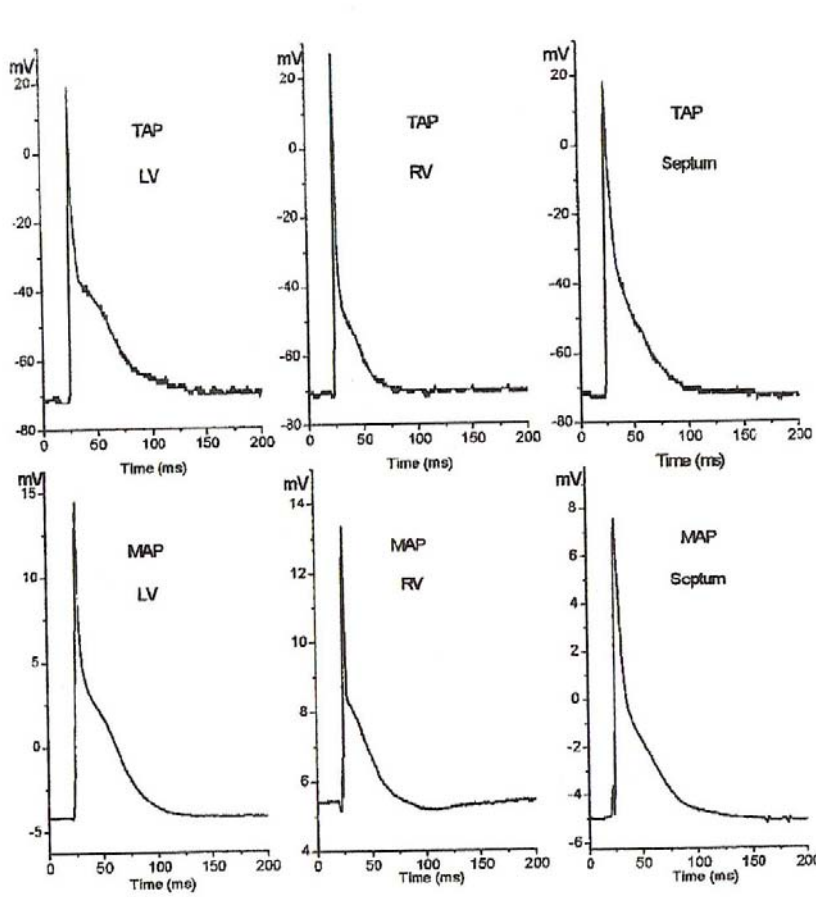

**Fig A1.4** Transmembrane action potentials (upper panels) compared to monophasic action potentials (lower panels) from normal mouse hearts. These traces illustrate the regional heterogeneity in waveform duration and amplitude, and marked difference in amplitude between MAPs and TAPs (Knollmann *et al*., 2001a)

**A1.3 Results**

50 mice were utilised while trialling MAP techniques. Expertise was gained in mounting hearts in the Langendorff apparatus and achieving good function (manifest as constant pressure, strong regular cardiac contractions and pink colour to the tissue). All hearts (*mdx* and C57) continued to beat for the duration of the experiment, which was often more than two hours.

Examples of MAPs achieved in *mdx* mice are shown in Figure A1.5

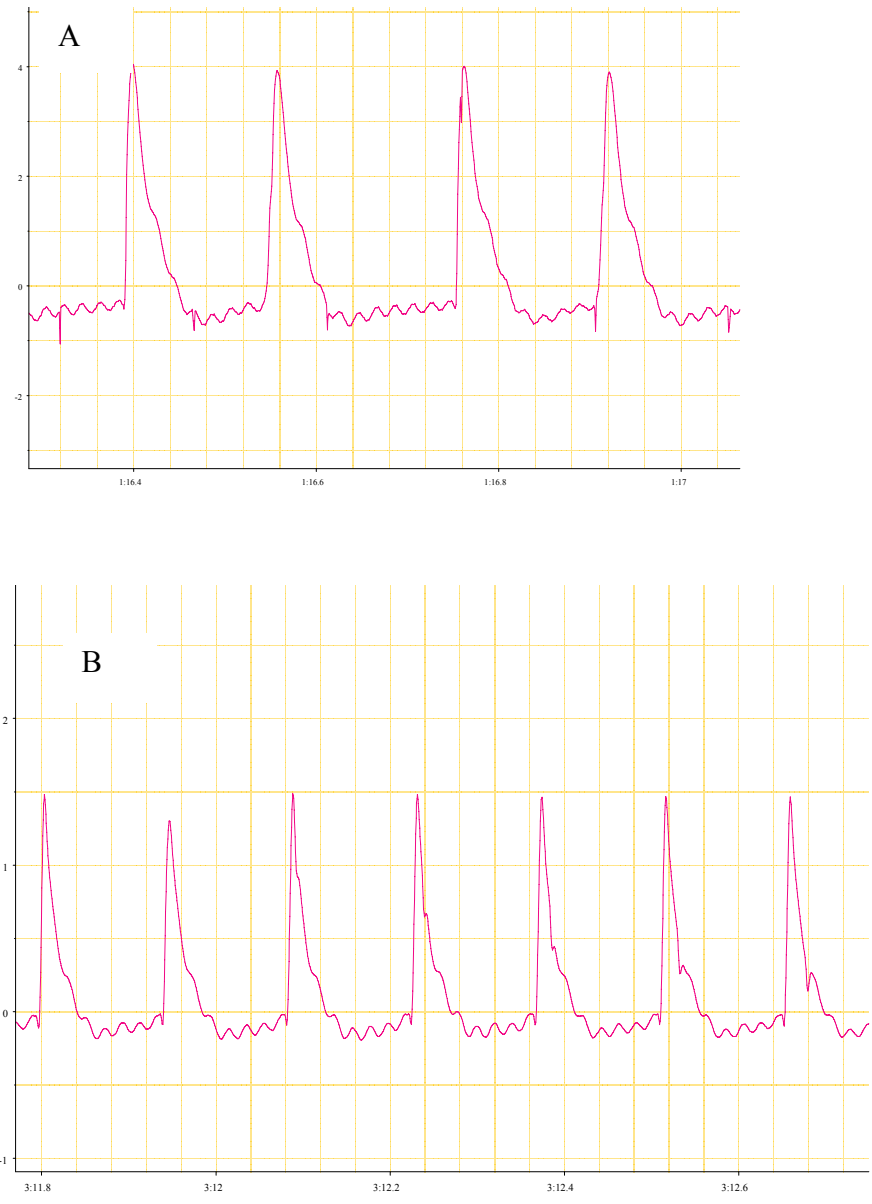

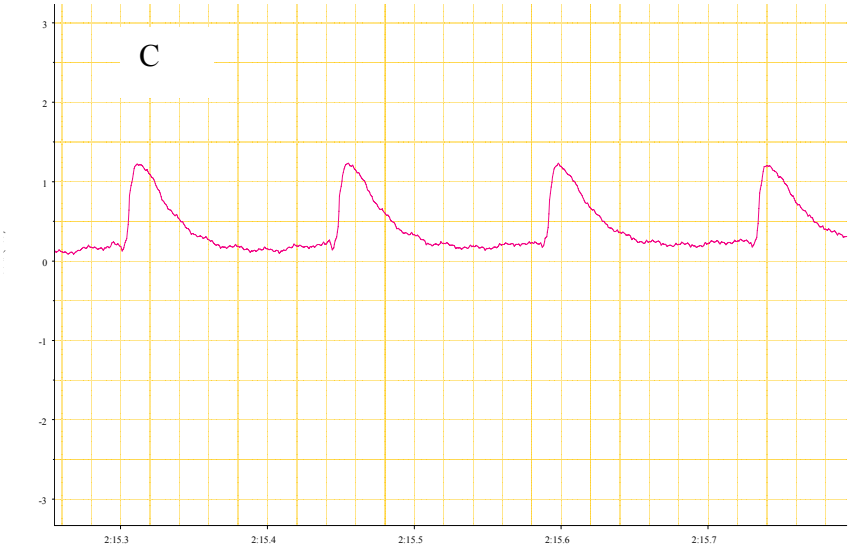


**Fig A1.5** Examples of monophasic action potential recordings achieved from epicardial surfaces of *mdx* hearts. These serve to illustrate the variation in MAP amplitude and wave forms experienced during these experiments. A. A typical left ventricular epicardial trace, with an amplitude of 4 mV. B. Another left ventricular recording from a different mouse recorded on a separate day. The amplitude was 2 mV and APD was also different to previous recording. C. This a third mouse reading with a 1mV amplitude, slower upstroke velocity and prolonged duration. Also apparent in these traces is the 50-cycle interference causing baseline and downstroke fluctuations.

There were three main areas of difficulty encountered during these experiments:

1.Reliability of MAP recordings

It was not possible to consistently and reliably obtain MAP recordings, despite efforts to replicate conditions and electrodes from previously successful experiments. Sometimes MAP recordings were achievable, but of very low amplitude (2-3 mV) making comparison between mice difficult. MAP electrodes were re-chlorided, or made again from new silver wire when problems were encountered. Two different commercial bio-amplifiers were trialled (Grass CP511 Amplifier and Animal Bioamp (ADI, Australia), and a custom made differential circuit was also made and tested unsuccessfully.

2.Electromagnetic interference

50-cycle interference was a significant problem throughout this series of experiments, with the degree of interference varying on a day-to-day basis. Initially the Langendorff

apparatus was disassembled and rebuilt in another area of the laboratory. An ultrasonic flow probe was also thought to be a major source of EMI initially, so its use was discontinued. Water baths, computers and amplifiers were moved as far from the heart and electrodes as possible. The stage for the tissue bath and the tissue bath itself was shielded using aluminium foil. Various combinations of filters were tried, and isolated ground amplifiers were chosen (with 50-Hz notch filter). Grounding of the heart was also attempted using earth electrodes.

3. Amplitude and morphology of MAPs

Variable MAP amplitudes are reported in the literature –for example 11-19mV (Knollmann *et al*., 2001a), 3.5-15.1mV (Danik *et al*., 2002) and 14.6-22.4mV (Liu *et al.*, 2004). Action potential amplitudes cannot be used as an absolute measure of cellular electrophysiology, but serve as a relative reference for acceptable signals. The maximum MAP amplitude achieved was 8.5mV, with the majority falling in the 2-4 mV range. Of greater concern than amplitude alone was the fidelity of waveforms, with many showing the appearance of Fig A1.5c, where there was not always typical depolarisation spikes with rapid repolarisation downstrokes.

**A1.4 Discussion**

MAP recordings provide precise information regarding local activation and repolarisation of the heart, and there is a need for verifying this information in *mdx* mice. Unfortunately there was a series of technical problems encountered during this experiment limiting the usefulness of the results, meaning *n* numbers were low and statistical tests could not be applied. The problem of 50-Hz interference was not overcome, despite seeking expert advice on this matter (A. Katchman, *pers comm*. 20.4.04). A commercial bioamplifier recommended and subsequently first used (Grass CP511) was found not to be a differential amplifier. Advice was also sought regarding waveform and amplitudes (B. Knollmann, , *pers comm* 20.5.04 and M. Franz, *pers comm*. 24.5.04) and it was felt that the problems encountered may be a combination of recording technique or MAP electrodes, although M. Franz indicated that recordings such as shown in Fig A1.5a and b were acceptable. This project was terminated due to inconsistencies in results and the time constraints of PhD studies.

# A2: TRANSMEMBRANE ACTION POTENTIALS AND FUNCTION OF VENTRICULAR TISSUE

## A2.1 Introduction

In recent years mouse trabeculae or small papillary muscle preparations have been utilised in studies of contractile function and calcium handling (Stull *et al.*, 2002; Gao *et al.*, 1999; Stuyvers *et al.*, 2002). They have the advantage over single cardiomyocytes in that intercellular connections are maintained, loaded contractions can be assessed and also there is the ability to maintain high pacing rates, similar to physiological frequencies (Stull *et al*., 2002). Ultra-thin muscles have less diffusion distance compared to thick ventricular wall preparations, so core hypoxia or accumulation of metabolites do not limit contractility. However, they suffer the disadvantage of a low incidence of geometrically suitable preparations (33% in one study (Stull *et al*., 2002)).

TAPs are superior to MAPs in providing information on resting membrane potentials, action potential amplitudes or upstroke velocity (Liu *et al.*, 2004), however achieving stable TAPs at very short cycle lengths can be difficult.

It was hoped that information gained from successful TAP studies in *mdx* and C57 mice would complement atrial data in aging mice (Chapter 3) and MAP studies in age matched mice (Appendix A1).

## A2.2 Methods

Hearts were isolated from 6-8 week old and 15 month old *mdx* and C57 mice. n=14-15/group

Mice were anaesthetised with 60 mg/kg sodium pentobarbital administered intra-peritoneally. A thoracotomy was performed and hearts were excised into room temperature perfusion fluid. The aorta was cannulated under magnification using a blunt ended 21 gauge needle, mounted onto a Langendorff apparatus and the coronary circulation perfused at 80 mmHg with modified Krebs-Henseleit buffer containing (mM) NaCl 119, $NaHCO_3$ 2, KCl 4.7, MgCl 1.2, $KH_2PO4$ 1.2, EDTA 0.5, glucose 11 and pyruvate 2. The concentration of $CaCl_2$ was 0.25M. The Krebs buffer was equilibrated with 95% $O_2$ and 5% $CO_2$ at 37$^{o}$C for 1 hour, giving a pH of 7.4, and was filtered inline

using 0.45 μm filter unit to remove microparticles. The heart was immersed in a jacketed glass bath maintained at 37$^{o}$C, where it rested horizontally and was perfused in 20mM 2,3-butanedione monoxime (BDM) to prevent cutting injury. The temperature of the perfusion fluid was continuously assessed by a needle thermistor at the entry of the aortic cannula.

The right ventricle was opened from base to apex by cutting parallel to the interventricular septum. Blood clots were washed out and a thin, uniform, nonbranched trabeculae or small pap muscle was carefully dissected leaving a block of tissue at one end from the RV free wall, and a small part of the tricuspid valve at the other end to facilitate mounting. Muscles were mounted between a stainless steel cradle glued to a force tranducer (Sensor Nor beam) and snared at the valve end by 9/0 monofilament nylon suture material (Ethilon brand) threaded into a 50 μm hollow stainless steel tube (Goodfellow, Cambridge,UK), according to published protocols for rat trabeculae (Ward *et al.*, 2003). Muscles were perfused initially with the same buffer as above (with the exception of BDM) at 37$^{o}$C, and stimulated at 0.5 Hz. Calcium and frequency was increased incrementally each 10 minutes over a 40-minute period until baseline conditions were reached (37$^{o}$C, 1.25 mM $Ca^{2+}$, 6.9 Hz.). Voltage was set at 20% greater than threshold, field stimulated at a pulse duration of 5 ms and perfusate flow rate at 8 mLs per minute.

Force development was determined at slack length (with no preload applied) and optimal length where force development is slightly below maximal (corresponding to an approximate sarcomere length of 2.2 μm (Stull *et al.*, 2002)).

Experimental apparatus was similar to that detailed in B4.2 (microelectrode apparatus) and A1.2.2 (Langendorff apparatus).

When muscles were equilibrated, force recordings were measured for 5 minutes, and a glass microelectrode was impaled into the tissue using a 3M KCl filled microelectrode of 10-50 mΩ resistance. Stable TAP recordings (at least 10 beats at 3-4 sites) were sought.

The muscles were measured at optimum length using a calibration reticule in the ocular of the dissection microscope after mounting. Cross-sectional areas were calculated assuming an ellipsoid shape (CSA=πab x length, where a= ½ minor diameter and b= ½ major diameter).

## A2.3 Results

Ventricular preparations from 32 mice were used while attempting to optimise experimental conditions. Experience was gained in the dissection and mounting of papillary muscles or trabeculae under magnification. Figure A2.1 shows force recordings and action potential recordings.

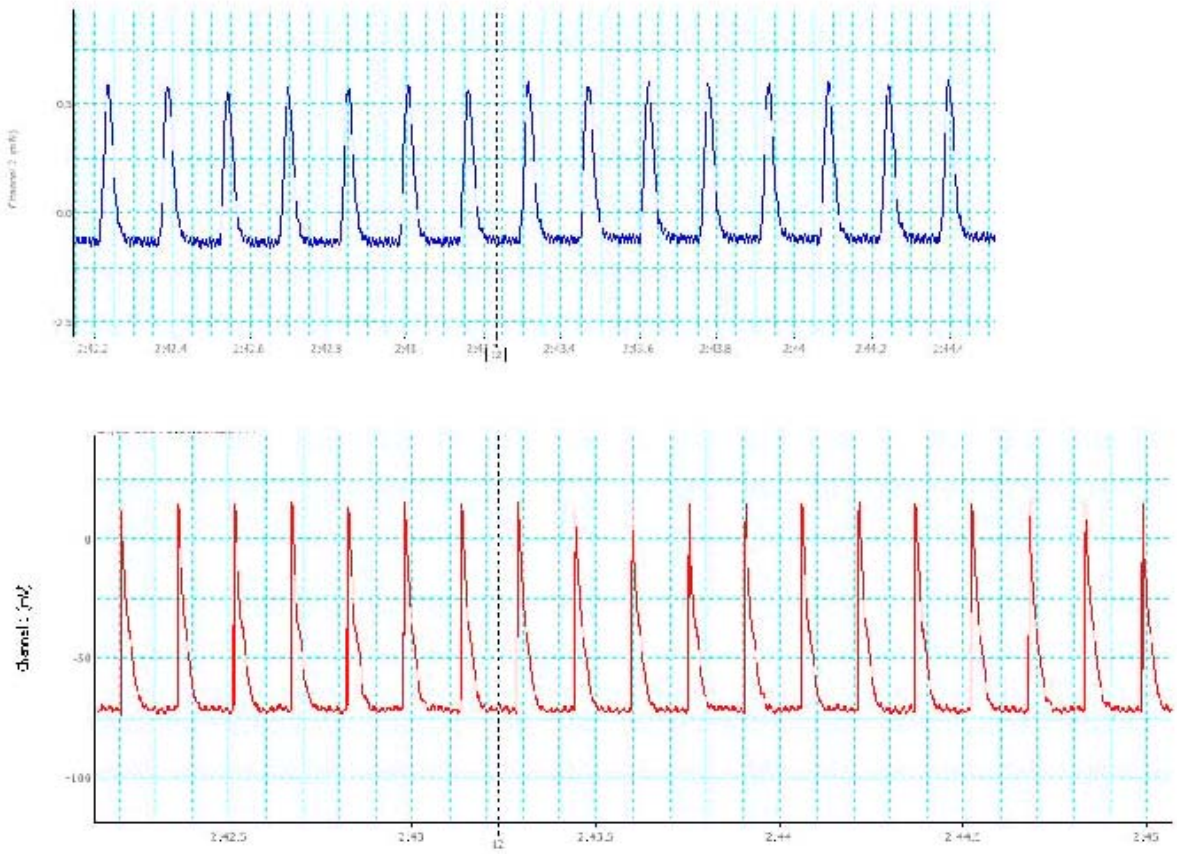

**Fig A2.1** Force recordings (above) and action potentials (below) achieved at a frequency of 6.8 Hz, or over 400bpm. These preparations were subjected to a temperature of 37$^{o}$C, and field stimulated at 5 ms pulse width and 30 volts.

The following observations were made regarding these experiments:

1.There was a low incidence of suitable linear, non-branched trabeculae necessitating the use of papillary muscles in most cases. The broad apical end of mouse papillary muscles made it difficult to mount these in the cradle of the force transducer, and the use of this cradle restricted contractions. Later in the experiment a fine (6/0 silk) noose was used to attach muscles to a hook glued onto the force transducer.

2. There was poor contractile function in many preparations. Rapid deterioration in function was encountered in mouse trabeculae at 37$^{o}$C in another published study, forcing these investigators to using non-physiological room temperatures for the remainder of their experiments (Gao *et al.*, 1998).

3. Achieving stable sequences of TAPs at high frequencies was very difficult.

4. Some technical difficulties were encountered including preload drift, and signal noise at high frequencies. This made measurement of small increments in force difficult.

This project was not pursued at the time because of difficulties in consistently achieving good ventricular function, making comparisons between strains problematical.

**A2.4 Discussion**

There are few reports that characterise fundamental cardiac physiology in *mdx* mice, and some are performed under non-physiological conditions (Sapp *et al.*, 1996) or in atrial preparations only (Sapp *et al*., 1996; Lu and Hoey, 2000a; Lu and Hoey, 2000b;). There is a need to further explore electrophysiological properties of *mdx* ventricular muscle as undertaken in transgenic mouse models of human cardiomyopathies. There is now an emphasis on replicating physiological temperatures and frequencies as far as possible (Stull *et al*., 2002; Ward *et al*., 2003) and ensuring optimum sarcomere length (Stull *et al*., 2002; Stuyvers *et al*., 2002). While these guidelines were adhered to as much as possible in this study it was unfortunate that statistical comparisons could not be made. Further improvements of apparatus and technique could include miniaturising the tissue bath further and use of laser diffraction techniques to accurately measure sarcomere length, rather than relying on optimal force production alone. It is possible that mouse trabeculae or papillary muscles are highly sensitive to stretch and are readily damaged.

**References.**

Bia, B., Cassidy, P., Young, M., Rafael, J., Leighton, B., Davies, K., Radda, G. and Clarke, K. (1999) Decreased myocardial nNOS, increased iNOS and abnormal ECGs in mouse models of Duchenne Muscular Dystrophy.,*J Mol Cell Cardiol,* **31,** 1857-62.

Casimiro, M. C., Knollmann, B. C., Ebert, S. N., Vary, J. C., Jr., Greene, A. E., Franz, M. R., Grinberg, A., Huang, S. P. and Pfeifer, K. (2001) Targeted disruption of the Kcnq1 gene produces a mouse model of Jervell and Lange- Nielsen Syndrome,*PNAS,* **98,** 2526-2531.

Chu, V., Otero, J., Lopez, O., Sullivan, M., Morgan, J., Amende, I. and Hampton, T. (2002) Electrocardiographic findings in mdx mice: a cardiac phenotype of Duchenne Muscular Dystrophy.,*Muscle Nerve,* **26,** 513-9.

Danik, S., Cabo, C., Chiello, C., Kang, S., Wit, A. L. and Coromilas, J. (2002) Correlation of repolarization of ventricular monophasic action potential with ECG in the murine heart,*Am J Physiol Heart Circ Physiol,* **283,** H372-381.

Franz, M. (1999) Current status of monophasic action potential recording: theories, measurements and interpretations.,*Cardiovasc Res,* **41,** 25-40.

Gao, W. D., Perez, N. G. and Marban, E. (1998) Calcium cycling and contractile activation in intact mouse cardiac muscle,*J Physiol (Lond),* **507,** 175-184.

Gao, W. D., Perez, N. G., Seidman, C. E., Seidman, J. G. and Marban, E. (1999) Altered cardiac excitation–contraction coupling in mutant mice with familial hypertrophic cardiomyopathy,*J. Clin. Invest.,* **103,** 661-666.

Knollmann, B., Katchman, A. and Franz, M. (2001a) Monophasic action potential recordings from intact mouse heart: validation, regional heterogeneity, and relation to refractoriness.,*J Cardiovasc Electrophysiol,* **12,** 1286-94.

Knollmann, B. C., Blatt, S. A., Horton, K., de Freitas, F., Miller, T., Bell, M., Housmans, P. R., Weissman, N. J., Morad, M. and Potter, J. D. (2001b) Inotropic Stimulation Induces Cardiac Dysfunction in Transgenic Mice Expressing a Troponin T (I79N) Mutation Linked to Familial Hypertrophic Cardiomyopathy,*J. Biol. Chem.,* **276,** 10039-10048.

Liu, G., Iden, J. B., Kovithavongs, K., Gulamhusein, R., Duff, H. J. and Kavanagh, K. M. (2004) In vivo temporal and spatial distribution of depolarization and repolarization and the illusive murine T wave,*J. Physiol.,* **555,** 267-279.

Lu, S. and Hoey, A. (2000a) Age- and sex-associated Changes in Cardiac B1-adrenoceptors from The Muscular Dystrophy (mdx) Mouse,*Journal of Molecular and Cell Cardiology,* **32,** 1661-1668.

Lu, S. and Hoey, A. (2000b) Changes in function of cardiac receptors mediating the effects of the autonomic nervous system in the muscular dystrophy (MDX) mouse.,*J Mol Cell Cardiol,* **32,** 143-52.

Pacioretty, L., Cooper, B. and Gilmour, R. (1992) Cellular Electrophysiology of Murine and Canine Cardiac Muscle in Duchenne Muscular Dystrophy,*Biophys. J.,* **61,** A306.

Perloff, J. (1984) Cardiac rhythm and conduction in Duchenne's muscular dystrophy: a prospective study of 20 patients.,*J Am Coll Cardiol,* **3,** 1263-8.

Sanyal, S. and Johnson, W. (1982) Cardiac conduction abnormalities in children with Duchenne's progressive muscular dystrophy: electrocardiographic features and morphologic correlates,*Circulation,* **66,** 853-863.

Sapp, J. L., Bobet, J. and Howlett, S. E. (1996) Contractile properties of myocardium are altered in dystrophin-deficient mdx mice,*Journal of Neurological Science,* **142,** 17-24.

Stull, L., Leppo, M., Marban, E. and Janssen, P. (2002) Physiological determinants of contractile force generation and calcium handling in mouse myocardium.,*J Mol Cell Cardiol,* **34,** 1367-76.

Stuyvers, B. D., McCulloch, A. D., Guo, J., Duff, H. J. and ter Keurs, H. E. D. J. (2002) Effect of stimulation rate, sarcomere length and Ca2+ on force generation by mouse cardiac muscle,*J. Physiol.,* **544,** 817-830.

Ward, M.-L., Pope, A. J., Loiselle, D. S. and Cannell, M. B. (2003) Reduced contraction strength with increased intracellular [Ca2+] in left ventricular trabeculae from failing rat hearts,*J Physiol (Lond),* **546,** 537-550.

Yotsukura, M., Yamamoto, A., Kajiwara, T., Nishimura, T., Sakata, K., Ishihara, T. and Ishikawa, K. (1999) QT dispersion in patients with Duchenne-type progressive muscular dystrophy.,*Am Heart J,* **137,** 672-7.

# APPENDIX B: RECIPES AND PROTOCOLS

# B1: HYDROXYPROLINE ASSAY

### B1.1 Equipment

2 mL flat based polypropylene tubes with lid

Spectrophotometer, semi-micro cuvettes (1.5-3 mL tapered)

Heating block or oven for heating at $107^0$C overnight.

Timer

Pippetors and tips, beakers, heat resistant tube rack.

Shaking water bath at $60^0$C

Manifold for bubbling off HCl (either a series of Silastic tubing and Y connectors with 18 gauge needles on ends, or custom made manifold (see Fig A.1))

Filter (Sartorius Midistart 0.2 μm) and tubing to connect from air tap to manifold

### B.1.2 Reagents

1.Hydroxyproline Standards

Stock of 1 mg/mL hydroxyproline (trans-4-hydroxy-L-proline, Sigma, Australia) prepared in distilled water.

Aliquot standards into 150 μL amounts and freeze.

Thaw prior to use for dilution into a standard series.

Require range of 0-20 μg HP, in assay vol of 500 μL. Mix reagents well.

2.Buffer Stock solution (pH 6)

Dissolve 50 g citric acid.$1H_20$ (analytical grade), 12 mLs acetic acid (96%), 120 g sodium acetate.$3H_20$ and 34 g of sodium hydroxide in $dH_20$ and bring up to 1 litre. Ten drops of toluene added as preservative.

The buffer is used in colour reaction by taking 500mLs and adding 100mLs water and 150mLs n-propanol= Working Solution. Stable for several months.

3.Chloramine T reagent (0.056 M) (keep in dark at $4^o$ for 3 weeks)

Dissolve 1.41g of Chloramine T in 10 mL water; add 10 mLs n-propanol and 80 mLs buffer at pH 6 (this is stable for several weeks, then discard)

4.Erlich's Reagent

Dissolve 15 g p-dimethylaminobenzaldehyde (Sigma, Australia) in 60 mLs n-propanol and 30 mLs perchloric acid, (2:1 n-propanol:perchloric acid) (or the amount required for that day's assays).

This is light sensitive and unstable, so needs to be prepared freshly.

This volume is enough for approx 360 samples (250 µLper sample)

Use fume hood with waterfall for preparation.

Perchloric acid and n-propanol can be mixed together and stored.

**B1.3 Sample Preparation**

Weigh tissue after trimming tendons, fat or capsular tissue. Place sample of tissue (or HP standard) in 6 N HCl. Use approx 10-20 mg tissue in 0.5 mL HCl in a cryotube. Tissue can be homogenised or cut into smaller pieces with scissors. Vortex thoroughly.

Seal tubes and hydrolyse at 107$^{o}$C for 18 hrs.

Next morning, open tubes and dry hydrolysed samples (blow off HCl with filtered compressed air in fume hood). This takes 1-2 hours, and results seem better if bubbling is not too vigorous, as this causes dried sample to adhere to walls of tube making them difficult to reconstitute. If tube rack is placed on heater block at 50$^{o}$C it speeds up drying process by evaporation also. Replace lids with fresh ones to avoid traces of HCl affecting assay.

Reconstitute dried sample with 500 µL $dH_20$. Vortex thoroughly, and get as much of dried sample from wall of tube. Despite the hydrochloric acid being removed in totality, the hydrolysate remains acid (pH 1-2).

**B1.4 Assay Procedure**

Use 0.5 mL reconstituted sample or standard

1.Add 250 µL of Chloramine T reagent. Ensure samples and chloramine T at room temperature. Vortex and incubate for 20 minutes at room temperature. (=oxidation step)

2.Add 250 µL Ehrlich's reagent to each sample and vortex. Incubate at 60$^{o}$C for 20 minutes (chromophore development stage) Cool tubes under tap water

3.Read absorbance of each sample at 550 nm using spectrophotometer.

Curve tends to plateau out, and some samples may be obviously dark red, but show HP in flat area. If too concentrated dilute sample with n-propanol and repeat absorbance reading. (Fig B.2)

4.Construct standard curve (determine curve fit and equation by entering values into KaleidaGraph v 3.5, Synergy Software, Reading, USA ). Calculate µg hydroxyproline in samples (Fig B.3).

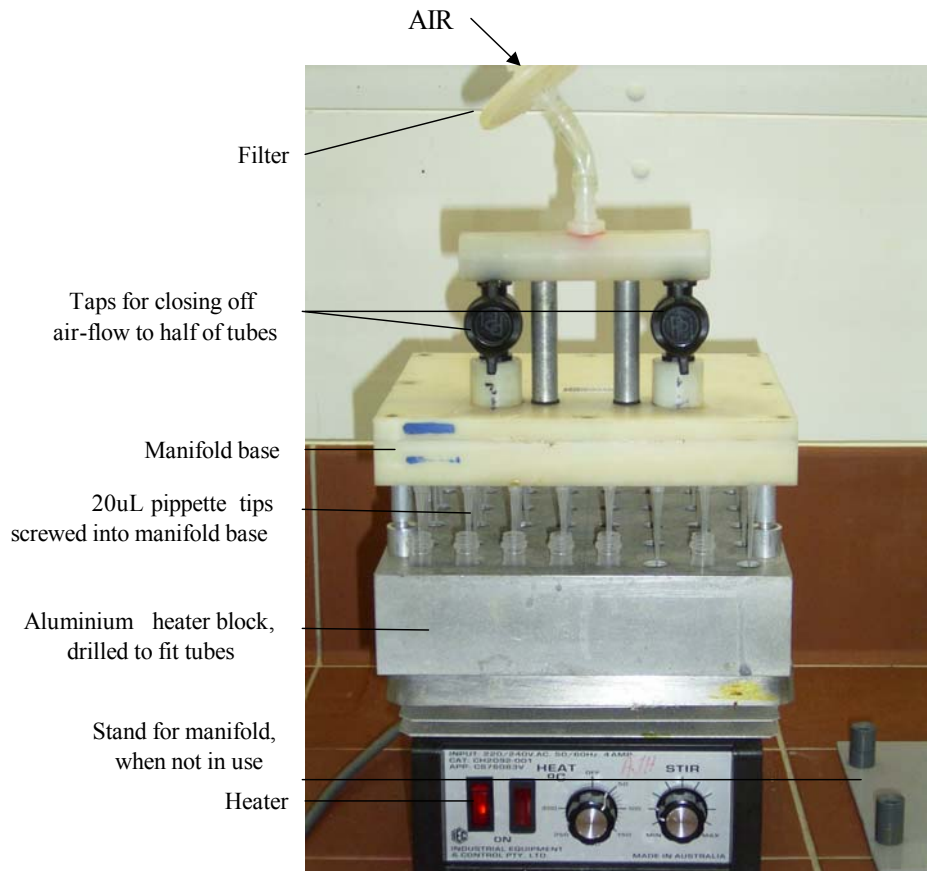


**Fig B1.1** Custom made manifold for drying hydrochloric acid from samples. The apparatus allows 40 samples to be handled at one time.

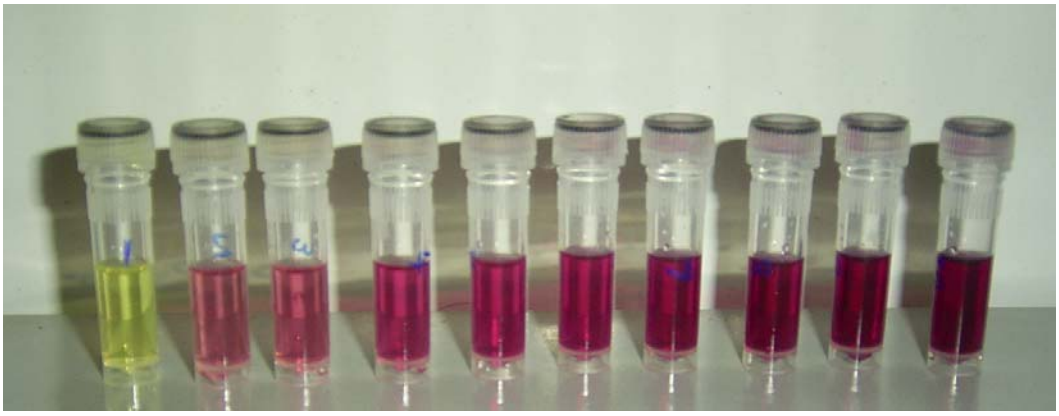

**Fig B1.2** Hydroxyproline standard series with dilutions from 1-20 µg hydroxyproline. This demonstrates the sensitivity of the assay, even in small tissue samples such as mouse atria.

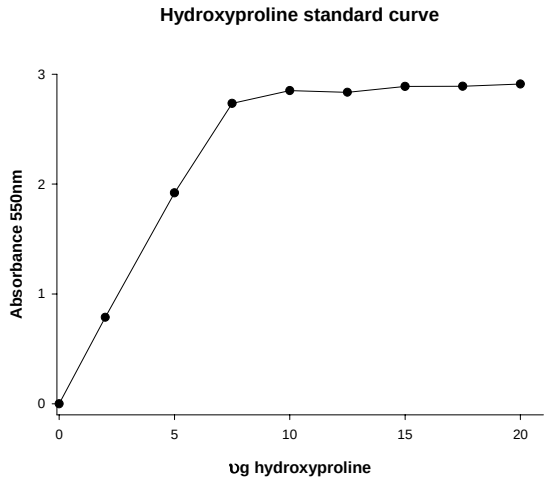


**Fig B1.3** Example of hydroxyproline standard curve. In the linear range of the graph R=0.99923

# B2: HISTOLOGY RECIPES AND PROTOCOLS

Histology protocols and recipes were courtesy of Assoc Prof Lindsay Brown's laboratory and Paul Addison, histologist, Department of Physiology and Pharmacology, University of Queensland. Procedures were adapted from hand processing to automatic processing to suit the equipment available at USQ.

**Figure B2.1** An overview of the steps required for preparation of H&E or Picrosirius Red stained sections.

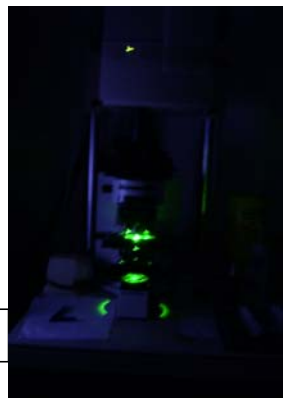

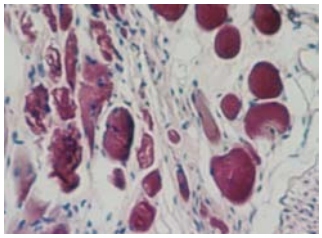

Steps in preparing histological slides

1.PRESTAIN AND FIXATIVE

2. TISSUE PROCESSING AND WAX EMBEDDING

3. CUTTING AND MOUNTING OF SECTIONS

5 µm sections

10 µm sections

Dewaxing and hydration
Stain HAEMATOXYLIN & EOSIN
Dehydration and rinse
Mounting and coverslipping

Dewaxing and hydration
Stain with PICROSIRIUS RED
Dehydration and rinse
Mounting and coverslipping

PHOTOGRAPHY AND ANALYSIS

**B2.1 Prestain and fixative recipes**

**1. Telly's fixative**

870 mL of 70% ethanol

44 mL $CH_3C00H$ (glacial acetic acid)

87 mL formaldehyde

**2. Modified Bouins's solution**

850 mL picric acid

100 mL formaldehyde

50 mL glacial acetic acid

Pin tissue onto cork, especially if thin tissue such as diaphragm or limb muscles

Place tissue in Telly's fixative for 3 days.

Remove Telly's and cover tissue in Modified Bouin's fluid for 24 hours.

Perform 3 changes of 70% Ethanol every 24 hours.

Store with tissue well covered by 70% Ethanol

**B2.2 Tissue processing and wax embedding.**

Equipment:

Shandon Elliot Duplex processor or Histokinette tissue processor with 9x 1L flask for ethanol and toluene

Fume hood

Tissue cassettes and baskets

Fisher Histo-Centre tissue embedding station

Simport embedding rings and plastic moulds

Paraplast Extra paraffin beads

Forceps

Toluene

Ethanol 100%, and beakers, measuring cylinders and funnel for diluting

Automatic processor times:

| Beaker | Solution | Time |
|---|---|---|
| 1. | 70% ethanol | 30 mins |
| 2. | 90% ethanol | 30 mins |
| 3. | 95% ethanol | 30 mins |
| 4. | 95% ethanol | 30 mins |
| 5. | Absolute ethanol | 30 mins |
| 6. | Absolute ethanol | 30 mins |
| 7. | Absolute ethanol | 30 mins |
| 8. | Toluene | 30 mins |
| 9. | Toluene | 30 mins |
| 10. | Wax (A) | 30 mins |
| 11. | Wax (B) | 30 mins |

**B2.3 Cutting and mounting**

Equipment:

Leica manual microtome

Feather brand disposable blades

Menzel- Glaser Polysine microscope slides

Heated water bath and heated trays

Paintbrushes, pencil

Sections cut at 5 μm (H&E) and 10 μm (picrosirius red)

**B2.4 Staining**

*Haematoxylin and Eosin recipes*:

**Mayer's Haematoxylin:**
0.5 g Mayer's Haematoxylin powder

500 mL $dH_2O$

Heat at 50-60$^oC$ on magnetic heater stirrer until dissolved.

Add 25 g aluminium potassium sulphate, mix until dissolved.

Add 100 mg sodium iodate - this oxidizes haematoxylin and changes colour to reddish.

Cool solution (preferably overnight)

Adjust pH by adding 0.5 g citric acid.

Add 10 g chloral hydrate to preserve solution.

Filter before use.

Do trial staining to determine the best staining times - 6.5 mins usually gives good nuclear staining.

This volume is usually sufficient for 500 slides, and is getting low in volume by 6-8 months.

Store at 4 $^oC$ when not in use.

**Eosin stain:**

Eosin used is Eosin yellowish (eosin Y) which is alcohol and water soluble.

Stock solution: 2 g powder, 40 mL $dH_2O$, 160 mL 95% EtOH

Working solution: Add 1 vol Stock solution : 3 vol 80% Ethanol (150: 450mL)

Store at 4 $^oC$

Adequate for 200 slides.

**Scott's solution**

4.5 g magnesium sulphate, 3.75 g sodium bicarbonate

Make up to 1 litre with $dH_2O$

Store at 4 $^oC$, can also keep solution in staining pots at RT, however discard regularly

*Picrosirius Red stains*:

**Phosphomolybdic Acid**

0.2% solution is used (ie 100 mg/100 mL $dH_2O$)

**0.01M HCl solution**

1mL 10 M HCl to 999 mL $dH_2O$

Discard after use.

**1% Lithium carbonate solution**

Add 5 g Li Carbonate to 500 mL $dH_2O$

**0.1% Picrosirius red stain**

0.1 g Sirius Red F3B (Chroma, Germany) in 100 mL $dH_2O$

**Staining procedure, Picrosirius red**

Place slides in racks in 56 $^{o}$C oven for 1 hour

Dewaxing:

1.XYLENE 5 mins

2.XYLENE 5 mins

3.XYLENE 5 mins

Hydration:

4.100% ETHANOL 3 mins

5. 100% ETHANOL 3 mins

6. 90% ETHANOL 3 mins

7. 70% ETHANOL 3 mins

8. Water bath 2 mins

9. Distilled water 1 min

10. PHOSPHOMOLYBDIC ACID 5 mins

11. Brief rinse in water bath

Stain:

12. PICROSIRIUS RED STAIN 90 mins

13. 0.01 M HCl 2 mins

Dehydration and rinse:

14. 70% ETHANOL 30 secs

15. 90% ETHANOL 30 secs

16. 100% ETHANOL 30 secs

17. 100% ETHANOL 30 secs

18 100% ETHANOL 30 secs

Mounting:

19 XYLENE 5 mins

20 XYLENE 5 mins

21 XYLENE 5 mins

22. Coverslip with Depex.

**Staining procedure, Haematoxylin and eosin**

Place slides in 56$^{o}$C oven for 1 hour

Follow dewaxing and rehydration as for Picrosirius Red staining protocol *until* step # 7

Omit Lithium Carbonate (step # 8)

Running water bath 2 mins

9. Distilled water 1 min

H&E staining

10 HAEMATOXYLIN STAIN 7 mins

Water bath 1 min

11 SCOTT'S SOLUTION 0.5-1 min

Water bath 4 mins

12 70% ETHANOL 1 min

13. EOSIN STAIN 11 mins

14. 95% ETHANOL 30 secs

15. 100% ETHANOL 30 secs

16. 100% ETHANOL 30 secs

17. 100% ETHANOL 30 secs

MOUNTING

As for Picrosirius Red, in fume hood. Continue from step # 19 of Picrosirius Red protocol.

B2.5 Photography and analysis

Equipment either:

A) Biorad MRC 1024 confocal scanning microscope with a krypton/argon laser and subjected to a Rhodamine/Texas Red filter of 568nm wavelength. Images were captured using a Biorad Lasersharp 2000 program.

Photomicrographs of 4 sections per heart were analysed and averaged for saturated pixel intensity corresponding to collagen fibres, using Scion Image software Beta 4.0.2 (http://www.scioncorp.com) density slice tool.

B) Nikon Eclipse E600 microscope, images captured with Q Imaging Micropublisher 5.0 Docu AnalySIS

Skeletal muscle regeneration was assessed by counting centronucleation (manual counting of 100 fibres per muscle). Cell diameters were calculated from digital photomicrographs and Scion Image software.

Some muscles were subjected to a visual grading scheme (see Chapter 4).

# B3 :WESTERN BLOT

Protocols courtesy of Renee Cornford-Nairn (USQ), Russell Johnsen and Kaite Honeyman (UWA)

B3.1 Recipes:

**Protein Treatment Buffer/ Protease Inhibitor/PMSF**

1 mL Protein treatment buffer (PTB) and 30 uL Protease Inhibitor (Sigma, Australia) and 2.5 µL PMSF solution.

PMSF= 0.5 mM phenylmethylsulfonyl fluoride in isopropanol (17.25 mg/0.5 mL)

**Transfer buffer (5X concentration)**

Tris base 30 g

Glycine 144 g

Sodium dodecyl sulfate (SDS) 0.5 g

adjust to pH 8.3 with concentrated HCl

Double distilled $H_20$ to make up to 1 L

SDS is used to enhance the transfer of large molecular weight proteins such as dystrophin.

**Loading (treatment) buffer**

125 mM TrisHCl (pH 8.8) 5 mLs

4% SDS 8 mL

40% glycerol 20 mL

d $H_20$ 17 mL

2 M urea was added as a denaturant, because samples are not sonicated. Range of urea= 2-8 M. 2 M= 6g urea in 50 mL

**TBST Buffer (Western washing buffer)**

| | **Concn (X1 solution)** | **1X working soln (1litre vol)** | **10X stock (2 L total volume)** |
|---|---|---|---|
| **Trizma base** | **10 mM** | **1.21 g** | **24.22** |
| **NaCl** | **150 mM** | **8.76 g** | **175.2 g** |
| **Tween 20** | **0.05%** | **500 µl** | **x** |

Adjust pH to 7.6 using HCl. Use Trizma not Tris HCl as base.

**TBS Buffer**

| | **Concn (X1 solution** | **1X working soln (1L vol)** | **10X stock (2 L total volume)** |
|---|---|---|---|
| **Trizma base** | **10 mM** | **1.21 g** | **24.22 g** |
| **NaCl** | **150 mM** | **8.8 g** | **176 g** |

**Blocking Buffer**

100 mL TBST

5 g skim milk powder

Place in beaker with magnetic flea. Stir to dissolve. Store in Schott bottle in fridge.

**SUMMARY OF WESTERN TRANSFER**

**1. Protein Extraction**

↓

**2. Protein Quantitation**

↓

**3. Mini Gel Electrophoresis**

↓

**4. Western Transfer**

↓

**5. $1^{o}$ Antibody incubation**

↓

**6. $2^{o}$ Antibody incubation**

↓

**7. Chemiluminescence detection**

B 3.2 Protein extraction

Prechill porcelain six-well mortars by placing in freezer. Chop tissue finely with scissors. Weigh tissue samples (10-30 mg tissue is optimum). Record weights. Place muscle tissue trimmed of tendons into labelled 1.5 mL eppendorf tube. Add 19 volumes of Protein Treatment Buffer/Protease Inhibitor/PMSF mix to frozen muscle sample on mortar- eg if tissue weighs 10 mg add 190 µL of mix. Use porcelain pestle to grind tissue, while keeping samples as cold as possible (use crushed ice or dry ice under mortar). Wash pestle thoroughly with distilled water after use to avoid contamination. Grinding takes some time and some tissue such as diaphragm is more difficult- grind as finely as possible. Pippette ground sample back into eppendorf tube and vortex thoroughly.

Store at -20$^{o}$C until needed.

B3.3 Protein Quantitation

This assay uses the scaled Lowry assay for protein estimation using a commercial kit (BioRad Protein Assay Kit) with concentrations (rather than µg of total protein calculated). (Note that this protocol will not work using buffers containing 2-mercaptoethanol). Aim of assay is to determine the concentration of total protein present in the tissue sample prior to loading the gel, with an optimum of 10 µg total protein loaded per lane.

Prepare a standard curve:

(Note the kit manual uses 4 mL plus volumes. ¼ suggested volumes are adequate for 1 mL microcuvettes)

Prepare 2mg/mL Bovine Serum Albumin (BSA) stocks and aliquot and freeze -20$^{o}$C until use.

| **Concentration** | **µl BSA stock** | **µl PTB** |
|---|---|---|
| Blank | 0 | 25 |
| 0.2mg/mL | 2.5 | 22.5 |
| 0.5mg/mL | 6.25 | 18.75 |
| 1.0mg/mL | 12.5 | 12.5 |
| 1.5mg/mL | 18.75 | 6.25 |
| 2mg/mL | 25 | 0 |

Prepare dilutions of samples.

| Dilution | µl Sample | µl PTB |
|---|---|---|
| 1/5 | 5 | 20 |
| 1/10 | 2.5 | 22.5 |

Other dilutions can be used (eg ½ and undiluted), however these may fall outside linear range of graph and are probably unnecessary.

Protocol for protein estimation:

Use freshly autoclaved tips, and wear gloves to avoid protein cross contamination.

Turn on spectrophotometer (750 nm).

Prepare a solution containing 125 µL of Reagent A per sample, and 20 µL Reagent S per mL of Reagent A. Dispense into a 15 mL Falcon tube or similar. Mix thoroughly. This mix is stable for 1 day.

Dispense 1 mL of Reagent B per sample into a 50 mL Falcon tube.

Briefly centrifuge thawed samples and standards (5000RPM)

Add 125 µL Reagent A-S mix into each tube. Vortex.

Add 1 mL Reagent B. DON'T MIX, STIR OR INVERT. Incubate for 15 minutes at room temp.

Read absorbance at 750 nm.

Use graphing program (eg Kaleidograph) to calculate total protein concentration (mg/mL) of unknown samples. Average both dilution readings.

B3.4 Mini Gel Electrophoresis

Uses Invitrogen NuPage Novex 4-12% Bis-Tris gradient gels and Invitrogen NuPage MOPS-SDS running buffer. Loading dye =4 µL mercaptoethanol + 1 µL bromphenol blue.

For C57 muscle samples load approximately 100 µg protein and make up volume of 35 µL with PTB and 5 µL loading dye to give 40 µL total volume/well. Add loading dye in fume hood due to use of mercaptoethanol.

For AO treated mice and *mdx* can use 35 µL of protein to maximise detection (dystrophin will be present in very low concentration)

Standard= Invitrogen E-Page SeeBlue pre-stained standard. Use 5 µL volume. No need to heat prior to electrophoresis. Standard extends from 20-260 kDa protein range.

Briefly centrifuge samples.

Denature proteins by heating at 95$^{o}$C for 10 minutes in heating block.

Remove gels from plastic bag (care with liquid inside bag as it contains sodium azide which is toxic.)

Rinse gels well in distilled water and remove white plastic strip from base.

Assemble gel apparatus. Pour 1 x MOPS-SDS running buffer into each compartment until ¾ full.

Place gel with writing facing towards you and comb facing away. If using 2 gels place back to back. Lock gel tension wedge in place to hold gels firmly. Fill inner chamber first and check for buffer leakage into outer chambers. Fill chambers to almost full.

Remove combs gently. See Figure B.3.1 for view of electrophoresis tank used.

Use a plastic transfer pipette to flush buffer into wells to wash them out thoroughly.

Load protein marker in left hand well.

Load other samples. Leave empty well between C57 sample and *mdx* if possible to avoid contamination. Use gel loading tips to fill wells.

Turn power unit on, adjust current to 20-25 mAmps. Run for approximately 3 hours for 1 gel or 5-6 hours for 2 gels, or until marker runs nearly to bottom of gel. Use water bath set with dip cooler at 15-18 $^{o}$C and heat exchange coil into tank to limit temperature to approximately 16$^{o}$C.

Can proceed to transfer immediately or alternatively leave gels in plastic soaked in buffer overnight at 4$^{o}$C.

**Fig B3.1** Mini Gel Apparatus

**View of the Invitrogen XCell *SureLock*™Mini Cell**

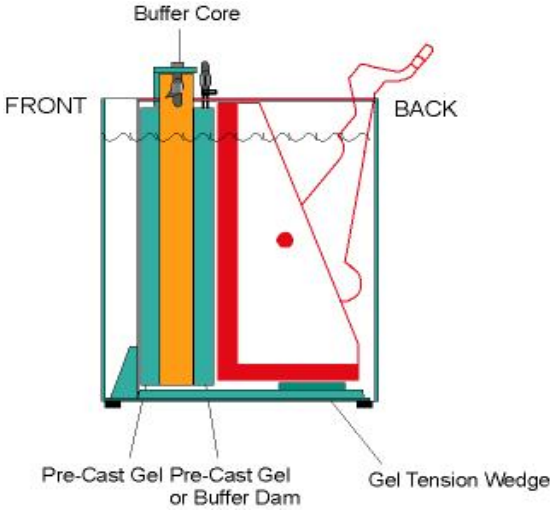


Preparation for Transfer:

Remove gel cassettes from electrophoresis unit and place in labelled plastic containers Cover in transfer buffer. Soak for 10-20 minutes.

Soak Scotch Brite pads in transfer buffer for a minimum of 4hours.

B3.5 Western Transfer

Have the following available:

BioRad unit for transfer (BioRad Mini-Protean II Cell Model and BioRad PowerPac3000)

1L Transfer Buffer

Container with transfer buffer to fit size of BioRad blot module components

Soaked blotting pads

Transfer membranes (Hybond-P membranes, Amersham Biosciences, Buckinghamshire UK). These membranes contain polyvinyldiflouride (PVDF), which have a high binding capacity compared to nitrocellulose membranes.

Use forceps to remove blue backing sheets after clipping top right hand corner of membrane for orientation (2 clips for second membrane). Dip in methanol for 10-20 seconds to activate, the give a 5 minute wash in distilled water.

Filter paper, soaked briefly in transfer buffer

Invitrogen NuPAGE gel cassette. This is opened by gently prising one side with plastic spatula to crack open cassette and expose gel while leaving it sitting on the larger plate. Trim below wells with edge of spatula. Discard gel waste into acrylamide waste bin.

The sandwich is assembled in container with transfer buffer using roller to roll out air bubbles. To turn out gel, place bottom layers onto cling film and turn gel face down onto wet filter paper layer. Cut foot of gel from unit using plastic spatula. Slide spatula carefully along gel to release. Finish preparing sandwich (Figure B 3.2).

Note that the gel is positioned closest to the black plate, and after sliding the plastic clasp closed to hold the sandwich together the module is inserted into the BioRad unit with the black plate closest to the black electrode. (Gel to Black and Black to Back)

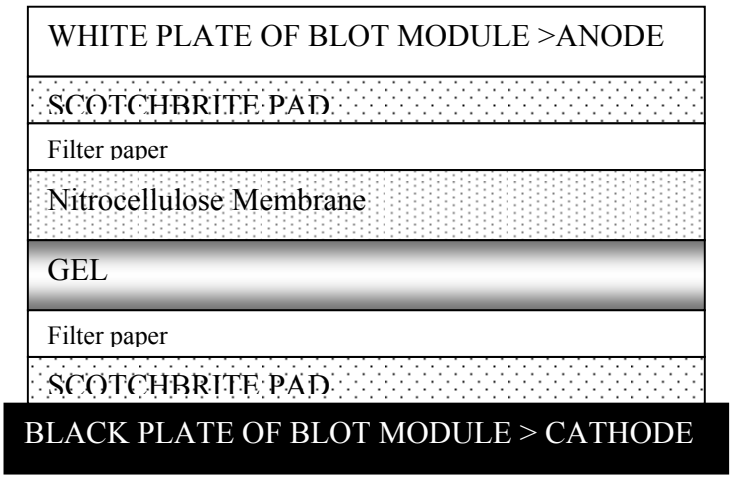


**Fig B3.2** Order of components of gel sandwich

Insert a frozen ice block into the back of the unit, and fill with transfer buffer. Insert a cooling coil to maintain temperature at 12$^{o}$C.

Place a magnetic flea into bottom of unit and position lid and electrical leads

Have a magnetic stirrer beneath this to facilitate mixing and cooling of buffer with magnetic flea.

Turn power pack on to a constant current of 300 mA at 15-18$^{o}$C overnight.
With 40 minutes of transfer time remaining, make up Blocking Buffer. Have TBST ready also and a shaking platform available.
With 10 minutes remaining make up Primary Antibody (Novocastra Laboratories Ltd, Newcastle upon Tyne, UK NCL-DYS2 mouse monoclonal antibody).
Antibody is diluted 1:100 (can be up to 1:33) with blocking buffer.

B3.6 Antibody incubation
Disassemble transfer apparatus and remove nitrocellulose membranes using forceps.
Cut off the lower half of the membrane below orange myoglobin marker.
Place each upper membrane is a small plastic container just big enough to fit membrane.
Wash 2 x in distilled water for 5 minutes each wash.
Incubate in Blocking Buffer for 60 minutes. Agitate gently on shaker for 1 hour.
Incubate membranes in antibody for 2 hours at room temperature. Add prepared DYS2 (Novocastra Laboratories, UK) diluted in blocking buffer.
Wash 3 x in TBST for at least 10 minutes. Place in blocking solution for 15 minutes.

B3.7 Antibody detection
Make up Secondary Antibody (Peroxidase-Conjugated Rabbit Anti-Mouse Immunoglobulins, DakoCytomation, Denmark) Dilute 1:1000 in Blocking Buffer.
Incubate for 120 minutes at room temperature.
Wash membranes twice in TBST and once in TBS each for 10 minutes. Make up chemiluminescent substrate during the last 10 minute wash

B3.8 Chemiluminescence and film development
Use Lumi-Light Western Blotting Substrate (Roche Diagnostics, Mannheim, Germany).
Mix 3mL each of Reagent 1 and 2 per membrane in a Falcon tube. Use fresh tips for each solution.
Place Lumi-light on top of membranes for 1 minute only. Drain off excess substrate.
Place membranes between 2 pieces of transparency film or plastic folder inserts. Use a tissue to gently wipe over plastic to remove air bubbles. Place in radiographic cassette.

In darkroom pour developer and fixer into shallow trays. Use photographic safelight only and remove piece of Amersham Bioscience radiographic film and cut to size. Cut one corner to orientate where protein marker is positioned. Film exposure time is variable, with C57 mice only needing 10 seconds exposure, and *mdx* requiring 5 or 10 minutes to maximise detection. Develop film for 30 secs with agitation, then wash, then fix for 2-3 minutes with gentle agitation. Give a final wash and hang in drying cupboard for a short period.

B3.9 Results of Western blotting for dystrophin

It was possible to consistently demonstrate the 427 kDa protein dystrophin in C57 muscle, whereas it was absent in *mdx* muscle (as expected) and antisense oligonucleotide (AO) injected *mdx* mice. Many repeat experiments were performed to improve detection of low levels of AO. Modifications such as the addition of PMSF to the Protein Treatment Buffer, using a methanol free Transfer Buffer, adding SDS to the Transfer Buffer to enhance transfer of large proteins and utilisation of the high binding capacity PVDF membranes were made. The low dose of AO used may have resulted in this failure to detect dystrophin in AO treated mice (see Chapters 6 and 7). Clear expression of dystrophin is shown in Figure B.3.3, where six dilutions of C57 extracted protein was used, ranging from 5-60 µg.

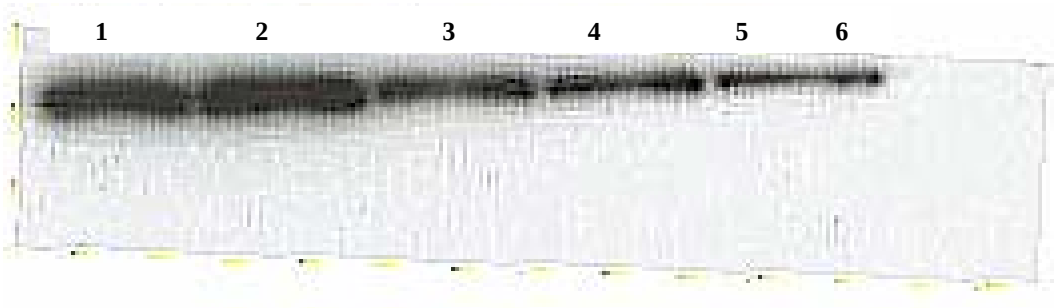


**Fig B.3.2** Detection of dystrophin in C57 limb muscles. Six dilutions of extracted protein were used to test for the sensitivity of the Western blotting procedure. Lane1 corresponds to 60 µg total protein, 2= 40 µg, 3=20 µg,, 4=15 µg, 5=10 µg and 6=5 µg.

# B4: SKELETAL MUSCLE ORGAN BATH PROTOCOL

## B4.1 KREBS PHYSIOLOGICAL SALINE SOLUTION (Krebs PSS)

Stock solutions (make up in 1 L volumes with $dH_20$):

Stock A:

NaCl 118 mM

KCl 4.7 mM

$MgSO_4.7H_2O$ 1.16 mM

$KH_2PO_4$ 1.18 mM

Stock B:

$NaHCO_3$ 25 mM

Stock C:

$CaCl_2.2H_20$ 2.5 mM

Store at $4^oC$

Working solution

Add 100 mL each of Stock A, B and C in MilliQ. Add 4.0 g glucose and make up to 2 L. Make fresh working solution each day.

## B4.2 Experimental equipment and protocol

Carbogen (95% $O_2$ and 5% $CO_2$) was bubbled through Krebs PSS for 30 minutes prior to experiment to bring buffer to correct pH (7.4). Ice-cold Krebs was used for dissections. Mice were anaesthetised with 70 mg/kg thiopentone sodium (Nembutal) by intraperitoneal injection. The skeletal muscles of interest were removed and placed in the Krebs PSS. Muscles were anchored by means of surgical silk to a fixed peg at one end, and attached to a force transducer at the tendon end, and placed within a 25 mL glass organ bath maintained at $24^oC$ (Figure B4.1). Tissues were field stimulated via a Grass S48 stimulator (W. Warwick, RI, USA) and current intensity was amplified using a pre-amplifier (EP500B. Audio Assemblies, Campbellfield, Victoria, Aust). Data was collected and analysed using Chart 4.1.1 software on an i Mac computer. A square pulse of 0.2 ms duration was dispersed via two platinum plate electrodes positioned at each side of the muscle.

Optimum preload (Lo) was defined as the length eliciting maximal single twitch force. Optimal voltage was also determined for each preparation, as was the frequency eliciting maximal tetanic force. Reported data was the average of 3 individual single twitches or tetanic stimulations per muscle strip, with those three values then averaged to give an overall mean for that muscle. A fatigue protocol (one tetanic stimulation every 5 secs for 5 minutes) and recovery from fatigue (a single tetanic stimulation 5 minutes later) was sometimes performed also. Muscle dimensions were measured at Lo using a digital micrometer, blotted for 3 secs then weighed prior to storage at –80$^{o}$C.

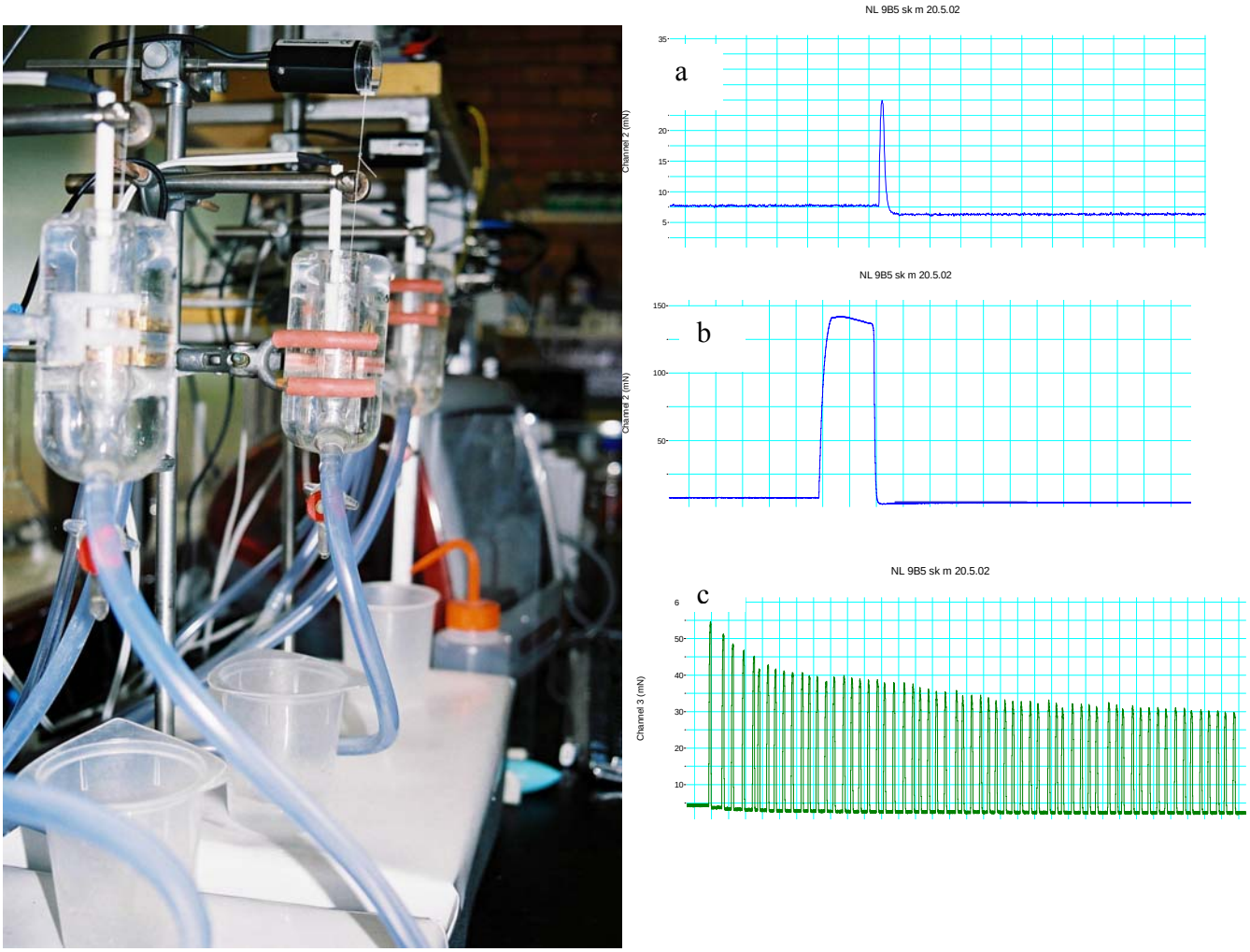


**Fig B4.1** Row of water-jacketed organ baths used for skeletal muscle contractility studies. The computer is to the right of the organ baths, and above it is positioned the stimulator and preamplifier. Recordings showing a) twitch b) tetanus and c) fatigue of representative diaphragm strips.

# B5 MICROELECTRODE STUDIES

## B5.1 TYRODES PHYSIOLOGICAL SALINE SOLUTION (TPSS)

Stock solutions (make up in 1 L volumes with $dH_20$):

Stock A:

NaCl 136.9 mM

KCl 5.4 mM

$MgCl_2.H_2O$ 1.05 mM

$NaH_2PO_4$. $H_2O$ 0.42 mM

Stock B:

$NaHCO_3$ 22.6 mM

Stock C:

$CaCl_2.2H_20$ 1.8 mM

Store at $4^oC$

Working solution

Add 100 mL each of Stock A, B and C in MilliQ. Add 2.0 g glucose, 0.2 g Ascorbic acid, and 0.4 mL of 9.5% $Na_2EDTA$ solution. Make up to 2 L.

Make working solution up freshly each day.

## B5.2 Experimental equipment

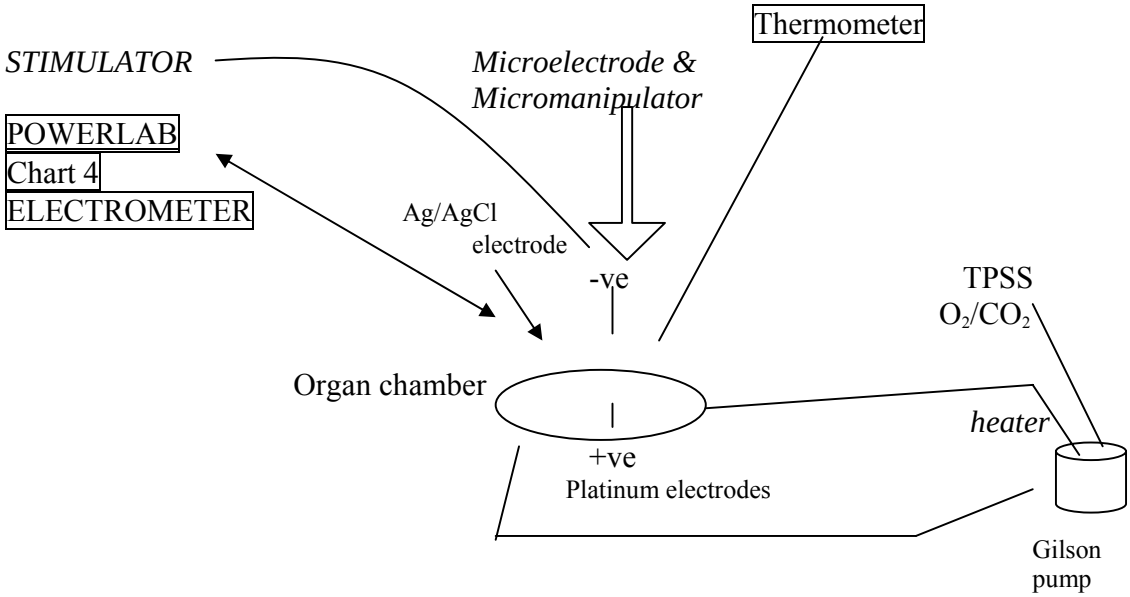


**Fig B5.1** Diagram of microelectrode apparatus used for atrial microelectrode and contractility studies.

**Pipette puller**- WPI microprocessor controlled vertical pipette puller. Microelectrodes of 10-50 MΩ resistance used.

**Perfusion pumps**- Gilson minipuls 3, set at 3 mL/minute.

**Stimulator**- Grass SD9 stimulator 8-10 V usually (can increase<20 V), Freq 1 Hz, pulse width 0.5 msecs,

Determine threshold voltage that elicits a contraction, add 20 %.

During an experiment it may be necessary to increase voltage to maintain contractions.

**WPI motorised micromanipulator** DC 3001R, MS 314 step arm controller

**WPI Electrometer-Cyto 721**

**Thermometer**-Fluke 50S K/J Temp =35+/- 0.5$^{o}$C

**Powersource** -Topward 3303D-4Volt, 1.18 amps, with flow through heater, custom made

**Force transducer**

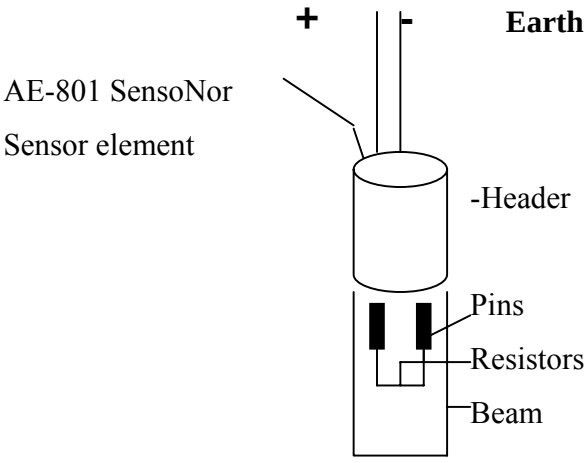


**Fig B5.2** Transducer consists of Wheatstone Bridge and crystal silicon beam with a 1000 Ohm resistor implanted each side, surrounded by 4 pins. An entomology pin was used as hook and a Plexiglass cover gave protection of transducer hook when not in use.

Figure B5.3 shows a photograph of the microelectrode apparatus enclosed in a mesh Faraday cage. Representative left atrial recordings and transmembrane action potentials are shown.

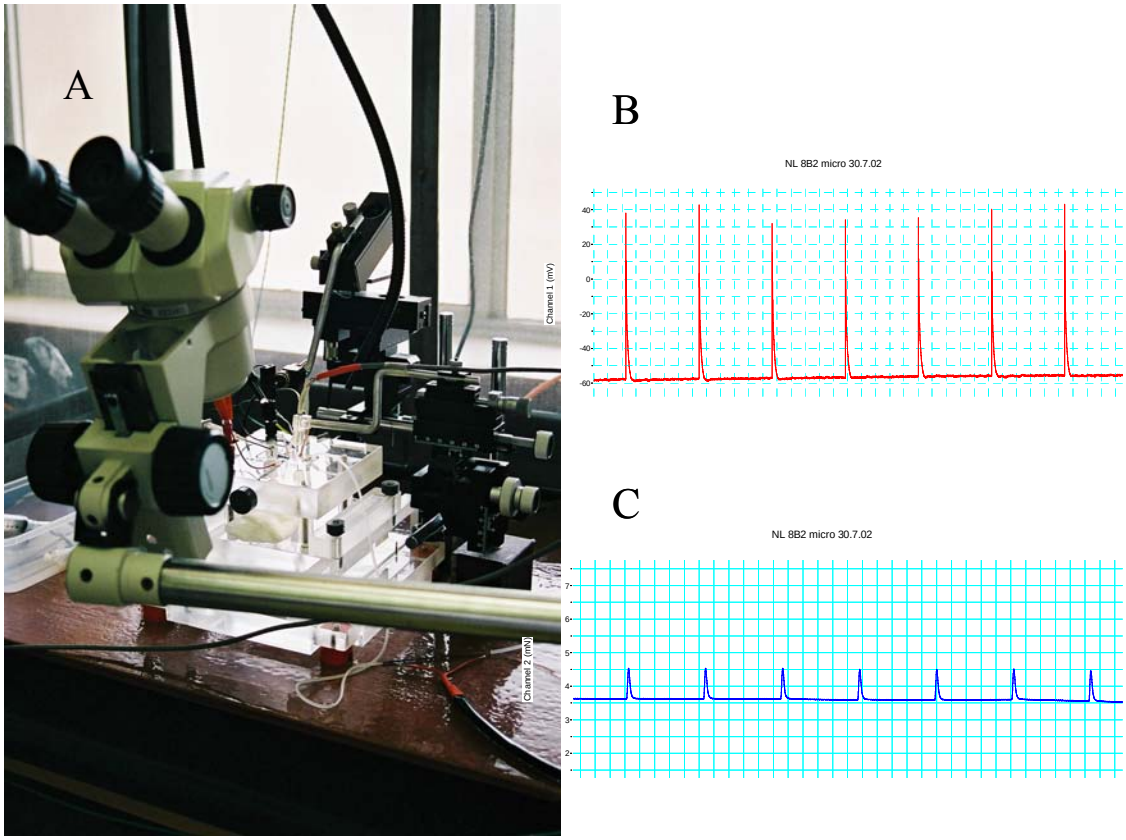


**Fig B5.3** Microelectrode stage holding tissue bath and left atria and microscope used for visualising impalements (A). The traces on the right show examples of left atrial transmembrane action potentials (B) and basal contractions at 1.8mM calcium (C).

**B5.3 Experimental protocol for Transmembrane action potentials and contractility of isolated atria**

The heart was quickly dissected in ice cold pre-carbogenated (95% $O_2$/5% $CO_2$) TPSS. The right atrium, right ventricular free wall and left ventricle and septum were dissected, blotted for 3 seconds and weighed. The left atria (LA) was removed and a stainless steel hook was positioned into the pulmonary vein opening, before transferring into a 1 mL Perspex organ bath. The LA was pinned onto a small rubber mat, and the hook connected to the force transducer (model AE801, SensoNor, Horten, Norway). The tissue was perfused continuously with carbogenated TPSS at a flow rate of 3mL/min and a temperature of 35±0.5$^{o}$C. The LA was held at an optimum preload of 3.5±0.5 mN

throughout the experiment, and field stimulated via platinum electrodes at 0.5 ms pulse width and 1 Hz, 25% above threshold (Grass SD9 stimulator, W. Warwick, RI, USA). After a 30 minute equilibration period the LA was impaled 4-5 times at different sites with a 3 M KCl filled glass microelectrode (World Precision Instruments, New Haven, CT, USA, 150F glass, 10-50 MΩ resistance). Data was recorded using a PowerLab and Chart 4.1.1 software (A.D. Instruments, Castle Hill, Australia), at 1000 samples/sec and then an average of the 4-5 recordings was calculated. A concentration response curve (CRC) to $CaCl_2$ was generated following transmembrane action potential (TAP) recordings.